



Helmholtz-Zentrum für Ozeanforschung Kiel

RV SONNE Fahrtbericht / Cruise Report S0277

OMAX: Offshore Malta Aquifer Exploration

Emden (Germany) – Emden (Germany)
14.08. – 03.10.2020



Berichte aus dem GEOMAR
Helmholtz-Zentrum für Ozeanforschung Kiel

Nr. 57 (N. Ser.)

January 2021



Helmholtz-Zentrum für Ozeanforschung Kiel

RV SONNE Fahrtbericht / Cruise Report S0277

OMAX: Offshore Malta Aquifer Exploration

Emden (Germany) – Emden (Germany)
14.08. – 03.10.2020



Berichte aus dem GEOMAR
Helmholtz-Zentrum für Ozeanforschung Kiel

Nr. 57 (N. Ser.)

January 2021

Das GEOMAR Helmholtz-Zentrum für Ozeanforschung Kiel
ist Mitglied der Helmholtz-Gemeinschaft
Deutscher Forschungszentren e.V.

The GEOMAR Helmholtz Centre for Ocean Research Kiel
is a member of the Helmholtz Association of
German Research Centres

Autor / Author:

Christian Berndt with contributions by Morelia Urlaub, Marion Jegen, Zarah Faghih, Konstantin Reeck, Gesa Franz, Kim Carolin Barnscheidt, Martin Wollatz-Vogt, Jonas Liebsch, Bettina Schramm, Judith Elger, Michel Kühn, Thomas Müller, Mark Schmidt, Timo Spiegel, Henrike Timm, Anina-Kaja Hinz, Thore Sager, Helene Hilbert, Lea Rohde, Torge Korbjuhn, Silvia Reissmann, Nicolaj Diller

GEOMAR Report

ISSN Nr. 2193-8113, DOI 10.3289/GEOMAR_REP_NS_57_2021

Helmholtz-Zentrum für Ozeanforschung Kiel / Helmholtz Centre for Ocean Research Kiel

GEOMAR
Dienstgebäude Westufer / West Shore Building
Düsternbrooker Weg 20
D-24105 Kiel
Germany

Helmholtz-Zentrum für Ozeanforschung Kiel / Helmholtz Centre for Ocean Research Kiel

GEOMAR
Dienstgebäude Ostufer / East Shore Building
Wischhofstr. 1-3
D-24148 Kiel
Germany

Tel.: +49 431 600-0
Fax: +49 431 600-2805
www.geomar.de

1 Cruise Summary

1.1 Summary in English

SO277 OMAX served two scientific projects. The objectives of the first project, SMART, were to develop multi-disciplinary methodologies to detect, quantify, and model offshore groundwater reservoirs in regions dominated by carbonate geology such as the Mediterranean Sea. To this end we acquired controlled-source electromagnetic, seismic, hydroacoustic, geochemical, seafloor imagery data off Malta. Preliminary evaluation of the geophysical data show that there are resistivity anomalies that may represent offshore freshwater aquifers. The absence of evidence for offshore springs means that these aquifers would be confined and that it will be difficult to use them in a sustainable manner. The objective of the second project, MAPACT-ETNA, is to monitor the flank of Etna volcano on Sicily which is slowly deforming seaward. Here, we deployed six seafloor geodesy stations and six ocean bottom seismometers for long-term observation (1-3 years). In addition, we mapped the seafloor off Mt. Etna and off the island of Stromboli to constrain the geological processes that control volcanic flank stability.

1.2 Zusammenfassung

SO277 OMAX diente zwei wissenschaftlichen Projekten. Ziel des ersten Projekts, SMART, war die Entwicklung multidisziplinärer Methoden zur Erkennung, Quantifizierung und Modellierung von Offshore-Grundwasserspeichern in Regionen, die durch Karbonatgeologie geprägt sind, wie z.B. dem Mittelmeerraum. Zu diesem Zweck haben wir vor Malta elektromagnetische, seismische, hydroakustische und geochemische Daten sowie Meeresboden-Videoaufnahmen erfasst. Die vorläufige Auswertung der geophysikalischen Daten zeigt, dass es auf dem Schelf vor Malta elektrische Leitfähigkeitsanomalien gibt, die auf Süßwasservorkommen hinweisen können. Das Fehlen jeglicher Anzeichen für größere Austritte von Frischwasser am Meeresboden zeigt jedoch, dass diese Grundwasserleiter heutzutage nicht signifikant mit dem meteorischen System in Verbindung stehen und es schwierig sein wird, sie auf nachhaltige Weise zu nutzen. Das Ziel des zweiten Projekts, MAPACT-ETNA, ist die Überwachung der Flanke des Ätna-Vulkans auf Sizilien, der sich langsam seewärts verformt. Hier haben wir sechs Geodäsiestationen und sechs Seismometer am Meeresboden für die Langzeitbeobachtung (1-3 Jahre) installiert. Außerdem haben wir den Meeresboden vor dem Ätna und vor der Insel Stromboli kartiert, um die geologischen Prozesse besser zu verstehen, die die Stabilität von Vulkanflanken mitbestimmen.

2 Participants

2.1 Principal Investigators

Name	Institution
Weymer, Bradley, Dr.	GEOMAR
Berndt, Christian, Prof.	GEOMAR

Jegen, Marion, Dr.	GEOMAR
Schmidt, Mark, Dr.	GEOMAR
Haroon, Amir, Dr.	GEOMAR

2.2 Scientific Party

Name	Discipline	Institution
Berndt, Christian, Prof.	Marine Geophysics / Chief Scientist	GEOMAR
Jegen, Marion, Dr.	Marine Geophysics / Lead EM	GEOMAR
Schmidt, Mark, Dr.	Marine Geochemistry / Lead Chemist	GEOMAR
Urlaub, Morelia, Dr.	Marine Geology / Lead Geodesy	GEOMAR
Elger, Judith, Dr.	Seismic acquisition	GEOMAR
Thomas Müller, Dr.	Hydrologist / chemist	GEOMAR
Schramm, Bettina	Ocean bottom seismometers	GEOMAR
Petersen, Florian	Geodesy	GEOMAR
Kühn, Michel	Seismic processing	GEOMAR
Reeck, Konstantin	EM	GEOMAR
Faghih, Zahra	EM	GEOMAR
Franz, Gesa	EM	GEOMAR
Hilbert, Helene	Watch keeper	GEOMAR
Kästner, Felix	Watch keeper	GEOMAR
Sager, Thore	Watch keeper	GEOMAR
Razeghi, Yousef	Watch keeper	GEOMAR
Barnscheid, Kim Carolin	Watch keeper	GEOMAR
Klein, Johanna	Watch keeper	GEOMAR
Hinz, Anina-Kaja	Watch keeper	GEOMAR
Timm, Henrike	Watch keeper	GEOMAR
Liebsch, Jonas	Watch keeper	GEOMAR
Spiegel, Timo	Geochemistry	GEOMAR
Wetzel, Gero	Seismic engineer	GEOMAR
Wollatz-Vogt, Martin	EM engineer	GEOMAR

Bartels, Thies	Airgun engineer	GEOMAR
Korbjuhn, Torge	AUV engineer	GEOMAR
Reissmann, Silvia	AUV engineer	GEOMAR
Diller, Nicolaj	AUV engineer	GEOMAR
Rohde, Lea	Apprentice	GEOMAR

2.3 Participating Institutions

GEOMAR Helmholtz-Zentrum für Ozeanforschung Kiel

3 Research Program

3.1 Description of the Work Areas

3.1.1 The Maltese shelf

Malta is representative for a large part of the Mediterranean coast line, and is also one of the ten poorest countries globally in terms of water resources per inhabitant (Vallée, D. et al. 2003). Stratigraphically, the islands consist of Oligocene and Miocene limestone formations: from top to bottom Upper Coralline Limestone, Greensand, Blue Clay, Globigerina Limestone and Lower Coralline Limestone. This stratigraphy makes it a type example for the geology in large parts of the Mediterranean. The archipelago hosts an excellent example of an unconfined carbonate rock aquifer onshore in the Lower Coralline Limestone, which is overlain by an aquitard the Globigerina Limestone. This aquitard continues offshore out to the shelf break. Existing borehole data and pockmarks indicate that the groundwater aquifer extends offshore, but so far it is unknown if the underlying aquifer also extends all the way to the shelf break or if it terminates somewhere on the shelf. Because of sea-level rise of 110 m after the last glacial maximum it is likely that the shelf and adjacent seafloor host both recharging and fossil aquifers. Groundwater is known to seep along the coastline and shallow seafloor (Micallef, A. et al. 2013).

3.1.2 The flank of Mt. Etna, Sicily

Mount Etna is Europe's largest active volcano. It rises to 3330 m above sea level. The volcanic edifice of Etna builds upon continental crust, but about 2/3 of its eastern flank locate under water in the Ionian Sea. The western Ionian Sea is a complex and active tectonic setting. Beside volcanism and flank instability the area is furthermore affected by strong bottom currents and diapirism.

3.1.3 Stromboli

Stromboli volcano is part of the Eolian Island backarc chain in the Tyrrhenian Sea north of Sicily. The volcano is 926 m above sea level and over 2700 m on average above the sea floor and has

been in almost continuous eruption for the past 2,000–5,000 years. A significant geological feature of the volcano is the Sciara del Fuoco ("stream of fire"), a big horseshoe-shaped depression created in the last 13,000 years by several collapses on the north-western side of the cone (Tibaldi et al. 2009).

3.2 Aims of the Cruise

SO277 contributes to two scientific projects and its agenda developed from the combination of two different ship time proposals: OMAX which was conceived to acquire a comprehensive data set to study freshened groundwater in the frame of the Helmholtz European partnering project SMART and GPF 18-1-89 MAPACT-ETNA (Monitoring and mAPping ACTive deformation of Mount ETNA).

3.2.1 Offshore groundwater

Coastal regions are the most densely-populated areas in the world with an average population density nearly 3 times higher than the global average (Small, C. 2003). Freshwater resources in coastal states and island nations are therefore under enormous stress, and their quantities and qualities are rapidly deteriorating. This problem is exacerbated by population growth, pollution, climate change and political conflicts (Bates, B. 2008). Problems are especially felt in arid areas, such as Malta, where groundwater is the only source of freshwater and the periods of highest demand (e.g., agricultural and tourist seasons) coincide with the periods of lowest recharge from precipitation (Post, V. 2005). By comparison, Cape Town, South Africa is the first major city in the modern era to face the threat of running out of drinking water, and other large cities like Jakarta, and Beijing are likely to follow suit.

Offshore aquifers (OAs) have been proposed as an alternative source of freshwater to cover demand by domestic, agricultural and tourist industries in coastal regions (Bakken, T. H. et al. 2012). During the Last Glacial Maximum (19-22,000 years ago), modern shelf areas were sub-aerially exposed, leading to the development of extensive water tables recharged by atmospheric precipitation (meteoric water), rivers, lakes and, in some areas, glacial meltwater (Burnett, W. et al. 2006). In view of the fact that sea level has been much lower than today for 80% of the Quaternary period (last 2.6 million years), and that meteoric groundwater systems migrate landwards more slowly than rising sea levels, remnants of meteoric groundwater occur extensively offshore (Evans, R. L. 2007). An OA has been defined by (Post, V. E. 2013) "*as a groundwater body with a minimum horizontal extent of 10 km, and a minimum concentration of total dissolved solids (TDS) less than 10 g/L, roughly 1/3 the salinity of seawater.*" Two types of OAs can be distinguished (Fig. 1). The first type (active) entails a present-day, permeable connection of the OA with a terrestrial aquifer recharged by meteoric water (Bratton, J. F. 2011, Johnston, R. H. 1983). Such aquifers tend to be wedge-shaped, becoming thinner and more saline with increasing

distance from the coast. However, onshore hydraulic heads are sometimes too low to drive water offshore (Kooi, H. et al. 2001) or a hydraulic connection between offshore and onshore aquifers may be absent (Person, M. et al. 2003). In such cases, offshore groundwater systems are associated with paleo-groundwater (fossil) systems that have been emplaced by meteoric recharge during lowered sea level periods (Leahy, P. et al. 1982) and that are no longer recharged.

Recent studies have estimated the volume of OAs to range between $\sim 3 \times 10^5 \text{ km}^3$ (Cohen, D. et al. 2010) and $4.5 \times 10^6 \text{ km}^3$ (Adkins, J. F. et al 2002), with a more robust estimate of $5 \times 10^5 \text{ km}^3$ (Post, V. E. et al. 2013). The latter is two orders of magnitude greater than what has been extracted globally from continental aquifers since 1900 ($4.5 \times 10^3 \text{ km}^3$). The salinity of OAs can range between freshwater and seawater values, and the salinity threshold defined by (Post, V. E. et al. 2013) corresponds to the upper limit of the salinity range used for the definition of brackish water for desalination (Greenlee, L. F. et al. 2009). Since submarine groundwater can be exploited using conventional technology from the oil and gas industry and onshore groundwater exploitation, and because the costs seem to be economically competitive with desalination (Bakken, T. H. et al. 2012), OAs have the potential to become an important resource that can relieve water scarcity and mitigate the adverse effects of groundwater depletion (e.g. land subsidence, saltwater intrusion) in densely populated coastal regions.

The characteristics of offshore groundwater systems remain poorly constrained, and there are many first-order questions, related to aquifer geometry and distribution, that need to be addressed. Conventional offshore groundwater aquifer and submarine groundwater discharge (SGD) methods rely on point-source data from boreholes, seepage meters, and chemical radionuclide tracer techniques that cannot provide continuous information of the groundwater system (Burnett, W. et al. 2006). Additionally, most measurements and research efforts have focused on the nearshore zone (up to several km from the shoreline) (Davidson-Arnott, R. et al. 1999), mainly because of accessibility, the presence of observable discharge at low tides, and its direct association with the unconfined surficial aquifer and topographically driven flow (Bratton, J. F. 2010).

The data to be acquired within this cruise address two of the overarching goals of the SMART project, which are: a) *To develop a best practice guide on how to combine geophysical measurements with geochemical characterisation to detect, characterise and monitor OAs*, and b) *To quantify the hydrologic budget of OAs*.

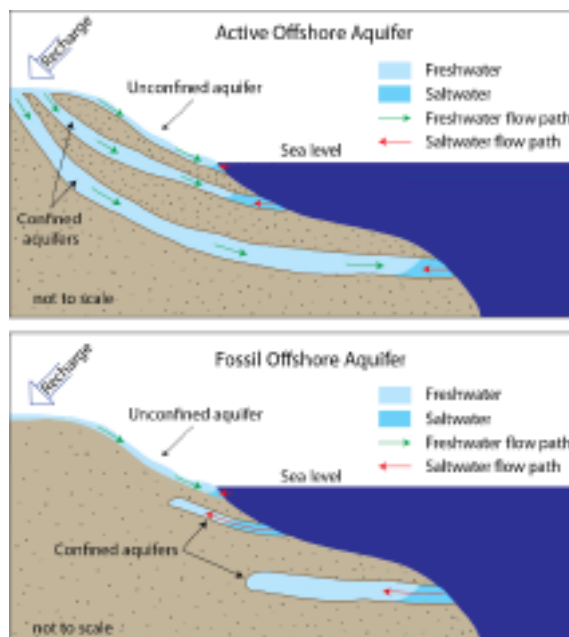


Fig. 3.1 Cartoon depicting the differences between active (connected) and fossil (disconnected) offshore aquifers. The modern day active aquifers are recharged by precipitation (green arrows). Fossil aquifers are no longer fed by meteoric water and are subject to saltwater intrusion (red arrows).

There are two working hypotheses driving the study design

Hypothesis 1: *The volume and spatial extent of offshore aquifers in carbonate settings can be determined by integrating seismic and electromagnetic methods*

Hypothesis 2: *The aquifers off Malta are active systems that discharge into the ocean.*

In order to test these hypotheses, we had three research objectives:

Objective 1: *Building a geological model and constraining the volume and spatial extent of offshore aquifer(s) by geophysical data acquisition*

Terrestrial hydrogeological investigations on Malta define two aquifers: a perched aquifer in the Upper Coralline Limestone (high porosity) and a mean sea-level Ghyben-Herzberg freshwater lens in the Lower Coralline Limestone with lower porosity, separated by an impermeable “Blue Clay” layer (i.e., Stuart, M. et al. 2010). The study area is located north of the Great Fault in Malta, where all the relevant formations hosting the aquifers occur and where the highest probability that an impermeable layer (Blue Clay) may extend offshore providing a seal for a potential offshore aquifer. The study area includes the widest and most gently sloping part of the Maltese continental shelf and bedrock/outcrop scarcity makes it the most suitable location for bottom towed CSEM experiments. Further indicators of the OA are a series of box canyons that are located upslope of a limestone cliff and are indicative of SGD and observations of flares in sub-bottom profiles reported by Micallef, Berndt and Debono (Micallef, A. et al. 2011). While the OA indications are indirect within the Malta region, extensive groundwater seeps have been located offshore in very similar geological settings, particularly offshore Sicily and the Levant (Bakalowicz, M. 2018). To achieve a focus on the region of interest, in October, 2018 we conducted marine 2D seismic and CSEM measurements extending the land EM profiles offshore east of the island on the R/V Hercules within the framework of the MARCAN project led by co-proponent Aaron Micallef. Terrestrial EM measurements were collected in July, 2018 by colleagues at UoM, and Texas A&M University.

We have conducted two types of seismic experiments. First, we collected 2D seismic data using the P-Cable system in 2D mode. The 2D seismic lines from the area between Malta and Gozo into the offshore study area allow us to correlate information from the boreholes.

Apart from mapping the stratigraphic changes, which are often associated with porosity changes, the move-out characteristics of the 2D seismic data and ocean bottom seismometer data will allow us to determine seismic velocities that provide rough porosity estimates and crucially show variations in petrophysical parameters away from the boreholes.

The second experiment was the collection of a high-resolution 3D seismic cube. The aim of this experiment was to image the entire subsurface in three dimensions. This will provide information on the geological variations such as faults, stratigraphic terminations, etc. that are crucial for building the hydrological models and constrain the geology for the inversion of the CSEM data. The cube includes the shelf break, i.e. across the area that was subaerially exposed during the sea-level lowstand during the last glacial maximum (LGM) and the area that was always submerged.

CSEM electromagnetic data were collected along profiles covering the seismic 2D profiles as well as 3D seismic cube. CSEM and seismic 3D cube lines as well as 2D regional seismic lines will be co-rendered to investigate first order correlation between resistivity changes and positions of

reflectors and/or velocity changes. This comparison will allow us to identify lithological changes and decipher changes in electrical conductivity due to porosity/clay content changes from electrical conductivity anomalies caused by potential fresh water saturation. Furthermore, physical properties (electrical conductivity, seismic velocity and porosity) of the gravity cores will be measured and analysed for fluid saturations with different salinities in order to characterize the physical property relationships in carbonates, which often defy standard effective medium theory models.

Objective 2: *Localize seep structures, which open a window into the aquifer at depth, using high resolution AUV based photo imagery, water column sensors and Parasound data.*

In order to understand the functioning of the aquifer and to direct seep sampling (Aim 3) it is necessary to localize groundwater seeps. In spite of extensive efforts using the video-CTD casts, gravity cores and AUV imagery it was not possible to discover any groundwater seeps.

Objective 3: *Characterize seeping groundwater to be able to interpret the geophysical data and provide background information for the hydrogeological models such as mixing, regional fluid flow rates, and age of the groundwater in the distal parts of the aquifer*

In the absence of seep sites it was not possible to obtain direct samples of offshore groundwater. Although much of the geochemical data still awaits analysis the comprehensive studies did not show signs of groundwater seepage. This would falsify the second hypothesis that the aquifers are connected to the ocean and suggests that the groundwater system off Malta is most probably a fossil system.

3.2.2 Slope stability of volcanic islands

Volcanoes are among the most rapidly growing geological structures on Earth. Consequently, volcanoes commonly suffer structural instability that may result in lateral flank collapses, such as the 1980 Mt St Helens collapse. Collapses of ocean island volcanoes or those along shorelines can trigger ocean-wide tsunamis with extreme effects. The world just witnessed a small example of such an event: the 22 December 2018 collapse of Anak-Krakatau in Indonesia that caused a tsunami with 430 fatalities at the surrounding coasts (Walter et al. 2019). Volcanic flank instability is a global and widespread phenomenon, and varying degrees of flank instability have been reported from all scales of volcanoes, such as Kilauea (Hawaii), the Canary Islands, Galapagos, and Tristan da Cunha (Poland et al. 2017).

Mount Etna, located on the coast of Sicily (Italy), is a basaltic stratovolcano located at the edge of the Calabria-Tyrrhenian slab. Right-lateral transtension between two slabs produce a vertical ‘slab window’, which allow magma to upwell. Mount Etna is one of the most intensively monitored

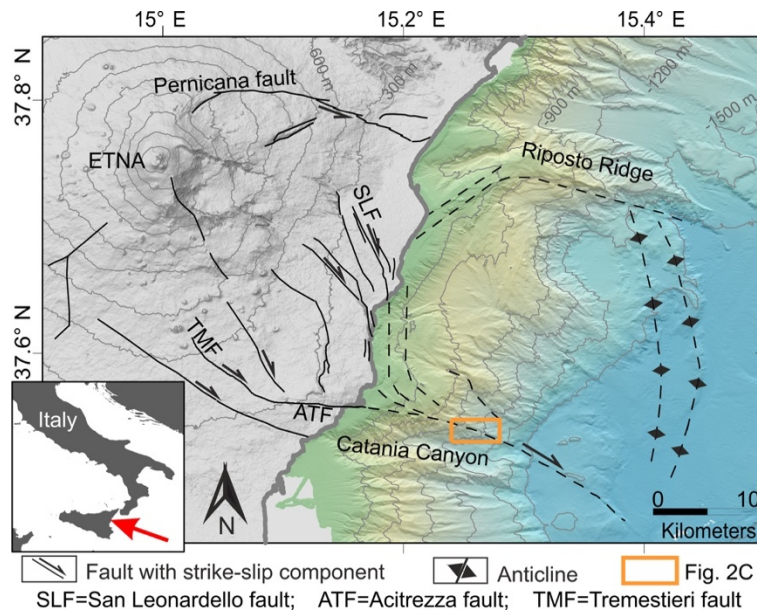


Fig. 3.2 Shaded relief map of Etna's eastern flank (grey: onshore, coloured: offshore) with the main faults that are kinematically related to seawards sliding of the volcano's unstable eastern flank (Urlaub et al. 2018).

and best studied volcanoes in the world. Repeated and ongoing GPS campaigns, permanent GPS monitoring onshore, and interferometric synthetic aperture radar (InSAR) data provide evidence for downward movement of the eastern and south-eastern flanks coupled with overall flank subsidence (e.g. Bonforte et al. 2011, Palano 2016). In contrast, the western flank is apparently more stable with no or only minor movement (e.g. Puglisi et al. 2001). Seaward motion of Mount Etna's southeastern flank manifests in continuous deformation as well as episodic 'slow slip' events that are aseismic and occur irrespective of volcanic activity (Palano 2016). Hence, displacement rates are highly variable over time, resulting in about 30-50 mm/year. Whereas vertical ground deformation due to magma overpressure reaches a maximum at the volcano summit, flank subsidence and seaward movement concentrates along the coast (Bonforte et al. 2011).

Large parts of Mount Etna's eastern part are covered by water, so that traditional geodetic measurements, such as those by GPS or InSAR, cannot be applied due to the opacity of seawater to electromagnetic waves. Consequently, offshore slip is highly unconstrained, resulting in high uncertainties in models that seek to fit the onshore GPS data. Hypotheses that attempt to explain Mount Etna's flank instability include the weight of the volcanic pile, increase of magma pressure (Borgia et al. 1992), a weak substrate (Nicolosi et al. 2014), combined magmatic inflation and continental margin instability (Chiocci et al. 2011), or a combined volcano edifice and continental margin instability (Gross et al. 2016). The disagreement on the causes of flank instability mainly originates from the lack of information on the dynamics of the submerged part of the volcano. Between 2016 and 2018, an acoustic telemetry network measured displacement of the submerged unstable flank at one location. The network recorded a minimum of 4 cm of slip during an eight-day sliding event in May 2017, while displacement on land peaked at ~4 cm at the coast. Such large deformation away from the magmatic system can only be explained by a gravitational effect that is further destabilized by magma dynamics (Urlaub et al. 2018). However, the observation period is less than two years and it is impossible to deduce long-term rates.

The spatial outline of the unstable flank is well defined onshore by geodetic, geophysical, and geological methods (e.g. Bonforte et al. 2011). Along the northern boundary of the unstable flank,

deformation focuses along the left-lateral Pernicana Fault that extends from the summit almost down to the coast (Fig. 3.2). Near the coast, this deformation is less focused and the Pernicana Fault appears to branch into a wider area. Diffuse deformation likely continues off the coast, as neither the bathymetric nor the seismic data show evidence for focused active faulting (Gross et al. 2016). In the south, the right-lateral Tremestieri-Acitrezza and Timpe fault systems (San Leonardello fault) mainly accommodate the flank movement on land (Fig. 3.2). Offshore, a right-lateral oblique transpressive fault north of Catania Canyon, interpreted as the offshore extension of both onshore fault systems, likely represents the southern boundary (Chiocci et al. 2011, Gross et al. 2016, Urlaub et al. 2018). Based on bathymetric and seismic data, Gutscher et al. (2016) speculate that this fault is further connected to a regional crustal structure; the North Alfeo Fault. According to Gutscher et al. (2016, 2017) the North Alfeo Fault is the surface expression of an active slab tear. The eastern and most distal end of the flank is less clear. A compressive feature might be expected. One candidate could be a plateau about 40 km off the coast, where seismic data indicates active uplift. This structure has been interpreted as a serpentinite diapir by others (Polonia et al. 2017).

Stromboli volcano has experienced two major eruptions in 2019. The eruptions were accompanied by strong ground deformation, landslides and large pyroclastic flows that entered the sea at the northwestern flank. While satellite imaging reveals morphological changes of the subaerial flank, changes at the seafloor remain hidden. Information on the distribution and the type of volcanic deposition will provide valuable insights into the growth of island volcanoes and the results will inform the analysis of potential weakness zones in volcanic edifices such as the flank of Mt. Etna.

Objectives

The first objective of GPF 18-1-89, side user on cruise SO277, was to install an autonomous seafloor geodetic array to understand deformation of Mount Etna's submerged flank over long terms. Our successful previous monitoring campaign (Urlaub et al. 2018) proved that (i) the technique is well suited to monitor unstable volcanic flanks under water, (ii) the location of the array coincides with the boundary of the unstable flank, (iii) the array design is ideal for monitoring flank instability, and (iv) the slip lies well within the resolution of the array. It is now important to analyse the displacement trend over long-terms (years to decades). In order to evaluate the hazard from a potential flank collapse it is crucial to know if the unstable flank is accelerating or decelerating.

The second objective is to collect high-resolution multibeam and Parasound data to identify if the active fault partitions into multiple faults in the landward direction and if it is linked to regional tectonic structures. If Mount Etna's unstable flank was connected to a deep, large-scale tectonic structure, its instability could in parts be controlled by the regional tectonic setting. A connection is not fully recognizable from existing bathymetric data with a grid spacing of 30 m (<1000 m water depth) and 100 m (>1000 m water depth). It could, however, be recognizable in multibeam data collected during dedicated surveys with the shipboard system.

The third objective is to map the distribution of the volcanic deposits associated with the 2019 eruptions at Stromboli. This is a unique opportunity because Italian colleagues have carried out a similar bathymetric survey of the flank of Mt. Stromboli in 2016 (Casalbore, pers. comm.). By calculating the difference between that data and our new data we will be able to identify the nature

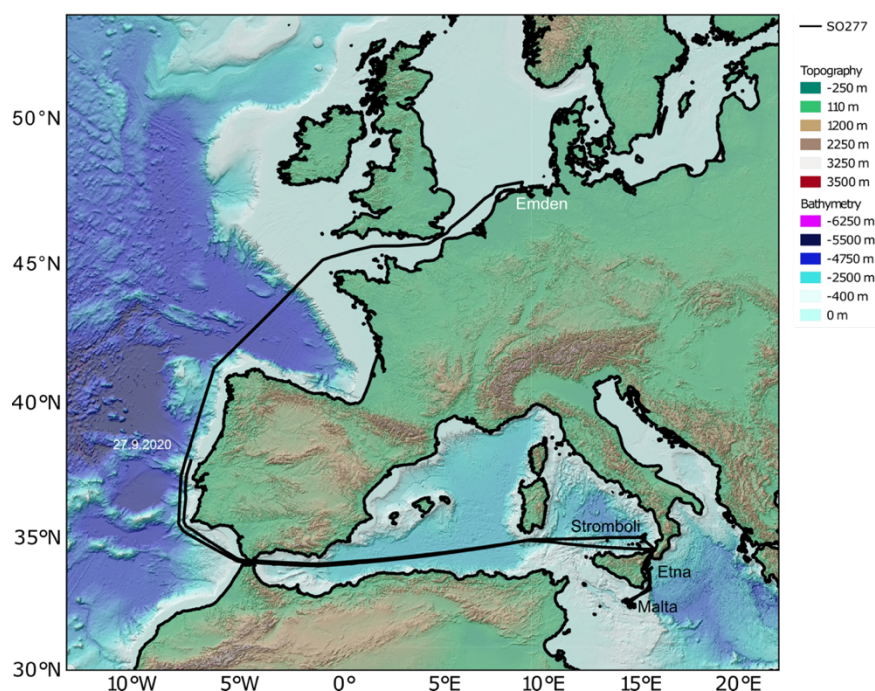


Fig. 2.3 Track chart of R/V SONNE CRUISE SO277. Bathymetry from Smith and Sandwell (1997). The three main working areas are labeled.

and distribution of volcanic deposits associated to the recent eruptions. These changes could include traces of pyroclastic flows, landslide scars, landslide blocks, all of which could have formed due to the recent major eruptions.

3.3 Agenda of the Cruise

The coronavirus situation in Germany required that three planned legs had to be combined: the two legs of Meteor cruise M170 that were originally scheduled to take place in December 2020 and parts of a Poseidon cruise that was already split up into Alkor cruise AL532 and Meteor cruise M169. The combination of these cruises and the reduced capacity to carry scientists meant that the work program had to be reduced by omitting the ROV that was planned for M170/2 and by reducing the capacity for geochemical analyses on board.

Sailing from Emden and back meant two long transits of eleven days each. The work was split into four packages. First, we deployed marine geodesy stations off Mt. Etna. Then we carried out the bulk of the work off the Maltese Islands before returning to Mt. Etna to double-check that the geodesy stations were operating properly and deploy six long-term ocean bottom seismometers. Finally, we used the remaining day of ship time that was saved for fixing the geodesy stations in case of problems to map the recent volcanic deposits off Stromboli a study that also addresses volcano flank stability.

4 Narrative of the Cruise

All times in the narrative are local times.

Monday, 14.8.2020

We departed from Emden at noon and started our long transit to Italy. Fortunately, the weather was fine for the entire transit allowing us to sail with 12 rather than the expected 11 knots which meant that we gained one day for work in the study area.

Sunday, 23.8.2020

From about midnight to the late morning we conducted the releaser tests for the marine geodesy stations, the ocean bottom seismometers, and the ocean bottom electromagnetic receivers in about 1700 m water depth north of Sicily. This took several hours because of the large number of instruments. Also, a sound velocity profile was measured to calibrate the hydroacoustic systems. Afterwards, we collected a single multibeam profile south of Volcano Island and continued our transit to the first study area off Mt. Etna passing through the Strait of Messina in the early evening.

Monday, 24.8.2020

We arrived in the study area off Catania at midnight and conducted a CTD cast that lasted until 07:00 in the morning. Apart from measuring the CTD profile we also used the video camera to obtain seafloor images in the area where the geodesy stations had to be deployed. The seafloor was covered with marine muds and showed abundant bioturbation but no clear signs of tectonic deformation. At 08:00 we began with the deployment of two geodesy stations which was completed by 15:00. While progressing to the first multi-beam line we spotted a bright red item at the location of the first deployment site. Concerned that one of the geodesy stations might have surfaced accidentally, we returned back only to find a bright red fairground balloon that was swimming in the water. Having sailed back to the deployment site, we made most of the opportunity and connected to both stations to check that they were operating properly before commencing with a multi-beam survey of Etna's flank during the night.

Tuesday, 25.8.2020

With a fresh northerly breeze, we continued to deploy the seafloor geodesy stations. The work progressed exceptionally well and we managed to place the remaining four stations on the seabed between 8:00 in the morning and 17:00. Afterwards, we continued to collect multi-beam data over the lower slope of Mount Etna.

Wednesday, 26.8.2020

In the morning at 08:00, we returned to the geodesy stations and communicated with them to ascertain that all were functioning properly. After we were satisfied that this was the case and that they could all range each other, we started our transit to the next study area off Malta. Initially we collected multi-beam data along the Malta Escarpment until we reached the boundary of our permitted work area. We arrived off Malta shortly before midnight.

Thursday, 27.8.2020

We started with a first CTD cast off Gozo to obtain a sound velocity profile for the calibration of the hydro-acoustic systems and to collect background water samples for the geochemistry. Afterwards until 07:00, we did a Video-CTD transect closer to the coast off the eastern tip of Gozo. At 08:00 we deployed the AUV off St. Paul's Bay and conducted a video survey of the seafloor in an area known for gas seepage. At 14:00 we retrieved the AUV and started to deploy 9 OBEMs until 19:00, then 10 OBS until 23:00. Afterwards, we carried out a multi-beam survey throughout the night.

Friday, 28.8.2020

We completed the multi-beam survey at 09:00 and started to deploy the 2D seismic system off Camino at 10:00. The system was up and running at 10:45, but after half an hour a fishing line got entangled and we had to retrieve the streamer to unhook it. From 13:00 onwards we acquired 2D seismic lines off the central and eastern parts of Malta.

Saturday, 29.8.2020

In fine weather we continued the 2D seismic data acquisition without further interruptions.

Sunday, 30.8.2020

In fine weather we continued the 2D seismic data acquisition.

Monday, 31.8.2020

In fine weather we continued the 2D seismic data acquisition.

Tuesday, 1.9.2020

We continued collecting 2D seismic data until 10:00 when the tow cable of the streamer started to show signs of malfunctioning. We retrieved the streamer and continued shooting into the OBS until 15:30. We then took on board the seismic source. Afterwards, we retrieved the two outermost OBS that were carrying the experimental mini-OBS because their batteries only last for five days. We also deployed three more OBEM in the study area off Gozo. Afterwards, we started a multi-beam survey beyond the shelf edge to ascertain that there are no obstacles for the CSEM tow that was planned for the following day.

Wednesday, 2.9.2020

At 08:00 we deployed the CSEM system and towed it along a track below and parallel to the escarpment along the NE coast of Gozo. Unfortunately, only the first two of the four receivers logged data but those are of good quality.

Thursday, 3.9.2020

We recovered the CSEM system between 07:00 and 09:00 in the morning. Interestingly, two pieces of slate were stuck to the depressor (pig) suggesting that the slates that are known to exist below the lower coralline limestone could be outcropping somewhere in the area. Afterwards we surveyed a video CTD track down the shelf edge across a phase reversal in the seismic data and crossing the CSEM line that was acquired in the night before. There were no signs of fluid escape along this track and the entire seafloor including the escarpment that forms the shelf edge turned out to be covered with soft sediment. Originally, we had planned to deploy the AUV in the morning but sometime between the previous AUV deployment on the 27.8. and the 3.9. the container that holds the AUV USBL modem must have opened and the transponder was lost. From 14:00 onwards we deployed the P-Cable 3D seismic system which was operational at 15:30 and we started to acquire 3D seismic data.

Friday, 4.9.2020

In spite of a fresh easterly breeze the P-Cable system was operating fine until one of the air pipes of the seismic source came loose and we had to take the source on board for repairs at 11:00. The system was back in operation at 14:00 and we continued acquisition of 3D seismic data.

Saturday, 5.9.2020

P-Cable acquisition continued without interruptions.

Sunday, 6.9.2020

P-Cable acquisition continued without interruptions.

Monday, 7.9.2020

We finished the planned P-Cable lines at 10:00 in the morning. Afterwards we began to acquire data in the numerous gaps caused by avoidance of fishing gear. At 17:00 a fishing line with hooks got entangled in the segment between streamer 11 and 12 and damaged the cross-cable segment and the T-junction. The port side paravane and streamers 11 to 16 had to be taken onboard and the cross-cable segment had to be replaced. Afterwards we continued filling the gaps in the P-Cable cube.

Tuesday, 8.9.2020

P-Cable acquisition finished at 14:30 in spite of some remaining holes in the fold map. These could not be filled because of fishing gear that was floating permanently at those locations. The system was back on board and the back deck was set up for CSEM operations. The CSEM system was deployed until 17:00 and we collected another CSEM profile beyond the shelf edge.

Wednesday, 9.9.2020

We recovered the CSEM system until 09:30 in the morning. The system was working well and all receivers collected data. At 10:30 we deployed the AUV close to Gozo and then started a first video-CTD transect near Sikka-i-Bajda reef. This was completed at 16:00 when we returned to the AUV station and retrieved the vehicle. We then started a second video-CTD transect at the pockmark field east off Gozo. Within the pockmarks the water was more turbid but no signs of fluid escape could be found. The station was finished at 22:00 and we collected several parallel Parasound profiles on the shelf to ascertain that there are no obstacles for the CSEM track planned for the next day.

Thursday, 10.9.2020

At 08:00 we started to recover four of the OBEM receivers. This was finished successfully by 11:00. Afterwards we conducted two CTD transects in the east and north off Gozo. During the first dive we could see the water column imaging anomaly east off Comino, but we could not detect a signal in the CTD or the other sensors. The second site confirmed the impression that the pockmarks below the shelf break are not active. At 16:00 we redeployed the CSEM system for another transect east off Gozo.

Friday, 11.9.2020

The CSEM transect was finished at 04:30 and the system was recovered until 06:30. Afterwards we steamed to the meeting point off Comino to take onboard the spare USBL modem for the AUV. This was delivered by boat at 09:00. From 10:00 to 11:30 we deployed four OBEM on a transect off northern Malta and the Comino channel and from lunch time to 16:00 we collected the first gravity cores. The first core consisted of fine sands and carbonate debris and it was possible to

centrifuge pore water. At the other two coring sites there was no penetration but some carbonate debris in the core catcher. During the night we conducted another CSEM tow north off Gozo.

Saturday, 12.9.2020

The CSEM system was successfully recovered in the morning and at 08:30 we deployed the AUV at the most prominent water column imaging anomaly southeast off Comino. Afterwards we collected three more gravity cores north off Gozo with mixed success before recovering the AUV at 14:00. Afterwards we retrieved the eight OBS and throughout the night we collected Parasound data to survey the track of the next CSEM deployment.

Sunday, 13.9.2020

At 10:00 we met with Dr. Owen Bonicci, the Maltese Minister of Education, who came out to visit us on a pilot boat. He was accompanied by Prof. Aaron Micallef and Dr. Axel Steuwer the University of Malta's vice rector. Because of coronavirus it was not possible for them to come onboard R/V Sonne but it was possible to exchange presents and talk over the side of the ship. Afterwards they stayed on to witness the deployment of the video CTD at the site of the most prominent water column anomaly that was identified in the multi-beam data.

When a violent thunderstorm came up, they left back for the harbor. The thunderstorm delayed the following AUV deployment until 14:00 because it was not safe to work on deck. The AUV carried out a short 1.5 hour-dive at the easternmost of the water column anomalies and from 16:00 onwards we began to acquire the next CSEM profile east off Sikka I Bajda reef.

Monday, 14.9.2020

We recovered the CSEM from 06:00 to 08:00. Although the Parasound profile had suggested that there was sufficient sediment cover along the track signs of wear and tear indicated the presence of several hard rock outcrops along the track and one receiver was damaged. From 08:00 to 10:30 we collected more Parasound data off the eastern tip of Malta to find out if another CSEM profile was possible in that region. Unfortunately, it also turned out to be too rough. We discovered, however, several water column anomalies in this area that indicate gas emissions from the seafloor. From 11:00 onwards we conducted three video-CTD casts at sites off eastern Malta where water column anomalies were reported previously. The first site turned out to be an unknown wreck in 118 m water depth. The other two sites did not show signs of fluid seepage either. From 19:00 onwards, we collected multibeam bathymetry data off Comino in extension of Markan CSEM profile 2 as a pre-survey for the final CSEM line.

Tuesday, 15.9.2020

In the morning at 08:00, we deployed the AUV at the northern water column anomaly off Comino in spite of a strong breeze (force 6-7). From 10:00 to 14:30 we collected three gravity cores further north before recovering the AUV at 15:30. The gravity cores showed mainly hemipelagic mud, but no evidence for methane in the sediments, authigenic carbonates but fragments of limestones. Afterwards we deployed the EM system in MMR mode (vertical dipole) that allows to tow the system also in rocky areas, but without a receiver. These signals were recorded by the OBEM.

Wednesday, 16.9.2020

The CSEM transmitter worked splendidly throughout the night and we recovered the system in the morning. At 08:00 we deployed the AUV at a gas flare off the shelf edge off Gozo. Afterwards we took three gravity cores at the northern water column anomaly off Comino. Core recovery was limited but it showed the correct interpretation of the AUV imagery. We then collected the AUV, before commencing with another CTD station at the same site where we took the gravity corers.

Thursday, 17.9.2020

From 08:00 onwards we collected two video-CTDs at an enigmatic mound NE off Malta that consists of carbonate rocks above the post Messinian soft sediments and at the flare site investigated with the AUV on the day before. With force 7 winds it was not possible to use the AUV. In the afternoon, we took one more gravity core from a box canyon NE of Gozo, before we deployed the CSEM system to acquire electrical resistivity data further offshore.

Friday, 18.9.2020

The windy conditions persisted during the day. At 08:00 in the morning, we recovered the CSEM system which was on deck by 09:30. Afterwards, we collected the twelve OBEM receivers. This was completed by 16:00. All instruments were safely retrieved and found to have recorded data, although one of the twelve data loggers had stopped after four days. In the evening, we conducted a final video-CTD cast at the southern water column anomaly off Comino before we left the study area to sail back to Sicily.

Saturday, 19.9.2020

We arrived off Mt. Etna in the early morning and set up communication with the seafloor geodesy stations. After we had downloaded the data from the past four weeks since their deployment and had ascertained that they were working correctly, we conducted one video-CTD dive near the geodesy array to see if there are obvious signs of flank deformation across the fault system, but apart from some elongate seafloor discolorations we could not find any anomalies. At 13:00 we started to deploy six ocean bottom seismometers which will stay in the area for one year to measure seismicity in the vicinity of the seafloor geodesy stations. This was completed by 16:00. Afterwards, we carried out a second video-CTD cast further down along the fault system in about 2000 m water depth. Towards the end of this dive we found signs of chemosynthetic ecosystems that were not expected. Analysis of the water samples will reveal the driving process for the associated fluid seepage. During the night we collected more multi-beam bathymetry data on this part of the slope.

Sunday, 20.9.2020

We continued multibeam surveying until 08:00 in the morning. Then we left the study area to proceed to our final study site off Stromboli. We arrived there at 15:00 and carried out a CTD cast. Afterwards, we started to survey the western flank of Stromboli using the multi-beam echosounder to image the recent deposits from Sciara del Fuoco.

Monday, 21.9.2020

The multi-beam survey and the scientific program were completed at 20:00 and we started the transit back to Emden.

Saturday, 3.10.2020

We arrived in Emden at 11:00.

5 Preliminary Results

5.1 Hydroacoustic methods

(M. Urlaub)

GEOMAR

During SO277 we used three types of hydroacoustic methods: multibeam echosounders, sediment echosounder (PARASOUND) and marine geodetic measurements. These are grouped under hydroacoustic methods, but we discuss the instrumentations, processing, preliminary results individually.

5.1.1 Multi-beam bathymetry

5.1.1.1 Instrumentation

Kongsberg multibeam echosounder systems are permanently installed on RV SONNE; the EM122 for full ocean depth and the EM710 system with a maximum acquisition depth of approximately 2000 m according to the manufacturer's data. In the working area off Malta with water depths <200 m only the EM710 was used. In the working areas off Sicily both systems were used in water depths <1400 m, while only the EM122 was used in greater depths. Altogether both systems recorded more than 700 million soundings during SO277.

In addition to bathymetric information the EM122 and the EM710 system register the amplitude of each beam reflection. The amplitude signals correspond to the intensity of the echo received at each beam. It is registered as the logarithm of the ratio between the intensity of the received signal and the intensity of the output signal, which results in negative decibel values. Both systems also allow recording the entire water column. The water column data correspond to the intensity of the echoes recorded from the instant the output signal is produced. All echoes coming from the water column, the seabed and even below the seabed are recorded for each beam. The water column data were stored in separate *.wcd files.

Both the EM122 and EM710 systems apply beam focusing to both transmit and receive beams in order to obtain the maximum resolution also inside the acoustic near-field. The systems are capable of producing more than one sounding per beam (so-called high density mode), such that the horizontal resolution is increased and is almost constant over the whole swath. In multiping mode, two swaths are generated per ping cycle, i.e. one beam is slightly tilted forward and the second ping slightly tilted towards the aft of the vessel, resulting in double the amount of soundings. As a

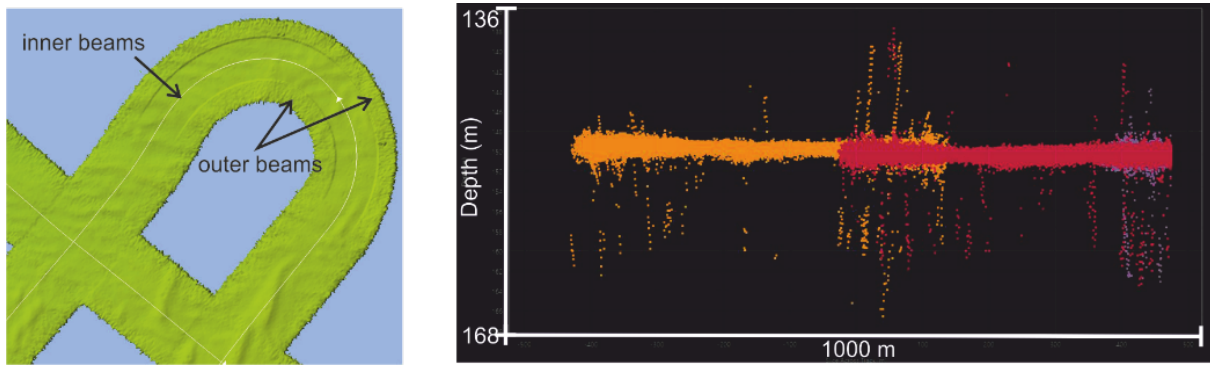


Fig. 5.1 Screenshots from Qimera showing the offset between outer and inner beams of the EM710 system in curves (left) and noise in EM710 data in areas with little topography (right).

consequence, both systems achieve a footprint of 0.5° across cruise direction and 1° in cruise direction. High-density equidistant and multiping modes were used and the Frequency Modulated chirp transmit pulse was selected throughout cruise SO277 for both systems.

Positioning is implemented onboard RV Sonne with conventional GPS/GLONASS plus differential GPS (DGPS) by using either DGPS satellites or DGPS land stations resulting in quasi-permanent DGPS positioning of the vessel. The operator station with the Seafloor Information System (SIS) acquisition software receives these signals. Ship motion and heading are compensated within the Seapath and SIS by using a Kongsberg MRU 5+ motion sensor.

Kongsberg EM710

The high-resolution shallow water multibeam echosounder transmits signals in the 70-100 kHz range. The system generates 256 beams providing 400 soundings. In multiping mode a maximum of 800 soundings per ping can be generated. The transmit fan is divided into three sectors to maximize range capability, but also to suppress interference from multiples of strong bottom echoes. The sectors are transmitted sequentially within each ping, and use distinct frequencies or waveforms. The maximum opening angle is 140° . In the working area off Malta the maximum ping frequency was reduced to 2 Hz to avoid persistent freezing of the SIS software. During SO277 the EM710 generally delivered high-quality data between 20 m to approximately 1400 m water depth and worked reliably. In turns, even in minor curves, a clear discrepancy in the quality between inner and outer beams became visible (Fig. 5.1). In areas of little topography the system produced a comparatively high number of erroneous soundings (Fig. 5.1).

Kongsberg EM122

The 12 kHz deep water multibeam echosounder generates 288 beams, resulting in 432 soundings per swath. In multi-ping mode, up to 864 soundings can be generated. The maximum opening angle is 150° and was chosen according to the needs of individual surveys. The EM 122 transducers are modular linear arrays in a Mills cross configuration. Beam inclination was set to automatic. The system provided high-quality data in the deep-water working areas off Sicily and worked without the need of user intervention.

Sound velocity probes

Beamforming requires sound speed data at the transducer head, which is available from a Valeport MODUS SVS sound velocity probe. The probe is located in centre of the vessel below the keel, and hence in the direct vicinity of the transducers. This signal goes directly into the SIS operator station. On 10 September 2020 the probe was removed because the adapter plate was needed for other operations. For the rest of the cruise the AML Oceanographic MicroX SV sound velocity sensor, which is part of the thermosalinograph (Self-cleaning Monitoring Box, SMB), provided the sound speed data for the SIS.

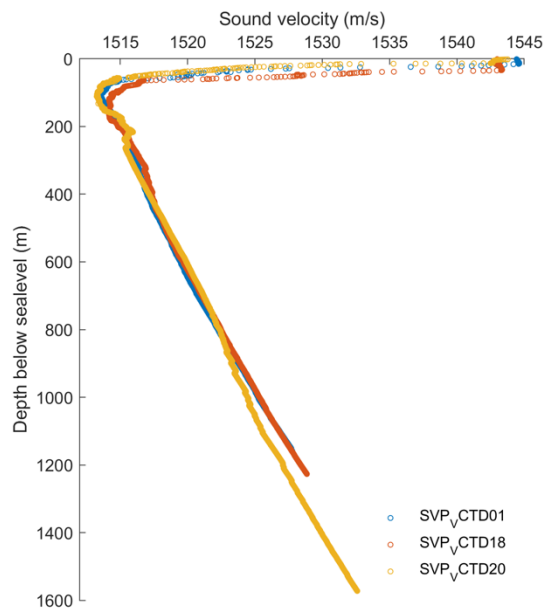


Fig. 3.2 Sound velocity profiles off Sicily in the Etna (blue, red) and Stromboli (orange) areas calculated from CTD data.

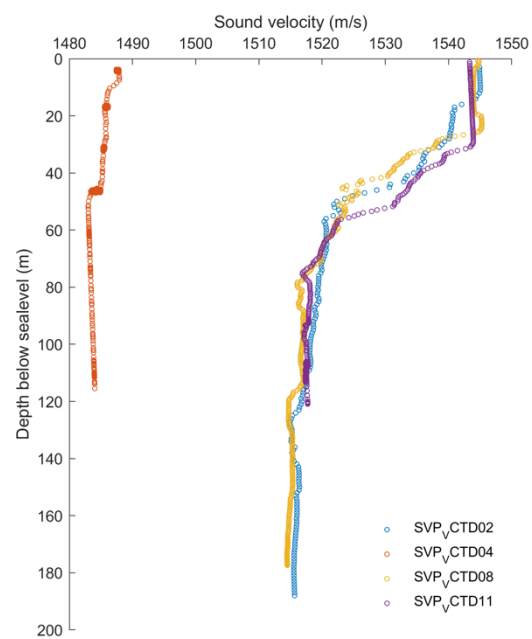


Fig. 5.3 Sound velocity profiles off Malta from CTD data.

Vertical sound velocity profiles were calculated from Video-CTD measurements following Wilson (1960). The sound velocity profile was updated each time a Video-CTD had been deployed. Because of deep water the sound velocity profiles off Sicily show little variability (Fig. 5.2). On the other hand, large variations in sound velocity were observed in the working area off Malta (Fig. 6). These variations are most likely combined effects of water column mixing by waves, diurnal variations, and internal currents owing to the shallow water environment.

5.1.1.2 Post processing

For multibeam post-processing and visualisation we used the software Qimera developed by QPS hydrographic and marine software solutions (<http://www.qps.nl/display/main/home>). When loading data from Kongsberg systems into Qimera, the software checks the detection class show flag to determine if soundings are accepted or rejected. Class 8 will always be rejected by default, as recommended by the manufacturer. Qimera then launches any required processing and applies

a weak filter to eliminate outliers to all loaded data. The soundings were then cleaned manually for further elimination of erroneous soundings. The grid calculated by Qimera and reflecting any edits

To visualize and analyze backscatter data from multibeam echosounders the cleaned soundings were exported to the *.gsf format. These were loaded into the FMGeocoderToolbox software, where radiometric corrections, filtering, an angle-varying gain and anti-aliasing filters are applied to the backscatter data before outputting a georeferenced mosaic.

The software FMMidwater reads, converts, and displays water column data. For fast screening of large data sets we converted the data using a data point reduction factor of 16 or 32 and visually inspected the lines in the stack view. Lines with clear water column anomalies were converted at higher resolution and analysed in detail.

5.1.1.3 Preliminary results

Etna

We conducted one dedicated multibeam survey and additionally recorded during transits between stations as well as on the transit to Malta using the EM122 system in water depths of 1000-2300 m and delivered a grid spacing of 30 m (Fig. 5.3). The first survey with EM710 and EM122 in 600-1200 m water depth covered Catania Canyon and the lineament north of it. The survey's target was to maximise horizontal resolution. Hence, the opening angle of both systems was 90° and the

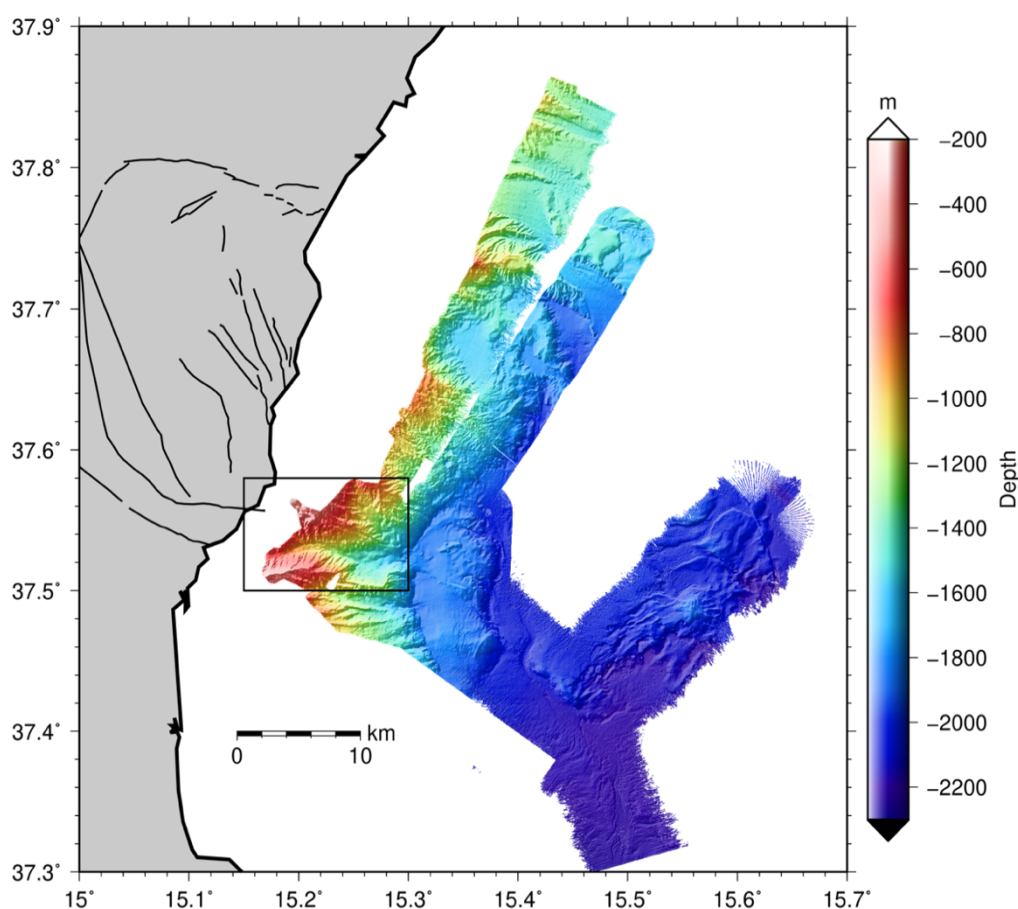


Fig. 5.4 Bathymetric map of the Catania Canyon and the lineament north of it.

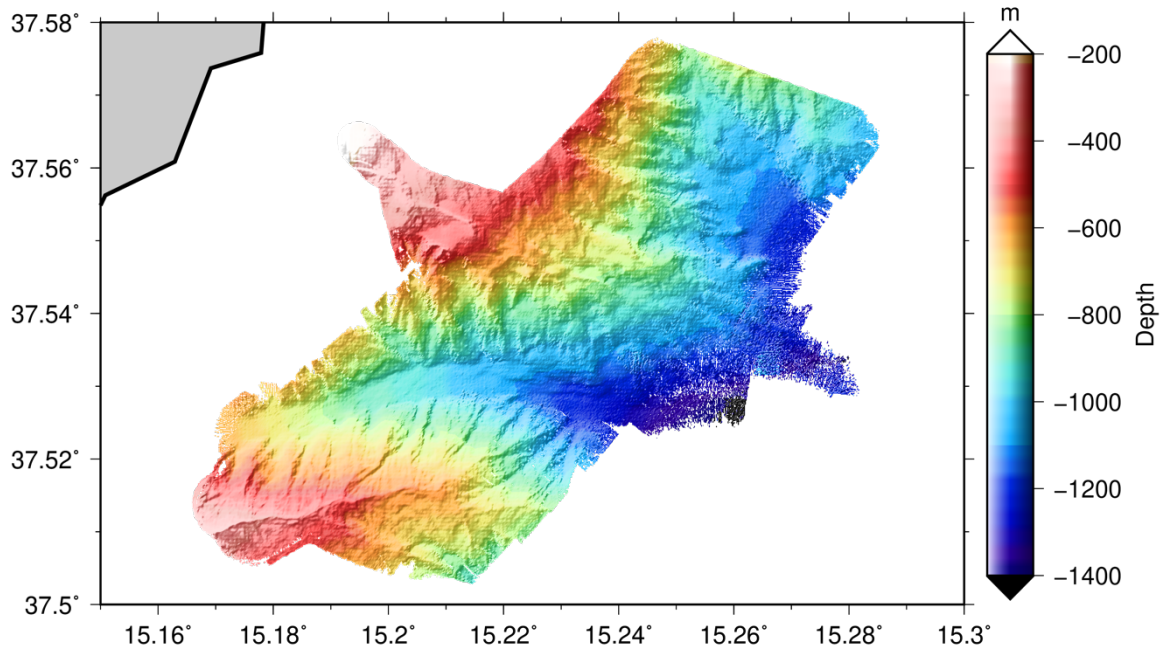


Fig. 5.5 Detailed bathymetric map of the selected area in the previous figure.

survey was designed to ensure a swath overlap of neighbouring profiles of at least 75%. After post-processing the data was gridded at 10 m spacing (Fig. 5.5).

The data collected during SO277 provides an improved seafloor map with respect to previous bathymetric data, in particular along the North Alfeo Fault, Catania Canyon, and the lineament north of Catania Canyon (Fig. 5.5). The fault trace comes out clearly and smaller-scale features, such as previously unrecognised en-echelon structures or landslide scars show up. The water column data does not yield evidence for any anomalies.

Stromboli

To map Stromboli's very steep northwestern flank the vessel followed slope-parallel profile lines from 200 m to 3000 m water depth. The opening angles of both the EM122 and EM710 systems were set to maximum on the shallow side and to 45° on the deep side and changed with each turn. The achieved grid spacing is 30 m for the entire survey with the EM122 system (Fig. 5.6) and 20 m for the depth range 200 – 1500 m with the EM710 system (Fig. 5.7).

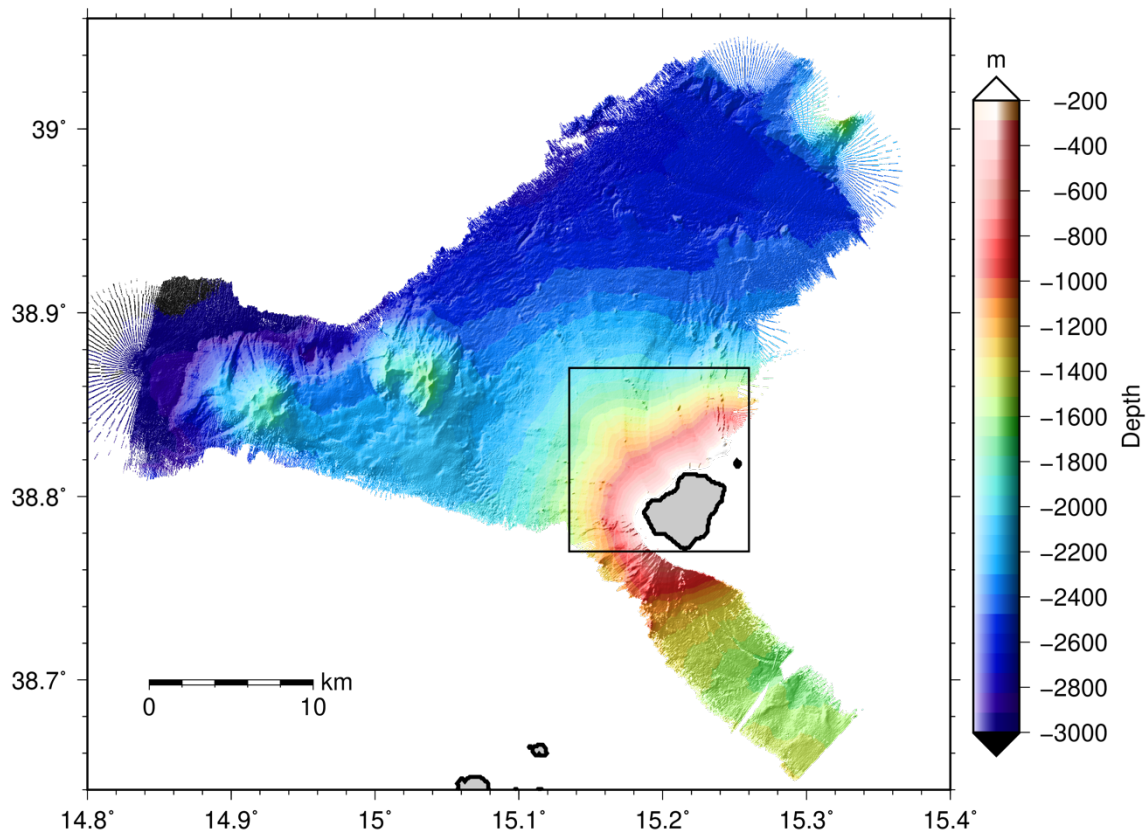


Fig. 5.6 Shaded relief map of the seafloor around Stromboli and parts of Stromboli channel from the EM122 system (30 m grid spacing).

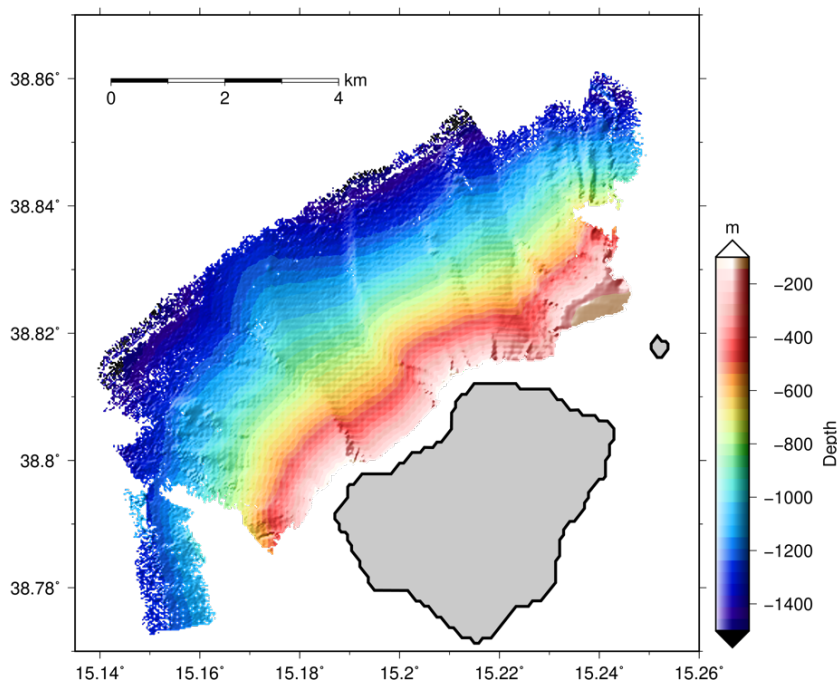


Fig. 5.7 Shaded relief map of the proximal area of Stromboli's northwestern flank recorded with the EM710 system (20 m grid spacing).

Malta

The area north-east of the Maltese Islands was the main target area of cruise SO277. This area has been mapped partly in great detail due to multiple overlaps of adjacent tracks and several dedicated multibeam surveys (Table 3). The water depth in the area ranged from 20 to 200 m, with an exception in the northwestern survey area, where water depths reach almost 500 m (Fig. 5.9). Overall grid spacing is 6 m with better resolution in areas of dedicated surveys.

Table 5.1 Multibeam surveys of SO277

	Date	File numbers	Remarks
Survey NE Malta	27/28 Aug 2020	52-70	
2D seismic profiling		71-385	
P-cable survey		385-532	
CSEM reconnaissance	10 Sep 2020	535-553	
CSEM reconnaissance	12 Sep 2020	560-582	
CSEM reconnaissance	14 Sep 2020	583-595	
CSEM reconnaissance	15 Sep 2020	597-630	Windy, 3-4 m swell
Survey SE Malta	16/17 Sep 2020	643-672	System failure multiple times

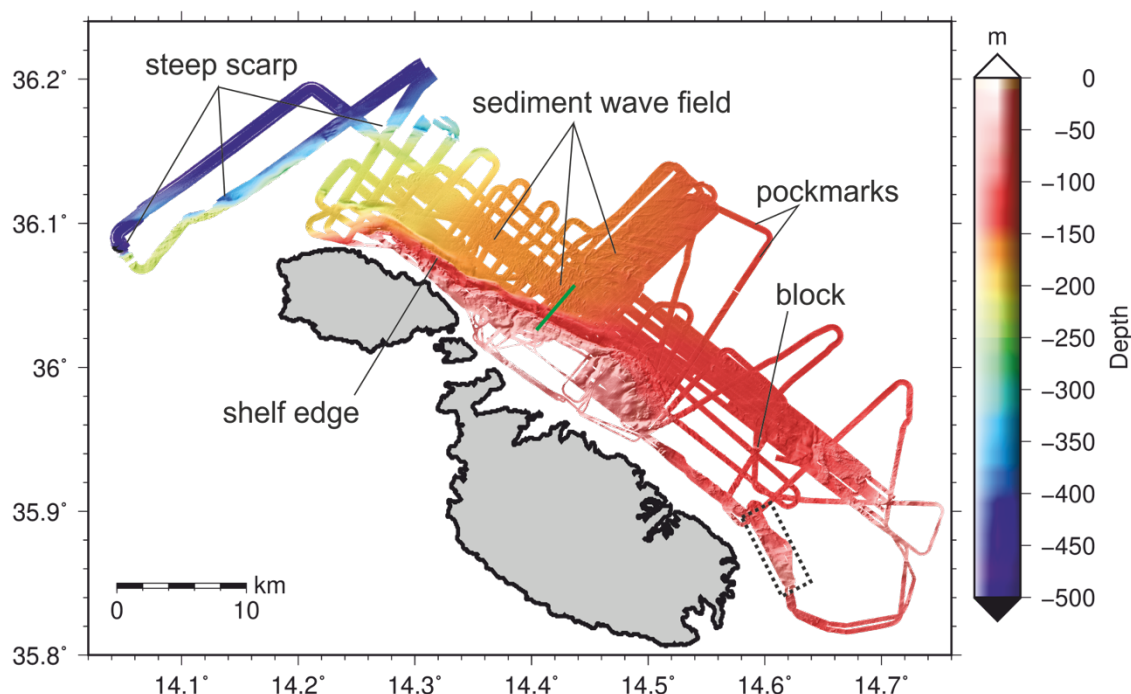


Fig. 5.9 Shaded relief map of the entire bathymetric data set collected with the EM710 system in the working area northeast of Malta during SO277. The green line shows the location of the downslope profile in Fig. 5.10. The dashed box shows the location of the backscatter image in Fig. 5.12.

The seafloor off Malta can be broadly distinguished into a shallow shelf reaching down to about 75 m water depth and a smooth sedimentary plain that is predominantly low in topography and reaches water depth of about 150 m (Fig. 5.10). The transition from the shelf to the sedimentary plain occurs in two ‘steps’. A presumably bottom-current induced sedimentary body lies at the foot of the shelf edge.

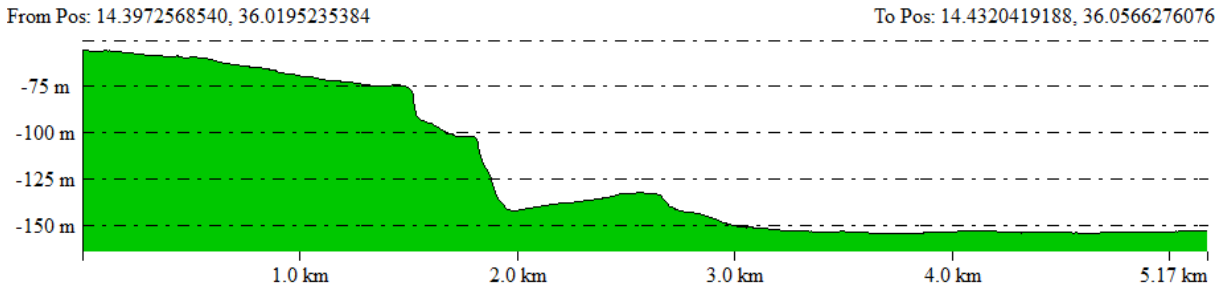


Fig. 5.10 Typical transect crossing the shelf to the sedimentary basin in the northeast of the Maltese Islands (for location see green line in Fig. 5.9).

The seafloor seawards of the shelf edge reveals tectonic, sedimentary, bottom current induced, and anthropogenic seafloor patterns. In the northwest a near-vertical, up to 250 m high scarp is prominent. A field of sediment waves of different shapes and sizes stretches out east of Comino. The new bathymetry also shows circular depressions in an area where pockmarks have previously been identified in side scan sonar data. We also note a singular block surrounded by smooth seafloor topography.

The water column images were analysed for anomalies in the water column that are caused by gas rising up from the seafloor. Gas pathways might also provide pathways for groundwater. The water column images showed several anomalies of varying shapes, sizes, and abundances (Fig. 5.11). Fish bladders have similar sizes as gas bubbles and therefore cause similar water column anomalies, making them hard to distinguish.

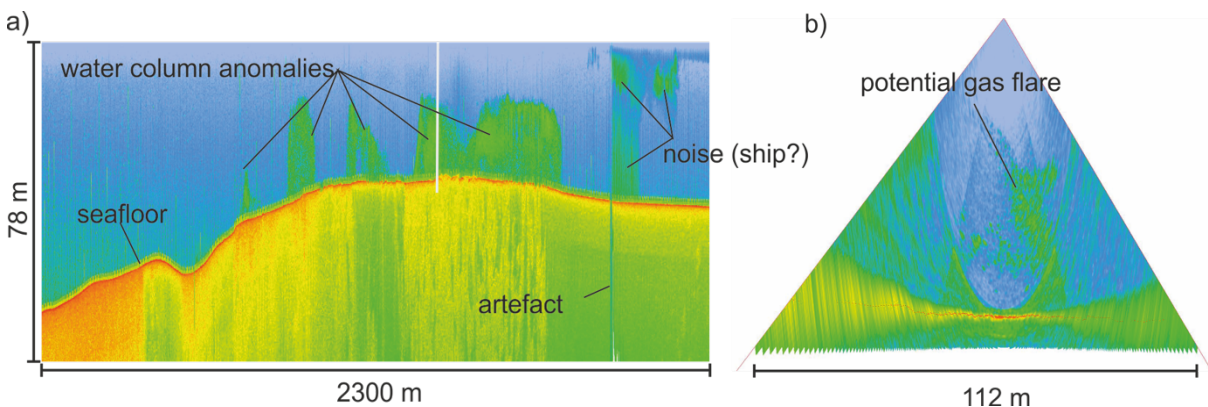


Fig. 5.11 Screenshots from the FMMidwater software showing examples of water column anomalies in the southeast of Comino. a) Stacked fans along the ship's track and b) water column image of one ping. The white line in a) indicates the location of the ping.

The backscatter data (Fig. 5.12) shows a clear difference in intensities between the shelf and the sedimentary basin. The shelf is predominantly made of hard grounds with high backscatter intensity. This is in contrast to the sedimentary basin with predominantly soft seafloor sediments.

In the area to the southeast of Malta the backscatter image shows circular structures of notably higher backscatter intensity than the surrounding seafloor. The circles have diameters of about 100 m and show up as very minor positive relief in the bathymetry data. In this area the water column images suggest the presence of multiple flares.

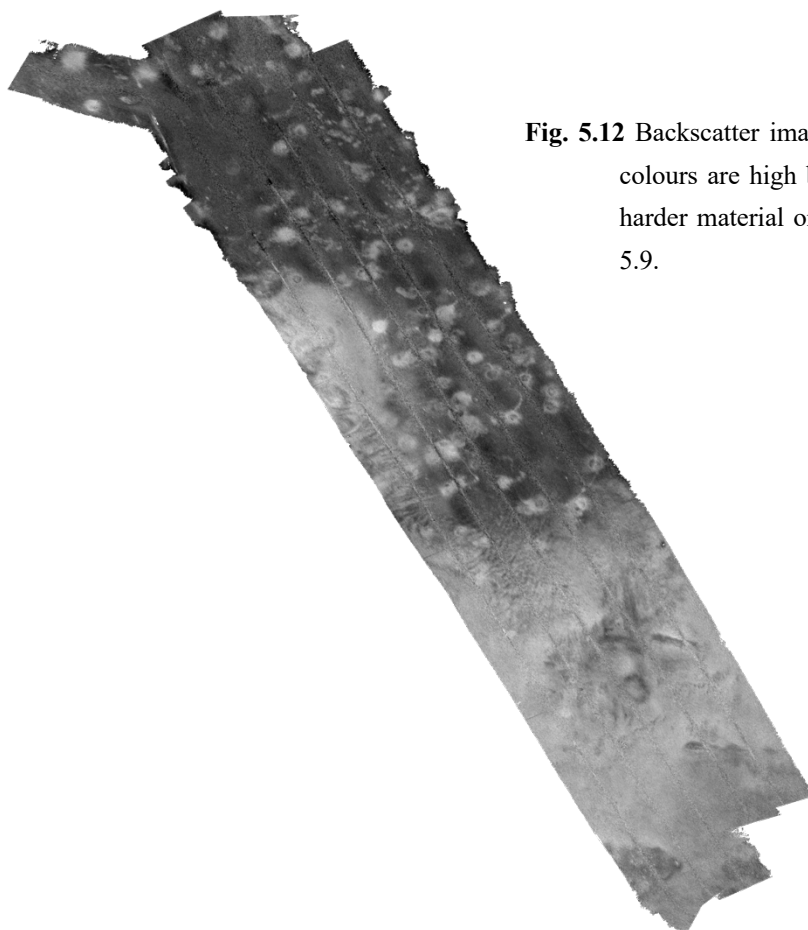


Fig. 5.12 Backscatter image of the shelf east of Malta. Light colours are high backscatter amplitudes, representing harder material on the seafloor. For location see Fig. 5.9.

5.1.2 Parasound

5.1.2.1 Method

RV Sonne is equipped with an Atlas Parasound DS P-70 parametric deep-sea sediment echosounder for full ocean depth. The system is a narrow beam sediment echosounder (opening angle $4.5^\circ \times 5.0^\circ$) that utilises the so-called parametric effect to generate a very low frequency secondary signal by emitting two primary signals of higher frequencies. The Parasound system transmits two independent pulse-modulated harmonic signals via the same transducer array. To generate and utilise the parameteric effect these signals must be generated with extremely high amplitudes. At such signal levels the seawater does not only serve as a propagation medium for the original signals but also generates additional new signal components at different frequencies. During SO277 the primary frequencies were 18 kHz and 22 kHz. The resulting secondary frequencies are 4 kHz and 40 kHz. For sediment penetration in particular the secondary low frequency is of interest.

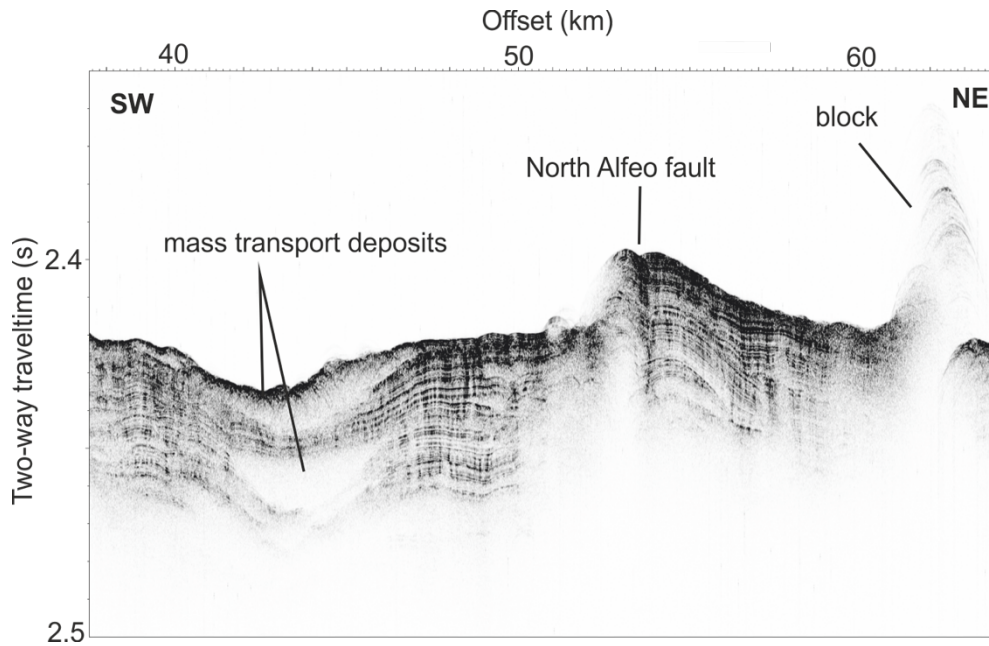


Fig. 5.13 Parasound profile cutting the North Alfeo fault at an almost vertical angle.

5.1.2.2 Parameter settings

In the deep-water settings at Etna and Stromboli as well as during the transit from Etna to Malta the Parasound system transmitted in a quasi-equidistant transmission sequence with a time interval of 1200 ms. In the working area off Malta the system emitted a rectangular frequency modulated single pulse. The receiver band width for both high frequencies was 66 % and for both low frequencies 33% of the output sample rate (12.2 kHz). The sound velocity was manually set to 1500 m/s.

5.1.2.3 Processing

All raw data were stored in the ASD data format (Atlas Hydrographic), which contains the data of the full water column of each ping for all four frequencies as well as the full set of system parameters. Additionally, a 200 m-long reception window centred on the seafloor of the primary high and the secondary low frequencies was recorded in the compressed PS3 data format after resampling the signal back at 12.1 kHz. This format is in wide usage in the PARASOUND user community and the limited reception window provides a detailed view of subbottom structures. All data were converted to SEG-Y format during the cruise using the software package ps32sgy version 15.9 (Hanno Keil, Uni Bremen). The software re-fits the different time windows, allows generation of one SEG-Y file for longer time periods, frequency filtering (low cut 2 kHz, high cut 6 kHz, two iterations), and the subtraction of mean. In this format the seismic interpretation software IHS Kingdom can easily read and display the parasound data.

5.1.2.4 Preliminary results

During SO277 we collected approximately 900 km of Parasound profiles. Technical problems did not occur. Imaging the sub-seafloor in volcanic areas was difficult due to steep slopes and hard sediments. Away from the continental slope of eastern Sicily penetration improved greatly. Several profiles cross the North Alfeo fault and document an active tectonic structure (Fig. 5.13).

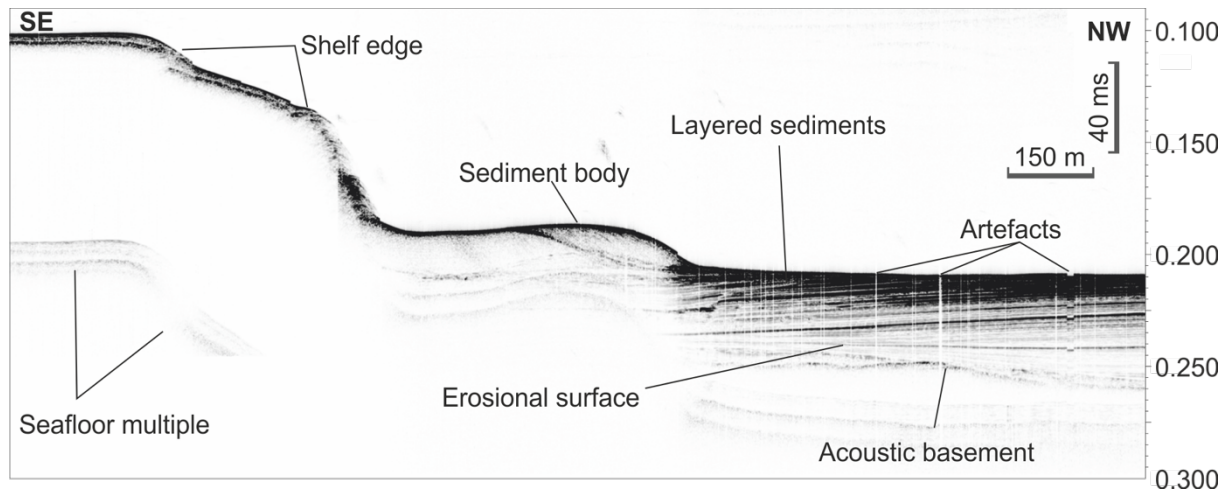


Fig. 5.14 Parasound profile inside the P-cable cube crossing the shelf, the sediment body adjacent to the shelf edge, and the sedimentary basin. Note that the transect cuts the shelf edge at a small angle.

In the Malta survey area the Parasound was mainly used for reconnaissance surveys for gravity coring and CSEM profiles. At the shelf almost all energy was reflected by the hard ground (Fig. 5.13). Penetration was slightly increased for channels cutting through the shelf and improved significantly seawards of the shelf edge.

Carbonates outcropping on the Maltese islands form the acoustic basement in the shelf area. A thin layer of sediments (<3 m) appears to cover the hard carbonates. Seawards of the shelf edge the Parasound data image a body with faint internal reflectors on top of the acoustic basement. We interpret this body as having formed by bottom current activity. Seawards of the sediment body a sequence of stratified sediments cover the acoustic basement. The sediment package is 0.05 s thick next to the drift body and thickens in the seaward direction. The sediment layers change their dip direction, with the two packages being separated by an erosional surface (Fig. 5.14).

The Parasound profiles also provide evidence for fluid escape structures in the sediments seawards of the shelf edge. Fig. 5.15 shows one example of a circular seafloor depression inside the P-Cable area. However, a flare was visible neither in the secondary low nor in the primary high frequencies. A later visit with the Video CTD did not return any active venting neither.

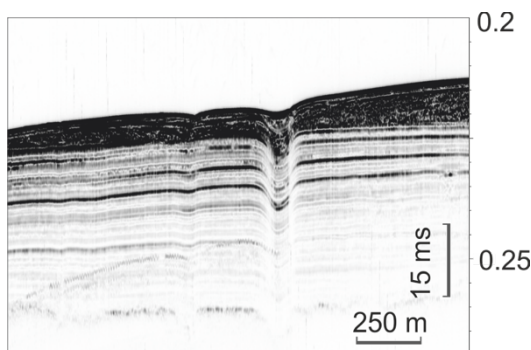


Fig. 5.15 Parasound profile across a circular seafloor depression.

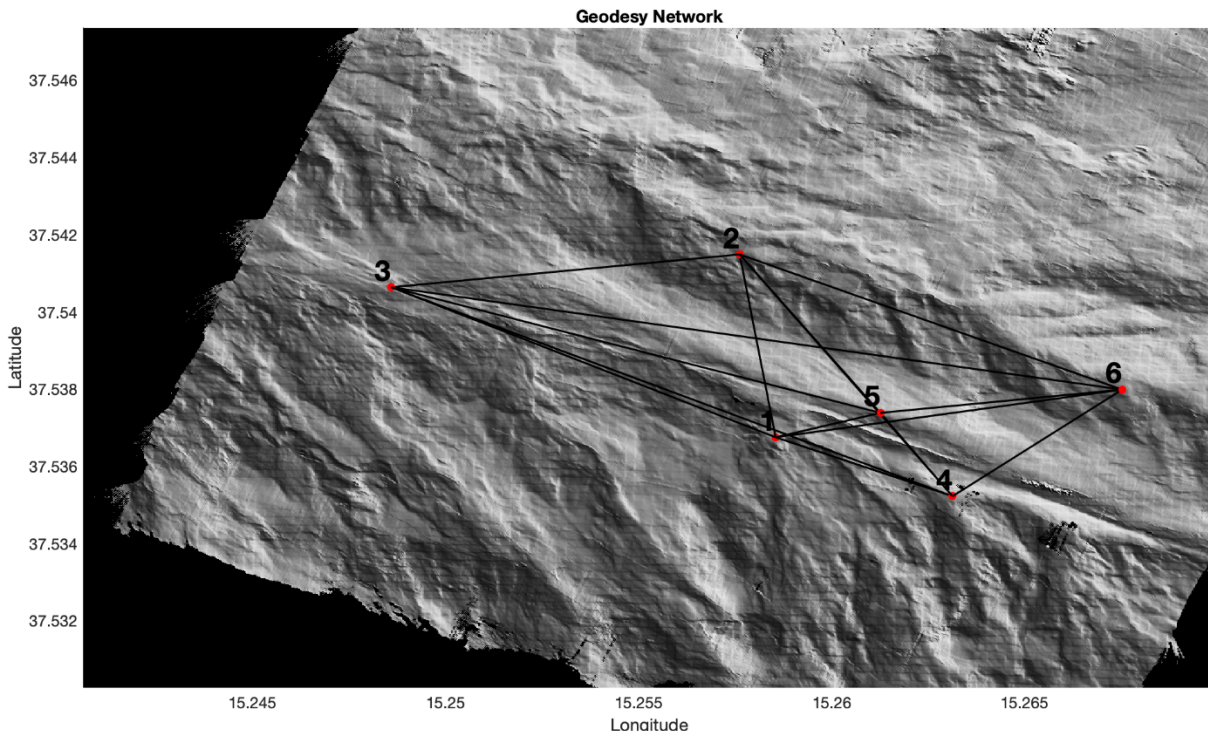


Fig. 5.16 The final network configuration consisting of six seafloor geodetic stations.

5.1.3 Seafloor geodesy

5.1.3.1 Method

Established satellite-based geodetic tools are not adaptable for use in the marine environment due to the opacity of seawater to electromagnetic waves. Underwater, distances can be estimated using sound speed of water and travel time measurements between transponders on the seafloor. Seafloor acoustic ranging methods provide relative positioning by using precision acoustic transponders (Autonomous Monitoring Transponder, AMT) that include: high-precision pressure sensors to monitor possible vertical movements as well as the tide effect, dual-axis inclinometers in order to measure instrument inclination as well as any change in the seafloor, high-resolution temperature sensors and sound velocity sensors to correct sound speed variations. Repeated interrogations over months to years allow the determination of displacements and, hence, deformation of the seafloor inside the network for extended periods, depending on battery capacity. This ‘direct-path ranging’ method provides relative deformation measurement since the absolute transponder positions are not determined (Petersen et al. 2019).

5.1.3.2 Network configuration

The AMTs are located at the outcrop of an active strike slip fault at the seafloor. Locations for individual transponders were chosen based on high resolution bathymetric map with a 2 m grid spacing that was collected in January 2020 with Autonomous Underwater Vehicle ‘ABYSS’ (Fig. 5.16). The network design ensures that at least two AMTs sit at each side of the fault and are in acoustic sight of each other.

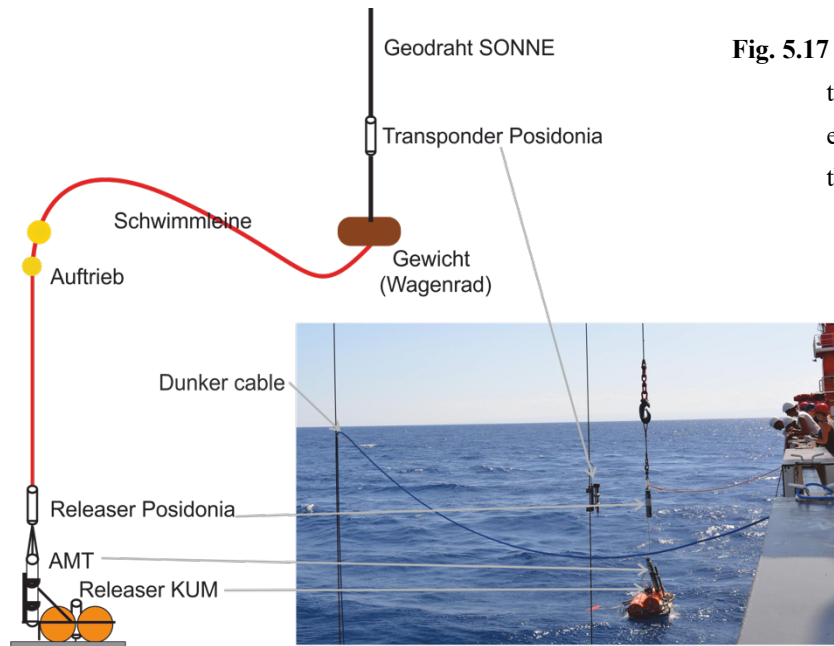


Fig. 5.17 Sketch of the deployment procedure of the seafloor geodetic stations after Kopp et al. 2017 (not to scale) and picture of the actual deployment during SO277.

5.1.3.3 Instrumentation

The six AMTs are part of GEOMAR's GeoSEA array and are of type 3505-6315 manufactured by Sonardyne International Ltd., UK. The transponders communicate with 8 ms phase-codes pulses and an 8 kHz bandwidth with a centered frequency of 18 kHz. For horizontal direct path measurements, the system utilizes acoustic ranging techniques with a ranging precision better than 15 mm (Sensor specifications for Sonardyne AMT Type 8305-6315) and long-term stability over 3 km distances. Vertical motion is obtained from pressure gauges (Sensor specifications: PreSens pressure sensor, precision: $\pm 0.0001\%$). Integrated inclinometers to monitor station settlement have an accuracy of $\pm 1^\circ$. Data are acquired and recorded autonomously subsea without system or human intervention at sample rates of 120 minutes for all baselines, temperature, and pressure. Battery checks, inclination, and sound velocity are acquired at every second to sixth cycle only in order to increase the battery lifetime. Lithium battery packs provide sufficient power for the estimated 3 years observation period. The data is time stamped and logged internally for recovery via integrated high-speed acoustic telemetry, allowing measurements to be made over a period of more than 3 years without requiring a surface vessel to be present to command the process. Each AMT is fitted with a 1 GB SD memory card that can store up to 2 Mio 512 byte pages in total. These data can then be recovered via the integrated high-speed acoustic telemetry link without recovering the AMTs by using a HPT dunker modem lowered to ~ 30 m water depth from the vessel. The HPT transceiver communicates with the AMT at 9000 bits/sec equivalent to 100 pages/minute.

5.1.3.4 Deployment

The transponders were pre-configured with the chosen log regime prior to deployment using a laptop with a serial test cable set up. Once programmed, the transponders are mounted on anchored buoyancy bodies equipped with an acoustic release for recovery (Fig. 5.17). The whole instrument is then lowered all the way to the seabed with the deep-sea cable of RV SONNE following a patented deployment procedure (Kopp et al. 2017). During deployment, a number of quality assessment checks are run from the vessel with the dunker modem to ensure that the unit is

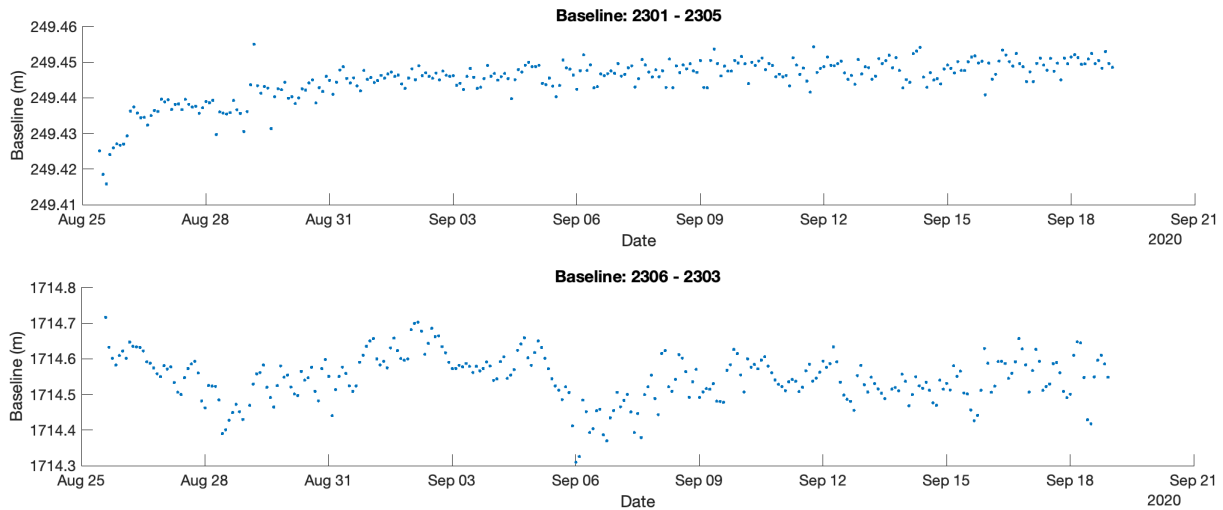


Fig. 5.18 Time series of a) the shortest and b) the longest baseline within the seafloor geodetic network. Note the different y-axes scales.

operating successfully and that line-of-sight is given with already deployed AMTs. Making use of the vessel's own IXBLUE (IXSEA) Posidonia system we successfully deployed all six AMTs with meter-precision resulting in 15 baselines with length between 250 and 1700 m. The seafloor geodetic network will remain in place for up to three years.

5.1.3.5 Preliminary results

After 24 working days off Malta, RV Sonne returned to the network in order to check the stations and download the first data set. The dunker modem successfully established acoustic links to all AMTs and retrieved data from five AMTs. One AMT stopped logging due to a memory card failure. Because it has continuously answered to the interrogations of all other station, and consequently the baselines are still established, no further action was taken. Following some basic processing, which includes the conversion of time-of-flight to distances we found that all baselines are stable and do not show any evidence for seafloor deformation. Some baselines show a period of settling or adjustment (e.g. baseline 2301-2303, Fig. 5.18a) expressed in approximately 0.02 m of relative distance change. Periodic variations appear to affect the longer baselines in particular (e.g. 2306-2303, Fig. 5.18b).

5.2 Electromagnetic surveying

(M. Jegen¹, Z. Faghih¹, K. Reeck¹, G. Franz¹, C. Barnscheidt¹, M. Wollatz-Vogt¹, J. Liebsch¹)

¹GEOMAR

5.2.1 Introduction

Marine controlled source electromagnetic (CSEM) is a geophysical exploration method used to derive the electrical properties, i.e. resistivity, of the seafloor. Electrical conduction in seafloor sediments occurs through ions in pore fluids, and therefore the conductivity (1/resistivity) of seafloor sediments depends mainly on the sediment porosity, pore space connectivity and the

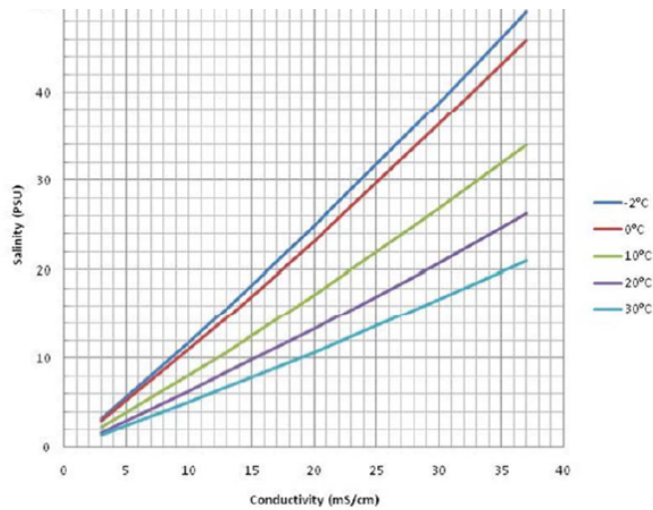


Fig. 5.19 Pore fluid conductivity for different salinity values and temperatures.

conductivity (ion content) of the pore fluid. An important source for ions is the amount of salt in the pore fluid, therefore the conductivity of the pore fluid depends strongly on its salinity. Fig. 5.19 shows the relationship between salinity and pore fluid conductivity for different temperature values. The relationship between the bulk resistivity of sediment, porosity and pore fluid resistivity may be described by the experimentally derived Archie's Law, which holds for most sediments with little clay content:

$$\rho_{\text{bulk}} = a \phi^{-m} S^{-n} \rho_{\text{fluid}}$$

Where ρ_{bulk} and ρ_{fluid} are the resistivities of the seafloor and pore fluid respectively, F is the porosity, S denotes the pore fluid saturation, and a , m and n are constants, which range between 0.5-1.5, 1.8-2.4 and ~ 2 respectively in marine sediments. Rocks containing large amounts of clay have a resistivity lower than predicted by Archie's law due to conductive pathways along the surface of negatively charged clay particles.

Typical seawater resistivity varies between 0.3 to 0.5 Ωm depending on seawater salinity and shallow marine sediments typical have a bulk resistivity of around 1 Ωm . Fresh water resistivity ranges between 1 and 10 Ωm , thus the bulk resistivity increases by a factor of 3 to 30 for fresh water saturated sediments.

Bulk electrical resistivity of marine sediments can be derived by a variety of methods, of which three (Magnetotellurics, CSEM and MMR) were used during OMAX. The difference between the methods arises from the geometry and frequency content of the electromagnetic source wave used and the geometry of the receiver. In magnetotellurics natural varying geomagnetic fields caused by currents in the ionosphere and worldwide lightning activity, give rise to electromagnetic source field. Since high frequency variations are damped by the conductive ocean above the measurement plane, the resolution in the upper kilometre is limited. However, bottom times of a few days or more allow the derivation of low frequency impedance values which allow for a depth of penetration of about 5 to 10 km. A shallow and higher resolution image of seafloor resistivities may be derived by controlled source electromagnetic measurements, which encompasses the use

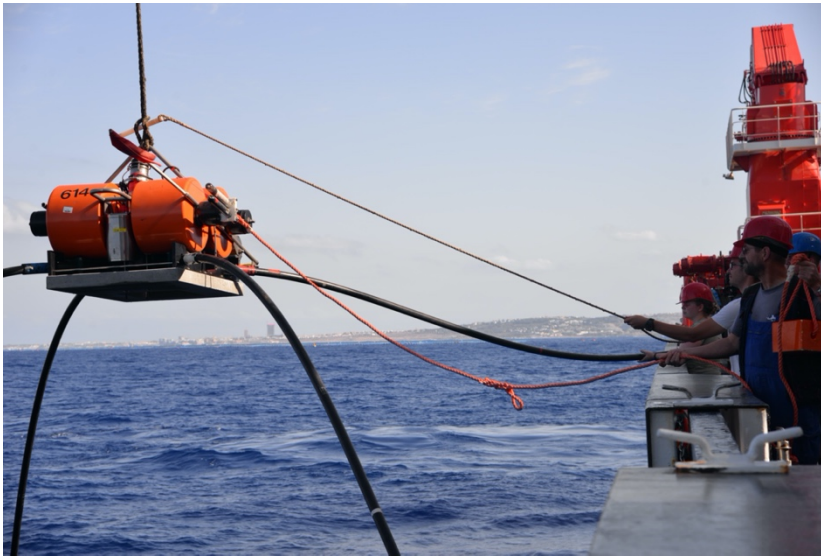


Fig. 5.20 GEOMAR OBEM lander.

of a transmitter to generate high frequency waves at the seafloor. Here we used a so called in line electric dipole-dipole systems, consisting of a horizontal electric dipole transmitter and inline dipole receivers. In addition to these more established methods, we also made a test measurement using the so called magnetometric resistance method (MMR). This method employs a vertical dipole as a source field and magnetic field receivers as receivers.

5.2.2 Magnetotellurics

5.2.2.1 Methodology

Natural varying magnetic field variations used in MT exhibit a plane wave characteristic. Frequency dependent electrical impedance measurements ($E(w)/B(w)$, where $E(w)$ denotes the electric and $B(w)$ the magnetic field as a function of frequency w) on the seafloor can in that case be shown to depend only on resistivity variations within the ocean and underlying seafloor. Impedance measurement can therefore be used to derive electrical resistivity models of the subsurface

In a homogenous half-space, the so-called skin depth d is a crude estimate of detection depth given by $d = 500 \sqrt{r T}$ in meters, where T is the period in seconds and r is the bulk resistivity. Due to the shallow water depth we expect a high frequency limit of approximately 1 Hz in the data. The lower frequency is bounded by the length of time that the instruments measure on the seafloor and will be on the order of 10^{-4} Hz. We therefore expect to be able to derive a background resistivity model of the area down to approximately 100 km with a highest resolution of the upper layers of about 1 km. The model at greater depth might be limited due to the proximity of the coast, which deviates the induced current in the ocean layer around the resistive island and might cause a bias in the model, unless considered explicitly with 3D modelling.

5.2.2.2 Instrumentation

The GEOMAR OBEM (Fig. 5.20) is mounted on an instrument carrier which consists of a titanium frame on which syntactic foam elements are mounted to give the frame a positive buoyancy. For deployment, a magnetically neutral concrete anchor slab is attached to the frame

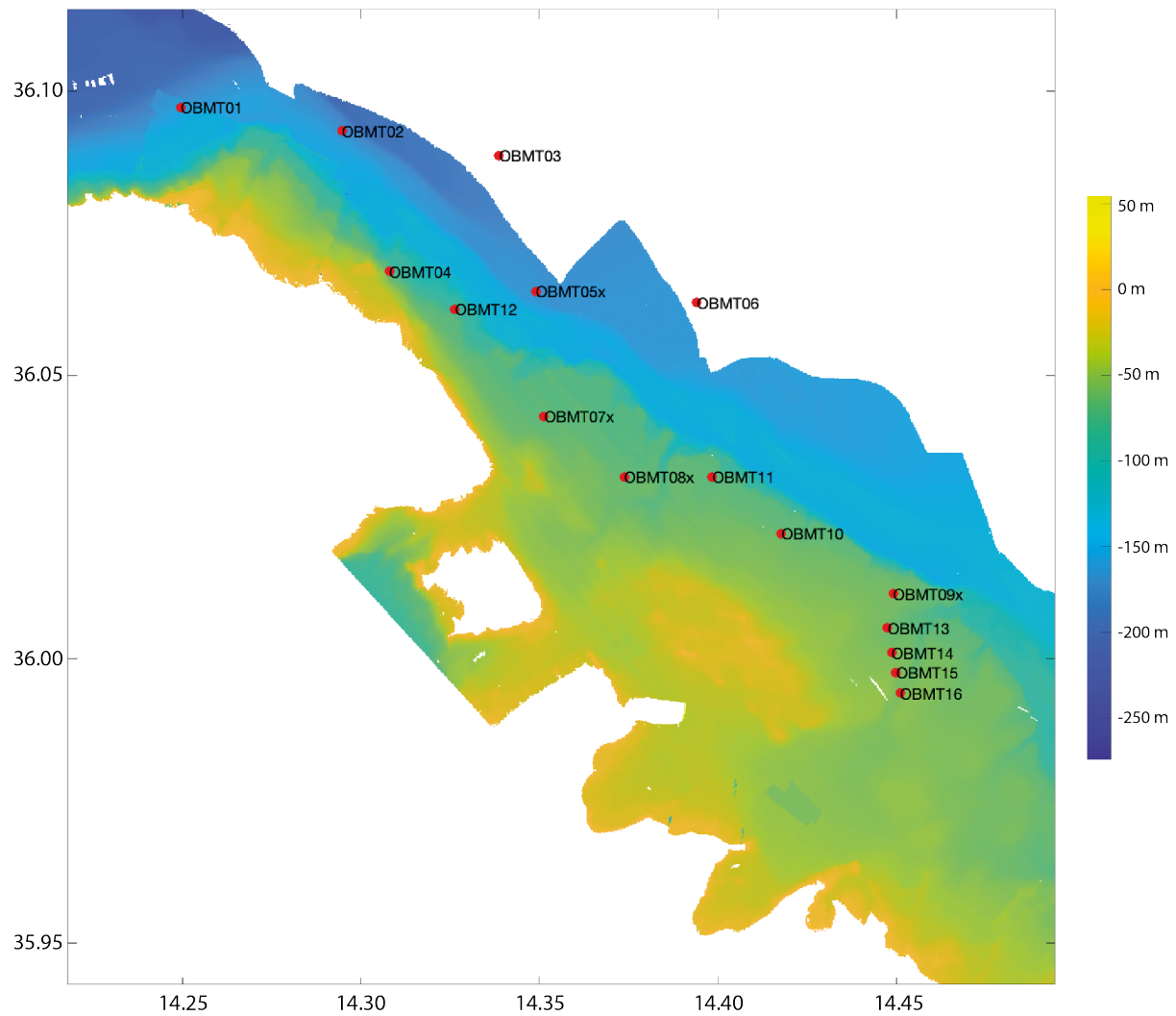


Fig. 5.21 OBEM stations occupied off Malta during SO277.

by a releaser. The frame is equipped with a titanium cylinder containing the battery pack and with a smaller titanium cylinder containing the 3-component fluxgate magnetometer with a precision of 10 pT/sqrt (Hz) and a data logger (both built by Magson GmbH, Berlin). The latter records magnetic and electric field variations, tilt variations, temperature and time. Timing of the measurement is kept via a Seascan temperature-controlled crystal which is synchronized to GPS prior to deployment (typical drift < 500 ms/year). The logged data is stored on a removable SMD card. Orthogonal horizontal electric field measurements are performed through voltage difference measurements between non-polarizable silver-silver chloride electrodes from Silvion, separated by plastic pipes mounted between frame and anchor to span a 10 m electric dipole.

The OBEMs can furthermore be used a CSEM receiver, sampling electric field variations at a frequency of 10 kHz. A mode switch between MT and CSEM is triggered by a signal to the release transponder. To facilitate recovery, the OBEMs are equipped with a strobe, radio, flag and a swimming line consisting of a rope with approximately 6 m lengths attached to a small flotation device.

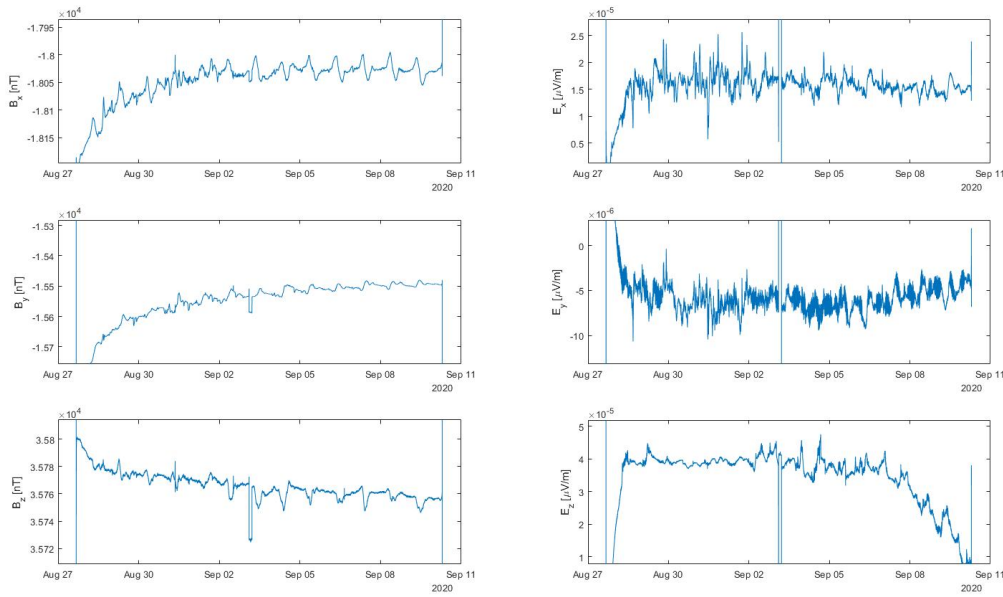


Fig. 5.22 Sample data set acquired by OBEM3, consisting of 3 component magnetic and electric field variations.

5.2.2.3 Data acquisition

Fig. 5.21 shows an overview of the stations that were occupied by OBEMs. Due to permitting restrictions, the OBEMs could only be deployed within the p-cable cube permission area. Nine OBEMs (OBEM1 to OBEM9) were deployed on August 27th, a further 3 (OBEM10 to OBEM12) on Sept. 2nd. OBEMs 5, 7, 8 and 9 were not equipped with a connection to the releaser and could therefore not be switched to CSEM modus during their deployment. For OBEM3 a test to measure a vertical electric field with the new three channel logger was performed by attaching a Silvion electrode to the swimming rope with the attached floatation device. The sampling frequency for OBEM 1 to 12 was chosen as 10 Hz.

On Sept. 10, OBEM 2,3,5 and 6 were recovered and redeployed as OBEM 13, 14, 15 and 16 onto the MMR profile (section 3) in order to record the MMR signal with a sampling frequency of 100 Hz. All stations were successfully recovered on Sept. 18th. Fig. 5.22 shows a sample raw data section for OBEM3, which also measured the vertical electric field. Clearly visible are a diurnal and semidiurnal signal, the expected correlation between electric and magnetic field variations as well as some spikes in all channels which we relate to the passing of RV Sonne over the instrument.

Table 5.2 Station list for the magnetotelluric experiments

Station-Number	System number	device ID	Longitude	Latitude	B fields	slow E-fields (MT)	fast E-fields (CSEM)	Comments
OBMT01	EM-07	59	14.249567	36.097133	good	good	-	
OBMT02	EM-09	50	14.294667	36.092950	good	good	-	05.-07.09.: Several peaks in total B-field, visible in all 3 components (e.g. 06.09. 01:25, also peak in E-field) 08.09. 16:30 – 18:45 CSEM mode
OBMT03	EM-01	45	14.338650	36.088667	good	good	-	
OBMT04	EM-08	53	14.308000	36.068250	good	good	-	09.09. 20:00 – 10.09. 04:00 strange peaks in total B-field (visible on all 3 components) → ship!

OBT05	EM-06	55	14.349050	36.064750	good	good	-	
OBT06	EM-02	62	14.394083	36.062783	good	Ex dead after switch to CSEM (02.09.)	-	02.09. 19:15-22:15 CSEM mode
OBT07	EM-03	47	14.351333	36.042767	Bz has drift of ~400 nT	good	-	03.-06.09. Peaks on B-fields → ship passing during P-cable survey 10.09. 14:30 16:30: strange peak on total B-field → ship passing by
OBT08	EM-04	58	14.373800	36.032100	Bz has drift of ~400 nT	good	-	03.-06.09. Peaks on B-fields → ship passing during P-cable survey
OBT09	EM-05	38	14.449167	36.011500	good	good	-	
OBT10	EM-12	40	14.417783	36.021517	good	good	-	
OBT11	EM-10	51	14.398000	36.031200	stopped after 4 days	stopped after 4 days	-	
OBT12	EM-11	41	14.326267	36.061333	good	good	-	03.09. 07:00-09:00 strong peak in total B-field (all 3 components + E-field) → ship!
OBT13	EM-02	62	14.447500	36.004500	good	good	good	16.09. 01:00 to 03:00 A.M. - visible signal from vertical dipole experiment
OBT14	EM-06	55	14.448900	36.001200	good	good	good	16.09. visible signal from vertical dipole experiment
OBT15	EM-01	45	14.449800	35.997600	good	good	good	15.09. 19:00-21:00 P.M. visible signal from vertical dipole experiment
OBT16	EM-09	50	14.451100	35.994100	good	good	good	15.09. 16:30-18:30 P.M. visible signal from vertical dipole experiment

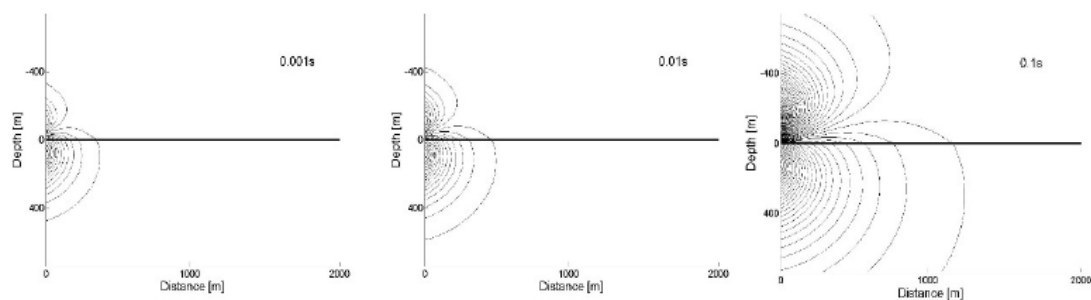


Fig. 5.23 Snapshots of the propagation of an electrical dipole field generated at the seafloor (black line) at 0.001, 0.01 and 1 sec after current switch on in transmitter dipole. The sea-layer and seafloor are assumed to be infinitely thick with a resistivity.

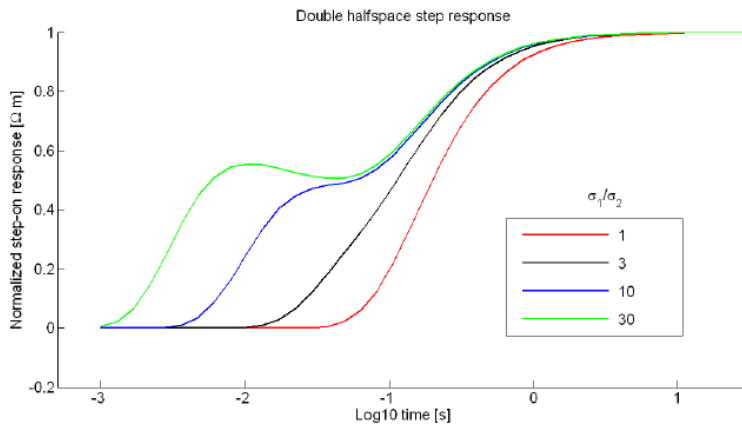


Fig. 5.24 Electric seafloor dipole-dipole response for a switch-on transmitter current wave form at 100 m transmitter-receiver offset. Responses are shown for different conductivity contrasts between a seafloor half space with σ_2 and an infinitely thick sea layer with conductivity of σ_1 (from R.N. Edwards).

5.2.3 Towed controlled source electromagnetic surveying

5.2.3.1 Methodology

In a CSEM experiment an electromagnetic wave is generated through a seafloor transmitter, which subsequently diffuses outward (Fig. 5.23). The wave's diffusion speed and amplitude damping are a function of seawater and seafloor resistivity. The diffusion speed increases with resistivity while amplitude damping decreases with increasing resistivity. Through monitoring the shape of the electromagnetic wave at different offsets, a resistivity model may be derived via inversion. The inversion is a statistical search process, which identifies resistivity models with responses that fit well with the measured responses. Short offset data and early time signals are most sensitive to shallow structures, while long offset data and late time signals contain information about the deeper structures (penetration depth is about 1/3 of offset).

Fig. 5.23 shows snap shots of the propagation of an electric dipole wave as created by the transmitter used in the experiment. The response as a function of time for a receiver 100 m away from the transmitter is shown in Fig. 5.24 for seawater/ subseafloor conductivity of (r_1/r_2) contrasts ranging between 1 and 30. The response changes significantly for different conductivity contrasts. For a high conductivity contrasts (e.g. low conductivity seafloor and a high conductivity sea layer) the early arrival of the seafloor wave can be easily distinguished from the later time arrival of the sub-surface layer wave. If there is not a strong contrast, the waves do not distinctly separate in time yet the transient is altered in amplitude.

Where CSEM measurements are performed in relatively shallow waters compared to the transmitter-receiver distance, the so-called airwave can have a big effect on the signal. For shallow oceans (where the ocean depth is in the same order as the transmitter-receiver offset) a fast or even the fastest path to the receiver may actually be through the sea layer into the very resistive air and back through the sea-layer to the seafloor receiver. This airwave may mask other arrivals of waves through seafloor resistors and thus makes a visual qualitative interpretation of the data more difficult. However, particularly for time domain EM data as used here, the airwave does not deteriorate the information content of the data.

5.2.3.2 Instrumentation

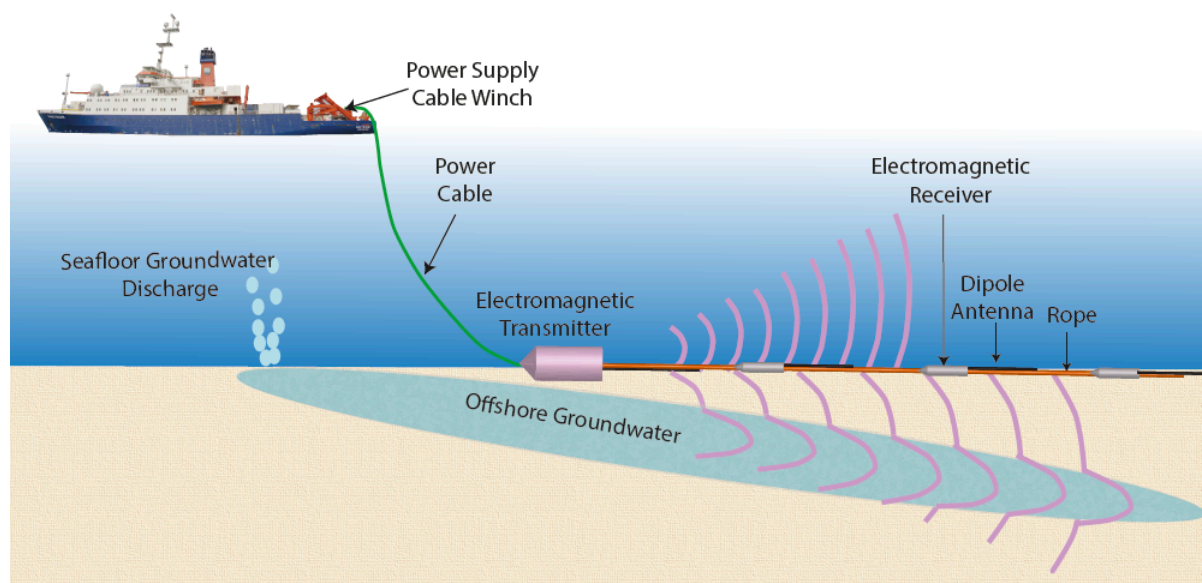


Fig. 5.25 Experimental set-up for the towed electric dipole-dipole system used in this experiment.

The electromagnetic data is acquired with a modular seafloor-towed CSEM Dipole-Dipole System. It consists of a 100 m-long electrical transmitting dipole and various electrical receiver units (Fig. 5.25). We use two different types of receiver dipoles: Three dipoles developed by the BGR (Hydra) and two receiver dipoles newly developed by GEOMAR (GEODIP). Transmitting dipole and receiving units are connected with ropes at offsets from 150 m to about 650 m. A stainless-steel tow-body termed “the pig” is attached to the front end of the seafloor array. It has the function of a weight to keep the array on the seafloor and serves as an instrument platform. It hosts the GEOMAR transmitter system that consists of three pressure cylinders containing the electronics and which is capable to transmit currents of up to 50A. The pig also contains a CTD sensor and an acoustic transponder for navigation purposes. A mobile winch with 700m of opto-electrical cable is used as an umbilical cord and to tow the array behind the ship.

Winch and block

The peak tension load of the winch is 16 tons (Fig. 5.26) (DT Marine Tow Winch Model 1020EHLWRS) and about 1.5 ton for the opto-electronical cable. For the cruise, the winch has been screwed onto the back deck at a distance of approximately 10 m from the stern. A block fitting the 22 mm cables was installed onto the A-frame of RV Sonne. In front of the winch, a smaller scale winch has been installed to facilitate the deployment and recovery of the receiver string.

Depressor (Pig)

The pig (Fig. 5.27) is a stainless-steel casing with a weight of 450 kg in air constituting the front end of the electric dipole-dipole seafloor array. The pig hosts the pressure vessels with GEOMAR transmitter electronics, a CTD sensor and an acoustic transponder provided by RV Sonne. The Pig was deployed through the A-frame at the stern of the ship. Usual readings on the tensiometer on

the DT winch were 300 to 400 kg at deployment with increasing tension readings during lowering to the seafloor (about 500 to 600 kg at 150 m water depth). At touch down, the readings decrease to about 100 kg. While towing on the seafloor, typical readings are about 200 kg to 300 kg.



Fig. 5.26 Left: Transmitter winch (blue with green cable) with opto-electrical cable and auxiliary receiver winch (red) for receiver deployment and recovery. Right: Block on A-frame.

The GEOMAR transmitter has been developed in-house and consists of an H-Bridge, three DC-DC converters and a data logger/controller with modem. Power to the transmitter is supplied by rechargeable lead gel buffer batteries, which are recharged during transmission s. The transmitter supplies up to 50 A current in a full or half duty cycle through copper current electrodes. The transmitter is linked to the ship by the DT 22mm electro-optical winch cable, which serves as a power lead to the transmitter and also as a modem line to communicate real-time with the transmitter. The transmitter is synched to a very stable, chip-scale atomic clock.

The distance of the copper current electrodes is for this experiment chosen to be 100, the period of the duty cycle was set to 8 seconds, and the current set to 20A. For safety reasons, the transmitter is switched on after it has been launched, usually at a water depth of approx. 20 m, and is switched off before it reaches the water surface at recovery.



Fig. 5.27 Stainless steel depressor (pig) containing GEOMAR transmitter (3 pressure housings with 1. lead batteries, 2. H-bridges and 3. electronics. CTD sensor is mounted within pig at the back end on one of the railings, transponder on white POM holder above.

Dipole receivers

Fig. 5.28 From left to right: GEOMAR Magson CSEM logger, GEOMAR logger housing with electrodes and dipole cable, BGR logger frame and BGR logger without housing.

The BGR-HYDRA (Fig. 5.26) receivers are battery-powered low-noise data loggers recording the receiver dipole voltages with 22-bit ADC at a sampling rate of 10 kHz. The receiver electronic has been developed and built by MAGSON GmbH Berlin. A precise time signal is provided by chip-scale atomic clocks, which is synchronized to GPS time prior to each deployment. The loggers are housed in titanium/POM frames which protect the pressure vessel of the data logger. The length of the attached receiver dipole is 25 to 30 m and is equipped with three electrodes. The outer electrodes consist of Silvion electrodes, whereas the central grounding dipole is a small steel rod. The electrodes and cables are attached to a rope, and the cables are collected into a y-junction onto a subcon connector which plugs into the receiver unit. The hydra receiver dipole unit is attached into the receiver array with a shekel.

The GEOMAR receivers GEODIP (Fig. 5.28) use an updated version of the MAGSON Hydra logger, which has slightly different dimensions. The main difference to the BGR HYDRA receiver consists in the mechanical setup. For the GEOMAR receivers, the electrodes and loggers are housed in protective POM units, which are attached onto a rope using knots.

5.2.3.3 Data acquisition

All together six bottom-towed CSEM lines were acquired (see Table 5 and Fig. 5.28) for an overview of the acquisition time line and profile locations). A test profile (CSEM1) was acquired Sept 2 to Sept 3 after the 2D and before the 3D seismic acquisition to ensure that all components functioned and to optimize the deployment and recovery routine. All other profiles were acquired during the night to avoid leisure and fishing boat traffic.

Identifying suitable profile lines was very difficult due to the lack of sediment coverage on part of the shelf, permanent seafloor installations such as power cables, fish farms and the presence of a multitude of wrecks in the area. To ensure that the dipole-dipole array did not get ensnared on carbonate blocks, the potentially dangerous profile lines were explored via Parasound (Fig. 5.29) and, if no multibeam data was available, with extra multibeam lines in the night prior to the CSEM deployment.

The shelf region itself was already covered by CSEM lines during the Marcan project. Finding new profile lines on the shelf proved difficult and plans for various CSEM profiles had to be

	Wed, Sept2	Thu, Sept2	Tue Sept 8	Wed Sept 9	Thu Sept 10	Fr Sept 11	Sa Sept 12	Su Sept 13	Mo Sept 14	Tue Sept 15	Wed Sept 16	Thu Sept 17	Fr Sept 18
0		CSEM1		CSEM2		CSEM3	CSEM4		CSEM5		MMR		CSEM6
1		30 WP		33 WP		17 WP	23 WP		22 WP		37WPs		29 WPs
2		13.5 km		9.4 km		4.4 km	5.7 km		5.5 km		1.8 km		7.3 km
3													
4													
5													
6													
7													
8													
9					4 OBMT Recovery								
10													
11						4 OBMT Deployment							12 OBMT recovery
12													
13													
14													
15													
16						OBS recovery							
17													
18													
19													
20													
21													
22													
23													
						CSEM	Deploy/Rec						
						CSEM	Acquisition						
						Bathy/Para							

Most profiles were acquired in the north of Malta offshore Gozo, since this region is deemed, based on the Marcan profiles and hydrogeological models, to be most prospective of offshore groundwater. Slightly less favourable conditions are met at the south of the Malta island. However, due to exposed carbonates, seafloor cables and fish farms it was not possible to acquire bottom towed CSEM data in this area. Due to seafloor installations and rough topography, it was not possible to acquire any data in the southern section of Malta and on parts of the shelf (these abandoned profiles are shown as pink lines on Fig. 5.29).

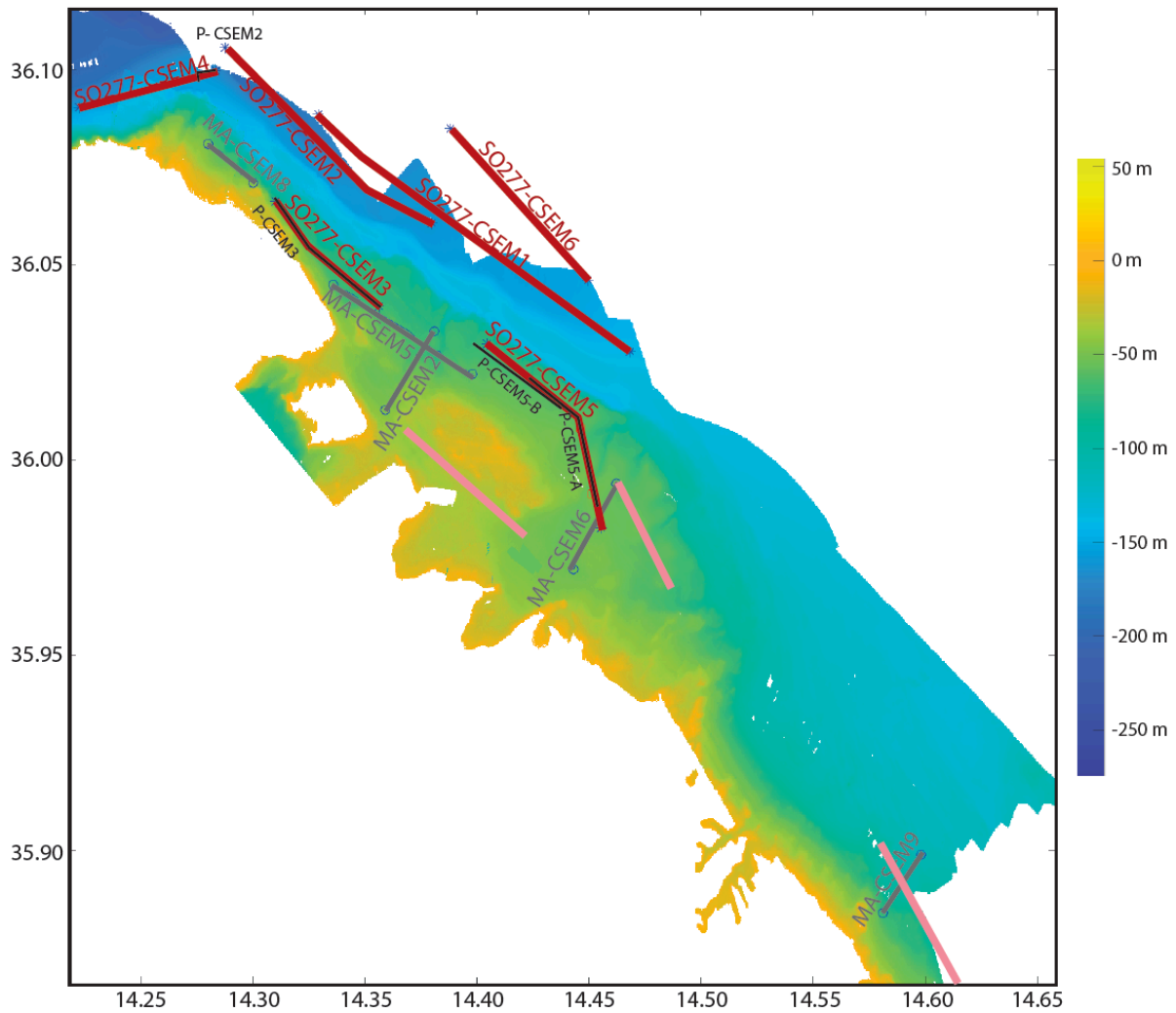


Fig. 5.29 Overview of CSEM lines acquired during Marcan project (grey) and SO277 OMAX cruise (red). Pink lines show CSEM profiles planned during SO277 OMAX cruise which had to be abandoned due to power cable, wrecks or rough topography. Black lines show the Parasound profiles (Figure 5.26) acquired before occupying the profile.

The transmitter current was set to 20 A with a wave form of a half duty cycle with a period of altogether 8 sec, i.e. 2 sec positive current, 2 sec off, 2 sec negative current, 2 sec off (Fig. 5.32). At each way point, we transmitted with above-described pattern for 60 sec, then paused for 60 sec to recharge the battery. This procedure was repeated 6 times at each station, such that we have six one-minute transmission cycles and 6 minutes pause. During transit to the next way point (with a speed of 0.3 up to 0.7 knots depending on topographic roughness), the cycle was set to 1-minute transmission and 2 minutes pause. Exceptions to these patterns are found for the first 10 waypoints of CSEM_1, where the duty cycle period was set to 4 seconds. Also, the recharging / pause period was smaller in the first two profiles, which led to a degeneration of the transmitter current in the last few waypoints of Line 1.

While the physical set up of the transmitter remained the same for all profiles, the length of the receiver arrays and positioning and sequence of receivers changed depending on topography as well as for testing purposes of the GEOMAR receivers (see Fig. 5.31).

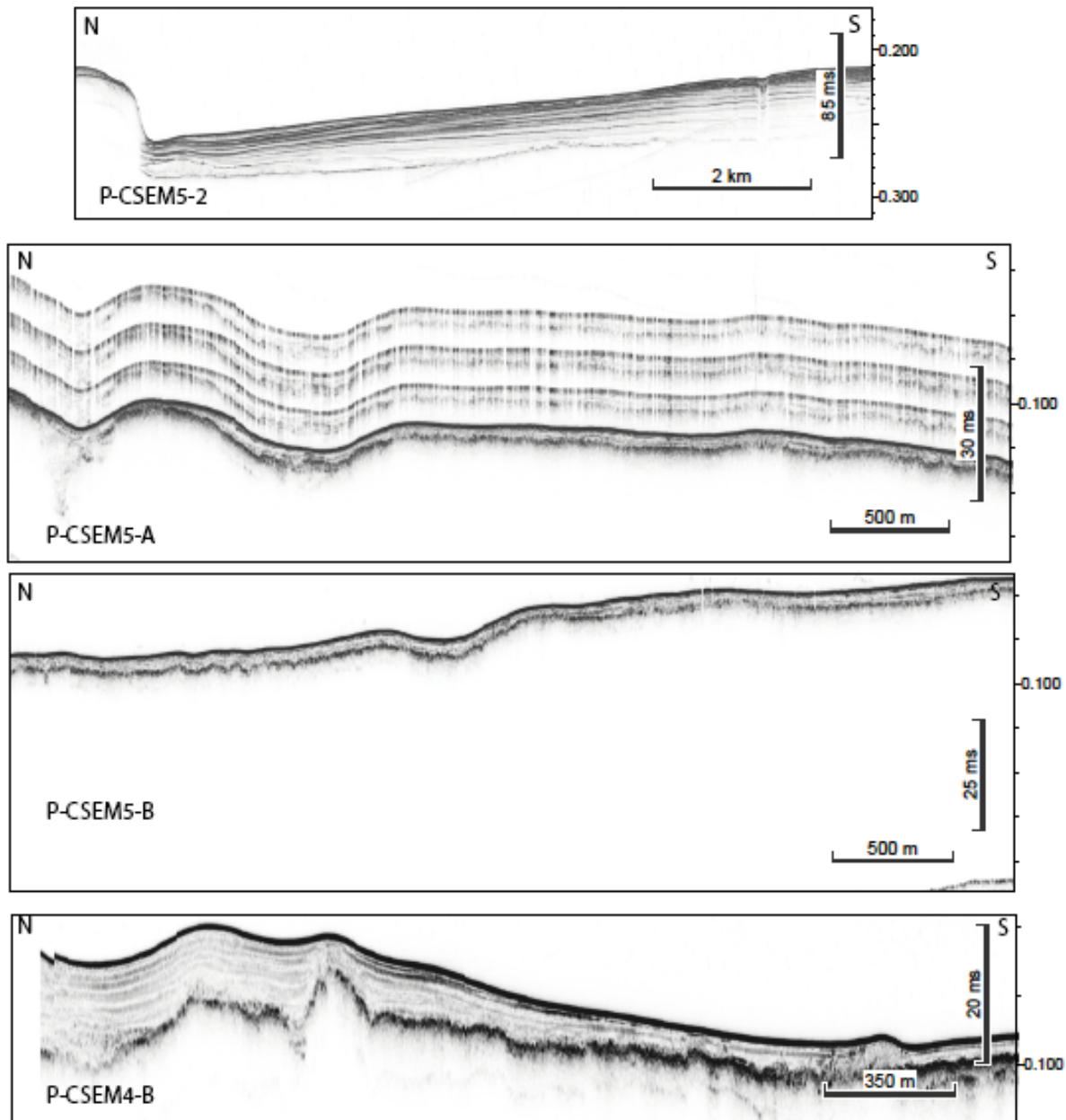


Fig. 5.30 Parasound profiles acquired along a selection of profiles, where carbonates were expected to be exposed.

For deployment and recovery, both the Toronto winch with the umbilical to the transmitter as well as the auxiliary winch were used. On the auxiliary winch, the connected ropes were wound. The transmitter section was wrapped at the bottom of wheel, followed by two 100 m ropes, and if measurements with very long offsets were possible, a 200 m rope, on the top. Prior to the deployment, the logger was synchronized, built into the container, connected to the dipoles and laid out on deck. For the deployment the last receiver dipole unit consisting of the logger and the

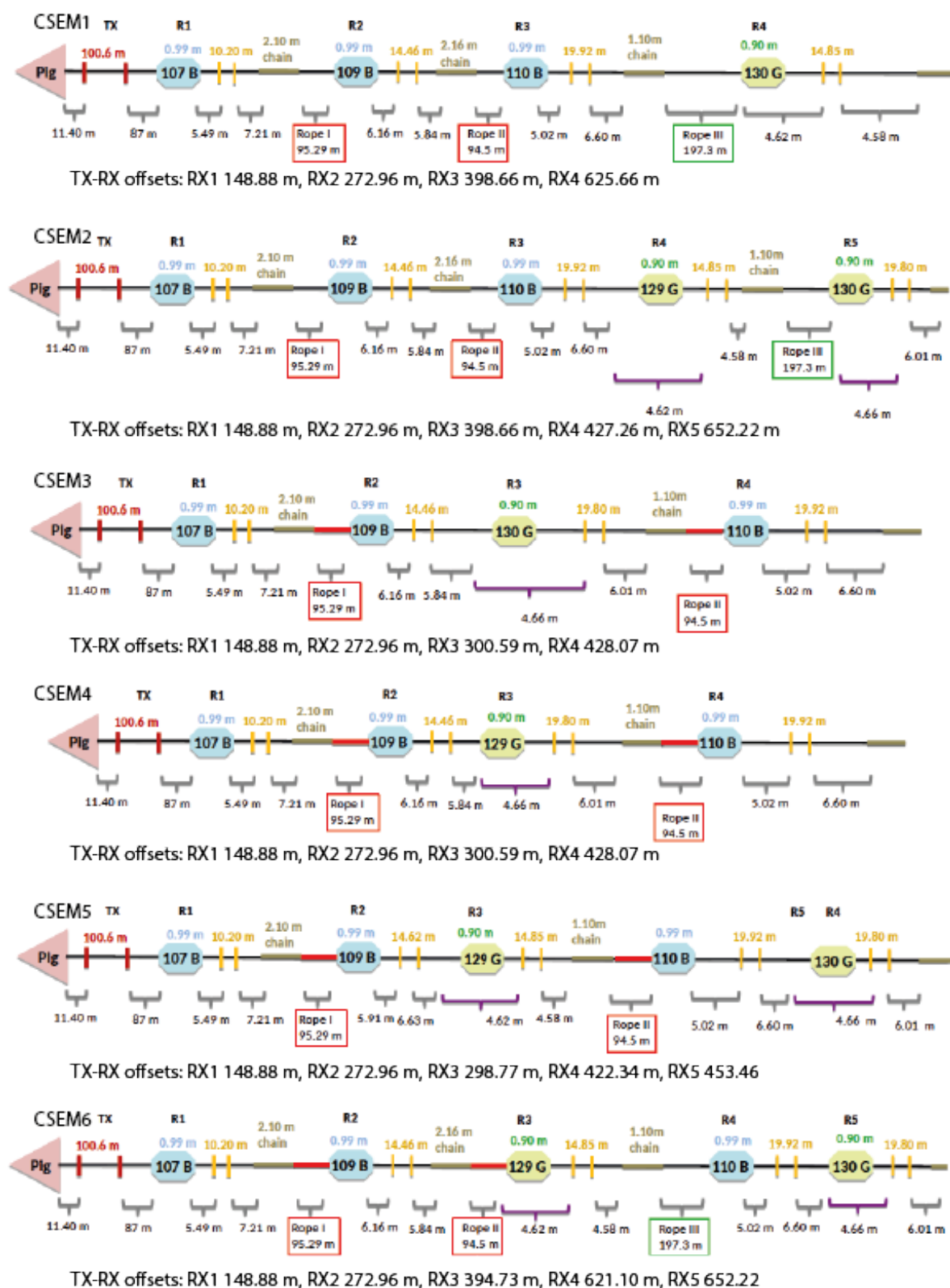


Fig. 5.31 Set up of CSEM array for lines 1 to 6.

attached dipole were connected to the top rope on the auxiliary winch and then deployed into the water. At the end of the first rope, the rope section was stopped on an eye on the deck and the second last receiver connected to the end of the rope in the water and the following rope, and the next section went into the water. This procedure was repeated for all segments. The last segment,

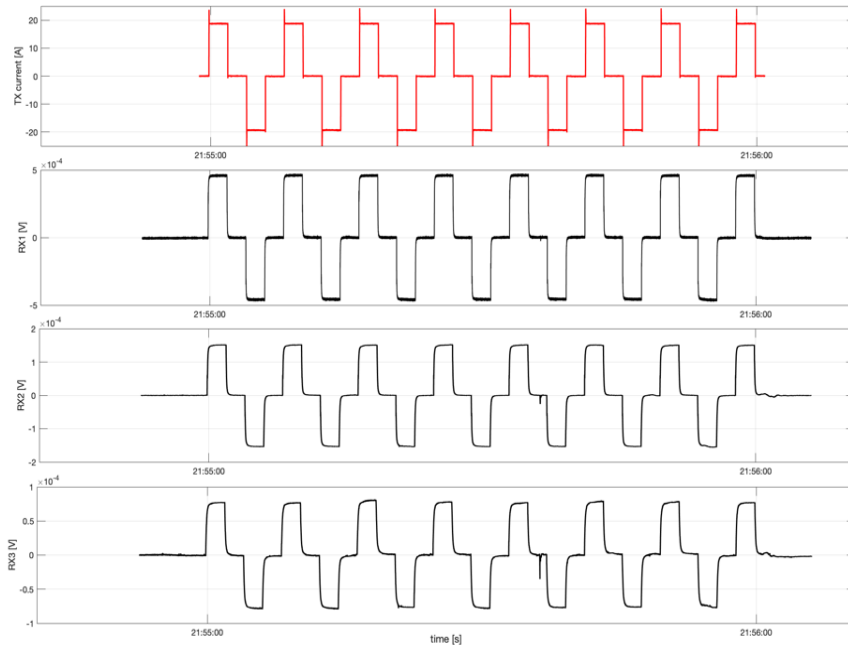


Fig. 5.32 Transmission wave form (upper panel) and received wave form at three receivers with increasing transmitter-receiver offset.

i.e. the transmitter unit, was then mechanically and electronically connected to the pig. After this, the transmitter on the pig was synchronized. The pig was deployed using the Toronto winch, the winch zeroed when the pig hit the water and lowered to the bottom. At 30 m depth, the winch was stopped and a test transmission executed. After the transmitter data was uploaded and the wave form checked, the pig was layer onto the seafloor. During deployment the ship was moving forward with approx. 0.3 to 0.5 knots, depending on the pull of the array. Deployment of the entire receiver string into the water took about 1 hour.

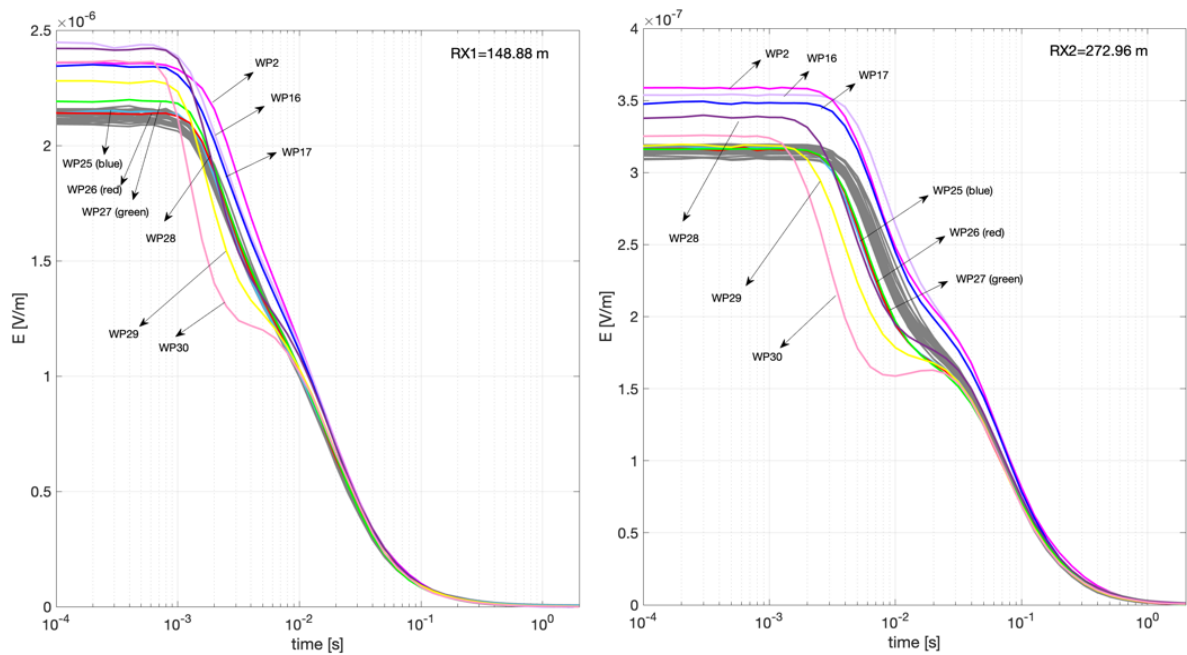


Fig. 5.33 Stacked transients of two receiver units for all WPs along Line 1.

After the deployment about one to two times the water depth of cable was paid out to make sure that the pig was not moved while the ship was heaving and ensure that the angle of the wire from the A-frame was large. A transponder on the pig was supposed to deliver exact USBL positioning, however, a transponder signal was only received occasionally, which we attributed to the fact that the angle of incidence of the pinger relative to the ship was very large due to the shallow water depth. The USBL data therefore needed to be interpolated using a common time base with the ship's GPS data.

Fig. 5.33 shows a sample data set for the transmitter signal as well as the signal at 3 receivers from profile 2. The data is processed by identifying the switch on/off times of the transmitter signal which are summarized in a shot table. Synchronous received signals are then identified based on the shot table. Transients of the receiver signals at one way point are then stacked to increase the signal to noise ratio. Figure 5.14 shows the processed transients at two receivers for all weigh points along profile 1. Earlier arrival times of the signal indicate a more resistive underground. For profile 1, a consistently anomalous resistive signal can be identified for the latter way points at the north of the profile.

Once processing has been finished and quality controlled, the data will be inverted to a 2D layered resistivity model using a linearized inversion.

Table 5.4 WPs along the six CSEM profiles.

CSEM Line 1		02.-03. 09.2020				CSEM Line 2		08.-09. 09.2020			
Name	USBL Long	USBL Lat	SHIP Long	SHIP Lat		Name	USBL Long	USBL Lat	SHIP Long	SHIP Lat	
'WP01'	14.4642	36.0306	14.4597	36.0314		'WP01'	14.2951	36.1017	14.2984	36.0996	
'WP02'	14.4620	36.0310	14.4578	36.0323		'WP02'	14.2978	36.1001	14.3011	36.0980	
'WP03'	14.4594	36.0318	14.4554	36.0334		'WP03'	14.3010	36.0982	14.3039	36.0964	
'WP04'	14.4569	36.0328	14.4529	36.0344		'WP04'	14.3032	36.0969	14.3066	36.0948	
'WP05'	14.4544	36.0338	14.4504	36.0353		'WP05'	14.3059	36.0953	14.3092	36.0932	
'WP06'	14.4519	36.0348	14.4479	36.0364		'WP06'	14.3087	36.0936	14.3120	36.0916	
'WP07'	14.4494	36.0358	14.4455	36.0374		'WP07'	14.3114	36.0920	14.3149	36.0901	
'WP08'	14.4470	36.0368	14.4430	36.0384		'WP08'	14.3142	36.0905	14.3177	36.0885	
'WP09'	14.4445	36.0378	14.4405	36.0395		'WP09'	14.3171	36.0889	14.3206	36.0869	
'WP10'	14.4420	36.0389	14.4380	36.0405		'WP10'	14.3200	36.0872	14.3233	36.0853	
'WP11'	14.4395	36.0399	14.4355	36.0415		'WP11'	14.3227	36.0858	14.3261	36.0837	
'WP12'	14.4371	36.0409	14.4331	36.0427		'WP12'	14.3254	36.0841	14.3289	36.0821	
'WP13'	14.4346	36.0420	14.4306	36.0437		'WP13'	14.3281	36.0826	14.3316	36.0805	
'WP14'	14.4321	36.0430	14.4282	36.0447		'WP14'	14.3308	36.0810	14.3342	36.0789	
'WP15'	14.4297	36.0441	14.4257	36.0457		'WP15'	14.3334	36.0795	14.3369	36.0774	
'WP16'	14.4271	36.0449	14.4230	36.0463		'WP16'	14.3362	36.0780	14.3397	36.0758	
'WP17'	14.4221	36.0468	14.4183	36.0488		'WP17'	14.3397	36.0759	14.3424	36.0743	
'WP18'	14.4169	36.0493	14.4134	36.0508		'WP18'	14.3420	36.0746	14.3451	36.0727	
'WP19'	14.4124	36.0512	14.4085	36.0529		'WP19'	14.3443	36.0733	14.3478	36.0712	
'WP20'	14.4076	36.0532	14.4037	36.0550		'WP20'	14.3463	36.0721	14.3497	36.0701	
'WP21'	14.3998	36.0566	14.3960	36.0582		'WP21'	14.3490	36.0708	14.3528	36.0691	
'WP22'	14.3921	36.0598	14.3881	36.0614		'WP22'	14.3518	36.0696	14.3558	36.0681	
'WP23'	14.3851	36.0626	14.3802	36.0647		'WP23'	14.3552	36.0685	14.3589	36.0673	
'WP24'	14.3766	36.0661	14.3723	36.0680		'WP24'	14.3578	36.0677	14.3619	36.0663	
'WP25'	14.3688	36.0694	14.3644	36.0712		'WP25'	14.3609	36.0667	14.3650	36.0653	
'WP26'	14.3600	36.0731	14.3565	36.0745		'WP26'	14.3640	36.0657	14.3681	36.0645	
'WP27'	14.3496	36.0773	14.3465	36.0786		'WP27'	14.3672	36.0647	14.3713	36.0634	
'WP28'	14.3408	36.0823	14.3378	36.0841		'WP28'	14.3703	36.0638	14.3744	36.0625	
'WP29'	14.3327	36.0874	14.3290	36.0896		'WP29'	14.3734	36.0628	14.3775	36.0615	
'WP30'	14.3312	36.0884	14.3275	36.0906		'WP30'	14.3764	36.0618	14.3806	36.0605	
						'WP31'	14.3796	36.0609	14.3837	36.0596	
						'WP32'	14.3827	36.0599	14.3868	36.0586	
						'WP33'	14.3858	36.0589	14.3899	36.0576	
CSEM Line 3		10.-11. 09.2020				CSEM Line4		11.-12. 09.2020			
Name	USBL Long	USBL Lat	SHIP Long	SHIP Lat		Name	USBL Long	USBL Lat	SHIP Long	SHIP Lat	
'WP01'	14.3521	36.0416	14.3496	36.0430		'WP01'	14.2880	36.1005	14.2838	36.0999	
'WP02'	14.3497	36.0429	14.3473	36.0442		'WP02'	14.2852	36.1001	14.2810	36.0994	
'WP03'	14.3474	36.0441	14.3449	36.0453		'WP03'	14.2826	36.0997	14.2782	36.0990	
'WP04'	14.3449	36.0453	14.3425	36.0465		'WP04'	14.2769	36.0988	14.2728	36.0981	
'WP05'	14.3424	36.0465	14.3401	36.0476		'WP05'	14.2742	36.0984	14.2701	36.0977	
'WP06'	14.3400	36.0478	14.3378	36.0488		'WP06'	14.2713	36.0979	14.2674	36.0973	
'WP07'	14.3371	36.0493	14.3349	36.0503		'WP07'	14.2687	36.0975	14.2647	36.0968	
'WP08'	14.3342	36.0507	14.3321	36.0517		'WP08'	14.2659	36.0970	14.2619	36.0964	
'WP09'	14.3313	36.0522	14.3292	36.0532		'WP09'	14.2632	36.0966	14.2592	36.0960	

'WP10'	14.3289	36.0534	14.3269	36.0544	'WP10'	14.2604	36.0962	14.2564	36.0956
'WP11'	14.3266	36.0548	14.3248	36.0558	'WP11'	14.2577	36.0957	14.2538	36.0951
'WP12'	14.3244	36.0561	14.3228	36.0573	'WP12'	14.2550	36.0953	14.2510	36.0947
'WP13'	14.3219	36.0579	14.3203	36.0591	'WP13'	14.2523	36.0949	14.2483	36.0942
'WP14'	14.3194	36.0597	14.3178	36.0609	'WP14'	14.2495	36.0945	14.2456	36.0939
'WP15'	14.3169	36.0615	14.3153	36.0627	'WP15'	14.2467	36.0940	14.2428	36.0934
'WP16'	14.3144	36.0633	14.3128	36.0644	'WP16'	14.2440	36.0936	14.2401	36.0931
'WP17'	NaN	NaN	14.3103	36.0662	'WP17'	14.2413	36.0932	14.2374	36.0926
					'WP18'	14.2385	36.0928	14.2346	36.0922
					'WP19'	14.2358	36.0924	14.2319	36.0918
					'WP20'	14.2336	36.0920	14.2292	36.0914
					'WP21'	NaN	NaN	14.2264	36.0910
					'WP22'	NaN	NaN	14.2237	36.0906
					'WP23'	NaN	NaN	14.2210	36.0901
CSEM Line 5					CSEM Line 6				
13.-14. 09.2020					17.-18. 09.2020				
Name	USBL Long	USBL Lat	SHIP Long	SHIP Lat	Name	USBL Long	USBL Lat	SHIP Long	SHIP Lat
'WP01'	14.4083	36.0282	14.4110	36.0268	'WP01'	14.4509	36.0454	14.4474	36.0476
'WP02'	14.4106	36.0270	14.4134	36.0257	'WP02'	14.4480	36.0472	14.4452	36.0490
'WP03'	14.4129	36.0256	14.4160	36.0248	'WP03'	14.4465	36.0481	14.4430	36.0504
'WP04'	14.4161	36.0245	14.4188	36.0233	'WP04'	14.4444	36.0495	14.4408	36.0517
'WP05'	14.4193	36.0231	14.4217	36.0220	'WP05'	14.4419	36.0511	14.4386	36.0531
'WP06'	14.4217	36.0220	14.4246	36.0207	'WP06'	14.4398	36.0524	14.4364	36.0544
'WP07'	14.4246	36.0207	14.4274	36.0193	'WP07'	14.4374	36.0538	14.4343	36.0558
'WP08'	14.4275	36.0193	14.4303	36.0179	'WP08'	14.4352	36.0546	14.4312	36.0542
'WP09'	14.4303	36.0179	14.4332	36.0166	'WP09'	14.4306	36.0578	14.4274	36.0603
'WP10'	14.4331	36.0165	14.4361	36.0153	'WP10'	14.4285	36.0594	14.4252	36.0617
'WP11'	14.4360	36.0151	14.4390	36.0139	'WP11'	14.4263	36.0608	14.4230	36.0631
'WP12'	14.4388	36.0137	14.4419	36.0126	'WP12'	14.4240	36.0622	14.4208	36.0645
'WP13'	14.4417	36.0123	14.4448	36.0112	'WP13'	14.4218	36.0636	14.4186	36.0659
'WP14'	14.4440	36.0112	14.4471	36.0102	'WP14'	14.4197	36.0649	14.4164	36.0673
'WP15'	14.4459	36.0095	14.4479	36.0076	'WP15'	14.4175	36.0663	14.4142	36.0687
'WP16'	14.4472	36.0070	14.4488	36.0050	'WP16'	14.4154	36.0677	14.4120	36.0701
'WP17'	14.4497	36.0032	14.4518	36.0012	'WP17'	14.4132	36.0691	14.4098	36.0715
'WP18'	14.4510	35.9989	14.4516	35.9967	'WP18'	14.4110	36.0705	14.4076	36.0728
'WP19'	14.4514	35.9963	14.4525	35.9941	'WP19'	14.4089	36.0719	14.4055	36.0742
'WP20'	14.4522	35.9937	14.4533	35.9915	'WP20'	14.4066	36.0733	14.4033	36.0756
'WP21'	14.4523	35.9929	14.4531	35.9905	'WP21'	14.4044	36.0747	14.4011	36.0770
'WP22'	NaN	NaN	14.4533	35.9879	'WP22'	14.4023	36.0761	14.3989	36.0784
					'WP23'	14.4001	36.0775	14.3968	36.0798
					'WP24'	14.3979	36.0789	14.3945	36.0811
					'WP25'	14.3957	36.0803	14.3923	36.0825
					'WP26'	14.3936	36.0817	14.3901	36.0839
					'WP27'	14.3913	36.0831	14.3879	36.0853
					'WP28'	14.3891	36.0845	14.3856	36.0867
					'WP29'	14.3869	36.0859	14.3835	36.0882

5.3.3 Magnetometric resistivity experiment

5.3.3.1 Methodology

Due to the rough topography of most of the shelf, which could be common scenario encountered on carbonate shelves, we decided to test the magnetometric resistivity (MMR) method for shallow water depths (Fig. 5.34). The experiment set up consist of a vertical dipole with a constant current. The OBEM measures the horizontal magnetic field arising from the overall current flow. The horizontal magnetic field measured is proportional, by Amperes law, through the net current which flows into the seafloor. If the seafloor would be infinitely resistive, no current flow would enter the seafloor and the resulting horizontal field would be zero. Vice versa, if it would be infinitely conductive, all current would flow into the seafloor and no return current through the water column would exist which would result in a maximum magnetic field. Assuming a resistivity of the sea layer of ρ_0 and a half space resistivity of the seafloor of ρ_0 , a water depth of D , a distance of the magnetometer to the dipole of R and the current in the dipole to be I , the magnetic field is given by:

$$B_H = \frac{\mu I D \rho_0}{4 \pi \rho_1 R^2}$$

The electrical resistivity can therefore be probed by measuring the horizontal magnetic field due to the vertical dipole at different distances from the dipole. The strength of the magnetic field, i.e.

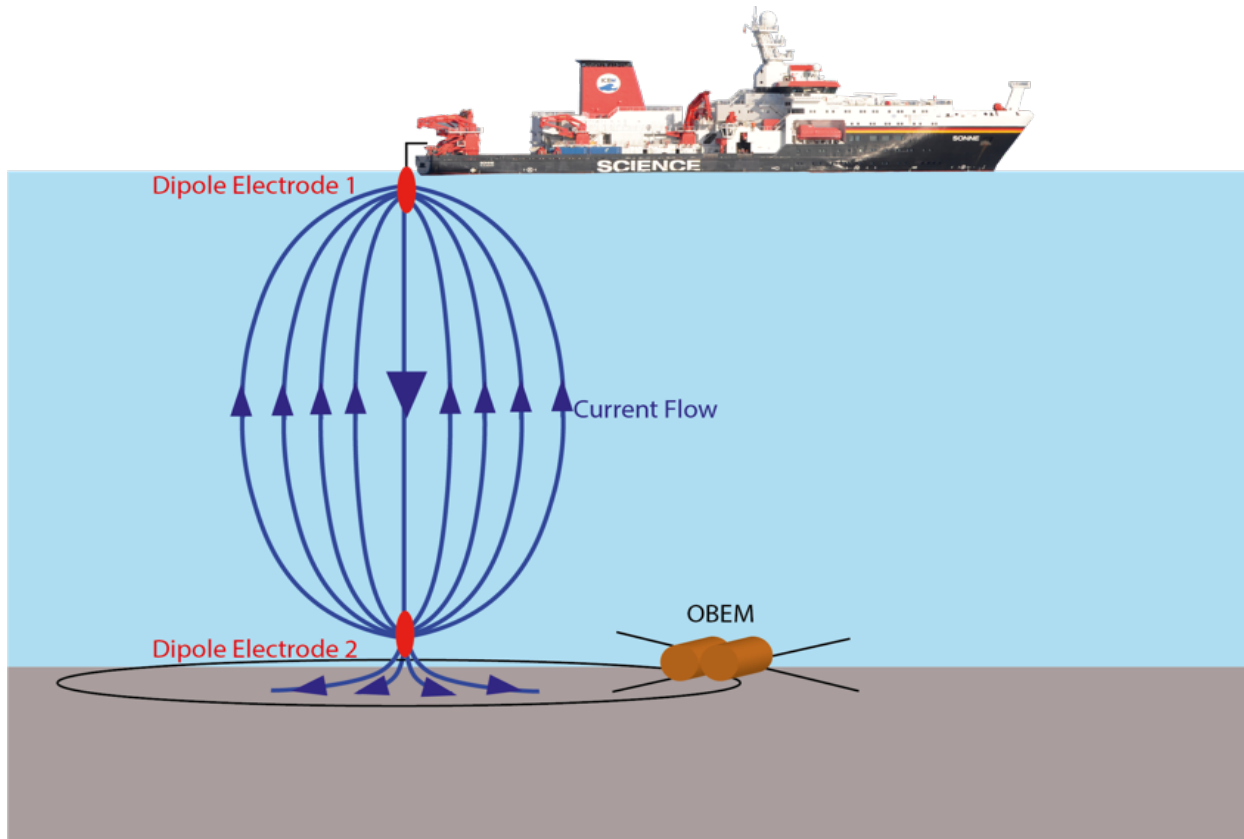


Fig. 5.34 Set up of a MMR experiment consisting of a vertical dipole spanned through the water column using current electrodes (red ellipses). The dipole current (blue lines) will cause a horizontal magnetic field at the OBEM, which is proportional to the net current flowing through an Ampere loop (black line).

signal to noise ratio above natural varying fields, is proportional to the dipole moment, i.e. the product of the current and the dipole length. To increase the dipole moment, the vertical dipole is spanned through the entire water column. Due to the shallow water depth the distance at which the magnetic field associated with the dipole can be detected is rather small but sufficiently large to be measured.

5.3.3.2 Data acquisition

To capture the MMR signal, 4 OBEMs were recovered from MT stations and placed along the planned profile separated by about 500 m from each other (Figure 5.35). The recording frequency of the electromagnetic fields was set to 100 Hz. The vertical dipole had a length of 35 m and the upper electrode was lowered to about 10 m. The water depth along the profile varied from 55 to 60 m. The transmission cycle was the same as for the CSEM experiment. Transmission occurred at way points with 50 m distance. Fig. 5.36 shows a sample data file for OBEM 15 at the centre of the profile. The horizontal part of the dipole transmitter currents is clearly visible in the electric field recordings for three transmission cycles. Anomalies in the horizontal magnetic field may be discerned from the varying background field. The data will be processed by removing the natural varying magnetic field variations using background data from adjacent OBEM stations. Stacking of the response at one station should increase the signal to noise ratio, such that we expect to be able to measure the response up to a distance of 150 m or more from the dipole.

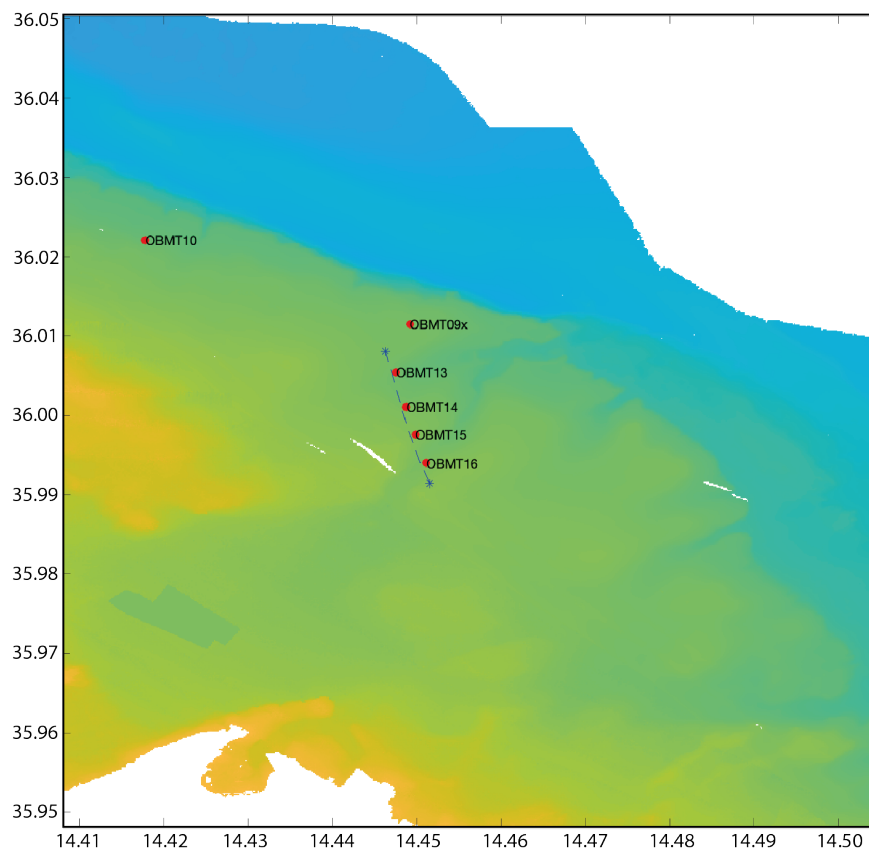


Fig. 5.35 MMR transmitter line and positions of OBEMs.

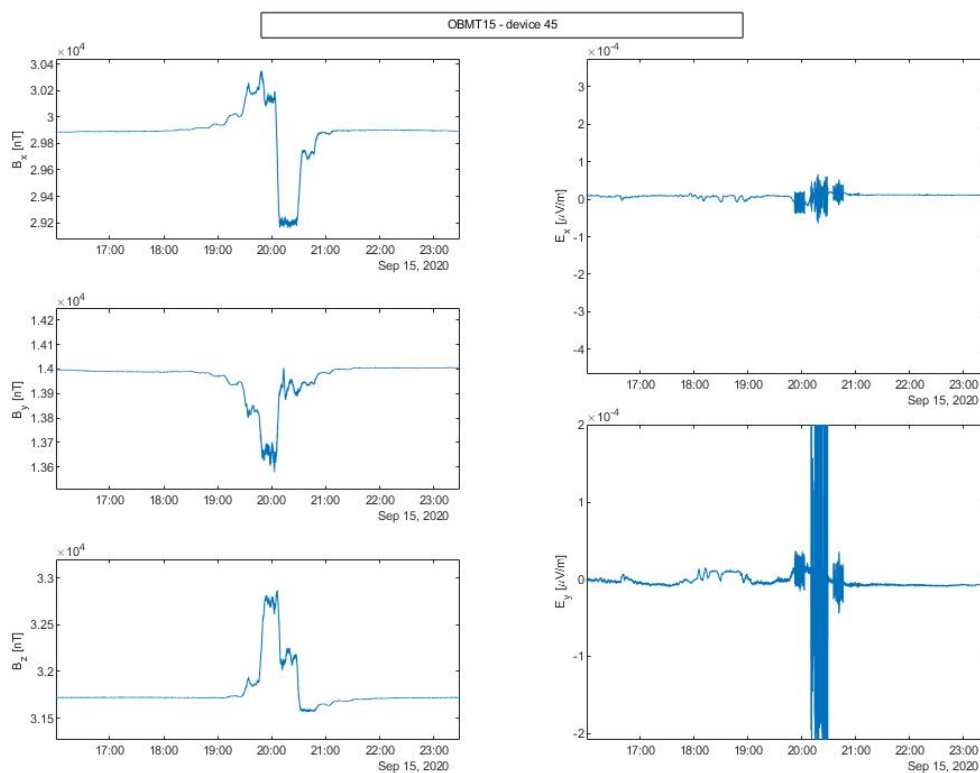


Fig. 5.36 Raw data received at OBEM 15 for three vertical dipole transmission approximately 50 m apart.

Table 5.5 Waypoints of vertical dipole transmission (Ship's GPS)

Name	SHIP_Lat	SHIP_Long
WP01	14.4519	35.9919
WP02	14.4515	35.9928
WP03	14.4513	35.9932
WP04	14.4511	35.9960
WP05	14.4510	35.9940
WP06	14.4508	35.9945
WP07	14.4507	35.9949
WP08	14.4505	35.9954
WP09	14.4505	35.9958
WP10	14.4503	35.9962
WP11	14.4502	35.9966
WP12	14.4500	35.9970
WP13	14.4498	35.9975
WP14	14.4497	35.9980
WP14	14.4497	35.9979
WP15	14.4995	35.9984
WP16	14.4494	35.9988
WP17	14.4492	35.9992
WP18	14.4490	35.9997
WP19	14.4490	36.0001
WP20	14.4488	36.0005
WP21	14.4487	36.0009
WP22	14.4486	36.0014
WP23	14.4485	36.0018
WP24	14.4483	36.0230
WP25	14.4483	36.0027
WP26	14.4482	36.0032
WP27	14.4481	36.0036
WP28	14.4480	36.0041
WP29	14.4479	36.0045
WP30	14.4477	36.0050
WP31	14.4476	36.0054
WP32	14.4475	36.0058
WP33	14.4475	36.0063
WP34	14.4473	36.0067
WP35	14.4472	36.0072
WP36	14.4471	36.0076
WP37	14.4470	36.0080

Table 5.6 Position of OBEMs receiving vertical dipole transmissions.

	System	Long	Lat	Depth (m)
OBMT13	EM-02	14.447500	36.004500	57
OBMT14	EM-06	14.448900	36.001200	51
OBMT15	EM-01 (with z electrode)	14.449800	35.997600	49
OBMT16	EM-09	14.451100	35.994100	51

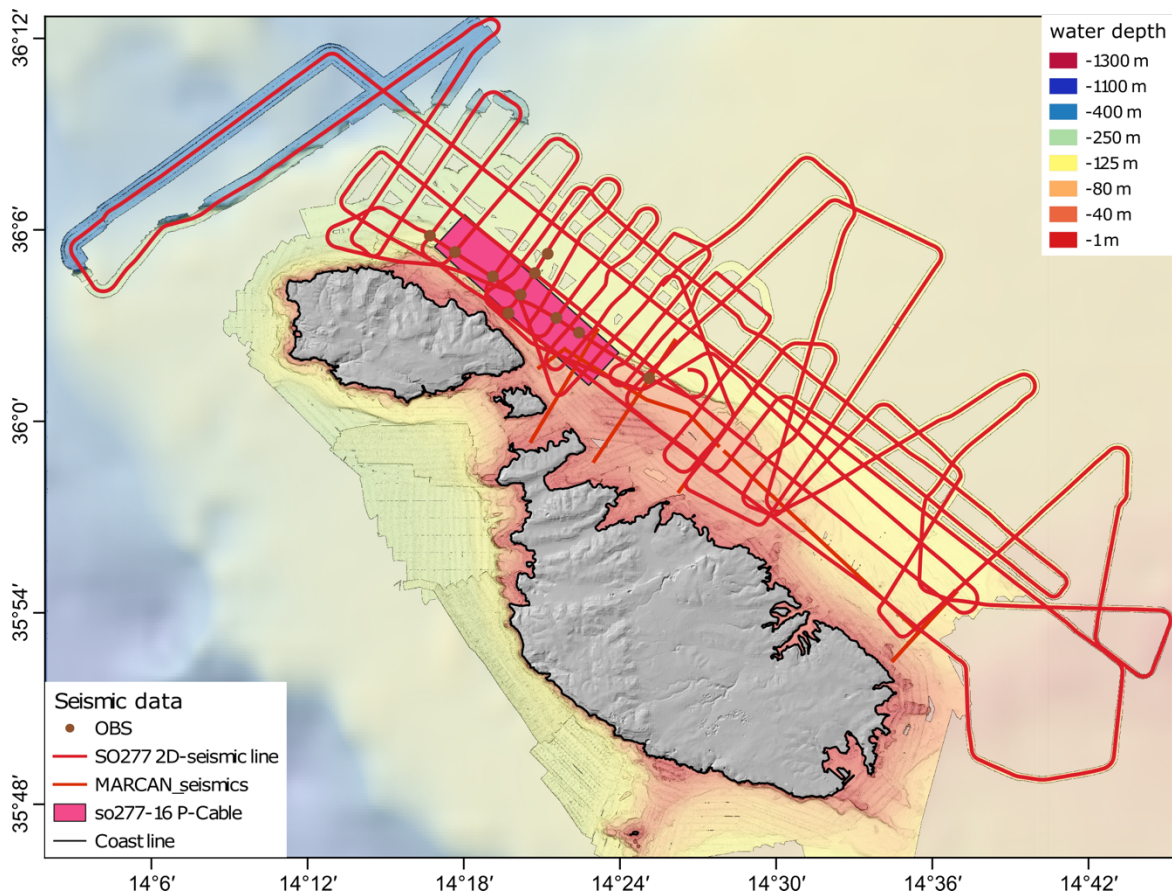
5.3 2D reflection seismic imaging

(J. Elger¹, M. Kühn¹)

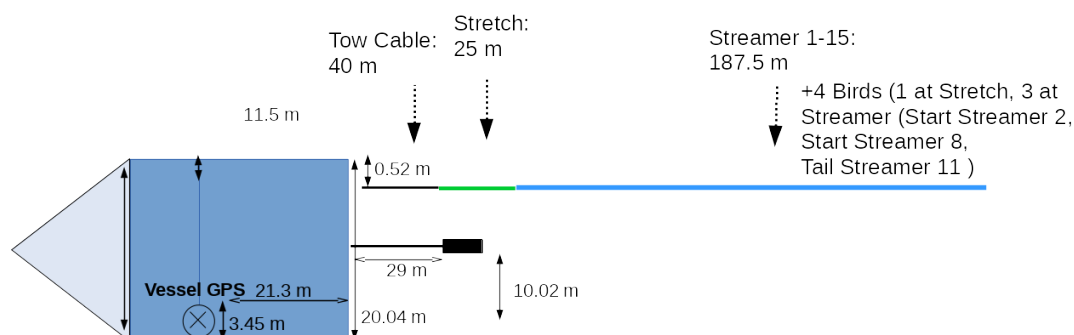
¹GEOMAR

5.3.1 Seismic data acquisition

High-resolution 2D seismic data were acquired north and east of Malta and Gozo (Fig. 5.36).

**Fig. 5.36** Seismic acquisition during SO277.

Survey: P1000



Streamers: 8 hydrophone groups with a group spacing of 1.5625 per streamer

Source: 2 GI-Gun in True GI mode

GPS-GUN-OFFSET: 6.57 m to portside, 50.3 m aft
GPS-STREAMER-OFFSET (FC): 16.43 m to portside, 86.3 m aft

Fig. 5.37 Deck geometry for the 2D seismic survey.

5.3.1.1 Streamer setup

We used 15 active streamer sections (Geometrics GeoEel streamer segments, each 12.5 m-long) with an overall digital streamer length of 187.5 m for recording the seismic signal. Deck geometry, streamer configuration and seismic gun setting for the 2D survey are illustrated in Fig. 5.37. The seismic recording unit consists of a tow cable, a 25 m-long vibro-stretch section behind the tow cable and the 15 active sections attached behind the stretch section. The tow cable had a length of 40 m behind the vessel's stern. Each active section contains 8 hydrophones with a group spacing of 1.56 m. Each active streamer section has its own analog-to-digital (AD) converter module with a small Linux computer. Communication between the AD digitizer modules and the recording system in the lab was established via TCP/IP protocol. A repeater was located between the deck cable and the tow cable (Lead-In). The streamer power supply unit managed the power supply and communication between the recording system and the AD digitizer modules. A small buoy was attached to the tail swivel of the 2D streamer.

Four Bird Remote Units (RUs) were deployed on the streamer during the survey. The RUs have adjustable wings that were controlled from the seismic lab.

Controller and RUs communicate via communication coils nested within the streamer. A twisted pair wire within the deck cable connects controller and coils.

Note that the deck geometry shown in Fig. 5.37 was changed for profile P1022 due to technical issues. On this profile the distance between vessel's stern and air guns was 30 m instead of 29 m and the distance between air gun to portside was 6.8 m instead of 10.02 m.

5.3.1.2 Seismic source

During the seismic experiment, two GI-Guns (Generator-Injector Guns) constituted the seismic source. The two guns were connected to a stringer by four 1 m-long steel chains above the guns. Two buoys attached to the stringer stabilized the gun's horizontal position at a water depth of

approximately 2 m. The GI guns were operated in true GI mode with a 45 in³ generator and 105 in³ injector chamber. An unfiltered frequency spectrum of one shot during the 2D seismic survey is shown in Fig. 5.38. A gun hydrophone provided both the time break and the shape of the near-field signal for permanent monitoring and quality control of the source signal. The injector pulse was triggered with a delay of 45 ms with respect to the generator pulse. This delay value was adopted for an approximate source depth of 2 m and a gun pressure of 200 bar. The shooting interval was adjusted to 5 seconds, resulting in a nominal shot point distance of 7.8 m with a ship's speed of approximately 3.5 knots through the water. There was a GPS mounted on the buoy of the first GI-Gun which recorded the location every second. This GPS recorded for the entire 2D survey but was lost early on during the 3D survey.

5.3.1.3 Data recording

Data were recorded with acquisition software provided by Geometrics. The analogue signal was digitized with a sampling rate of 0.5 ms. The seismic data were recorded in SEG-D format. Recording length was 3 seconds. One file with all channels within the streamer configuration was generated per shot. The corresponding logged shot file reports shot number and time information contained in an RMC string. The acquisition PC allowed online quality control by displaying shot gathers, a noise window, and the frequency spectrum of each shot. The cycle time of the shots were displayed as well. The vessel's position was simultaneously logged in the RMC string along with logged time and position information with a GPS antenna.

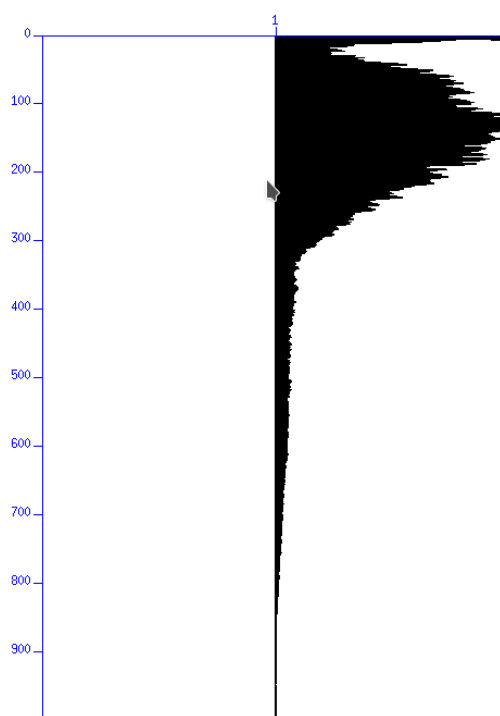


Fig. 5.38 Unfiltered frequency spectra for the 2D seismic experiment.

5.3.2 On-board Processing

On-board processing included streamer geometry configuration, delay calculations and source and receiver depth control. From the seismic data a delay of -43 ms was evaluated. A receiver ghost effect in the seismic data could not be detected. The source-receiver locations were then binned with a common-midpoint bin spacing of 1.5625 m. Different filter tests were performed and the frequency spectra were analyzed (Fig. 5.38). Seismic traces were balanced and filtered using a bandpass filter with corner frequencies at 25, 45, 450, 500 Hz (Fig. 5.39) and a f-x deconvolution with a window width of 12 traces and a filter width of 4 traces (Random Noise Attenuation). Subsequently, a normal move out correction (with a constant velocity of 1522.00 m/s, derived from a first CTD measurement) and stacking were applied. The stack was migrated with a 2D Stolt

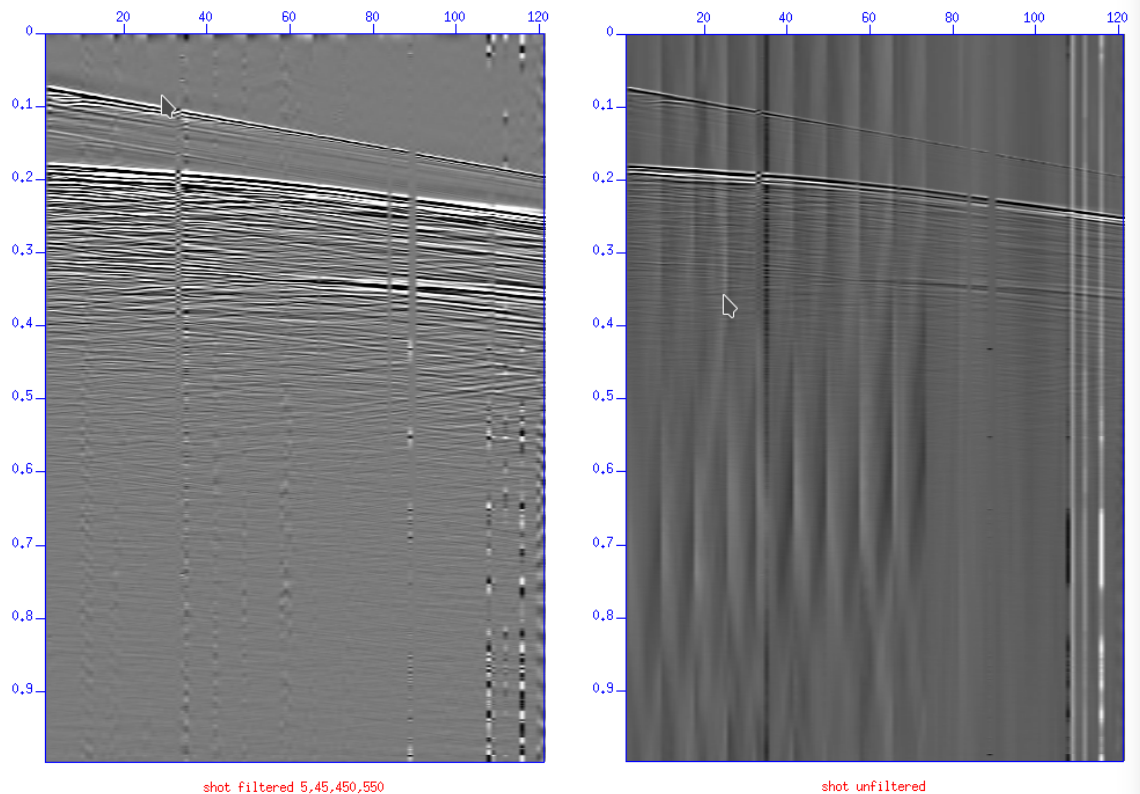


Fig. 5.39 Left: Unfiltered shot gather with travel time on the y-axis and channel number on the x-axis showing the first arrival of the direct wave (uppermost signal) and reflections from the subsurface afterwards. Low-frequency noise overlies the signal. Right: Bandpass-filtered shot gather using filter corner frequencies 5, 45, 450, 550. The final bandpass filter used for processing had corner frequencies 25, 45, 450, 550.

migration algorithm using constant velocity models. Due to rapid velocity changes within the subsurface, all profiles were migrated with three different constant velocity models (1500 m/s, 2800 m/s, 3400 m/s) to improve seismic imaging. Additionally, reflection coefficient calculations using the Zoeppritz equation were done using the CREWES Zoeppritz Explorer software tool (www.crewes.org). These calculations indicated an improved imaging by only using the first 15 channels of the streamer.

5.3.3 Preliminary results

In total, we collected more than 780 km of 2D seismic profiles (Fig. 5.36) on the east coast off Gozo and Malta. The acquired profiles are of good quality and will provide important information to understand the geological setup. Due to great differences in seismic properties between overlying sediments and limestones, which are characteristic for the regional geology, the seismic imaging is very challenging. Units of horizontal bedded reflectors off the shelf are resolved well using all 120 available channels (Fig. 5.40, down to about 0.3 s). The units below, most properly hard rock, e.g. limestones (compare drilling results in Gatt 2012), bear more challenges for the seismic imaging. In some places coherent reflections can resolve dipping layers, interrupted by aligned offsets which show a broad network of faults. Here, the interface between the horizontally layered reflectors and the underlying units is characterized by a moderate amplitude reflection. Elsewhere, this interface is represented by a very high amplitude reflection with nearly no energy

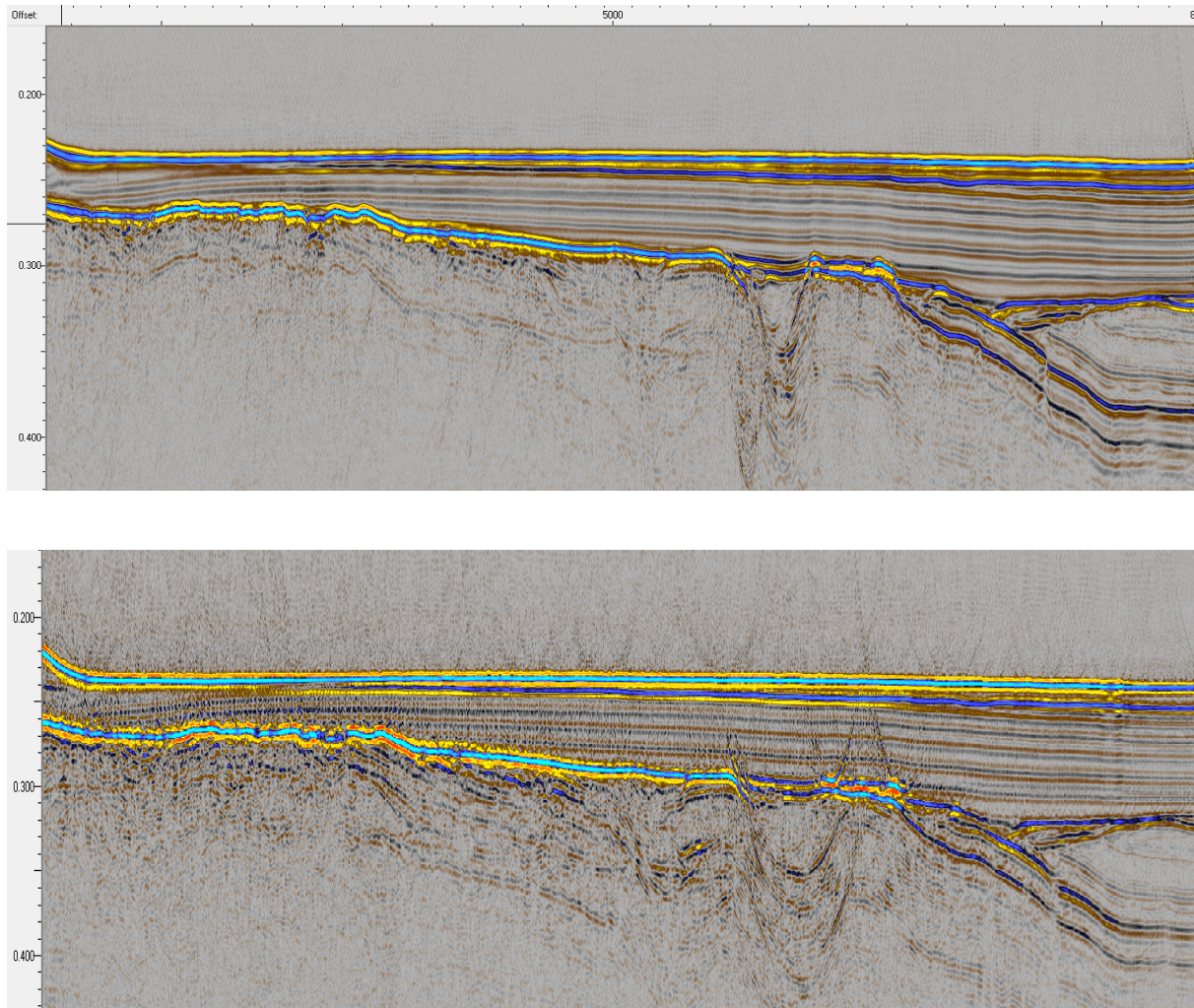


Fig. 5.40 3D seismic reflection profile 1045 east of Gozo on the outer margin in two different procession versions:
 a) Stolt migration with 1500 m/s of all 120 channels, and b) Stolt migration with 2800 m/s of the first 15 channels.

recorded below (Fig. 5.40a). This is the result of high reflection coefficients at angles higher than about 25° . They are caused by low water depth, about 160 m, and the potentially high acoustic impedance contrast between soft sediments at the top and limestone below (compare sonic velocities of about 3400 m/s in Gatt, 2012). As a result, using only the first 15 channels of the MCS (with lower angles), the 2D data can reveal more structures below the top of the limestones (Fig. 5.40b).

The 2D seismic data show abundant fault systems, horizontally deposited pelagic sediments in the distal part and the high amplitude Messinian reflections below. The MCS data provide insights into the nature of a prominent morphological terrace along Malta's shelf break (Fig. 5.36). It runs nearly parallel to the east coast off Gozo and Malta at the bottom of the shelf break. The MCS data reveal the internal sedimentary structure which suggests that it is formed as a contourite drift or an old shoreline deposit from a previous sealevel lowstand (Fig. 5.41).

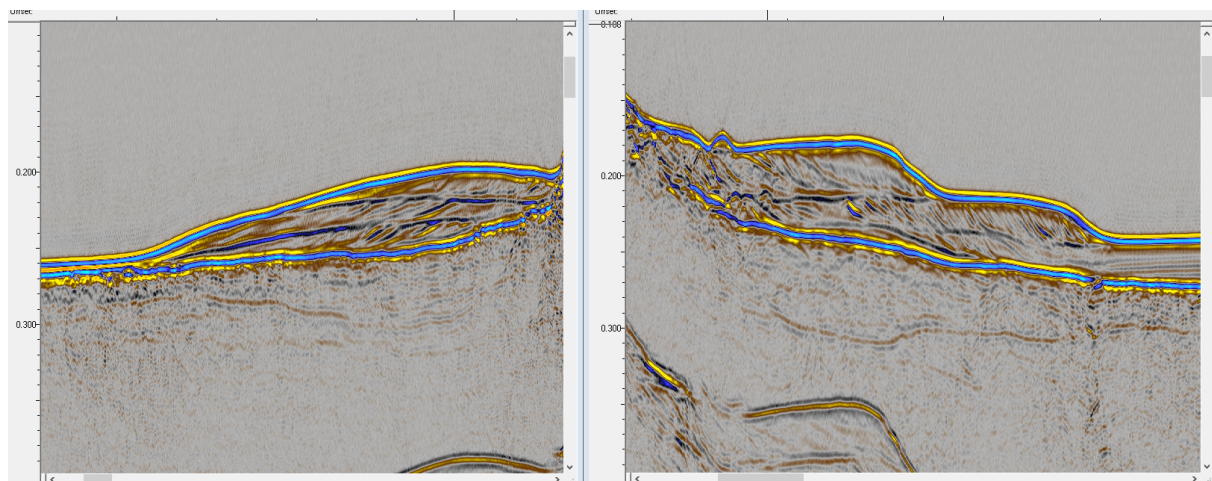


Fig. 5.41 Sections of 2D seismic reflection profiles 1039 (a) and 1028 (b) east of Gozo at the morphological step that runs parallel to the coast. Both profiles show the internal sediment structure with prograding sediments separated by horizontal reflectors at similar depth suggesting that their deposition was sealevel controlled.

5.4 3D reflection seismic imaging

(J. Elger¹, M. Kühn¹)

¹GEOMAR

5.4.1 Seismic data acquisition

High resolution 3D seismic data were with the P-Cable system covering a 12 km by 2.5 km area north of Malta. The survey was planned with an inline spacing of 60 m.

5.4.1.1 Streamer setup

During the 3D seismic survey, 16 streamer sections were attached to the 199 m long cross cable and dragged in a hyperbolic shape behind vessel (Fig. 5.42). The outer three streamer sections were spaced approximately 14 m apart and the inner ten segments were spaced approximately 9 m apart. Each active streamer section contained 8 hydrophones with a group spacing of 1.56 m. Each section had an analog-to-digital (AD) converter module, connected to the junction boxes on the cross cable via a 5 m long lead-in cable. Communication between the cross cable and the recording system in the lab was established via TCP/IP protocol. The streamer power supply unit in the lab managed the power supply and communication between the recording system and the AD digitizer modules. Spherical floats were attached to each junction box, except at the outermost streamers. Additionally, five floats were tied to the cross cable between streamers 6, 7, 8, 9, 10 and 11. For the survey we used Geometrics GeoEel streamer segments (oil filled streamers as well as solid state streamers).

Diagram illustrating the experimental setup for the 2019-2020 season, showing the vessel, paravane (starboard), paravane (port), and streamers.

Vessel GPS: 21.3 m (horizontal distance), 3.45 m (vertical distance).

Paravane (starboard): 17.03 m (depth), 14.42 m (depth), 14.32 m (depth), 14.16 m (depth), 9.22 m (depth), 9.10 m (depth), 9.30 m (depth), 9.10 m (depth), 9.20 m (depth), 9.45 m (depth), 9.40 m (depth), 9.20 m (depth), 9.35 m (depth), 14.10 m (depth), 14.20 m (depth), 13.95 m (depth), 14.30 m (depth).

Streamers: 16 streamers (streamer 1 to streamer 16) are deployed from the paravane (starboard).

Legend:

- paravane GPS antenna
- float at each junction box but the outer ones
- float between streamers 6, 7, 8, 9, 10, 11

Source: 2 GI-Guns in harmonic mode

GPS-GUN-OFFSET: 6.57 m to portside, 50.3 m aft

5.4.1.2 Seismic source

5.4.1.3 Data recording

Data were recorded with acquisition software provided by Geometrics. The analogue signal was digitized with a sampling rate of 0.5 ms. The seismic data were recorded in SEG-D format. Recording length was 3 seconds. One file with all channels within the streamer configuration was generated per shot. The corresponding logged shot file reports shot number and time information contained in an RMC string. The acquisition PC allowed online quality control by displaying shot gathers, a noise window, and the frequency spectrum of each shot. The cycle time of the shots

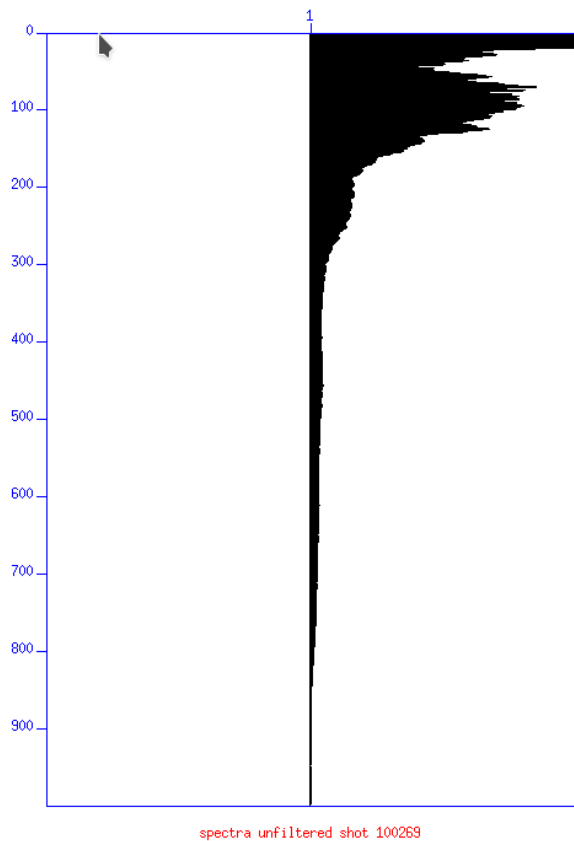


Fig. 5.43 Unfiltered frequency spectra for the 3D seismic experiment.

were displayed as well. The vessel's position and the positions of the P-Cable paravanes were simultaneously logged in the RMC string along with logged time and position information with GPS antennas.

5.4.2 On-board Processing

On-board processing included streamer geometry configuration, delay calculations and source and receiver depth control. From the seismic data a delay of -68 ms was evaluated. Post-stack quality control revealed this value to be too low, further evaluation has to be carried out at post-cruise processing. A receiver ghost effect in the seismic data could not be detected. Seismic traces (Fig. 5.44) were balanced and filtered using a bandpass filter with corner frequencies at 5, 45, 600, 800 Hz (Fig. 5.44) and a F-X deconvolution with a window width of 12 traces and a filter width of 4 traces (Random Noise Attenuation). The source and receiver locations were calculated and the traces were binned on a 6.25 m by 6.25 m grid, resulting in an even fold and reasonable coverage (Fig. 5.45). Subsequently, a normal move out correction (with a constant velocity of 1544.00 m/s, derived from a local CTD measurement) and stacking were applied. The stacked data were interpolated and then migrated in two passes (first cross-line then in-line) with a 2D Stolt migration algorithm using a constant velocity model (1500 m/s).

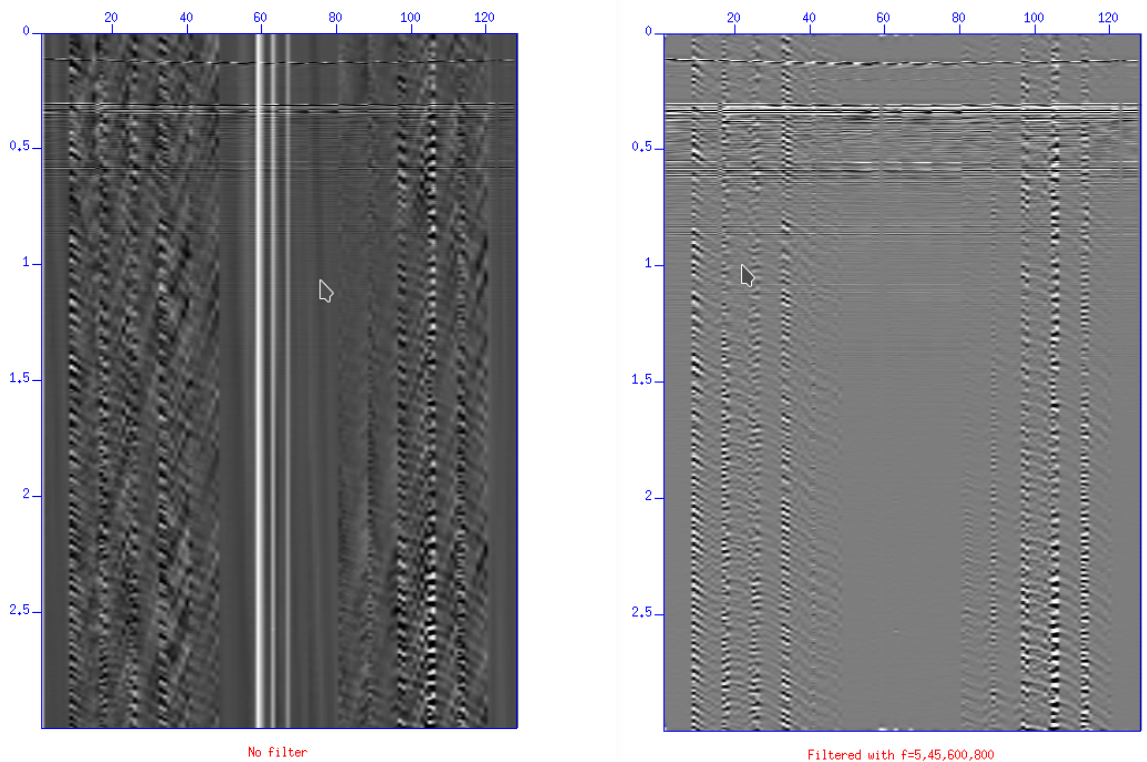


Fig. 5.44 Left: Unfiltered shot gather with travel time on the y-axis and channel number on the x-axis showing the first arrival of the direct wave (uppermost signal) and reflections from the subsurface afterwards. Low-frequency noise overlies the signal. Right: Bandpass-filtered shot gather using filter corner frequencies 5,45,450,550. The final bandpass filter used for processing had corner frequencies 25,45,450,550.

5.4.3 Preliminary results

The acquired P-cable seismic dataset covers an area of about 33 km² (Fig. 5.46). It covers part of the upper shelf, the morphological step, that we interpreted in the 2D seismic lines as an old coastline, and the horizontally layered deposits in the distal shelf. On board it was possible to process a first 3D cube including interpolation of the minor gaps in the fold map and Stolt migration with water velocity. The data processing will be refined when back at GEOMAR. The final data set will be used to map small-scale structures such as Karst features and faults to constrain the nature of the potential aquifers.

5.5 Multi-component ocean bottom seismometer deployments

(B. Schramm¹)

¹GEOMAR

5.5.1 Experimental setup

Ten multi-component Ocean Bottom Seismometers (OBS) were deployed to (1) record compressional and shear waves during the active source experiment around Malta and (2) six OBSs to record microseismic activity during a year-long deployment in the Etna area. OBSs are

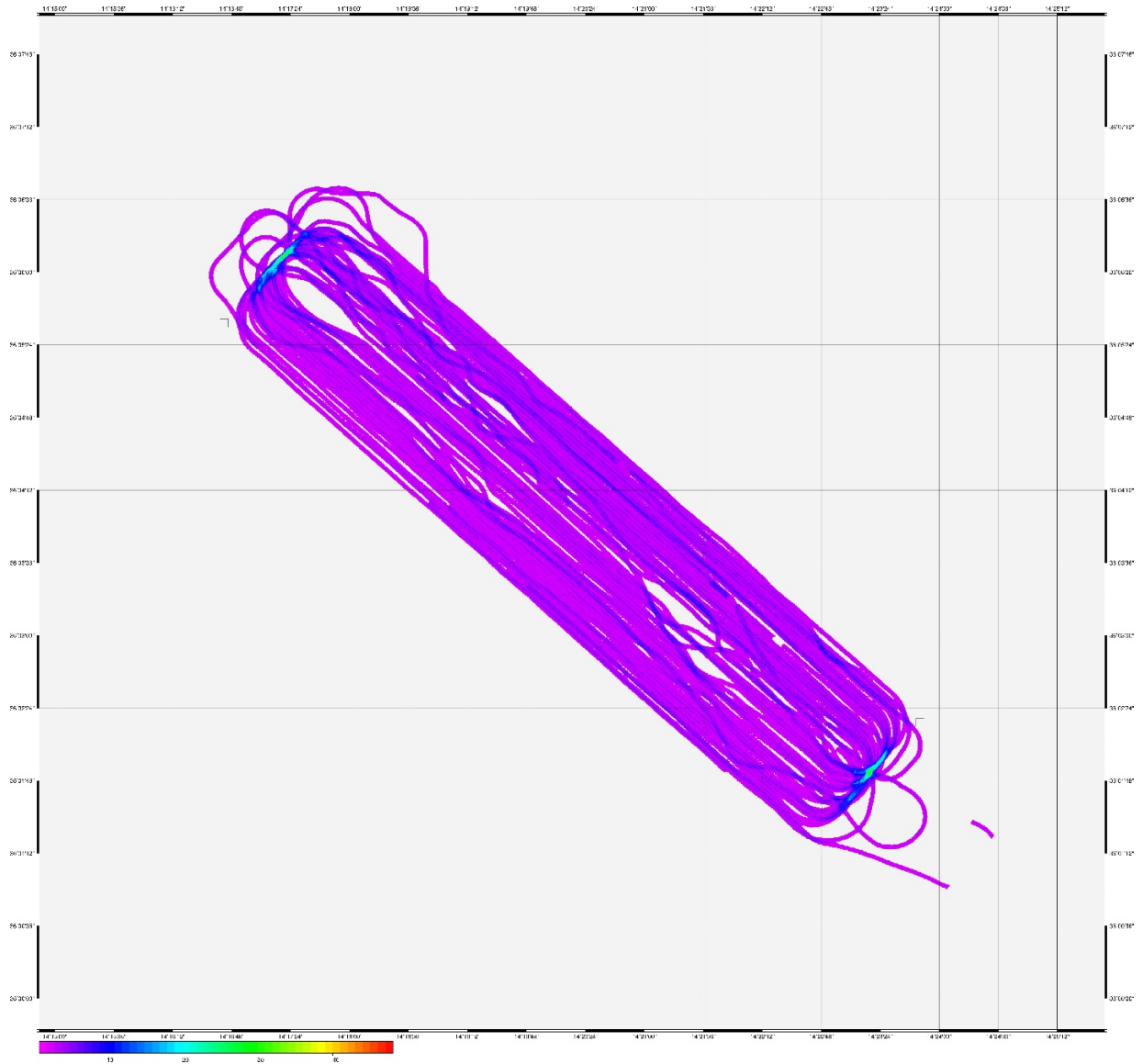


Fig. 5.45 Fold map of the 3D seismic experiment. Purple color indicates good fold coverage (traces per grid cell).

autonomous seafloor recording platforms, designed to record both, compressional and shear waves reflected and refracted through the sediment. They consist of four floats, which are connected to a frame and generally they are equipped with a 4.5 Hz three-component seismometer, a hydrophone and a data recorder encased in a high-pressure tube (Fig. 5.47).

All sensors are connected to the recording unit and continuously record the incoming signals. The system itself is less dense than water, so in order to deploy the device to the ocean bottom a weight is mounted to the frame and attached to a releaser. This releaser has an acoustic communication unit, which can be addressed from the ship to release the weight after the experiment. The OBS will then ascend to the sea surface and can be recovered. A flashlight, radio transmitter, and a flag are attached to the frame to increase the visibility of the OBS and to facilitate an easy and quick recovery.

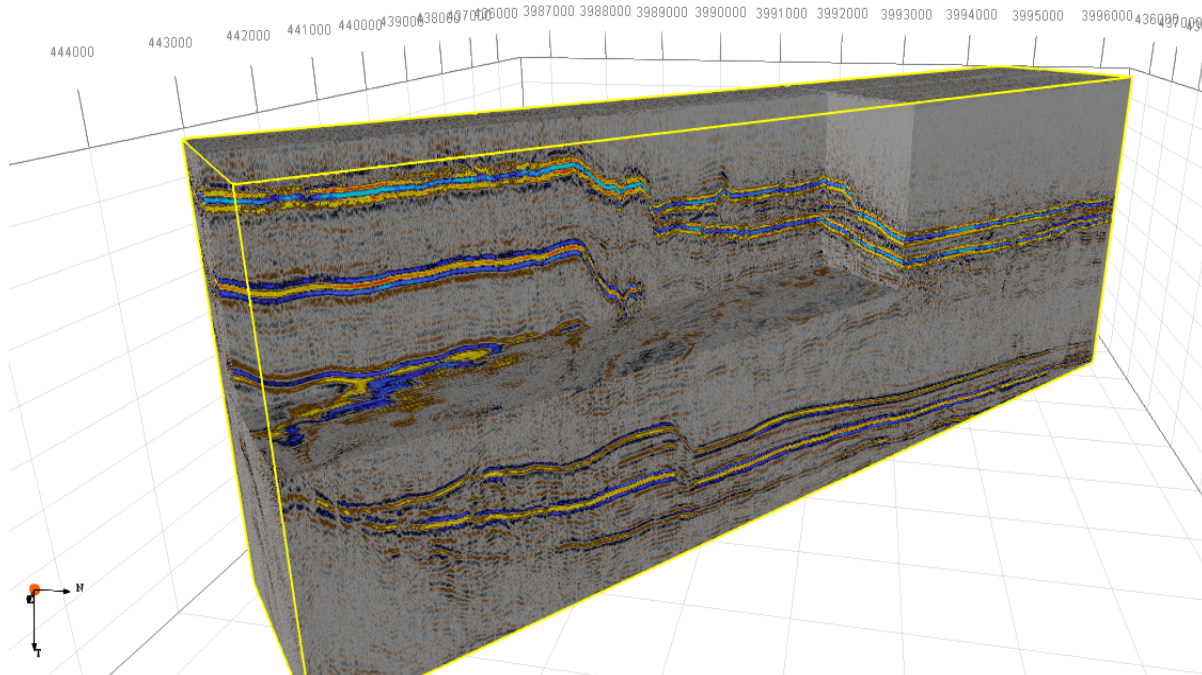


Fig. 5.46 Chair cut animation of the 3D data that cover an area from the upper slope down to the distal part.

Two different types of recorders were used during SO277: GEOLOGS and 6D6. The sample rate of all OBS recorders was set to 1000 Hz. The gain of the input channels was set to 16 for the three geophone components and to 1 for the hydrophone for the GEOLOG recorders. For the 6D6 recorders we used a gain of 1 for the hydrophone and 2 for the three geophone components. The station list is given in the appendix.

Additionally, two OBSs were equipped with a pressure tube of a new OBS prototype, a development for the ACT SENSE project. Unfortunately, just one of these Mini OBSs recorded data. They were attached to OBS01 and OBS10.

For the long-term deployment off Mt. Etna the sampling rate was reduced to 250 Hz in order to limit the data volume.

5.5.2 Preliminary results

Ten OBS were prepared and deployed in the 3D-MCS-cube on August the 27th 2020 (Fig. 5.36). The OBS array was designed to provide arrivals times for a seismic velocity analysis.

The two OBS equipped with an extra pressure tube (OBS1 and OBS10) were meant to record for six days during the 2D seismic experiment, but as mentioned above the Mini OBS on OBS10 did malfunction. The other instruments recorded data during both the 2D and 3D seismic experiments. A first quality control shows promising data (Figs. 5.48 and 5.49), but a detailed processing will have to be carried out after the cruise at GEOMAR. Especially the tomography on the shelf of Malta and the hard ground will pose a processing challenge.

Following the active source experiment, six of the OBS were prepared for long-term deployment in order to record micro-seismic activity related to tectonics and the stability of the Etna area. They were successfully deployed on September the 19th 2020.

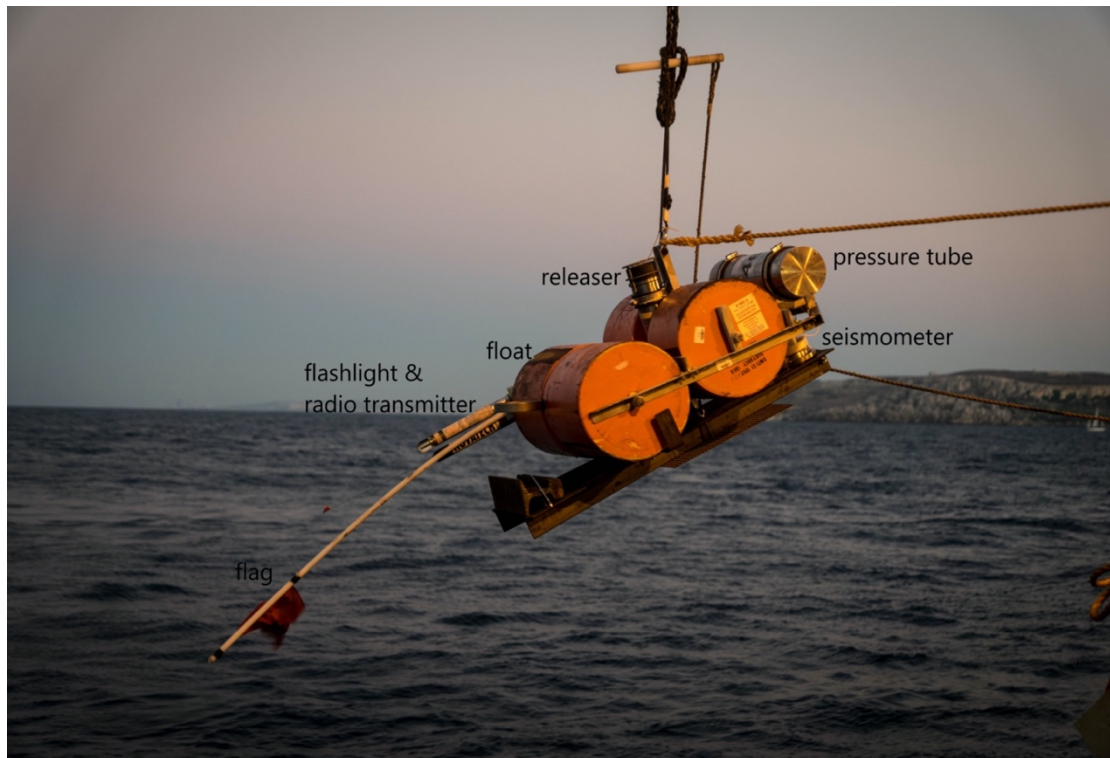


Fig. 5.47 Ocean bottom seismometer during the deployment in front of Malta.

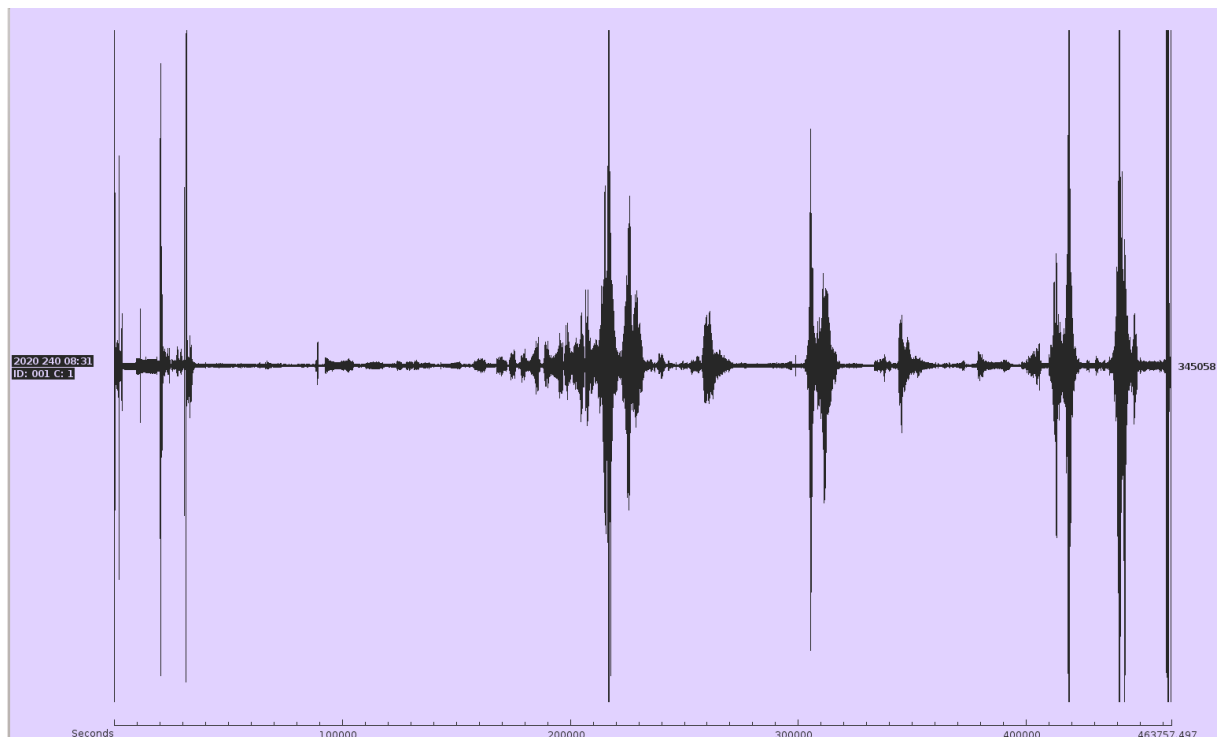


Fig. 5.48 OBS data example showing reflections on OBS09.

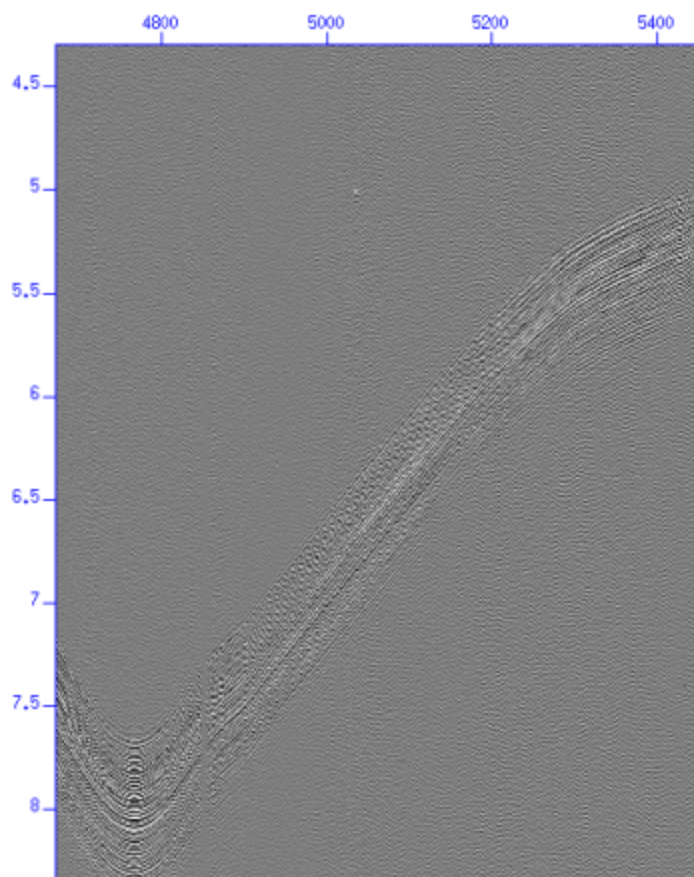


Fig. 5.49 OBS data example showing reflections on OBS09.

5.6 Geochemistry

(Thomas Müller¹, Mark Schmidt¹, Tino Spiegel¹, Henrike Timm¹, Anina-Kaja Hinz¹, Thore Sager¹, Morelia Urlaub¹, Helene Hilbert¹, Lea Rohde¹)

¹ GEOMAR Helmholtz Centre for Ocean Research Kiel

5.6.1 Introduction

The focus of interest of the SMART project are offshore aquifers, how they can be detected and characterized. To achieve this goal, three research objectives have been formulated for the OMAX cruise:

Objective 1 Building a geological model and constraining the volume and spatial extent of offshore aquifer(s) by geophysical data acquisition

Objective 2 Localize seep structures, which open a window into the aquifer at depth, using high resolution AUV based photo imagery, water column sensors and Parasound data

Objective 3 Characterize seeping groundwater to be able to interpret the geophysical data and provide background information for the hydrogeological models such as mixing, regional fluid flow rates, and age of the groundwater in the distal parts of the aquifer



Fig. 5.50 Deploying the online Video-CTD. Water sampler (11x10 L Niskin) rosette includes SBE9plus-CTD, O₂, turbidity (Chelsea), methane (Contros), CO₂ (Contros), pH (SBE), nitrate (SBE) and altimeter sensors.

The geochemical work can contribute in particular to objectives 2 and 3. The following tools were available for this purpose:

- Seafloor monitoring with a variety of sensors and by using a video camera
- Water column sampling
- Sediment and porewater sampling

The seafloor monitoring is used to detect anomalies, visually or in the sensor data. Expected anomalies are, for example, structures in the seabed that indicate fluid or gas leaks, elevated methane, nitrate or CO₂ concentrations or decreased salinity values of the water. If such anomalies occur, water samples can be taken and these places are then preferred locations for sediment sampling (Gravity core). Further locations for gravity coring have been derived from preliminary investigations and have been continuously adapted to the state of knowledge during the cruise. Pore-water samples taken from the gravity core samples may then provide insight into the original groundwater signal, as pore waters were expected to be less diluted by seawater especially in deeper segments.

5.6.2 Water column chemistry

5.6.2.1 Methodology

A video-guided Water Sampler Rosette/CTD system (VCTD, Fig. 5.50) was used to study oceanographic characteristics of the water column and to monitor the seafloor for fluid release structures and chemical/physical bottom water anomalies. The CTD (Sea-Bird Electronics, Inc. SBE9plus underwater unit) was a real-time data acquisition system transmitting data via coaxial

cable to the deck unit (Linke et al., 2015). The Water Sampler frame was equipped with Niskin bottles (11x10 L) to take water samples at interesting spots. An HD-Video camera (Canon LEGRIA HF G10) and LED light sources were attached to the lower part of the frame and are controlled by the telemetry deck unit via the 18 mm cable (~11 km total length) of winch 1 (“Speicherwinde 1”) onboard RV Sonne. The digital video and data telemetry system (Linke et al., 2015) providing real-time monitoring of the seafloor was also used to control the distance to the seafloor in “bottom view” mode. The VCTD rosette was equipped with additional sensors e.g. for dissolved gases, i.e. CO₂ and CH₄, and pH to monitor chemical anomalies near the seafloor (Schmidt et al., 2015). Veering (lowering) and heaving of the VCTD during station work was done with a rope speed of 0.5 m s⁻¹. The ship moved with 0.3 to 0.5 knts along predefined transects in bottom view mode.

The SBE9plus underwater unit was equipped with 2 pressure sensors, 2 temperature sensors, 2 oxygen sensors and 2 conductivity sensors. Furthermore, an altimeter sensor measuring distance between VCTD and seafloor, and a turbidity sensor (Chelsea Nephelometer) measuring suspended particulates and colloids were attached. The SBE underwater unit and Niskin bottle carousel motor were powered via the winch’s coaxial-cable by using the modem/power unit from Sea&Sun Technology (Linke et al., 2015). CTD data recording and triggering Niskin bottles were controlled with SEASAVE software (SBE7.21) on an external laptop. CTD data were recorded with 24 Hz. The ship’s GPS position data (SeaPath, Kongsberg SP 320-5+) was logged parallel to the CTD and Video data from NMEA-string of RV Sonne.

Hydro-casts and hydrographic data from towed SBE-CTD were processed by using SBE software SBE7.22.1. Usually, data files of 1 second bins and 1 meter bins were created from raw data files and exported to ASCII. CTD data was combined with data sets from external sensors by correlating their individual UTC time stamps.

HydroCTM-CH₄ sensors

The membrane inlet methane sensor (CH4P-1019-001, 4H-Jena Contros) had been mounted to the rosette frame replacing one Niskin bottle. The highly sensitive methane sensor was able to detect even smallest increases of dissolved CH₄ above an average background level of 1-2 nM (Schmidt et al., 2013). The sensor was connected to 5V external sensor connector of the SBE CTD underwater unit (A/D voltage channel 7) enabling online CH₄-data visualisation during recording. The methane sensor was powered by three NiMH-rechargeable battery packs (24 V, 9 Ah, 6000 m rated), which were mounted to the rosette frame.

SBE27-pH/O.R.P. sensor

The pH-sensor (SBE27-0287) combines a pressure balanced glass-electrode, Ag/AgCl reference probe, and a platinum O.R.P. electrode (1200 m rated).

HydroCTM-CO₂ sensors

The HydroC-CO₂ (CO₂-0412-005, 4H-Jena Contros) sensors, equipped with pumped (Seabird SBE-5T) sensor heads, were integrated into the Video-CTD device (Schmidt et al., 2015). Measured pCO₂-data is stored internally on SD card, however, the sensors reading is also monitored onboard by using one analogue 0-5 V channel of the SBE9plus. When running in VCTD-mode the HydroCTM-CO₂ is powered by an external NiMH-power unit (>10h at ~16°C).

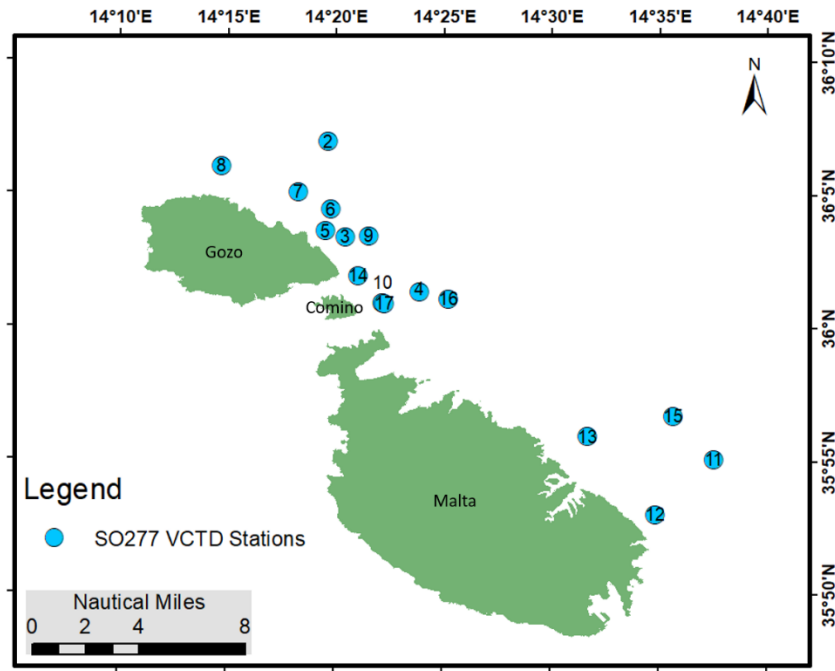


Fig. 5.51 Locations of Video-CTD stations at the eastern coast of Malta. Stations 10 and 17 were at the same location (different profiles).

Submersible Ultraviolet Nitrate Analyzer SUNA V2 (2k)

The SUNA nitrate sensor (SBE) is a chemical-free sensor which can be used in fresh, brackish and salt water. It is designed to measure the concentration of nitrate ions in water (Johnson and Coletti, 2002). The principle behind is the In-Situ Ultraviolet Spectroscopy (ISUS), developed at MBARI, California. Measurements are in units of micromoles per litre (μM). Internal data storage provides calibrated nitrate concentrations after sensor recovery. However, during this cruise not only power supply was provided via SBE9+ but also the serial port of the SUNA sensor was connected to analogue 0-5V input of SBE-device.

Nephelometer

A nephelometer (S/N 107513-001, Chelsea) powered by and connected to the SBE9+ underwater unit was attached in the lower department of the rosette frame. The sensor signal was used to detect turbidity anomalies in bottom waters.

5.6.2.2 Video-CTD stations

Towed Video-CTD measurements were performed in three different working areas. 16 stations were conducted east of off Malta (Fig. 5.51); 3 stations were conducted east off Sicily near volcano Etna (Fig. 5.52); and one station was performed near volcano Stromboli (Fig. 5.52). Details about VCTDs sampling locations etc. are summarized in table 1.

The stations off Malta are all located within a distance of maximum 8 miles to the coast. Selection criteria for station locations and towed tracks of the VCTD were based on preliminary investigations or were adapted to the current state of knowledge during the expedition. The former are largely related to electromagnetic investigations, water column anomalies and structural abnormalities (i.e. pockmarks) in the underground derived from backscatter data, the latter mainly to results of seismic data and bathymetric investigations. The working depths along the eastern

coast of Malta were always <200 metres, off Sicily the working depth was up to 2100 m, while in the Stromboli working area the VCTD was lowered to a maximum depth of 1579 m. Detailed information about VCTD stations, e.g. coordinates, time in the water, etc. are summarized in Table 9.

5.6.2.3 Recorded data sets

For each Video-CTD station the following sensor data were collected and were provided to shipboard scientific party after station end as xlsx-files which contain the following information: Time (UTC), water depth (m), conductivity (S m^{-1}), temperature ($^{\circ}\text{C}$), density (kg m^{-3}), sound velocity (m s^{-1}), oxygen ($\mu\text{mol L}^{-1}$), salinity, latitude ($^{\circ}\text{N}$), longitude ($^{\circ}\text{W}$), pressure (db), methane (ppm), carbon dioxide (μatm), turbidity (FTU), pH, potential temperature ($^{\circ}\text{C}$).

In addition to the continuous video recordings in HD, seafloor images of selected spots were taken in bottom view mode.

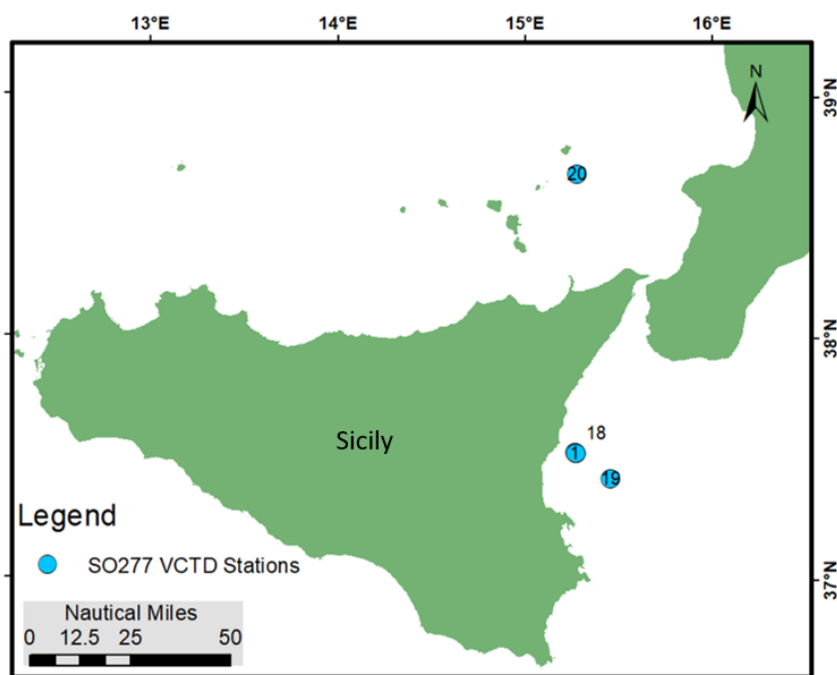


Fig. 5.52 VCTD stations at Sicily (1 and 18 were at the same location, 19) and at Stromboli (20).

Table 5.7 Overview of Video-CTD stations 01 - 05.

Name	Station	Location	Date	Activity	Time [UTC]	Lat	Lon	depth [m]	Comment
VCTD 01	2	Etna	23.08.2020	Station Start	22:05:02	37° 32,307	15° 15,615	-	no Niskin samples
				CTD in the water	22:18:10	37° 32,325	15° 15,649	-	
			24.08.2020	Bottom sight	01:35:25	37° 32,327	15° 15,645	1118,6	SL 1148 m
				Station End	04:34:39	37° 32,190	15° 15,652	1130,6	
VCTD 02	6	Malta depth profile	26.08.2020	Station Start	21:10:14	36° 06,954	14° 19,647	183,8	difficulties with winch, several stops, heaven with 0.1 m/s
				CTD in the water	21:23:27	36° 06,950	14° 19,618	184,0	
				Bottom sight	21:37:05	36° 06,953	14° 19,618	184,2	SL 187 m
				Station End	22:21:52	36°06,949	14° 19,616	184,2	
VCTD 03	7	Gozo south; pockmarks, gases,	27.08.2020	Station Start	00:12:04	36° 03,244	14° 20,317	75,4	no Niskin samples
				CTD in the water	00:15:27	36° 03,244	14° 20,317	75,4	
				Bottom sight	01:27:46	36° 03,240	14° 20,317	72,5	SL 72 m
				Station End	03:46:34	36° 03,524	14° 20,585	261,6	
VCTD 04	13	EM Line 5	01.09.2020	Station Start	22:06:22	36° 01,341	14° 23,908	52,8	CTD Start on Deck 21:20, in the water 22:10
				CTD in the water	22:10:01	36° 01,345	14° 23,897	52,5	
			02.09.2020	Bottom sight	22:16:28	36° 01,343	14° 23,898	52,7	Niskin samples 1 - 6, 8 -11 SL 52 m
				Station End	02:08:38	36° 02,399	14° 23,461	129,7	
VCTD 05	15	Seismic Line, (Profile 1027), pockmarks	03.09.2020	Station Start	07:44:27	36° 03,600	14° 19,536	67,5	CTD Start on deck; no Altimeter
				CTD in the water	07:46:51	36° 03,600	14° 19,537	67,7	
				Bottom sight	07:54:11	36° 03,597	14° 19,538	67,7	Niskin samples 1 - 4 SL 66 m
				Station End	11:16:17	36° 04,815	14° 20,673	165,0	

Table 5.8 continued Overview of Video-CTD stations 06 - 10.

Name	Station	Location	Date	Activity	Time [UTC]	Lat	Lon	depth [m]	Comment
VCTD 06	19	depresssion/ big pockmark	09.09.2020	Station Start	11:45:11	36° 04,412	14° 19,758	163,0	no Posidonia, no Altimeter Niskin samples 1 - 3 SL 158 m
				CTD in the water	11:48:01	36° 04,413	14° 19,775	163,0	
				Bottom sight	12:07:05	36° 04,415	14° 19,782	155,9	
				Station End	14:28:15	36° 04,379	14° 19,803	-	
VCTD 07	20	pockmarks eastern Gozo	09.09.2020	Station Start	16:30:19	36° 05,079	14° 18,277	136,5	no Altimeter, Problems to start Camera, Start after 10min in the water no Niskin samples SL 139 m
				CTD in the water	16:32:11	36° 05,078	14° 28,275	136,5	
				Bottom sight	17:01:19	36° 05,077	14° 18,276	136,1	
				Station End	20:05:33	36° 05,088	14° 18,069	136,3	
VCTD 08	23	vertical profile	10.09.2020	Station Start	10:05:56	36° 06,035	14° 14,726	175,2	no Altimeter, no Niskin samples CTD could not start SL 177 m
				CTD in the water	10:12:04	36° 06,035	14° 14,727	173,5	
				CTD back on deck	10:20:14	36° 06,035	14° 14,723	173,0	
				CTD in the water	10:30:34	36° 06,035	14° 14,728	172,0	
				Bottom sight	10:43:38	36° 06,036	14° 14,724	177,0	
				Station End	10:55:41	36° 06,036	14° 14,725	171,0	
VCTD 09	24	flare	10.09.2020	Station Start	11:40:12	36° 03,427	14° 21,543	133,5	no Altimeter, no Niskin samples SL 136 m
				CTD in the water	11:42:20	36° 03,430	14° 21,548	132,2	
				Bottom sight	11:58:44	36° 03,430	14° 21,550	133,0	
				Station End	13:31:12	36° 03,467	14° 21,596	135,5	
VCTD 10	36	flare Comino south	13.09.2020	Station Start	08:07:34	36° 00,922	14°22,215	33,5	no Altimeter, no Niskin samples SL 28 m
				CTD in the water	08:12:24	36° 00,925	14°22,215	34,0	
				Bottom sight	08:18:24	36° 00,928	14°22,212	34,5	
				Station End	09:54:34	36° 00,848	14°22,282	33,0	

Table 5.9 continued Overview of Video-CTD stations 11 - 14.

Name	Station	Location	Date	Activity	Time [UTC]	Lat	Lon	depth [m]	Comment
VCTD1 1	40	Pockmarks and Water column anomaly	14.09.2020	Station Start CTD in the water	10:43:05	35° 54,794	14° 37,847	116,5	no Altimeter, no Posidonia, no Niskin samples SL 119 m continue on profile SL 122 m
					10:44:55	35° 54,794	14° 37,859	116,4	
				Bottom sight CTD back on deck	10:56:28	35° 54,794	14° 37,868	116,6	
				CTD in the water	12:21:19	35° 54,775	14° 37,866	116,3	
					12:46:08	35° 55,106	14° 37,517	119,2	
				Bottom sight	12:55:35	35° 55,076	14° 37,529	118,4	
				Station End	13:50:11	35° 55,042	14° 37,317	118,1	
VCTD1 2	41	Water column anomaly	14.09.2020	Station Start CTD in the water	14:27:04	35° 53,001	14° 34,852	63,3	no Altimeter, no Posidonia, no Niskin samples SL 65 m
					14:29:30	35° 53,004	14° 34,854	63,4	
				Bottom sight	14:37:40	35° 53,001	14° 34,851	62,5	
				Station End	14:58:03	35° 52,980	14° 34,831	58,7	
VCTD1 3	42	EM Line 9	14.09.2020	Station Start CTD in the water	15:35:56	35° 55,925	14° 31,744	96,7	no Altimeter, no Niskin samples SL 100 m
					15:39:30	35° 55,918	14° 31,726	96,7	
				Bottom sight	16:00:25	35° 55,919	14° 31,714	96,7	
				Station End	17:26:19	35° 55,895	14° 31,979	99,4	
VCTD1 4A	54	Flare Comino Nord	16.09.2020	Station Start CTD in the water	13:39:11	36° 01,936	14° 21,069	39,0	VCTD 14: Camera could not start, VCTD back on deck no Altimeter, no Niskin samples SL 34 m
					14:31:31	36° 01,939	14° 21,075	37,8	
				Bottom sight	14:38:04	36° 01,939	14° 21,075	39,0	
				Station End	16:16:26	36° 01,772	14° 21,213	41,1	

Table 5.10 continued Overview of Video-CTD stations 15 – 20.

Name	Station	Location	Date	Activity	Time [UTC]	Lat	Lon	depth [m]	Comments
VCTD1 5A	56	hard rock structure at the seafloor	17.09.2020	Station Start CTD in the water	06:02:46	35° 56,701	14° 35,667	121,7	VCTD 15: Camera could not start, stop firing, stop CTD, wait 20 min, Restart no Altimeter, no Niskin samples
					06:04:20	35° 56,699	14° 35,669	121,7	
				Bottom sight	06:32:51	35° 56,703	14° 35,671	120,5	
				Station End	09:06:07	35° 56,688	14° 35,410	120,8	
VCTD1 6	57	Flare 12	17.09.2020	Station Start CTD in the water	10:19:21	36° 01,058	14° 25,243	54,5	no Altimeter, no Niskin samples
					10:25:24	36° 01,063	14° 25,246	55,5	
				Bottom sight	10:34:18	36° 01,065	14° 25,244	54,5	
				Station End	11:59:05	36° 01,359	14° 25,425	65,0	
VCTD1 7	61	Flare Comino S	18.09.2020	Station Start CTD in the water	15:06:26	36° 00,879	14° 22,216	33,8	no Altimeter, no Niskin samples
					15:07:17	36° 00,881	14° 22,285	34,5	
				Bottom sight	15:15:36	36° 00,882	14° 22,275	34,2	
				Station End	16:25:29	36° 00,882	14° 22,285		
VCTD1 8	65	Etna 1	19.09.2020	Station Start CTD in the water	07:02:02	37° 32,133	15° 15,892	1192,5	no Altimeter, no Niskin samples
					07:05:10	37° 32,127	15° 15,891	1196,2	
				Bottom sight	07:49:15	37° 32,161	15° 15,878	1192,3	
				Station End	09:32:52	37° 32,114	15° 15,836	1198,7	
VCTD1 9	67	Etna 2	19.09.2020	Station Start CTD in the water	14:19:09	37° 25,778	15° 26,670	1966,2	no Altimeter, CTD Start on Deck Niskin samples: 1, 2, 3, 5, 6, 8
					14:20:36	37° 25,778	15° 26,669	1965,4	
				Bottom sight	15:20:09	37° 25,786	15° 26,670	1964,5	
				Station End	18:40:43	37° 25,822	15° 25,702	2173,8	
VCTD2 0	69	Stromboli	20.09.2020	Station Start CTD in the water	12:05:03	38° 41,529	15° 16,335	1577,0	no Altimeter, no Posidonia, no Niskin samples, CTD Start on Deck
					12:11:53	38° 41,528	15° 16,333	1576,2	
				Bottom sight	13:10:35	38° 41,529	15° 16,333	1578,4	
				Station End	14:16:48	38° 41,527	15° 16,336	1579,0	

Niskin water sampling

Niskin water samplers triggered at selected spots at the seafloor were subsampled after retrieval on deck for various onshore laboratory analyses (Tab. 10). Major and trace element concentrations of seawater samples will be determined by using ICP-OES. Nutrients like nitrate and phosphate will be measured on 10 ml subsamples, filtered (0.2 µm) and frozen at -20°C, with an autoanalyser at GEOMAR. Ion chromatography will be used to analyse chloride, bromine, iodine and sulphate

content of the samples. Headspace gas sampling was performed by filling 120 ml glass vials, crimped with butyl-rubber stoppers, and replacing 10 ml of water by helium gas and poisoning with HgCl₂-solution. DIC samples (8 ml of seawater) were stored in glass vials after poisoning with 30 microliters of saturated HgCl₂-solution. Subsamples for IC (1.8 ml), ICP-OES (3 ml, acidified with 30 microliter HNO₃), and stable isotopes of water (~1.5 ml) were subsampled into plastic vials and stored at 4°C until onshore laboratory analysis.

Table 5.11 Niskin bottles sampled for onshore laboratory analyses.

Station	Date	Sampled Niskins (bottle no.)	ICP-OES	IC	DIC	Nutrients	$\delta^{18}\text{O}/\delta\text{D-H}_2\text{O}$	Headspace gas
Station 13 VCTD04	01.09.2020- 02.09.2020	1-6, 8-11	x	x	x	x	x	x
Station 15 VCTD05	03.09.2020	1-4	x	x	x	x	x	x
Station 19 VCTD06	09.09.2020	1-3	x	x	x	x	x	x
Station 67 VCTD19	19.09.2020	1-6, 8	x	x	x	x	x	x

5.6.2.4 Preliminary results

Malta

The recorded vertical profile (upcast) data of VCTD02 plotted in Fig. 5.53 shows oceanographic profiles characteristic of shallow Mediterranean waters in summer (i.e. temperature, salinity, oxygen, turbidity, and pH data). The data is highly variable between stations VCTD02 and VCTD17 as demonstrated with salinity vs. depths profiles (Fig. 5.54), but variability is comparable to other shelf areas in the Mediterranean Sea, when compared to e.g. Vargas-Yáñez et al., 2017. Neither salinity anomalies (freshening) nor temperature deviations from background data could be determined during towed VCTDs in bottom view mode. Measured partial pressure data of methane in bottom water is only slightly enriched by up to 2 ppm compared to surface water (Figs. 5.55 and 5.60). The calculated methane concentrations are ranging between 1.9 nM (surface water equilibrium) and maximum concentrations of 4.4 nM (bottom water). Dissolved oxygen maximum and dissolved CO₂-minimum at about 50 m water depth (VCTD06, Fig. 5.55) indicate productive photosynthesis above the pycnocline. No CO₂ anomalies differing from background were detected in bottom view mode.

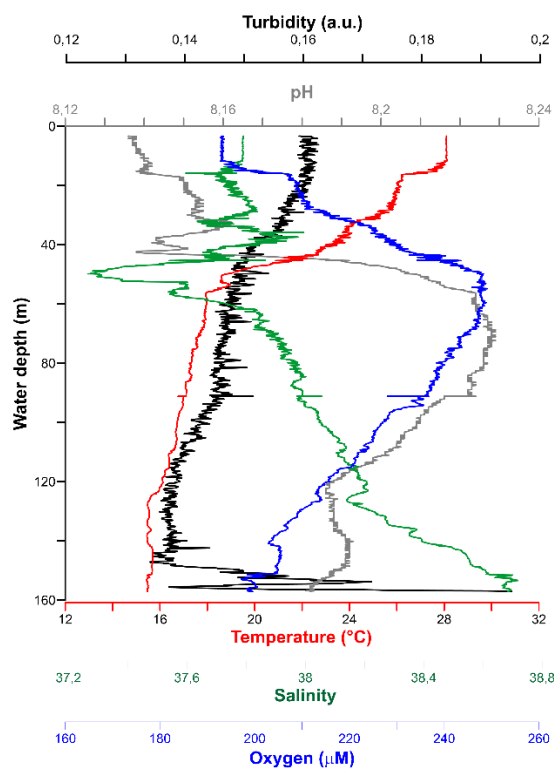


Fig. 5.53 VCTD02 as an example of different hydrographic parameters measured east off Malta in September.

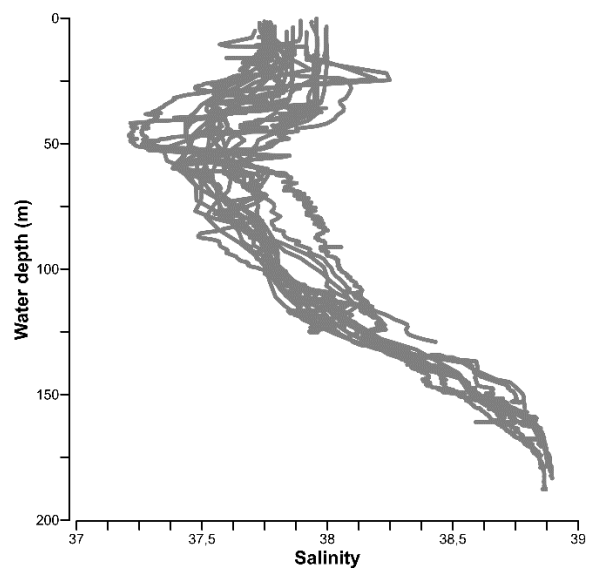


Fig. 5.54 VCTD02- VCTD17 demonstrates the range of salinity measured between 0 and 170 m below sea level east off Malta in September 2020.

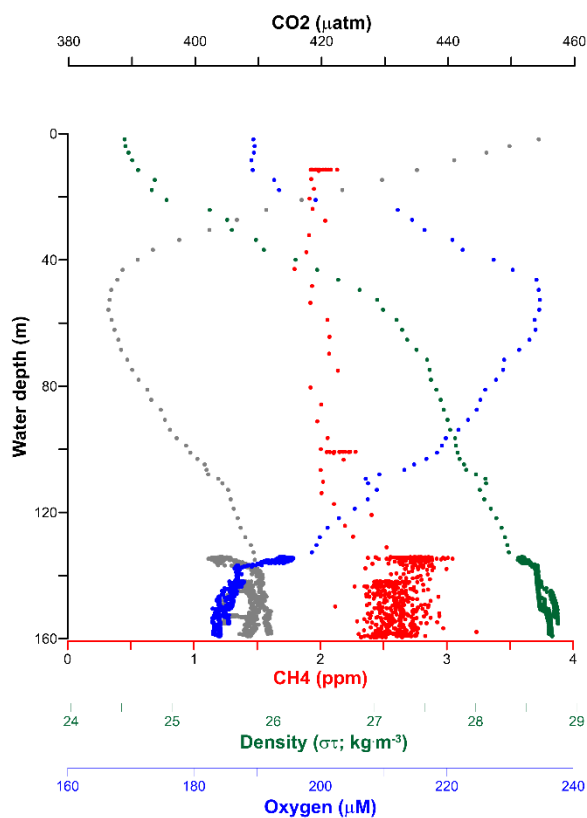


Fig. 5.55 Measured dissolved gas concentrations of station VCTD06 plotted with density.

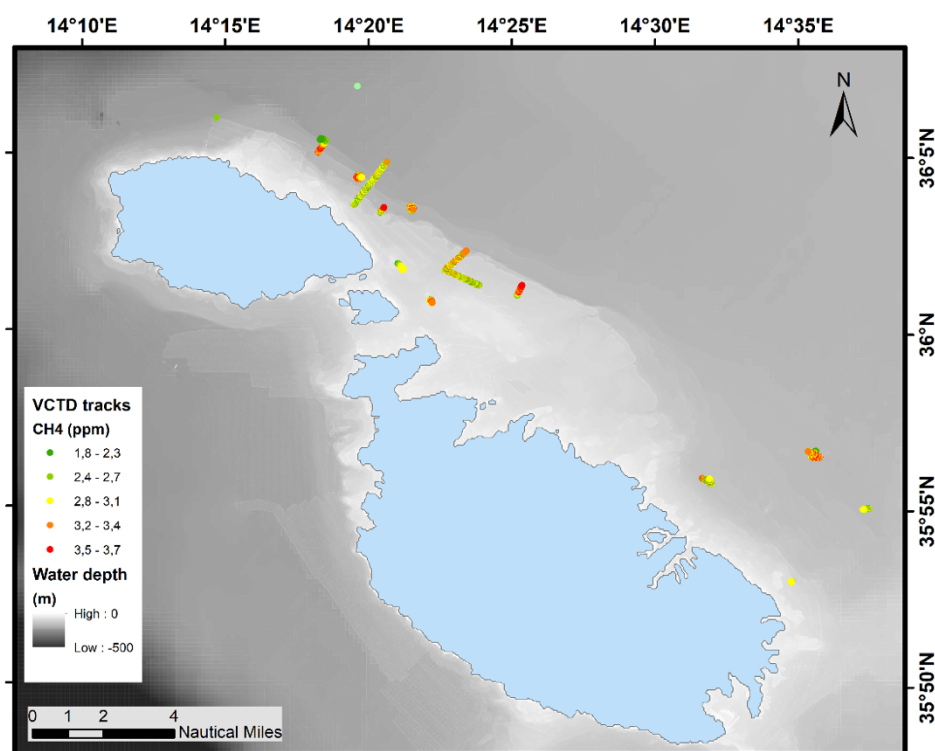


Fig. 5.56 Towed Video-CTD tracks indicating only minor changes of methane concentrations in bottom water at 1.5-3 m distance to seafloor (1.8-3.7 ppm).

Etna – Stations 2, 65, 67

In the working area east off Sicily in the Ionian Sea, submarine landslides and transform faults associated with volcanic and tectonic activities were of research interest. Three VCTD stations (VCTD 1,18, 19) were conducted in this area to mainly record sound velocity data and seafloor images. Luckily, a strong methane anomaly could be detected in a submarine channel at about 2100 mbsl (Fig. 5.57). The geological setting 40 km SE of Etna in combination with the methane anomaly, (authigenic?) rocks in the channel, and tube worm colonies living in the methane-rich bottom water raised questions about recent gas formation processes, e.g. by serpentinization (e.g. Schrenk et al., 2013; Polonia et al., 2017), methanogenesis related to organic matter degradation in sapropels (e.g. Bayon et al., 2013), or volcanic activity (e.g. Alessandro et al., 1997).

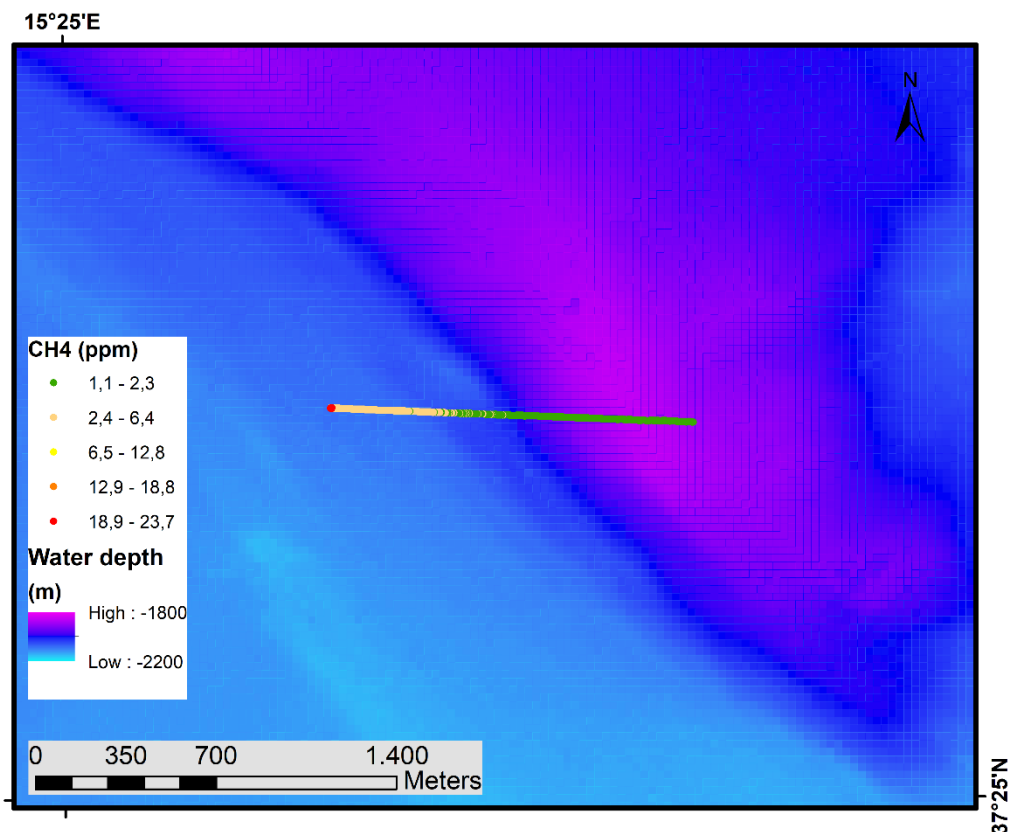
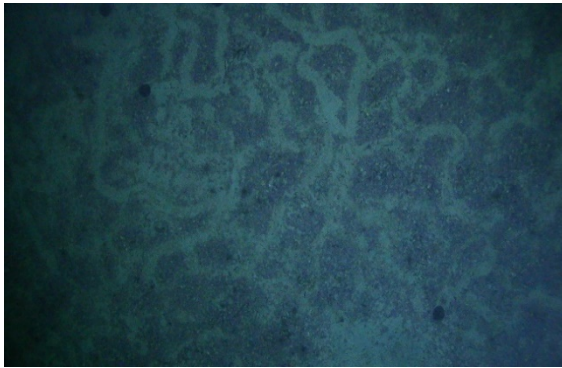


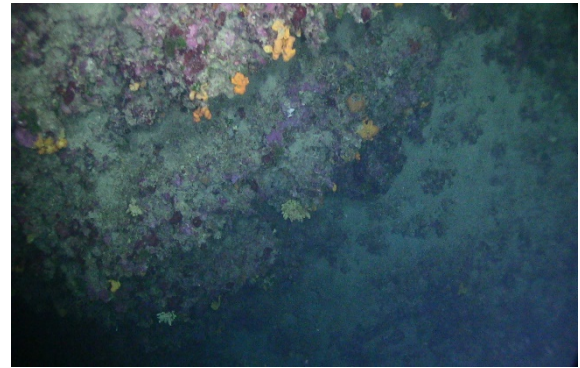
Fig. 5.57 Near-seafloor partial pressure data of dissolved methane measured during VCTD19 deployment in the working area ~40 km SE of volcano Etna, Ionian Sea.

Marine Life

Various marine organisms have been discovered on the seabed (Fig 5.58).



VCTD04 sea urchins grazing the solid seafloor



VCTD04 coral overgrown carbonate crusts/block



VCTD14 thick seagrass



VCTD14 seagrass, breeding area for fish?



VCTD17 seagrass on reef carbonates



VCTD19 tube worm colony in deep sea channel

Fig. 5.58 Marine organisms spotted at the seafloor during the towed VCTD tracks.

Marine Litter

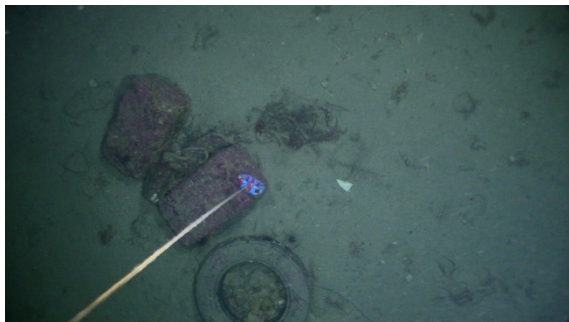
During the observations of the seafloor, marine litter was found at some locations. Quite often these were fishing lines or parts of fishing nets, but also beverage cans, glass bottles or concrete parts were spotted (Fig. 5.59).



VCTD03



VCTD09



VCTD13



VCTD13

Fig. 5.59 Marine Litter observed at the Seafloor. Clockwise from top left: soda can (VCTD 03), glass bottle (VCTD09), car tire and anchor weight/chain (VCTD13), fishing line (VCTD 13).

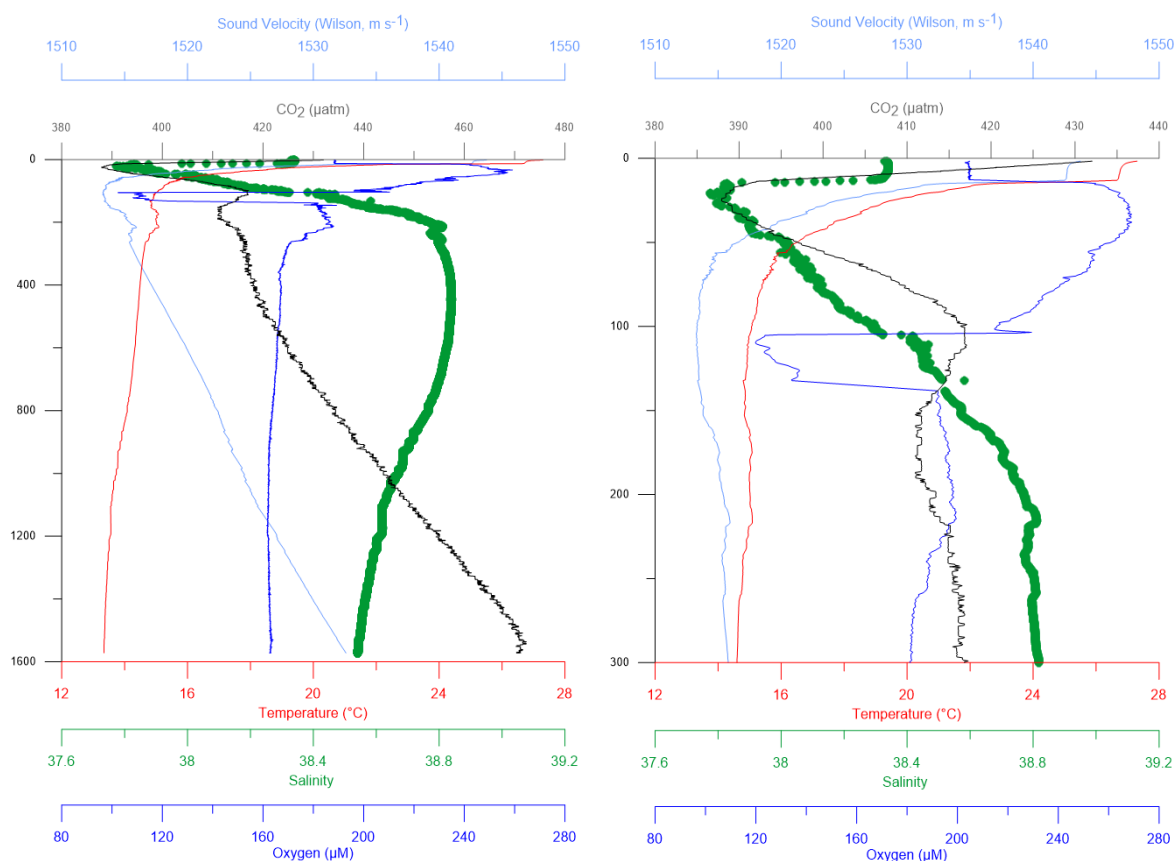


Fig. 5.60 Vertical profiles of sound velocity, CO₂, temperature, salinity and oxygen plotted against water depth of VCTD20 carried out next to Stromboli. left: total depth, right: upper 300 m.

Depth profile Stromboli Station 69 – VCTD20

The depth profile at Stromboli was taken to generate a profile of sound velocity which is an important prerequisite for the mapping of bathymetric data (generated by Parasound).

In the surface ocean CO₂ concentrations are characterized by a minimum at 390 µatm, most likely representing CO₂ consumption during primary production (Fig. 5.60). Afterwards concentrations continuously increase probably reflecting respiration in deeper waters, where CO₂ is produced by metabolism of organisms. Oxygen shows an opposite trend to CO₂ in that it increases in the surface ocean to a maximum of 260 µM, most likely due to O₂ production during photosynthesis of primary producers and decreases afterwards to a minimum of 100 µM in a pronounced horizon at about 100 m water depth, where respiratory processes partly consume the available oxygen. In deeper waters, O₂ concentrations show an either stable or gently decreasing trend. Temperatures decrease from 27°C to 15°C within the uppermost 100 m of the water column and gently decrease afterwards to a minimum of 13.5°C at 1600 m. Salinities decrease to a minimum 37.8 psu in the upper few meters of the water column and increase thereafter to a maximum of 38.8 psu at 200 m water depth. Below, salinity decreases again, this time with a gentle gradient to 38.5 psu at 1600 m water depth. Sound velocities through the water column are dependent on salinity, temperature and density. As such, they first decrease with increasing salinity and decreasing temperatures up to about 100 m water depth to 1514 m s⁻¹ and afterwards steadily increase to a maximum of 1532 m s⁻¹ at 1600 m.

Titration of total alkalinity and chloride

Total alkalinity concentrations in the water column range between 2.4 and 2.7 mmol l⁻¹, while chloride concentrations range from 585 to 620 mM. No obvious trends or anomalies can be seen in the water column profiles that point towards groundwater discharge (Fig. 5.62; Attachment 1).

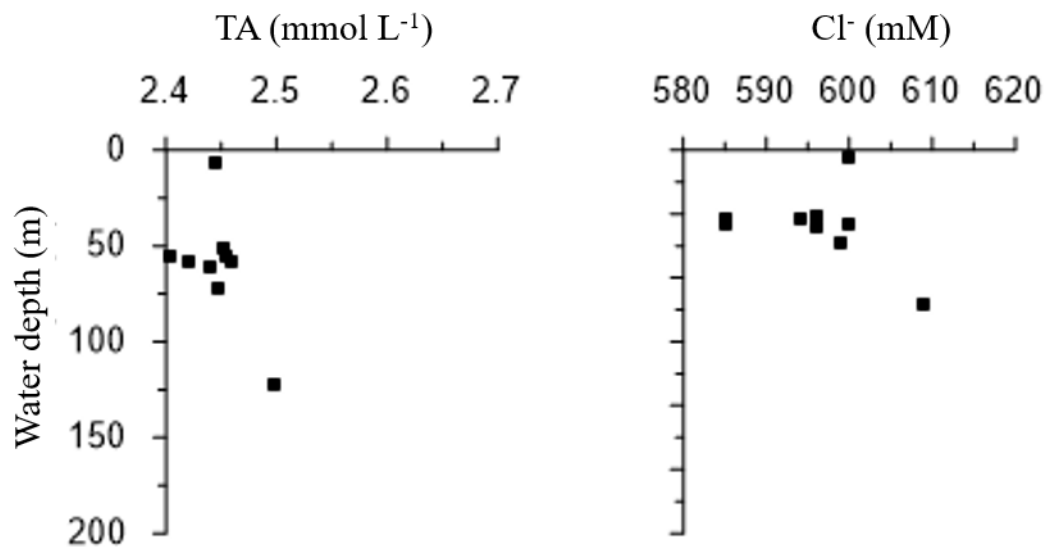


Fig. 5.61 Total alkalinity and chloride concentrations plotted against water depths of station 13 (VCTD04).

5.6.3 Gravity cores and pore water sampling

5.6.3.1 Methodology

Gravity coring

A gravity corer with 3 m stainless steel tube, inner plastic liner, and 1.25 tons head-weight was deployed for sediment sampling (Fig. 5.62). The speed of penetration at the seafloor was 1 m per second. The recovered sediment cores were cut in archive and working halves aboard and were subsequently processed at laboratory conditions (22°C).

Wet sediment subsampling

About 5 ml of wet sediment were taken in approximately 30 cm intervals and were collected in small plastic cups for porosity and TCNS analyses at GEOMAR. Three milliliters of sediment were added to 20 ml headspace vials filled with 1.5 g NaCl and 9 ml of saturated NaCl solution (Sommer et al., 2009). Vials were crimped with rubber stoppers and stored after mixing for further gas chromatographic and stable isotope measurements at GEOMAR. Five millilitres pre-cut plastic syringes were filled with wet sediment stored in aseptic plastic bags and frozen for subsequent microbial and biomarker analyses at ETH Zurich.



Fig. 5.62 Deploying the gravity corer.

Porewater sampling

Two different methods were applied to extract pore water from split cores halves. Where silty sand allowed Rhizon-extraction the method according to Seeberg-Elverfeldt et al. (2005) was applied. If not enough pore water for subsampling could be extracted by Rhizones, wet subsamples of sandy sediment had to be centrifuged for 5 minutes at 4000rpm at 25°C. As such, more than 10 ml of pore water were extracted every 30 cm with both methods. Aliquots of the extracted pore water were sub-sampled for various onboard and further home-based laboratory analyses. Subsamples for ICP-OES analysis were acidified with 10 µl of conc. suprapure HNO₃ per 2 ml of pore water sample (i.e., pH < 1) and ~1.8 ml subsamples for δD-, δ¹⁸O-H₂O and 1.8 ml for DIC were treated with 10 µl of HgCl₂ to inhibit further microbial degradation. All samples for home-based analyses were stored refrigerated and gas-tight.

Chemical titrations aboard

Chloride and alkalinity of pore water aliquots (1 ml) were immediately determined aboard according to Grasshoff et al. (1999).

5.6.3.2 Gravity coring stations

Gravity coring (GC) stations off Malta are all located within a distance of at maximum 6 miles to the coast (Fig. 5.63). Twenty attempts were made at 14 stations, with water depths between 38 and 148 meters (Table 11). At 7 stations a sediment core could be taken with sediment lengths from 67 to 284 cm. At the other locations, small amounts of sediment were obtained in the core catcher.

Selection criteria for station locations were based on preliminary investigations such as water column anomalies or elevated methane concentrations, high resistivity of the underlying formations as indicated from the electromagnetic data, or were adapted to the current state of knowledge during the expedition. These are, for example, the results from hydroacoustic and seismic data, indicating fluid or gas migration in the subsurface or flares imaged in the water column. Gravity core 9, for example, was taken because the seismic data (Line 1027) showed a change in polarity pointing to buried free gas in the Lower Coralline stratigraphic unit which is known as the main sub-terrain aquifer of Malta. The area around GC 9 was thus considered for detailed investigations by using four (Seismic, CSEM, VCTD, GC) different observation tools (Fig 5.64).

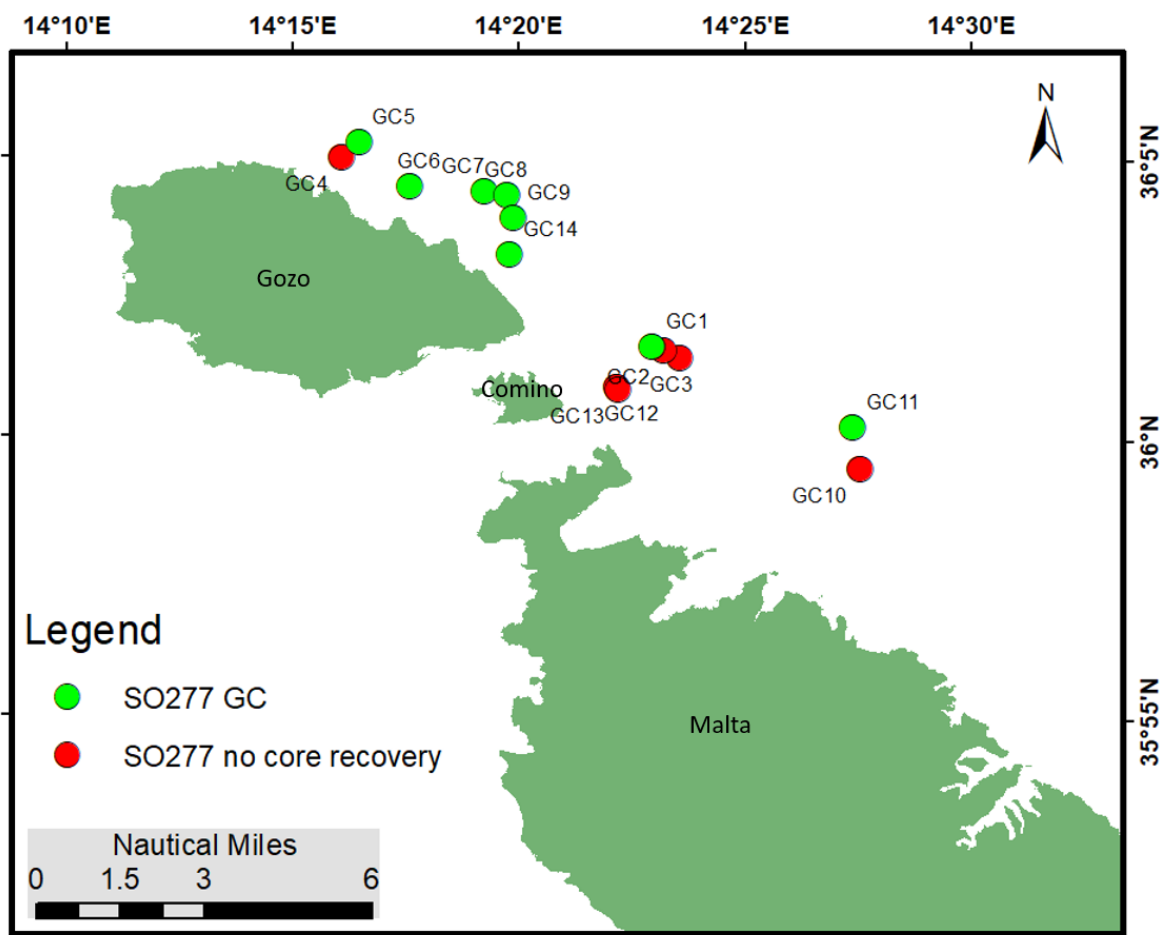


Fig. 5.63 Gravity core locations are marked in green (full segment of sediment liner) and marked in red (some sediment in core catcher only).

Table 5.12 Overview of gravity core locations.

GC	Station	date	Lat	Lon	depth [m]	Info	Sample	Sample length [cm]
GC1	27	11.0 9.	36° 01,656	14° 22,986	66	elev. methane, channel sediments, close to Line 5	GC1	192
GC2	28	11.0 9.	36° 01,591	14° 23,225	62	high Res EM Line 5	GC2 - empty, core catcher sample	Core catcher - sample
GC3	29	11.0 9.	36° 01,458	14° 23,593	60	high Res EM Line 5	GC3 - empty, core catcher sample	cc-sample
GC4	32	12.0 9.	36° 05,018	14° 16,103	53	channel sediments, Globigerina	GC4 - empty, core catcher sample	cc-sample
GC5	33	12.0 9.	36° 05,299	14° 16,478	92	channel sediments, Lower Coralline	GC5, GC5B	270; 273
GC6	34	12.0 9.	36° 04,496	14° 17,622	60	EM Line 8	GC6	278
GC7	45_1; 45_2	15.0 9.	36° 04,427	14° 19,258	126	dissolved gases	GC7, GC7A	67; 85
GC8	46	15.0 9.	36° 04,369	14° 19,748	148	seismics Line 5	GC8	155
GC9	47_1; 47_2	15.0 9.	36° 03,958	14° 19,913	131	big depression/ pockmark	GC9, GC9A	140; 150
GC10	50	16.0 9.	35° 59,49	14° 27,6	57	high Res EM Line 6	GC10, GC10A empty, core catcher sample	cc-sample
GC11	51	16.0 9.	36° 00,243	14° 27,425	68	elev. methane, channel sediments	GC11	76
GC12	52	16.0 9	36° 00,936	14° 22,218	38	Depression (sediment trap) in area of flares	GC12; 12A, empty, core catcher sample	cc-sample
GC13	53	16.0 9.	36°00,89 1	14° 22,246	40	Outcrop covered with sea gras	GC13; 13A, empty, core catcher sample	cc-sample
GC14	58	17.0 9.	36° 03,298	14° 19,833	68	Sediment slump area	GC14	2,84

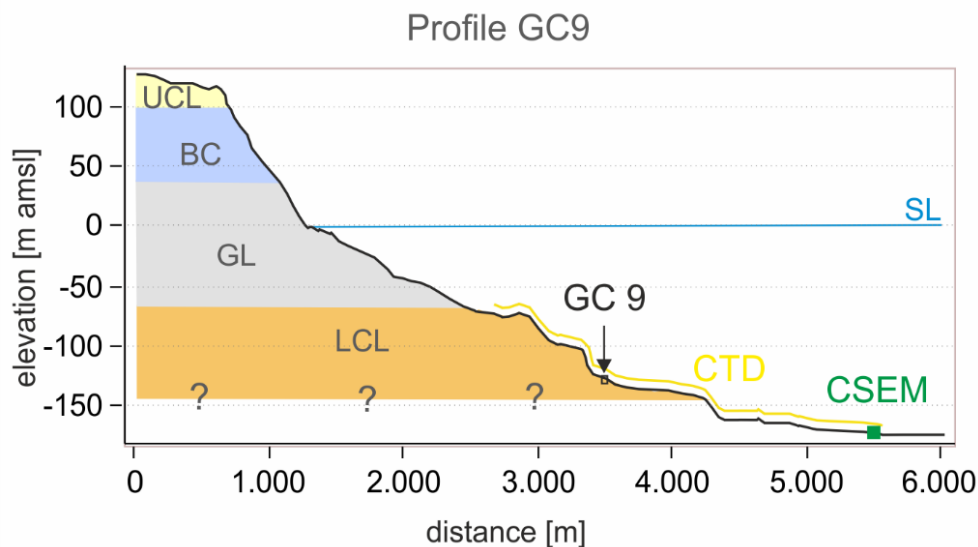


Fig. 5.64 Gravity core 9 was taken at the Seismic Profile Line 1027 at a depth of 131 m below sea level.

5.6.3.3 Preliminary results

A mixture of sand, silt and clay was found in the sediment cores (see appendices 2 to 19). The sediments are quite uniform across the sites, predominantly fine-grained and grey-greenish in color (Fig 5.65). Through all locations remnants of algae and seagrass are mixed with the sediments and fragments of corals and shells can be found. While only fragments of it are found in some sections of the cores (for example GC1), others have larger proportions (for example GC7).

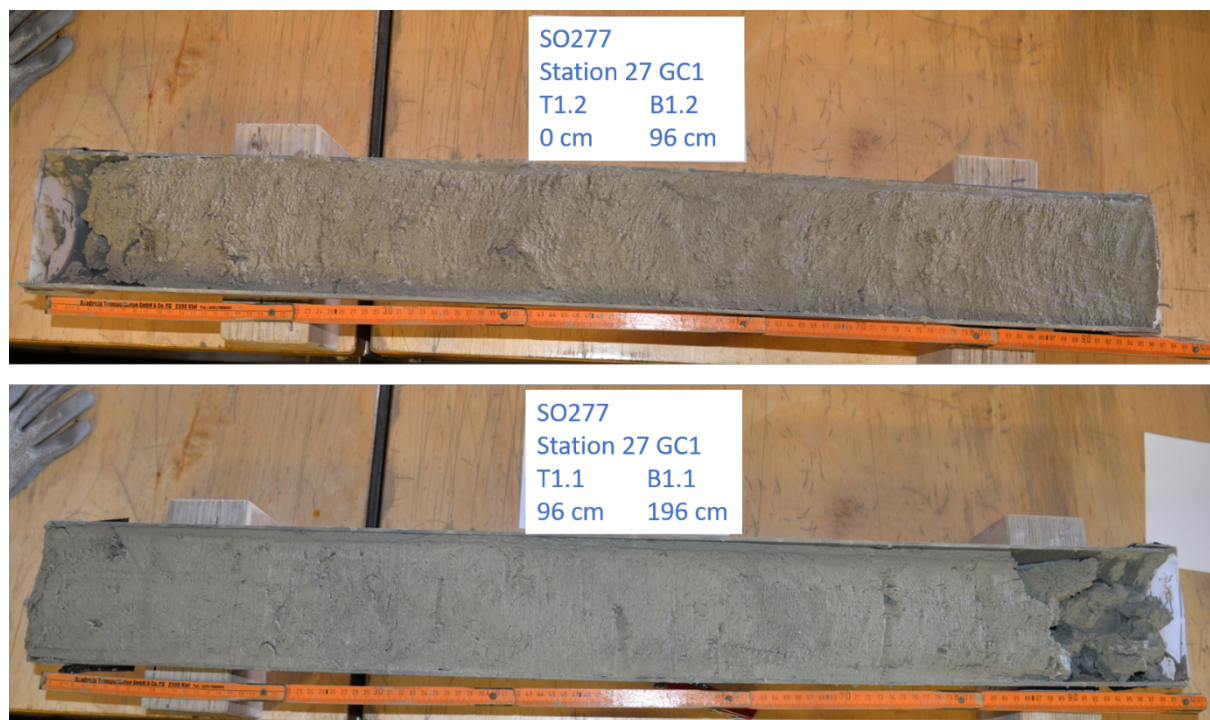


Fig. 5.65 Core photography of GC1. Mostly fine-grained grey to greenish sediments were found in GC1.



Fig. 5.66 Surface sediments obtained from core catcher; in clockwise direction starting from top left: GC3; GC2; GC5

Seabed description

Surface material (obtained from core catcher)

At locations where there was only little material in the core catcher, sediment samples were taken and will be classified at a later stage. At a first glance, it can be said that Maerl was found at some locations (Fig 5.66). This would support the results of Sciberras et al. 2009, who describe a maerl bed off the northeastern coast of Malta.

Titration of total alkalinity and chloride

Total alkalinity concentrations range between 2.2 and 3.1 mmol/l and are characterized by some downcore variability but generally little spatial variability between different sampling locations (Fig 5.67, Attachment 3). Despite being characterized by a distinct H_2S smell (see gravity core description, Attachment 1), total alkalinity concentrations at site GC14 do not illustrate a different trend due to sulfate reduction compared to other stations. Chloride concentrations are comparable

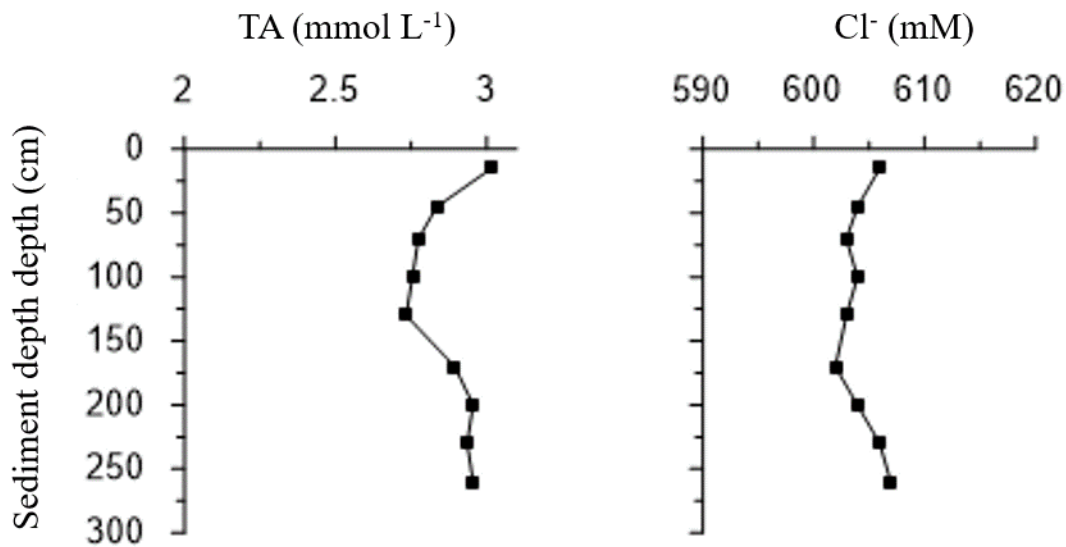


Fig. 5.67 Total alkalinity and chloride concentrations plotted against sediment depth. Pore water samples were taken at approximately 30 cm intervals (GC14).

between different sites, thus, indicating no distinct salinity anomalies in pore waters due to ground water influence.

5.7 AUV dives

(T. Korbjuhn¹, S. Reissmann¹, N. Diller¹)

¹GEOMAR

5.7.1 System overview

Anton and Luise are reconfigurable autonomous underwater vehicles (AUV) of the type Girona 500 (Fig. 5.68). They are designed for a maximum operating depth of up to 500m. The vehicle is composed of an aluminium frame, which supports three torpedo-shaped hulls of 0.3 m in diameter and 1.5 m in length as well as other elements like the thrusters. This design offers a good hydrodynamic performance as long as the space in between is not too occupied with additional payload. Nevertheless, it also offers a large space for housing the equipment while maintaining a compact size, which allows operating the vehicle from small boats.

The overall dimensions of the vehicle are 1 m in height, 1 m in width, 1.5 m in length and a weight of less than 200kg. The two upper hulls, which contain the flotation foam and the electronics housing, are positively buoyant, while the lower one contains the heavier elements such as the batteries and the payload. This particular arrangement of the components makes the separation between the center of gravity and the center of buoyancy about 11 cm, which is significantly more than any typical torpedo shape design. This provides the vehicle with passive stability in pitch and

roll, making it suitable for imaging surveys. One characteristic of the Girona 500 is its capability to reconfigure for different tasks.

The Cola2 infrastructure on those AUVs is the central control software, developed by IQUA Robotics (Girona, Spain). The communication under and above water is controlled by BELUGA. This marine command and software is developed by the AUV group GEOMAR. It also includes the USBL (Ultrashort Baseline) positioning. The belonging transducer/modem is mounted on the ship and is part of the BELUGA ad hoc network.

Besides the navigational sensors like INS (Inertial Navigation System), DVL (Doppler Velocity Log), Pressure Sensor, USBL and GPS it has a CTD (Conductivity, Temperature, Depth) type Seabird FastCAT SBE49 mounted by default. As one optional payload a CoraMo mk II Camera, which is developed by the GEOMAR AUV group, is mounted on both vehicles. This down or forward-looking camera system for photographic surveys

can take up to 2 images per second with a resolution of 12.34MP. CoraMo brings connection for 8 high power LEDs. There are several other payload available like a DeltaT multibeam or a magnetometer. During this cruise, AUV LUISE carried a nitrate sensor.

Missions (Fig. 5.68) can have a duration of up to 9 hours and a total length of about 10 kilometers, depending on settings, payload and environmental conditions like currents. The maximum speed is 1m/s while the minimum speed is not limited, even hovering at one point for an arbitrary amount of time is possible.

5.7.2 Sensors

5.7.2.1 Navigational

INS: iXblue Phins Combat C3

The internal navigation unit that processes sensor data and provides position information. The error of this INS is in range of $0,15^\circ$ for heading and $0,05^\circ$ for roll and pitch. This leads to a 0,3% DT position accuracy.

DVL: Teledyne RDI Explorer 600kHz

This device measures the velocity relative to the sea floor and its altitude.

Pressure sensor: Valeport ultraP

This sensor measures the pressure and converts it to water depth.

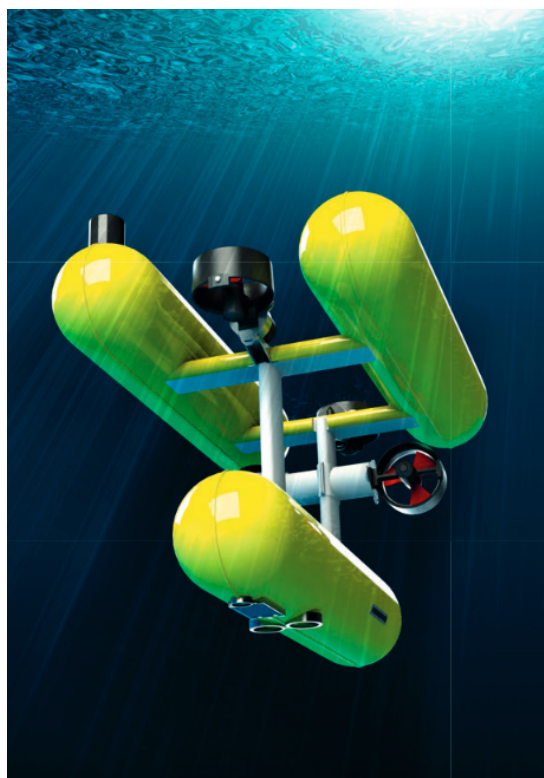


Fig. 5.68 Girona 500 AUV.

USBL: Evologics S2CR 18/34

The Evologics S2CR 18/34 modem combines underwater acoustics and positioning.

GPS: Quectel l86 GNSS module

The GPS is used to determine the absolute position at the surface.

5.7.2.2 Payload

CTD: Sea-Bird SBE 49 FastCAT

This measurement device acquires the conductivity, temperature and the pressure of the water and calculates the sound velocity. A csv file with the data is produced for each mission and can be found in the missions “01_exports” directory. Each line contains a timestamp, the position (latitude and longitude as decimal degrees) and the CTD data itself: pressure [dBar], salinity [psu], temperature [°C], conductivity [S/m] and sound velocity [m/s].

CoraMo mk II Camera

The images and the corresponding metadata can be found in the missions “03_pictures” directory. The camera has several parameters that can be set for every dive. For each image, a csv file containing information about parameter settings of the camera and the coramo system in total as well as navigational and environmental information (e.g. position and temperature) from the time the image was taken is written. It has the same name as the corresponding image. Additionally one combining file containing each single csv files data line is created after a dive (images_metadata.csv) and can also be found in the pictures directory. Depending on the settings, a second file with metadata (00_metadata_information.csv) is written during the dive. It contains less information about camera and system parameters and focuses more on the information needed

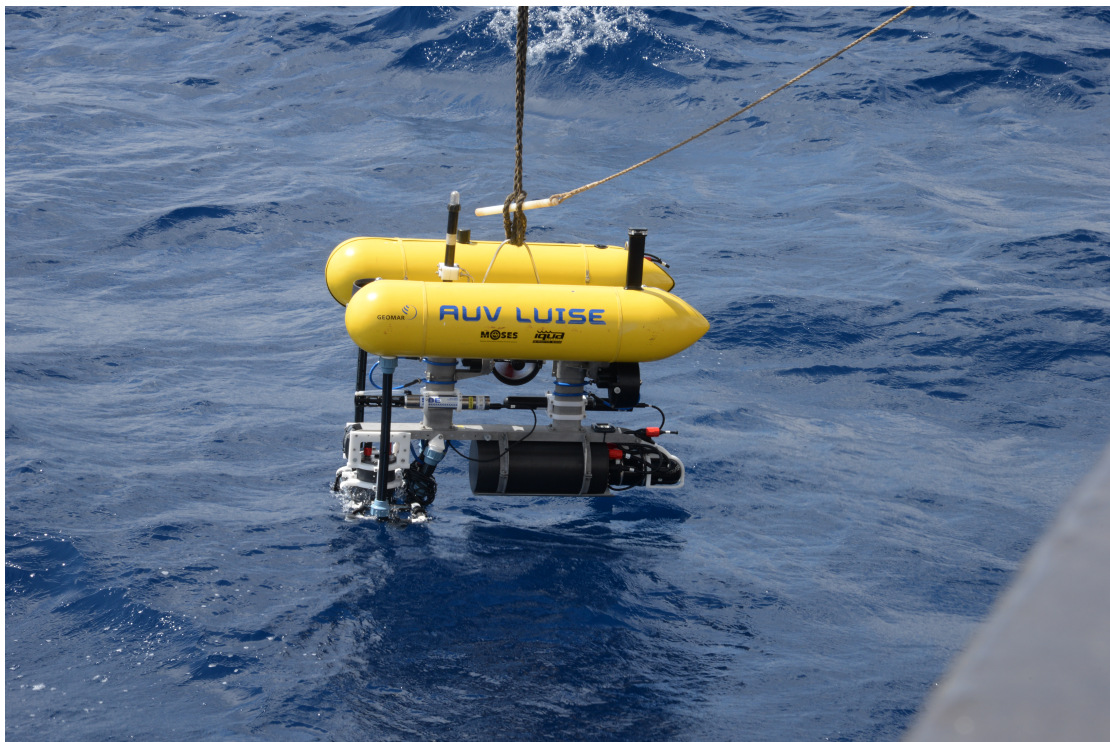


Fig 5.69 Deployment of AUV LUISE.

to build mosaics from the images like position, rotation and general information about the camera equipment.

Imagenex 837B DeltaT 4000

The optionally mounted multibeam sonar is used for mapping purposes. It has not been used on SO277.

Nitrate Sensor Sea-Bird SUNA V2

This nitrate sensor was mounted on AUV LUISE and supplied with power by the AUV. It is not integrated into the system. The sensor was maintained by geochemistry group on SO277.

5.7.3 Dives

In total six AUV dives took place on this cruise. The basic information about those can be found in the Table 12 followed by a short description of each dive and some example images taken by the AUV.

Table 5.13 Dive overview

Station	Date 2020	AUV	Dive No.	Center Position	Area	Mission Time	Altitude	Depth	Speed	Length	Data
008	27.8	Luise	42	35° 57.972 N 14° 26.177 E	150m x 65m	4.5h	1.5m	~47m	0.4m/s	5966m	~4700 images, CTD, Nitrate
018	09.9	Luise	43	36° 4.460 N 14° 17.682 E	750m x 16m	4.5h	1.8m	~70m	0.4m/s	6020m	~15500 images, CTD, Nitrate
028	12.9	Luise	44	36° 00.920 N 4° 22.226 E	140m x 140m	6.5h	2.0m	~40m	0.4m/s	8383m	~22500 images, CTD, Nitrate
037	13.9	Luise	45	36° 1.293 N 14° 25.425 E	45m x 45m	1h	1.7m	~70m	0.4m/s	984m	~3500 images, CTD, Nitrate
044	15.9	Luise	46	36° 1.771 N 14° 21.247 E	170m x 100m	6h	1.7m	~47m	0.4m/s	7797m	~14000 images, CTD, Nitrate
049	16.9	Luise	47	36° 3.566 N 14° 26.421 E	190m x 100m	6.5h	1.7m	~150m	0.4m/s	8560m	~15000 images, CTD, Nitrate

Total

~29h mission time

~75200 images

~37700 m length

27.08.2020, Station 008, Luise_042, 07:00 – 11:30 UTC

The first AUV dive on OMAX cruise was placed close to the coast of Malta near to the city Qawra. In this area, pockmarks were assumed. A second reason to choose that region was the idea to use the AUV images to get permission for gravity cores there. Due to technical reasons, the camera did not record the whole dive. Because of the shallow water, coring would not have been possible in that region. On the images recorded and the depth profile of the dive, no pockmarks could be found.

09.09.2020, Station 018, Luise_043, 11:00 – 15:30 UTC

This dive area in front of Gozo was again chosen because permission for gravity cores should be requested with the images. The dive area included two possible pockmarks, which could not be detected in the images of the AUV. The planned core was permitted and taken later on the cruise. The images show some sandy regions as well as overgrown ones (Fig. 5.70).

12.09.2020, Station 028, Luise_044, 06:00 – 12:30 UTC

The next dive was placed in front of Comino, in the direction of Malta. In that area flares were assumed and gravity cores were planned. The dives images show stony, overgrown as well as sandy regions. The mosaic matches well with backscatter data of that region. The flares could not be detected in the images but gravity cores could be taken in that area later on the cruise after getting permission.

13.09.2020, Station 037, Luise_045, 12:30 – 13:30 UTC

This dive was shortened to about one-hour mission time because of bad weather conditions, which only allowed deploying the AUV about two hours later than planned. The dive took place in front of Malta close to a possible old river structure on the ground. The images of that dive do all show

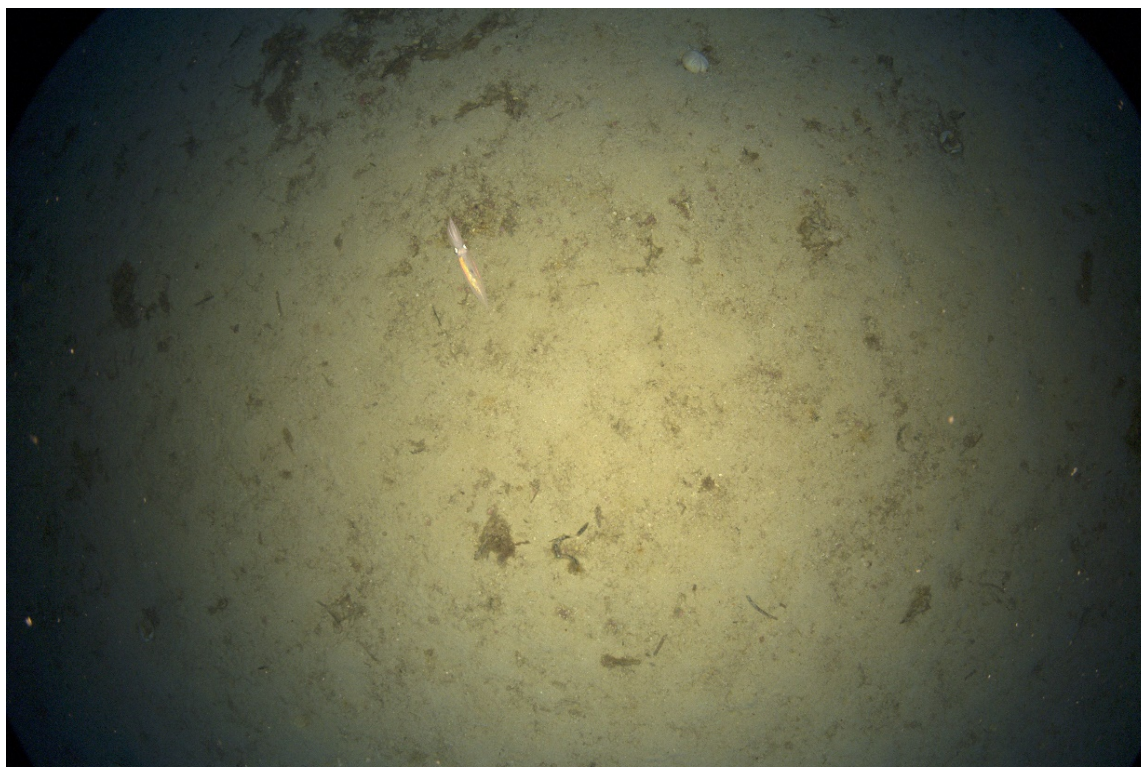


Fig. 5.70 Example photograph taken on dive Luise_043 showing sediment covered seafloor and a squid.

the same structures, which contain of sandy parts on the ground and groups of small stones and other things. These structures show a pattern, which may be the result of bioturbation. No flares could be detected in the images.

15.09.2020, Station 044, Luise_046, 06:30 – 12:30 UTC

Luisen dive number 46 took again place in front of Comino, in the direction of Gozo this time. Again, a possible flare was chosen. The images do again show stony overgrown as well as sandy regions. The portion of plants in that regions seems to be increased compared to the first Comino dive (Luise_044). In the images, no flare could be detected so far.

16.09.2020, Station 049, Luise_047, 06:00 – 12:30 UTC

This dive took place in front of the plateau in front of the islands at a depth of about 150 meters. Because of the depth and the lack of DVL bottom lock, some drift in the navigation of the AUV was expected. It is not possible to say how much the drift was when the AUV reached the ground but when Luise reached the surface the offset was about 50m in south east direction. Again, some possible flares were the reason to choose that area. The images do all look quite similar for the whole dive. The floor consists of some sand or sediment that seems to be relatively soft. The whole ground shows some small holes of different sizes. The images show some string like objects that might be bubble chains but might also be some biological structures. In the area covered several skeletons of marine mammals were found (Fig. 5.71).



Fig. 5.71 Example photograph taken during dive Luise_047 showing the carcass of a marine mammal.

6 Station List SO277

Table 1: Overall Station List.

Date	Station	Gear	Time	Depth	Latitude	Longitude	Remarks
2020	SONNE		UTC	[m]	[°N]	[°E]	
23.8.	SO277_1-1	MB	14:08:00	1303,99	38° 21.636' N	014° 48.500' E	rwK: 093°; d= 11nm
23.8.	SO277_1-1	MB	15:00:14	608,06	38° 20.851' N	014° 59.875' E	rwK = 090°, d= 24nm
23.8.	SO277_1-1	MB	15:11:00	852,91	38° 20.851' N	015° 02.632' E	Unterbrechung wg. Verlassen Aufzeichnungsgebiet
23.8.	SO277_1-1	MB	20:00:00	1154,45	37° 51.752' N	015° 26.567' E	Eintritt in neues Aufzeichnungsgebiet
24.8.	SO277_2-1	CTD	01:35:25	1118,58	37° 32.327' N	015° 15.645' E	BOSI, SL: 1148m
24.8.	SO277_2-1	CTD	02:25:32	1135,55	37° 32.185' N	015° 15.646' E	Beginn hieven
24.8.	SO277_3-1	AGSS	06:30:30	1021,07	37° 32.489' N	015° 15.478' E	Geosea GDS 2
24.8.	SO277_3-1	AGSS	06:31:16	1021,28	37° 32.490' N	015° 15.477' E	(Modem)
24.8.	SO277_3-1	AGSS	06:44:54	1024,01	37° 32.488' N	015° 15.482' E	Gewichte zu Wasser
24.8.	SO277_3-1	AGSS	06:47:15	1024,02	37° 32.488' N	015° 15.482' E	Bei SL: 10m Transponder am Draht
24.8.	SO277_3-1	AGSS	06:58:37	1024,50	37° 32.487' N	015° 15.479' E	AGSS zu Wasser, FW2/SPW2
24.8.	SO277_3-1	AGSS	08:09:56	0,00	37° 32.497' N	015° 15.472' E	SLmax: 1024m
24.8.	SO277_3-1	AGSS	08:12:23	0,00	37° 32.498' N	015° 15.472' E	AGSS ausgelöst
24.8.	SO277_3-1	AGSS	08:12:57	0,00	37° 32.498' N	015° 15.472' E	Beginn hieven
24.8.	SO277_3-1	AGSS	08:53:53	0,00	37° 32.500' N	015° 15.477' E	Gewicht an Deck
24.8.	SO277_3-1	AGSS	09:00:15	0,00	37° 32.501' N	015° 15.477' E	Modem an Deck, Ende Station
24.8.	SO277_3-2	AGSS	11:02:00	1186,87	37° 32.115' N	015° 15.784' E	Geosea GDS 4
24.8.	SO277_3-2	AGSS	11:03:05	1185,44	37° 32.115' N	015° 15.784' E	Modem zu Wasser über SB70 mit EL2
24.8.	SO277_3-2	AGSS	11:10:12	1185,34	37° 32.114' N	015° 15.784' E	Modem auf Tiefe, SL: 54m
24.8.	SO277_3-2	AGSS	11:14:50	1187,04	37° 32.113' N	015° 15.782' E	Gewicht zu Wasser über SB250 mit SPW2
24.8.	SO277_3-2	AGSS	11:17:27	1190,74	37° 32.113' N	015° 15.781' E	Transponder bei SL: 10m angebracht und zu Wasser
24.8.	SO277_3-2	AGSS	11:20:03	1188,86	37° 32.113' N	015° 15.779' E	AGSS Geosea + Auftriebskörper zu Wasser über Kran1
24.8.	SO277_3-2	AGSS	12:26:01	0,00	37° 32.120' N	015° 15.779' E	Ausgelöst, SLmax: 1165m
24.8.	SO277_3-2	AGSS	13:12:54	1175,79	37° 32.122' N	015° 15.781' E	Transponder an Deck
24.8.	SO277_3-2	AGSS	13:15:08	1172,76	37° 32.123' N	015° 15.781' E	Gewicht + Auftriebskörper an Deck
24.8.	SO277_3-2	AGSS	13:21:31	1173,24	37° 32.123' N	015° 15.781' E	Modem an Deck
24.8.	SO277_4-1	MB	15:49:33	447,26	37° 30.888' N	015° 10.363' E	rwK: 046°, d: 5nm
24.8.	SO277_4-1	MB	16:35:48	907,09	37° 34.103' N	015° 15.874' E	rwK = 226°, d= 5nm
24.8.	SO277_4-1	MB	17:24:38	517,39	37° 30.911' N	015° 10.992' E	rwK = 046°, d= 5nm
24.8.	SO277_4-1	MB	18:11:40	833,09	37° 34.244' N	015° 15.776' E	rwK = 226°, d = 5nm
24.8.	SO277_4-1	MB	19:00:01	514,33	37° 30.698' N	015° 11.558' E	rwK = 046°, d = 5nm
24.8.	SO277_4-1	MB	19:51:14	879,07	37° 34.214' N	015° 15.953' E	rwK= 226°, d = 5nm
24.8.	SO277_4-1	MB	20:38:24	594,02	37° 30.646' N	015° 11.786' E	rwK = 046°, d = 5nm
24.8.	SO277_4-1	MB	21:30:32	897,04	37° 34.174' N	015° 16.191' E	rwK = 226°, d = 5nm
24.8.	SO277_4-1	MB	22:15:43	689,88	37° 30.534' N	015° 12.250' E	rwK: 046°, d: 5nm
24.8.	SO277_4-1	MB	23:05:06	872,34	37° 34.192' N	015° 16.112' E	rwK: 225°, d: 5nm
24.8.	SO277_4-1	MB	23:52:06	767,51	37° 30.478' N	015° 12.501' E	rwK: 046°, d: 5nm
25.8.	SO277_4-1	MB	00:38:42	882,12	37° 34.177' N	015° 16.251' E	rwK: 225°, d: 5nm
25.8.	SO277_4-1	MB	01:26:21	893,09	37° 30.334' N	015° 12.763' E	Profilwechsel, rwK: 130°, d: 2nm
25.8.	SO277_4-1	MB	01:43:07	1173,70	37° 28.878' N	015° 14.806' E	rwK: 014°, d: 3nm

Date	Station	Gear	Time	Depth	Latitude	Longitude	Remarks
2020	SONNE		UTC	[m]	[°N]	[°E]	
25.8.	SO277 4-1	MB	02:15:45	1341,25	37° 32.050' N	015° 16.572' E	Switch on Parasound
25.8.	SO277 4-1	MB	02:23:30	1591,15	37° 31.897' N	015° 17.510' E	rwK: 192°, d: 3nm
25.8.	SO277 4-1	MB	03:04:00	1342,12	37° 28.895' N	015° 15.826' E	rwK = 014°, d = 3nm
25.8.	SO277 4-1	MB	03:50:37	1716,88	37° 31.896' N	015° 17.851' E	rwK = 189°, d = 3nm
25.8.	SO277 4-1	MB	04:34:05	1357,19	37° 28.885' N	015° 16.039' E	rwK = 012°, d = 3nm
25.8.	SO277 4-1	MB	05:19:47	1818,95	37° 31.842' N	015° 18.308' E	rwK = 188°, d= 3nm
25.8.	SO277 4-1	MB	05:29:34	1826,77	37° 30.896' N	015° 18.383' E	Unterbrechung Profil
25.8.	SO277 4-1	MB	15:00:00	1119,42	37° 32.252' N	015° 15.548' E	Fortsetzung Profil, rwK = 198°, d= 3nm
25.8.	SO277 4-1	MB	15:49:14	1242,00	37° 28.595' N	015° 15.838' E	rwK = 011°, d= 3nm
25.8.	SO277 4-1	MB	16:30:50	1473,21	37° 32.231' N	015° 17.192' E	rwK = 192°, d = 3nm
25.8.	SO277 4-1	MB	17:19:52	1594,84	37° 28.344' N	015° 17.917' E	rwK = 008° d = 2nm
25.8.	SO277 4-1	MB	17:57:19	1843,23	37° 31.931' N	015° 18.563' E	Ende Profil Nr. 2, Anfahrt Profil Nr. 3
25.8.	SO277 4-1	MB	18:19:20	1656,36	37° 33.777' N	015° 19.255' E	Beginn Profil Nr. 3 rwK = 185°, d= 6nm
25.8.	SO277 4-1	MB	19:21:37	1696,40	37° 27.458' N	015° 18.803' E	rwK = 004°, d = 6nm
25.8.	SO277 4-1	MB	20:28:51	1862,02	37° 33.512' N	015° 20.180' E	rwK = 184°, d = 6nm
25.8.	SO277 4-1	MB	21:35:43	1861,48	37° 26.988' N	015° 20.076' E	rwK = 004°, d = 6,5nm
25.8.	SO277 4-1	MB	22:44:01	1885,91	37° 33.328' N	015° 21.147' E	rwK: 183°, d: 7nm
25.8.	SO277 4-1	MB	23:52:47	1930,44	37° 26.536' N	015° 21.313' E	rwK: 003°, d: 7nm
26.8.	SO277 4-1	MB	01:07:25	1979,92	37° 33.257' N	015° 22.340' E	Profilwechsel, rwK: 308°, d: 2nm
26.8.	SO277 4-1	MB	01:24:12	1604,87	37° 34.452' N	015° 19.887' E	rwK: 034°, d: 13nm
26.8.	SO277 4-1	MB	03:26:15	1589,74	37° 45.141' N	015° 30.210' E	rwK: 214°, d: 13nm
26.8.	SO277 4-1	MB	05:15:28	1866,37	37° 34.445' N	015° 21.622' E	Ende Profil Nr. 4
25.8.	SO277 3-3	AGSS	05:56:46	0,00	37° 32.213' N	015° 15.548' E	GeoSea GDS 1
25.8.	SO277 3-3	AGSS	05:58:15	0,00	37° 32.214' N	015° 15.544' E	Modem zu Wasser (EL 2)
25.8.	SO277 3-3	AGSS	06:06:15	0,00	37° 32.216' N	015° 15.522' E	Gewicht zu Wasser (FW2/SPW2)
25.8.	SO277 3-3	AGSS	06:08:27	0,00	37° 32.216' N	015° 15.517' E	bei SL: 10m Transponder am Draht
25.8.	SO277 3-3	AGSS	06:09:48	0,00	37° 32.215' N	015° 15.518' E	AGSS
25.8.	SO277 3-3	AGSS	07:03:40	0,00	37° 32.216' N	015° 15.504' E	AGSS ausgelöst, SLmax: 1106m
25.8.	SO277 3-3	AGSS	07:47:59	0,00	37° 32.213' N	015° 15.512' E	Transponder + Auftriebskörper
25.8.	SO277 3-3	AGSS	07:49:32	0,00	37° 32.212' N	015° 15.511' E	Gewicht an Deck
25.8.	SO277 3-3	AGSS	07:54:13	0,00	37° 32.215' N	015° 15.509' E	Modem an Deck, Ende Station
25.8.	SO277 3-4	AGSS	08:19:41	0,00	37° 32.249' N	015° 15.680' E	GeoSea GDS 5, Modem zu Wasser (EL 2)
25.8.	SO277 3-4	AGSS	08:26:54	0,00	37° 32.250' N	015° 15.678' E	Gewicht zu Wasser (FW2/SPW2)
25.8.	SO277 3-4	AGSS	08:28:25	0,00	37° 32.249' N	015° 15.677' E	Bei SL: 10m Transponder am Draht
25.8.	SO277 3-4	AGSS	08:30:23	0,00	37° 32.248' N	015° 15.675' E	AGSS zu Wasser
25.8.	SO277 3-4	AGSS	09:28:06	0,00	37° 32.250' N	015° 15.669' E	AGSS ausgelöst, SLmax: 1125m
25.8.	SO277 3-4	AGSS	10:10:44	0,00	37° 32.251' N	015° 15.668' E	Transponder an Deck
25.8.	SO277 3-4	AGSS	10:13:14	0,00	37° 32.251' N	015° 15.668' E	Gewicht + Auftriebskörper an Deck
25.8.	SO277 3-4	AGSS	10:19:47	0,00	37° 32.251' N	015° 15.672' E	Modem an Deck
25.8.	SO277 3-5	AGSS	10:37:03	0,00	37° 32.433' N	015° 14.893' E	Geosea GDS 3
25.8.	SO277 3-5	AGSS	10:39:01	0,00	37° 32.436' N	015° 14.901' E	Modem zu Wasser
25.8.	SO277 3-5	AGSS	10:42:19	0,00	37° 32.434' N	015° 14.902' E	Modem auf Tiefe, SL: 34m
25.8.	SO277 3-5	AGSS	10:45:22	0,00	37° 32.432' N	015° 14.902' E	Gewicht zu Wasser

Date	Station	Gear	Time	Depth	Latitude	Longitude	Remarks
2020	SONNE		UTC	[m]	[°N]	[°E]	
25.8.	SO277_3-5	AGSS	10:47:47	0,00	37° 32.431' N	015° 14.899' E	Transponder bei SL: 10m angebracht
25.8.	SO277_3-5	AGSS	10:49:41	0,00	37° 32.431' N	015° 14.899' E	AGSS + Auftriebskörper zu Wasser
25.8.	SO277_3-5	AGSS	10:50:45	0,00	37° 32.431' N	015° 14.900' E	Beginn Fieren
25.8.	SO277_3-5	AGSS	11:25:58	0,00	37° 32.448' N	015° 14.906' E	BOKO, SLmax: 944m
25.8.	SO277_3-5	AGSS	11:33:53	0,00	37° 32.448' N	015° 14.907' E	AGSS ausgelöst
25.8.	SO277_3-5	AGSS	11:34:20	0,00	37° 32.448' N	015° 14.907' E	Beginn Hieven
25.8.	SO277_3-5	AGSS	12:09:26	0,00	37° 32.448' N	015° 14.907' E	Transponder an Deck
25.8.	SO277_3-5	AGSS	12:11:52	0,00	37° 32.448' N	015° 14.907' E	Gewicht + Auftriebskörper + Releaser an Deck
25.8.	SO277_3-5	AGSS	12:17:01	0,00	37° 32.445' N	015° 14.903' E	Modem an Deck
25.8.	SO277_3-6	AGSS	12:36:04	0,00	37° 32.264' N	015° 16.044' E	Geosea GDS 6
25.8.	SO277_3-6	AGSS	12:36:32	0,00	37° 32.265' N	015° 16.044' E	Modem zu Wasser
25.8.	SO277_3-6	AGSS	12:40:17	0,00	37° 32.272' N	015° 16.047' E	Modem auf Tiefe, SL: 34m
25.8.	SO277_3-6	AGSS	12:48:09	0,00	37° 32.278' N	015° 16.050' E	Gewicht zu Wasser
25.8.	SO277_3-6	AGSS	12:50:10	0,00	37° 32.281' N	015° 16.050' E	Transponder bei SL: 10m angebracht
25.8.	SO277_3-6	AGSS	12:52:24	0,00	37° 32.281' N	015° 16.050' E	AGSS + Auftriebskörper + Releaser zu Wasser
25.8.	SO277_3-6	AGSS	12:54:35	0,00	37° 32.282' N	015° 16.048' E	Beginn Fieren
25.8.	SO277_3-6	AGSS	13:44:14	0,00	37° 32.289' N	015° 16.046' E	BOKO, SLmax: 1185m
25.8.	SO277_3-6	AGSS	13:47:02	0,00	37° 32.288' N	015° 16.046' E	AGSS ausgelöst
25.8.	SO277_3-6	AGSS	13:47:21	0,00	37° 32.288' N	015° 16.046' E	Beginn Hieven
25.8.	SO277_3-6	AGSS	14:31:36	0,00	37° 32.287' N	015° 16.051' E	Ankerstein mit Auftriebskörper an Deck
25.8.	SO277_3-6	AGSS	14:45:10	0,00	37° 32.291' N	015° 16.050' E	Modem an Deck
26.8.	SO277_5-1	MB	07:41:06	1074,19	37° 32.345' N	015° 15.373' E	rwK: 142°, d: 3,5nm, v: 8kn
26.8.	SO277_5-1	MB	08:11:18	1837,58	37° 29.590' N	015° 18.167' E	rwK: 162°, d: 8nm
26.8.	SO277_5-1	MB	09:10:31	1967,40	37° 22.083' N	015° 21.330' E	rwK: 140°, d: 7nm
26.8.	SO277_5-1	MB	10:00:38	2261,94	37° 16.997' N	015° 26.623' E	rwK: 177°, d: 18nm
26.8.	SO277_5-1	MB	12:13:27	2617,18	36° 59.151' N	015° 27.804' E	rwK: 168°, d: 23nm
26.8.	SO277_5-1	MB	15:08:42	3226,56	36° 36.747' N	015° 32.855' E	Ende Profil
26.8.	SO277_6-1	CTD	21:10:14	183,76	36° 06.954' N	014° 19.647' E	Clean Ship liegt an
26.8.	SO277_6-1	CTD	21:23:27	184,00	36° 06.950' N	014° 19.618' E	FW1/SPW1
26.8.	SO277_6-1	CTD	21:37:05	184,23	36° 06.953' N	014° 19.618' E	Bodensicht, SLmax: 187m
26.8.	SO277_6-1	CTD	21:37:38	183,87	36° 06.953' N	014° 19.619' E	SZmax: 3,7kN
27.8.	SO277_7-1	CTD	00:20:21	72,89	36° 03.245' N	014° 20.316' E	Transponder bei SL: 10m angebracht
27.8.	SO277_7-1	CTD	00:52:09	73,11	36° 03.245' N	014° 20.325' E	Transponder an Deck
27.8.	SO277_7-1	CTD	01:19:24	72,28	36° 03.239' N	014° 20.317' E	Transponder bei SL: 10m angebracht
27.8.	SO277_7-1	CTD	01:27:46	72,49	36° 03.240' N	014° 20.317' E	BOSI, SL: 72m
27.8.	SO277_7-1	CTD	01:29:34	73,34	36° 03.242' N	014° 20.321' E	rwK: 037°
27.8.	SO277_7-1	CTD	03:38:35	258,36	36° 03.522' N	014° 20.586' E	Transponder an Deck
27.8.	SO277_7-1	CTD	03:43:27	258,66	36° 03.524' N	014° 20.587' E	CTD an Deck
27.8.	SO277_8-1	AUV_L	05:52:48	43,70	35° 58.225' N	014° 26.322' E	FW1/SPW1
27.8.	SO277_8-1	AUV_L	05:53:58	43,20	35° 58.224' N	014° 26.320' E	AUV ausgelöst
27.8.	SO277_8-1	AUV_L	05:59:12	43,50	35° 58.227' N	014° 26.326' E	Beginn Mission
27.8.	SO277_8-1	AUV_L	06:29:41	44,00	35° 58.225' N	014° 26.323' E	Mission zum 2. mal gestartet

Date	Station	Gear	Time	Depth	Latitude	Longitude	Remarks
2020	SONNE		UTC	[m]	[°N]	[°E]	
27.8.	SO277 8-1	AUV L	11:44:25	44,70	35° 58.222' N	014° 26.321' E	Mission beendet, Beginn Auftauchen
27.8.	SO277 8-1	AUV L	12:00:57	44,00	35° 58.224' N	014° 26.324' E	AUV aufgetaucht
27.8.	SO277 9-1	OBE M	12:58:59	54,34	36° 00.691' N	014° 26.945' E	OBMT 09
27.8.	SO277 9-1	OBE M	13:34:25	62,38	36° 01.925' N	014° 22.427' E	OBMT 08
27.8.	SO277 9-1	OBE M	14:05:42	67,11	36° 02.566' N	014° 21.079' E	OBMT 07
27.8.	SO277 9-1	OBE M	14:32:13	151,43	36° 03.766' N	014° 23.638' E	OBMT 06
27.8.	SO277 9-1	OBE M	14:56:46	152,78	36° 03.890' N	014° 20.932' E	OBMT 05
27.8.	SO277 9-1	OBE M	15:18:10	68,86	36° 04.103' N	014° 18.470' E	OBMT 04
27.8.	SO277 9-1	OBE M	16:06:35	169,61	36° 05.319' N	014° 20.320' E	OBMT 03
27.8.	SO277 9-1	OBE M	16:30:15	155,46	36° 05.559' N	014° 17.700' E	OBMT 02
27.8.	SO277 9-1	OBE M	16:54:27	156,09	36° 05.825' N	014° 14.974' E	OBMT 01
01.9.	SO277 9-1	OBE M	14:31:06	60,87	36° 01.293' N	014° 25.067' E	OBMT 10
01.9.	SO277 9-1	OBE M	15:30:19	67,95	36° 01.879' N	014° 23.881' E	OBMT 11
01.9.	SO277 9-1	OBE M	16:11:08	87,96	36° 03.680' N	014° 19.577' E	OBMT12
27.8.	SO277 10-1	SEIS OBR	17:20:26	146,96	36° 05.920' N	014° 16.506' E	OBS 1
27.8.	SO277 10-1	SEIS OBR	17:46:53	142,02	36° 05.414' N	014° 17.534' E	OBS 02
27.8.	SO277 10-1	SEIS OBR	18:12:18	127,22	36° 04.662' N	014° 19.005' E	OBS 03
27.8.	SO277 10-1	SEIS OBR	18:39:32	165,98	36° 05.373' N	014° 21.065' E	OBS 04
27.8.	SO277 10-1	SEIS OBR	19:00:45	167,15	36° 04.796' N	014° 20.594' E	OBS 05
27.8.	SO277 10-1	SEIS OBR	19:17:44	134,96	36° 04.112' N	014° 20.063' E	OBS 06
27.8.	SO277 10-1	SEIS OBR	19:33:52	67,31	36° 03.523' N	014° 19.608' E	OBS 07
27.8.	SO277 10-1	SEIS OBR	19:57:31	132,04	36° 03.370' N	014° 21.442' E	OBS 08
27.8.	SO277 10-1	SEIS OBR	20:18:14	86,91	36° 02.894' N	014° 22.320' E	OBS 09
27.8.	SO277 10-1	SEIS OBR	20:52:52	66,98	36° 01.507' N	014° 25.037' E	OBS 10
12.9.	SO277 10-1	SEIS OBR	13:08:27	123,70	36° 03.095' N	014° 22.221' E	Hydrophon zu Wasser, OBS ausgelöst
12.9.	SO277 10-1	SEIS OBR	13:10:22	121,00	36° 03.097' N	014° 22.221' E	Hydrophon an Deck
12.9.	SO277 10-1	SEIS OBR	13:36:19	137,70	36° 03.196' N	014° 21.542' E	Hydrophon zu Wasser, OBS ausgelöst
12.9.	SO277 10-1	SEIS OBR	13:37:15	135,50	36° 03.200' N	014° 21.533' E	Hydrophon an Deck
12.9.	SO277 10-1	SEIS OBR	14:09:42	88,20	36° 03.497' N	014° 19.854' E	Hydrophon zu Wasser, OBS ausgelöst
12.9.	SO277 10-1	SEIS OBR	14:10:22	87,50	36° 03.493' N	014° 19.851' E	Hydrophon an Deck
12.9.	SO277 10-1	SEIS OBR	14:33:24	128,00	36° 03.874' N	014° 19.946' E	Hydrophon zu Wasser
12.9.	SO277 10-1	SEIS OBR	14:33:48	127,20	36° 03.872' N	014° 19.947' E	Hydrophon an Deck
12.9.	SO277 10-1	SEIS OBR	14:44:32	134,70	36° 04.098' N	014° 20.033' E	OBS an Deck
12.9.	SO277 10-1	SEIS OBR	14:57:24	163,00	36° 04.573' N	014° 20.436' E	Hydrophon zu Wasser
12.9.	SO277 10-1	SEIS OBR	14:58:06	163,50	36° 04.575' N	014° 20.440' E	Hydrophon an Deck
12.9.	SO277 10-1	SEIS OBR	15:00:05	166,70	36° 04.576' N	014° 20.446' E	aufgetaucht

Date	Station	Gear	Time	Depth	Latitude	Longitude	Remarks
2020	SONNE		UTC	[m]	[°N]	[°E]	
12.9.	SO277	10-1 SEIS OBR	15:10:02	165,20	36° 04.780' N	014° 20.599' E	OBS an Deck
12.9.	SO277	10-1 SEIS OBR	15:20:01	166,50	36° 05.188' N	014° 20.914' E	Hydrophon zu Wasser
12.9.	SO277	10-1 SEIS OBR	15:20:54	165,20	36° 05.188' N	014° 20.921' E	Hydrophon an Deck
12.9.	SO277	10-1 SEIS OBR	15:22:45	164,20	36° 05.188' N	014° 20.936' E	aufgetaucht
12.9.	SO277	10-1 SEIS OBR	15:31:46	166,70	36° 05.357' N	014° 21.068' E	OBS an Deck
12.9.	SO277	10-1 SEIS OBR	15:56:38	124,70	36° 04.452' N	014° 19.072' E	Hydrohon zu Wasser
12.9.	SO277	10-1 SEIS OBR	15:57:09	125,00	36° 04.453' N	014° 19.066' E	Hydrophon an Deck
12.9.	SO277	10-1 SEIS OBR	15:58:50	124,20	36° 04.453' N	014° 19.053' E	aufgetaucht
12.9.	SO277	10-1 SEIS OBR	16:08:00	130,20	36° 04.666' N	014° 18.977' E	OBS an Deck
12.9.	SO277	10-1 SEIS OBR	16:25:44	135,50	36° 05.189' N	014° 17.507' E	Hydrophon zu Wasser
12.9.	SO277	10-1 SEIS OBR	16:26:37	136,70	36° 05.194' N	014° 17.498' E	Hydrophon an Deck
12.9.	SO277	10-1 SEIS OBR	16:38:19	142,70	36° 05.423' N	014° 17.525' E	OBS an Deck
27.8.	SO277	11-1 MB	22:03:02	199,93	36° 07.760' N	014° 17.368' E	rwK: 128°, d: 8nm
27.8.	SO277	11-1 MB	23:17:04	146,98	36° 02.555' N	014° 25.892' E	rwK: 308°, d: 8nm
28.8.	SO277	11-1 MB	00:33:16	200,37	36° 07.946' N	014° 17.978' E	rwK: 128°, d: 8nm
28.8.	SO277	11-1 MB	01:49:19	146,65	36° 02.703' N	014° 26.042' E	rwK: 308°, d: 8nm
28.8.	SO277	11-1 MB	03:02:04	200,46	36° 08.015' N	014° 18.223' E	rwK: 128°, d: 8nm
28.8.	SO277	11-1 MB	04:18:33	146,69	36° 02.815' N	014° 26.137' E	rwk = 308°, d= 8nm
28.8.	SO277	11-1 MB	05:34:53	203,19	36° 08.288' N	014° 19.130' E	rwK = 128°, d= 21nm
28.8.	SO277	11-1 MB	06:40:18	148,77	36° 03.806' N	014° 26.514' E	Abbruch Profil
01.9.	SO277	11-1 MB	17:55:57	127,41	36° 01.982' N	014° 25.216' E	Start Profil M8-Survey 3, rwK= 128°, d=6nm
01.9.	SO277	11-1 MB	18:36:48	96,25	35° 58.606' N	014° 30.543' E	rwK = 308°, d= 3nm
01.9.	SO277	11-1 MB	19:06:56	109,14	36° 00.777' N	014° 27.632' E	rwK: 128°, d: 3nm
01.9.	SO277	11-1 MB	19:36:36	98,14	35° 58.641' N	014° 30.659' E	rwK: 308°, d: 5nm
01.9.	SO277	11-1 MB	20:21:27	134,91	36° 02.103' N	014° 25.835' E	rwK: 130°, d: 3nm
01.9.	SO277	11-1 MB	20:46:40	128,05	36° 01.223' N	014° 28.479' E	rwK: 095°, d: 1nm
01.9.	SO277	11-1 MB	20:52:13	131,71	36° 01.108' N	014° 29.295' E	rwK: 130°, d: 2nm
01.9.	SO277	11-1 MB	21:09:23	124,80	35° 59.687' N	014° 31.420' E	rwK: 308°, d: 4nm
01.9.	SO277	11-1 MB	21:40:00	132,50	36° 01.562' N	014° 27.417' E	Abbruch Profil
02.9.	SO277	11-1 MB	02:33:03	134,81	36° 01.688' N	014° 27.211' E	Fortsetzung Profil Survey 3, rwK = 308°, d = 1nm
02.9.	SO277	11-1 MB	02:38:07	140,79	36° 02.027' N	014° 26.598' E	rwK = 144°, d = 2nm
02.9.	SO277	11-1 MB	02:57:48	67,31	36° 00.777' N	014° 27.505' E	rwK = 128°, d = 3nm
02.9.	SO277	11-1 MB	03:45:34	110,32	35° 58.971' N	014° 31.050' E	rwK = 308°, d= 6nm
28.8.	SO277	12-1 SEIST R	07:58:27	41,88	36° 00.944' N	014° 21.636' E	Beginn aussetzen Airguns
28.8.	SO277	12-1 SEIST R	08:00:49	42,12	36° 00.989' N	014° 21.697' E	Airguns zu Wasser
28.8.	SO277	12-1 SEIST R	08:12:40	45,51	36° 01.187' N	014° 21.901' E	Beginn aussetzen Streamer
28.8.	SO277	12-1 SEIST R	08:22:57	50,03	36° 01.314' N	014° 22.043' E	1. Bird zu Wasser
28.8.	SO277	12-1 SEIST R	08:25:41	50,75	36° 01.342' N	014° 22.080' E	2. Bird zu Wasser
28.8.	SO277	12-1 SEIST R	08:29:19	50,74	36° 01.381' N	014° 22.125' E	3. Bird zu Wasser

Date	Station	Gear	Time	Depth	Latitude	Longitude	Remarks
2020	SONNE		UTC	[m]	[°N]	[°E]	
28.8.	SO277_12-1	SEIST R	08:31:04	51,05	36° 01.400' N	014° 22.146' E	4. Bird zu Wasser
28.8.	SO277_12-1	SEIST R	08:47:06	55,50	36° 01.563' N	014° 22.333' E	komplett ausgesteckt, 280m
28.8.	SO277_12-1	SEIST R	08:53:41	57,94	36° 01.737' N	014° 22.481' E	1. Schuss , Beginn Profil, rwK: 042°, d: 10nm
28.8.	SO277_12-1	SEIST R	09:25:57	150,26	36° 03.328' N	014° 24.162' E	Airguns ausgeschaltet, Fischereizeichen im Streamer verhängen
28.8.	SO277_12-1	SEIST R	09:30:18	151,33	36° 03.486' N	014° 24.355' E	Beginn hieven Streamer
28.8.	SO277_12-1	SEIST R	09:34:12	151,46	36° 03.583' N	014° 24.486' E	4. Bird an Deck
28.8.	SO277_12-1	SEIST R	09:36:46	150,97	36° 03.639' N	014° 24.552' E	3. Bird an Deck
28.8.	SO277_12-1	SEIST R	09:40:20	150,80	36° 03.706' N	014° 24.637' E	2. Bird an Deck
28.8.	SO277_12-1	SEIST R	09:54:24	150,40	36° 03.993' N	014° 24.990' E	Longline wieder frei und im Wasser
28.8.	SO277_12-1	SEIST R	10:00:51	150,95	36° 04.140' N	014° 25.165' E	2. Bird zu Wasser
28.8.	SO277_12-1	SEIST R	10:07:27	150,84	36° 04.293' N	014° 25.346' E	3. Bird zu Wasser
28.8.	SO277_12-1	SEIST R	10:09:53	150,63	36° 04.350' N	014° 25.413' E	4. Bird zu Wasser
28.8.	SO277_12-1	SEIST R	10:13:12	151,23	36° 04.427' N	014° 25.504' E	Streamer komplett ausgesteckt, SL: 280m
28.8.	SO277_12-1	SEIST R	10:16:27	151,93	36° 04.502' N	014° 25.599' E	Airgun zu Wasser, Fortsetzung Profil
28.8.	SO277_12-1	SEIST R	11:33:52	146,17	36° 08.354' N	014° 30.775' E	rwK: 132°, d: 2nm
28.8.	SO277_12-1	SEIST R	12:00:04	141,80	36° 07.360' N	014° 32.659' E	rwK: 196°, d: 10nm
28.8.	SO277_12-1	SEIST R	14:14:23	66,08	35° 57.754' N	014° 29.573' E	rwK: 059°, d: 10nm
28.8.	SO277_12-1	SEIST R	16:19:25	129,32	36° 01.611' N	014° 39.707' E	rwK = 212°, d= 9nm
28.8.	SO277_12-1	SEIST R	18:03:18	107,63	35° 55.130' N	014° 35.475' E	rwK: 091°, d: 8nm
28.8.	SO277_12-1	SEIST R	19:45:35	64,71	35° 54.301' N	014° 44.771' E	rwK: 200°, d: 1,7nm
28.8.	SO277_12-1	SEIST R	20:15:20	53,53	35° 52.421' N	014° 44.453' E	rwK: 307°, d: 2nm
28.8.	SO277_12-1	SEIST R	20:43:23	60,62	35° 53.196' N	014° 42.385' E	rwK: 011°, d: 7nm
28.8.	SO277_12-1	SEIST R	22:02:07	112,74	35° 58.847' N	014° 43.465' E	rwK: 227°, d: 9nm
29.8.	SO277_12-1	SEIST R	00:09:06	92,44	35° 53.515' N	014° 35.063' E	rwK: 313°, d: 1nm
29.8.	SO277_12-1	SEIST R	00:27:04	89,05	35° 54.163' N	014° 33.946' E	rwK: 032°, d: 5nm
29.8.	SO277_12-1	SEIST R	01:35:51	126,24	35° 58.446' N	014° 37.036' E	rwK: 312°, d: 3nm
29.8.	SO277_12-1	SEIST R	02:20:32	134,43	36° 00.705' N	014° 34.177' E	rwK: 222°, d: 5nm
29.8.	SO277_12-1	SEIST R	03:25:48	59,22	35° 57.266' N	014° 30.012' E	rwK = 291°, d = 2nm
29.8.	SO277_12-1	SEIST R	03:40:04	47,16	35° 57.557' N	014° 28.797' E	rwK = 038°, d = 6nm
29.8.	SO277_12-1	SEIST R	04:50:56	138,05	36° 02.042' N	014° 32.171' E	rwK = 310°, d = 2nm
29.8.	SO277_12-1	SEIST R	05:10:11	140,04	36° 02.619' N	014° 30.793' E	rwK = 215°, d= 6nm
29.8.	SO277_12-1	SEIST R	06:23:20	46,17	35° 58.608' N	014° 26.547' E	rwK = 306°, d = 1nm
29.8.	SO277_12-1	SEIST R	06:33:16	44,59	35° 58.851' N	014° 25.763' E	rwK: 040°, d: 6nm
29.8.	SO277_12-1	SEIST R	07:56:01	145,19	36° 03.841' N	014° 29.541' E	rwK: 310°, d: 2,2nm
29.8.	SO277_12-1	SEIST R	08:17:40	147,78	36° 04.976' N	014° 28.406' E	rwK: 218°, d: 6,7nm
29.8.	SO277_12-1	SEIST R	08:24:25	149,14	36° 05.035' N	014° 28.090' E	Airguns abgeschaltet

Date	Station	Gear	Time	Depth	Latitude	Longitude	Remarks
2020	SONNE		UTC	[m]	[°N]	[°E]	
29.8.	SO277_12-1	SEIST R	08:40:35	148,97	36° 04.736' N	014° 27.463' E	Airguns wieder angeschaltet
29.8.	SO277_12-1	SEIST R	09:39:43	53,13	36° 01.344' N	014° 24.128' E	rwK: 039°, d: 5nm
29.8.	SO277_12-1	SEIST R	10:57:12	150,50	36° 05.340' N	014° 27.310' E	rwK: 303°, d: 1nm
29.8.	SO277_12-1	SEIST R	11:16:09	153,67	36° 06.093' N	014° 26.263' E	rwK: 220°, d: 6nm
29.8.	SO277_12-1	SEIST R	12:35:04	48,65	36° 01.820' N	014° 21.613' E	rwK: 040°, d: 6nm
29.8.	SO277_12-1	SEIST R	14:03:25	157,16	36° 06.692' N	014° 25.213' E	rwK: 217°, d: 6nm
29.8.	SO277_12-1	SEIST R	15:14:13	69,15	36° 02.876' N	014° 21.031' E	rwK = 035°, d = 6nm
29.8.	SO277_12-1	SEIST R	16:33:09	165,66	36° 07.573' N	014° 23.770' E	rwK = 213°, d= 5nm
29.8.	SO277_12-1	SEIST R	17:57:36	91,20	36° 04.107' N	014° 18.732' E	rwK = 036°, d= 5nm
29.8.	SO277_12-1	SEIST R	19:14:51	208,96	36° 08.890' N	014° 21.715' E	rwK: 220°, d: 6nm
29.8.	SO277_12-1	SEIST R	20:38:51	86,09	36° 05.243' N	014° 16.433' E	rwK: 037°, d: 6nm
29.8.	SO277_12-1	SEIST R	21:52:20	285,81	36° 09.563' N	014° 19.915' E	rwK: 304°, d: 1nm
29.8.	SO277_12-1	SEIST R	22:09:20	322,61	36° 10.420' N	014° 19.065' E	rwK: 213°, d: 6nm
29.8.	SO277_12-1	SEIST R	23:34:57	135,76	36° 05.268' N	014° 14.398' E	rwK: 033°, d: 8nm
30.8.	SO277_12-1	SEIST R	01:33:07	402,24	36° 12.279' N	014° 18.980' E	rwK: 234°, d: 16nm
30.8.	SO277_12-1	SEIST R	05:00:10	223,61	36° 04.093' N	014° 03.878' E	rwK: 327°, d: 2nm
30.8.	SO277_12-1	SEIST R	05:17:49	485,02	36° 05.123' N	014° 02.815' E	rwK = 053°, d = 10nm
30.8.	SO277_12-1	SEIST R	07:32:19	451,77	36° 11.515' N	014° 12.397' E	rwK = 128°, d= 32nm
30.8.	SO277_12-1	SEIST R	14:30:35	61,39	35° 52.694' N	014° 43.084' E	rwK = 200° d= 3nm
30.8.	SO277_12-1	SEIST R	15:08:37	89,56	35° 49.737' N	014° 42.980' E	rwK = 268°, d= 5nm
30.8.	SO277_12-1	SEIST R	16:08:29	91,53	35° 49.655' N	014° 37.660' E	rwK = 359°, d = 3nm
30.8.	SO277_12-1	SEIST R	16:44:34	86,29	35° 52.467' N	014° 37.262' E	rwK = 307°, d= 19nm
30.8.	SO277_12-1	SEIST R	20:52:15	64,30	36° 03.980' N	014° 18.617' E	rwK: 313°, d: 5,5nm
30.8.	SO277_12-1	SEIST R	21:58:03	193,56	36° 06.687' N	014° 13.302' E	rwK: 041°, d: 2nm
30.8.	SO277_12-1	SEIST R	22:29:03	212,10	36° 08.508' N	014° 14.518' E	rwK: 128°, d: 24nm
31.8.	SO277_12-1	SEIST R	03:47:01	119,36	35° 54.729' N	014° 37.686' E	rwK = 310°, d= 12nm
31.8.	SO277_12-1	SEIST R	06:11:39	140,93	36° 02.189' N	014° 27.623' E	rwK: 238°, d: 2nm
31.8.	SO277_12-1	SEIST R	06:44:45	53,99	36° 01.224' N	014° 24.978' E	rwK: 294°, d: 4,5nm
31.8.	SO277_12-1	SEIST R	07:41:43	62,25	36° 02.698' N	014° 20.297' E	rwK: 313°, d: 2nm
31.8.	SO277_12-1	SEIST R	08:04:35	50,68	36° 03.795' N	014° 18.792' E	rwK: 035°, d: 4,5nm
31.8.	SO277_12-1	SEIST R	09:03:52	173,11	36° 07.304' N	014° 22.027' E	rwK: 128°, d: 20nm
31.8.	SO277_12-1	SEIST R	13:30:12	92,53	35° 55.284' N	014° 41.102' E	rwK: 309°, d: 11nm
31.8.	SO277_12-1	SEIST R	15:54:08	133,10	36° 00.880' N	014° 30.567' E	rwK = 216°, d = 4nm
31.8.	SO277_12-1	SEIST R	16:36:46	49,72	35° 58.642' N	014° 27.813' E	rwK = 300° d = 4nm
31.8.	SO277_12-1	SEIST R	17:19:56	18,37	36° 00.529' N	014° 24.378' E	rwK = 046°, d = 7nm
31.8.	SO277_12-1	SEIST R	18:36:40	145,42	36° 04.772' N	014° 28.934' E	rwK: 046°, d: 3nm

Date	Station	Gear	Time	Depth	Latitude	Longitude	Remarks
2020	SONNE		UTC	[m]	[°N]	[°E]	
31.8.	SO277_12-1	SEIST R	19:18:56	143,00	36° 06.999' N	014° 31.833' E	rwK: 115°, d: 4nm
31.8.	SO277_12-1	SEIST R	20:05:34	134,89	36° 05.703' N	014° 35.957' E	rwK: 213°, d: 10nm
31.8.	SO277_12-1	SEIST R	22:23:15	42,08	35° 56.990' N	014° 29.462' E	rwK: 297°, d: 3nm
31.8.	SO277_12-1	SEIST R	23:00:02	41,93	35° 58.033' N	014° 26.534' E	rwK: 036°, d: 3nm
31.8.	SO277_12-1	SEIST R	23:36:07	65,63	36° 00.204' N	014° 28.200' E	rwK: 339°, d: 5nm
01.9.	SO277_12-1	SEIST R	00:41:12	150,55	36° 04.639' N	014° 26.136' E	rwK: 222°, d: 6nm
01.9.	SO277_12-1	SEIST R	01:52:40	42,23	36° 00.965' N	014° 21.625' E	rwK: 340°, d: 4nm
01.9.	SO277_12-1	SEIST R	02:40:07	131,20	36° 03.971' N	014° 19.991' E	rwK: 284°, d: 7nm
01.9.	SO277_12-1	SEIST R	04:01:57	176,10	36° 05.564' N	014° 12.813' E	rwK = 067°, d = 2nm
01.9.	SO277_12-1	SEIST R	04:29:13	211,54	36° 06.779' N	014° 14.423' E	rwK = 122°, d= 11nm
01.9.	SO277_12-1	SEIST R	06:56:16	60,38	36° 00.972' N	014° 26.431' E	rwK: 303°, d: 11nm
01.9.	SO277_12-1	SEIST R	07:25:58	129,91	36° 01.702' N	014° 26.117' E	Datenprobleme, Beginn einholen Streamer
01.9.	SO277_12-1	SEIST R	07:35:34	131,51	36° 01.618' N	014° 25.783' E	Airguns abgeschaltet, Beginn einholen der Airguns
01.9.	SO277_12-1	SEIST R	07:40:37	133,08	36° 01.657' N	014° 25.587' E	Bird 4 an Deck
01.9.	SO277_12-1	SEIST R	07:44:35	132,81	36° 01.700' N	014° 25.428' E	Bird 3 an Deck
01.9.	SO277_12-1	SEIST R	07:48:27	129,71	36° 01.747' N	014° 25.265' E	Bird 2 an Deck
01.9.	SO277_12-1	SEIST R	07:51:03	129,84	36° 01.779' N	014° 25.156' E	Bird 1 an Deck
01.9.	SO277_12-1	SEIST R	07:53:22	127,37	36° 01.805' N	014° 25.060' E	Streamer an Deck
01.9.	SO277_12-1	SEIST R	07:57:05	126,27	36° 01.836' N	014° 24.912' E	Fortsetzung Profil, ohne Streamer nur mit Airguns
01.9.	SO277_12-1	SEIST R	07:57:38	125,73	36° 01.842' N	014° 24.888' E	Airguns ausgesteckt und schießen wieder
01.9.	SO277_12-1	SEIST R	08:49:51	57,56	36° 00.869' N	014° 26.553' E	Erneut Profilbeginn ab WP 1, rw: 303°, d: 11nm
01.9.	SO277_12-1	SEIST R	11:16:04	201,56	36° 06.498' N	014° 15.336' E	rwK: 099°, d: 5nm
01.9.	SO277_12-1	SEIST R	12:29:02	167,33	36° 06.027' N	014° 21.473' E	rwK: 212°, d: 3nm
01.9.	SO277_12-1	SEIST R	13:26:14	71,66	36° 03.738' N	014° 19.212' E	Airgun an Deck
01.9.	SO277_10-2	SEIS OBR	14:43:58	64,13	36° 01.483' N	014° 24.691' E	Recovery OBS 01, Hydrophon zu Wasser
01.9.	SO277_10-2	SEIS OBR	16:41:23	146,65	36° 05.698' N	014° 16.606' E	Recovery OBS 10, Hydrophon zu Wasser
01.9.	SO277_10-2	SEIS OBR	16:43:18	147,38	36° 05.695' N	014° 16.611' E	OBS 10 ausgestellt
01.9.	SO277_10-2	SEIS OBR	16:44:55	146,80	36° 05.696' N	014° 16.612' E	Hydrophon an Deck
01.9.	SO277_10-2	SEIS OBR	16:45:57	147,55	36° 05.698' N	014° 16.612' E	aufgetaucht
01.9.	SO277_10-2	SEIS OBR	16:57:00	147,10	36° 05.952' N	014° 16.408' E	OBS 10 an Deck
01.9.	SO277_13-1	CTD	22:06:22	52,76	36° 01.341' N	014° 23.908' E	clean ship liegt an
01.9.	SO277_13-1	CTD	22:16:28	52,70	36° 01.343' N	014° 23.898' E	BOSI, SL: 52m
01.9.	SO277_13-1	CTD	22:21:09	52,20	36° 01.338' N	014° 23.903' E	rwK: 294°, d: 1nm
02.9.	SO277_13-1	CTD	00:00:02	58,70	36° 01.768' N	014° 22.717' E	rwK: 049°, d: 1nm
02.9.	SO277_13-1	CTD	01:12:25	123,20	36° 02.312' N	014° 23.464' E	Beginn Hieven
02.9.	SO277_14-1	CSE M	06:32:56	134,73	36° 01.699' N	014° 28.221' E	Erster Dipol zu Wasser

Date	Station	Gear	Time	Depth	Latitude	Longitude	Remarks
2020	SONNE		UTC	[m]	[°N]	[°E]	
02.9.	SO277_14-1	CSE M	06:44:02	135,05	36° 01.713' N	014° 28.180' E	Zweite Messstrecke zu Wasser
02.9.	SO277_14-1	CSE M	06:57:13	135,23	36° 01.725' N	014° 28.160' E	Dritte Messstrecke zu Wasser
02.9.	SO277_14-1	CSE M	07:08:58	135,38	36° 01.733' N	014° 28.124' E	Vierte Messstrecke zu Wasser
02.9.	SO277_14-1	CSE M	08:00:00	135,83	36° 01.772' N	014° 28.070' E	Schweinchen zu Wasser
02.9.	SO277_14-1	CSE M	08:17:33	136,38	36° 01.826' N	014° 28.017' E	Schwein am Grund
02.9.	SO277_14-1	CSE M	09:00:00	138,16	36° 01.890' N	014° 27.590' E	rwK: 297°, d: 6nm
02.9.	SO277_14-1	CSE M	19:14:40	148,20	36° 03.176' N	014° 24.511' E	Hydrophone zu Wasser
02.9.	SO277_14-1	CSE M	19:17:42	147,50	36° 03.170' N	014° 24.512' E	Hydrophone an Deck
02.9.	SO277_14-1	CSE M	20:06:13	148,20	36° 03.300' N	014° 24.225' E	Hydrophone zu Wasser
02.9.	SO277_14-1	CSE M	20:09:14	149,00	36° 03.298' N	014° 24.230' E	Hydrophone an Deck
02.9.	SO277_14-1	CSE M	22:47:41	152,00	36° 03.881' N	014° 22.809' E	Hydrophon zu Wasser
02.9.	SO277_14-1	CSE M	22:53:01	151,20	36° 03.880' N	014° 22.808' E	Hydrophon an Deck
03.9.	SO277_14-1	CSE M	02:30:56	164,20	36° 04.719' N	014° 20.790' E	Hydrophon zu Wasser
03.9.	SO277_14-1	CSE M	02:37:12	165,20	36° 04.717' N	014° 20.790' E	Hydrophon an Deck
03.9.	SO277_14-1	CSE M	02:38:23	165,50	36° 04.719' N	014° 20.787' E	rwK = 308°
03.9.	SO277_14-1	CSE M	05:03:09	171,50	36° 05.441' N	014° 19.650' E	Beginn hieven
03.9.	SO277_14-1	CSE M	05:04:04	172,70	36° 05.440' N	014° 19.650' E	Hydrophon zu Wasser
03.9.	SO277_14-1	CSE M	05:13:06	173,50	36° 05.434' N	014° 19.651' E	Hydrophon an Deck
03.9.	SO277_14-1	CSE M	05:23:53	174,20	36° 05.435' N	014° 19.642' E	Schweinchen an Deck
03.9.	SO277_14-1	CSE M	06:06:43	173,00	36° 05.423' N	014° 19.680' E	Erste Messkette an Deck
03.9.	SO277_14-1	CSE M	06:18:41	171,20	36° 05.420' N	014° 19.683' E	Zweite Messkette an Deck
03.9.	SO277_14-1	CSE M	06:27:04	171,50	36° 05.419' N	014° 19.682' E	Dritte Messkette an Deck
03.9.	SO277_14-1	CSE M	06:43:23	173,00	36° 05.424' N	014° 19.676' E	CSEM komplett an Deck
03.9.	SO277_15-1	CTD	07:46:51	67,70	36° 03.600' N	014° 19.537' E	FW1/SPW1
03.9.	SO277_15-1	CTD	07:54:11	67,70	36° 03.597' N	014° 19.538' E	Bodensicht, SL: 66m
03.9.	SO277_15-1	CTD	07:59:36	68,20	36° 03.602' N	014° 19.540' E	Beginn Profil, rwK: 037°, d: 1nm, v: 0,5kn
03.9.	SO277_15-1	CTD	11:03:37	166,00	36° 04.815' N	014° 20.672' E	Beginn Hieven, SL: 171m
03.9.	SO277_16-1	SEIST R	12:06:15	54,50	36° 01.238' N	014° 24.942' E	STB-Scherbrett zu Wasser
03.9.	SO277_16-1	SEIST R	12:49:07	46,00	36° 01.179' N	014° 23.473' E	Streamer zu Wasser
03.9.	SO277_16-1	SEIST R	13:01:25	42,70	36° 01.154' N	014° 23.067' E	BB-Scherbrett zu Wasser
03.9.	SO277_16-1	SEIST R	13:23:01	57,50	36° 01.619' N	014° 22.192' E	Airgun zu Wasser
03.9.	SO277_16-1	SEIST R	13:32:06	51,00	36° 01.935' N	014° 21.762' E	rwK: 312°, d: 5nm
03.9.	SO277_16-1	SEIST R	15:33:34	192,24	36° 06.462' N	014° 17.327' E	rwK = 132°, d= 6nm
03.9.	SO277_16-1	SEIST R	17:43:43	64,89	36° 01.633' N	014° 23.073' E	rwK = 312°, d= 6nm
03.9.	SO277_16-1	SEIST R	19:48:15	159,86	36° 05.986' N	014° 16.928' E	rwK: 132°, d: 7nm
03.9.	SO277_16-1	SEIST R	22:18:57	64,27	36° 01.746' N	014° 23.185' E	rwK: 312°, d: 6nm

Date	Station	Gear	Time	Depth	Latitude	Longitude	Remarks
2020	SONNE		UTC	[m]	[°N]	[°E]	
04.9.	SO277_16-1	SEIST R	00:17:12	168,20	36° 05.998' N	014° 17.183' E	rwK: 132°, d: 6nm
04.9.	SO277_16-1	SEIST R	02:53:09	63,03	36° 01.552' N	014° 23.014' E	rwK: 312°, d: 6nm
04.9.	SO277_16-1	SEIST R	04:53:58	160,84	36° 05.906' N	014° 17.136' E	rwK = 132°, d = 6nm
04.9.	SO277_16-1	SEIST R	07:07:48	68,78	36° 02.025' N	014° 23.139' E	rwK = 312°, d = 6nm
04.9.	SO277_16-1	SEIST R	08:52:42	93,14	36° 04.107' N	014° 18.804' E	Airgun-Probleme, Airgun abgeschaltet und wird eingeholt
04.9.	SO277_16-1	SEIST R	08:58:57	93,90	36° 04.274' N	014° 18.553' E	Airgun an Deck
04.9.	SO277_16-1	SEIST R	09:09:23	119,21	36° 04.647' N	014° 18.058' E	Airgun zu Wasser
04.9.	SO277_16-1	SEIST R	09:14:44	129,22	36° 04.848' N	014° 17.771' E	Airgun wird wieder eingeholt
04.9.	SO277_16-1	SEIST R	09:18:17	125,93	36° 04.974' N	014° 17.590' E	Airgun an Deck
04.9.	SO277_16-1	SEIST R	09:30:59	131,65	36° 05.440' N	014° 16.954' E	rwK: 132°, d: 6nm
04.9.	SO277_16-1	SEIST R	10:11:14	162,29	36° 05.240' N	014° 18.570' E	Airgun zu Wasser
04.9.	SO277_16-1	SEIST R	10:30:11	157,84	36° 04.650' N	014° 19.388' E	Airgun an Deck
04.9.	SO277_16-1	SEIST R	11:53:45	74,42	36° 02.152' N	014° 22.849' E	Airgun zu Wasser
04.9.	SO277_16-1	SEIST R	11:59:12	85,70	36° 01.980' N	014° 23.075' E	Airgun zugeschaltet
04.9.	SO277_16-1	SEIST R	12:03:56	70,14	36° 01.685' N	014° 23.118' E	rwK: 312°, d: 6nm
04.9.	SO277_16-1	SEIST R	13:52:49	151,59	36° 05.733' N	014° 16.910' E	rwK: 132°, d: 6nm
04.9.	SO277_16-1	SEIST R	16:18:45	64,34	36° 01.620' N	014° 23.057' E	rwK = 312°, d= 6nm
04.9.	SO277_16-1	SEIST R	18:03:36	138,41	36° 05.411' N	014° 17.121' E	rwK = 132°, d = 6nm
04.9.	SO277_16-1	SEIST R	20:44:15	95,57	36° 02.224' N	014° 23.126' E	rwK: 312°, d: 6nm
04.9.	SO277_16-1	SEIST R	22:54:17	159,83	36° 05.896' N	014° 17.099' E	rwK: 132°, d: 6nm
05.9.	SO277_16-1	SEIST R	01:12:17	62,37	36° 01.925' N	014° 23.316' E	rwK: 312°, d: 6nm
05.9.	SO277_16-1	SEIST R	03:22:16	185,77	36° 06.044' N	014° 17.235' E	rwK = 132°, d= 6nm
05.9.	SO277_16-1	SEIST R	05:39:50	62,89	36° 01.759' N	014° 23.235' E	rwK = 312°, d = 6nm
05.9.	SO277_16-1	SEIST R	07:51:47	150,29	36° 05.617' N	014° 17.252' E	rwK = 132°, d = 6nm
05.9.	SO277_16-1	SEIST R	10:15:19	67,20	36° 01.921' N	014° 23.412' E	rwK: 312°, d: 6nm
05.9.	SO277_16-1	SEIST R	12:12:10	165,20	36° 05.902' N	014° 17.154' E	rwK: 132°, d: 6nm
05.9.	SO277_16-1	SEIST R	14:32:45	67,37	36° 01.845' N	014° 23.277' E	rwK = 312°, d = 6nm
05.9.	SO277_16-1	SEIST R	16:23:02	195,74	36° 06.146' N	014° 17.358' E	rwK = 132°, d= 6nm
05.9.	SO277_16-1	SEIST R	18:48:37	97,41	36° 02.343' N	014° 23.278' E	rwK = 312°, d= 6nm
05.9.	SO277_16-1	SEIST R	21:05:00	151,71	36° 05.683' N	014° 17.349' E	rwK: 132°, d: 6nm
05.9.	SO277_16-1	SEIST R	23:42:53	64,80	36° 02.023' N	014° 23.433' E	rwK: 312°, d: 6nm
06.9.	SO277_16-1	SEIST R	01:40:16	182,53	36° 06.013' N	014° 17.262' E	rwK: 132°, d: 6nm
06.9.	SO277_16-1	SEIST R	04:15:40	62,14	36° 01.830' N	014° 23.263' E	rwK = 312°, d= 6nm
06.9.	SO277_16-1	SEIST R	06:00:29	153,85	36° 05.682' N	014° 17.417' E	rwK = 132°, d = 6nm
06.9.	SO277_16-1	SEIST R	08:23:31	133,15	36° 02.402' N	014° 23.367' E	rwK: 312°, d: 6nm
06.9.	SO277_16-1	SEIST R	10:34:20	165,15	36° 05.939' N	014° 17.088' E	rwK: 132°, d: 6nm

Date	Station	Gear	Time	Depth	Latitude	Longitude	Remarks
2020	SONNE		UTC	[m]	[°N]	[°E]	
06.9.	SO277_16-1	SEIST R	12:53:12	91,27	36° 02.160' N	014° 23.542' E	rwK: 312°, d: 6nm
06.9.	SO277_16-1	SEIST R	15:00:32	186,25	36° 06.271' N	014° 17.882' E	rwK = 132°, d= 6nm
06.9.	SO277_16-1	SEIST R	17:12:25	69,96	36° 02.013' N	014° 23.461' E	rwK = 312°, d= 6nm
06.9.	SO277_16-1	SEIST R	19:18:32	163,58	36° 05.756' N	014° 17.392' E	rwK = 132°, d = 6nm
06.9.	SO277_16-1	SEIST R	21:44:52	139,38	36° 02.455' N	014° 23.473' E	rwK: 312°, d: 6nm
07.9.	SO277_16-1	SEIST R	00:00:21	165,47	36° 05.921' N	014° 17.144' E	rwK: 132°, d: 6nm
07.9.	SO277_16-1	SEIST R	02:42:02	70,36	36° 01.977' N	014° 23.569' E	rwK: 312°, d: 6nm
07.9.	SO277_16-1	SEIST R	04:57:41	193,89	36° 06.576' N	014° 17.633' E	rwK = 132°, d = 6nm
07.9.	SO277_16-1	SEIST R	07:01:01	137,09	36° 02.545' N	014° 23.478' E	rwK = 312°, d= 6nm
07.9.	SO277_16-1	SEIST R	09:28:57	175,30	36° 06.163' N	014° 16.933' E	rwK: 131°, d: 0,4nm
07.9.	SO277_16-1	SEIST R	09:52:00	184,94	36° 06.059' N	014° 17.904' E	rwK: 107°, d: 0,25nm
07.9.	SO277_16-1	SEIST R	09:58:07	181,57	36° 05.931' N	014° 18.291' E	rwK: 132°, d: 1,5nm
07.9.	SO277_16-1	SEIST R	11:43:17	63,85	36° 01.928' N	014° 23.194' E	rwK: 311°, d: 6nm
07.9.	SO277_16-1	SEIST R	14:00:09	139,06	36° 05.365' N	014° 17.087' E	rwK: 132°, d: 6nm
07.9.	SO277_16-1	SEIST R	14:05:42	145,22	36° 05.507' N	014° 16.940' E	Airgun an Deck
07.9.	SO277_16-1	SEIST R	14:28:22	182,18	36° 06.119' N	014° 17.034' E	Airguns zu Wasser
07.9.	SO277_16-1	SEIST R	14:52:50	189,45	36° 05.827' N	014° 17.849' E	rwK = 132°, d = 6nm
07.9.	SO277_16-1	SEIST R	15:18:08	156,91	36° 04.748' N	014° 19.180' E	Profilunterbrechung wegen elektr. Problem am Streamer
07.9.	SO277_16-1	SEIST R	15:30:11	144,68	36° 04.359' N	014° 19.706' E	Airguns an Deck
07.9.	SO277_16-1	SEIST R	15:32:16	140,22	36° 04.321' N	014° 19.792' E	Streamer auf 60m vorholen
07.9.	SO277_16-1	SEIST R	16:13:05	98,61	36° 03.152' N	014° 21.060' E	Bb-Scherbrett an Deck
07.9.	SO277_16-1	SEIST R	16:31:10	70,61	36° 02.731' N	014° 21.712' E	5 Streamer an Deck
07.9.	SO277_16-1	SEIST R	17:00:24	65,58	36° 02.009' N	014° 22.696' E	Beginn aussetzen Streamer
07.9.	SO277_16-1	SEIST R	17:16:51	60,38	36° 01.752' N	014° 23.372' E	Streamer ausgesteckt
07.9.	SO277_16-1	SEIST R	17:20:13	61,94	36° 01.712' N	014° 23.508' E	Bb-Scherbrett zu Wasser
07.9.	SO277_16-1	SEIST R	17:32:30	59,22	36° 01.568' N	014° 23.988' E	Scherbretter auf 110m ausgesteckt, Beginn Drehung über Stb.
07.9.	SO277_16-1	SEIST R	18:20:44	50,12	36° 01.347' N	014° 22.686' E	rwK = 312°, d= 6nm
07.9.	SO277_16-1	SEIST R	20:29:33	138,94	36° 05.360' N	014° 17.109' E	rwK: 041°, d: 1nm
07.9.	SO277_16-1	SEIST R	20:49:52	194,23	36° 06.208' N	014° 17.435' E	rwK: 132°, d: 2,5nm
07.9.	SO277_16-1	SEIST R	21:37:58	175,30	36° 05.000' N	014° 19.807' E	rwK: 123°, d: 0,3nm
07.9.	SO277_16-1	SEIST R	21:44:10	173,33	36° 04.827' N	014° 20.120' E	rwK: 130°, 0,7nm
07.9.	SO277_16-1	SEIST R	23:04:10	113,69	36° 02.226' N	014° 23.739' E	rwK: 311°, d: 6nm
08.9.	SO277_16-1	SEIST R	01:14:52	194,83	36° 06.164' N	014° 17.440' E	rwK: 136°, d: 7nm
08.9.	SO277_16-1	SEIST R	04:00:54	58,43	36° 01.330' N	014° 23.756' E	rwK = 311° d= 7nm (NW-Kurse)
08.9.	SO277_16-1	SEIST R	06:12:26	148,09	36° 05.601' N	014° 17.074' E	rwK: 131°, d: 7nm SE Kurse
08.9.	SO277_16-1	SEIST R	08:25:26	66,48	36° 01.858' N	014° 23.389' E	rwK: 304°, d: 1,5nm

Date	Station	Gear	Time	Depth	Latitude	Longitude	Remarks
2020	SONNE		UTC	[m]	[°N]	[°E]	
08.9.	SO277_16-1	SEIST R	09:04:24	75,70	36° 02.478' N	014° 22.007' E	rwK: 288°, d: 1,7nm
08.9.	SO277_16-1	SEIST R	09:39:53	91,90	36° 03.300' N	014° 20.018' E	rwK: 033°, d: 1,5nm
08.9.	SO277_16-1	SEIST R	10:45:18	101,41	36° 03.192' N	014° 21.246' E	rwK: 308°, d: 6nm
08.9.	SO277_16-1	SEIST R	12:15:21	150,91	36° 05.928' N	014° 16.446' E	Airgun abgeschaltet
08.9.	SO277_16-1	SEIST R	12:31:10	188,86	36° 06.357' N	014° 15.731' E	Airgun an Deck
08.9.	SO277_16-1	SEIST R	13:07:25	206,08	36° 07.525' N	014° 15.847' E	BB-Scherbrett an Deck
08.9.	SO277_16-1	SEIST R	13:31:42	209,60	36° 07.984' N	014° 15.391' E	Streamer an Deck
08.9.	SO277_16-1	SEIST R	13:51:06	205,00	36° 07.819' N	014° 14.637' E	STB-Scherbrett an Deck
08.9.	SO277_17-1	CSE M	14:43:49	188,40	36° 06.374' N	014° 17.394' E	1.Messstrecke zu Wasser
08.9.	SO277_17-1	CSE M	14:52:51	187,50	36° 06.314' N	014° 17.448' E	2.Messkette zu Wasser
08.9.	SO277_17-1	CSE M	14:54:16	187,50	36° 06.304' N	014° 17.456' E	3.Messkette zu Wasser
08.9.	SO277_17-1	CSE M	15:02:11	186,50	36° 06.264' N	014° 17.492' E	4.Messkette zu Wasser
08.9.	SO277_17-1	CSE M	15:08:57	186,50	36° 06.244' N	014° 17.517' E	5.Messkette zu Wasser
08.9.	SO277_17-1	CSE M	15:41:39	186,20	36° 06.196' N	014° 17.575' E	Schweinchen zu Wasser
08.9.	SO277_17-1	CSE M	16:07:38	183,70	36° 06.073' N	014° 17.746' E	Schweinchen auf Grund
08.9.	SO277_17-1	CSE M	16:28:50	181,80	36° 05.974' N	014° 17.907' E	Hydrophon zu Wasser
08.9.	SO277_17-1	CSE M	16:33:53	182,10	36° 05.974' N	014° 17.905' E	Hydrophon an Deck
08.9.	SO277_17-1	CSE M	18:37:57	178,70	36° 05.593' N	014° 18.552' E	Hydrophon zu Wasser
08.9.	SO277_17-1	CSE M	18:46:02	175,60	36° 05.592' N	014° 18.552' E	Hydrophon an Deck
09.9.	SO277_17-1	CSE M	08:16:33	150,00	36° 03.456' N	014° 23.398' E	Beginn Einholen der Messinstrumente
09.9.	SO277_17-1	CSE M	08:36:27	149,60	36° 03.459' N	014° 23.396' E	Schweinchen an Deck
09.9.	SO277_17-1	CSE M	09:04:07	149,60	36° 03.479' N	014° 23.306' E	Erste Messstrecke an Deck
09.9.	SO277_17-1	CSE M	09:13:03	149,60	36° 03.488' N	014° 23.301' E	Zweite Messstrecke an Deck
09.9.	SO277_17-1	CSE M	09:21:30	150,90	36° 03.490' N	014° 23.301' E	Dritte Messstrecke an Deck
09.9.	SO277_17-1	CSE M	09:24:05	151,20	36° 03.496' N	014° 23.288' E	Vierte Messstrecke an Deck
09.9.	SO277_17-1	CSE M	09:30:53	151,20	36° 03.495' N	014° 23.284' E	Alles an Deck
09.9.	SO277_18-1	AUV_ L	10:58:01	62,70	36° 04.393' N	014° 17.870' E	Hydrophon zu Wasser
09.9.	SO277_18-1	AUV_ L	11:00:05	62,50	36° 04.392' N	014° 17.869' E	AUV abgetaucht
09.9.	SO277_18-1	AUV_ L	11:07:22	62,50	36° 04.393' N	014° 17.872' E	Hydrophon an Deck
09.9.	SO277_18-1	AUV_ L	14:54:44	63,00	36° 04.390' N	014° 17.874' E	Modem zu Wasser
09.9.	SO277_18-1	AUV_ L	15:59:10	62,70	36° 04.388' N	014° 17.875' E	AUV L an Deck
09.9.	SO277_18-1	AUV_ L	15:59:49	62,70	36° 04.388' N	014° 17.875' E	Modem an Deck
09.9.	SO277_19-1	CTD	11:45:11	160,03	36° 04.412' N	014° 19.758' E	Clean Ship
09.9.	SO277_19-1	CTD	12:07:05	155,94	36° 04.415' N	014° 19.782' E	BOSI, SL: 158m
09.9.	SO277_20-1	CTD	16:37:15	136,08	36° 05.081' N	014° 18.271' E	Transponder SL = 10m zu Wasser
09.9.	SO277_20-1	CTD	17:01:19	136,05	36° 05.077' N	014° 18.276' E	Bodensicht SL = 139m

Date	Station	Gear	Time	Depth	Latitude	Longitude	Remarks
2020	SONNE		UTC	[m]	[°N]	[°E]	
09.9.	SO277_20-1	CTD	17:02:25	136,06	36° 05.077' N	014° 18.276' E	rwK = 032°, d = 0,5nm
09.9.	SO277_20-1	CTD	18:10:30	178,72	36° 05.413' N	014° 18.538' E	rwK: 294°, d: 0,15nm
09.9.	SO277_20-1	CTD	18:46:25	179,63	36° 05.466' N	014° 18.373' E	rwK: 214°, d: 0,45nm
09.9.	SO277_20-1	CTD	19:57:03	136,25	36° 05.088' N	014° 18.069' E	Beginn hieven
09.9.	SO277_20-1	CTD	20:02:48	136,30	36° 05.088' N	014° 18.069' E	Transponder an Deck
09.9.	SO277_20-1	CTD	20:04:55	136,30	36° 05.088' N	014° 18.069' E	CTD an Deck
09.9.	SO277_21-1	PS	20:23:08	60,39	36° 04.035' N	014° 18.482' E	rwK:131°, 1nm
09.9.	SO277_21-1	PS	20:31:59	64,88	36° 03.261' N	014° 19.570' E	rwK: 122°, d: 1,7nm
09.9.	SO277_21-1	PS	20:40:30	72,77	36° 02.643' N	014° 20.767' E	rwK: 189°, d: 1,2nm
09.9.	SO277_21-1	PS	20:55:22	48,73	36° 01.122' N	014° 21.170' E	rwK: 125°, d: 3,9nm
09.9.	SO277_21-1	PS	21:37:09	48,54	35° 58.518' N	014° 25.354' E	rwK: 305°, d: 3,9nm
09.9.	SO277_21-1	PS	22:48:41	68,68	36° 04.217' N	014° 18.252' E	rwK: 134°, d: 8nm
10.9.	SO277_21-1	PS	00:03:01	48,44	35° 58.896' N	014° 25.136' E	Parasound
10.9.	SO277_21-1	PS	00:16:03	42,64	35° 58.844' N	014° 25.105' E	EM710, rwK: 314°, d: 8nm
10.9.	SO277_21-1	PS	01:24:07	36,83	36° 04.044' N	014° 18.363' E	rwK. 134°, d: 8nm
10.9.	SO277_21-1	PS	02:35:41	43,79	35° 58.783' N	014° 25.543' E	rwK = 305°, d= 4nm
10.9.	SO277_21-1	PS	03:08:53	40,17	36° 00.806' N	014° 21.555' E	rwK = 125°, d = 4nm
10.9.	SO277_21-1	PS	03:46:01	43,62	35° 58.817' N	014° 25.384' E	rwK = 305°, d= 5nm
10.9.	SO277_21-1	PS	04:17:40	34,65	36° 00.646' N	014° 21.793' E	rwK = 356°, d = 2nm
10.9.	SO277_21-1	PS	04:30:49	60,88	36° 02.269' N	014° 21.374' E	rwK = 302°, d = 2nm
10.9.	SO277_21-1	PS	04:41:59	60,97	36° 03.104' N	014° 19.800' E	rwK = 311°, d = 2nm
10.9.	SO277_22-1	OBE M	06:00:48	140,50	36° 05.358' N	014° 17.651' E	Hydrophon zu Wasser
10.9.	SO277_22-1	OBE M	06:13:40	140,00	36° 05.357' N	014° 17.649' E	OBMT 01 ausgelöst
10.9.	SO277_22-1	OBE M	06:18:22	141,20	36° 05.356' N	014° 17.646' E	Hydrophon an Deck
10.9.	SO277_22-1	OBE M	06:30:16	149,20	36° 05.490' N	014° 17.663' E	OBMT 01
10.9.	SO277_22-1	OBE M	06:55:52	168,20	36° 05.155' N	014° 20.256' E	Hydrophon zu Wasser
10.9.	SO277_22-1	OBE M	06:57:59	168,20	36° 05.156' N	014° 20.252' E	OBMT 02 ausgelöst
10.9.	SO277_22-1	OBE M	07:03:24	169,00	36° 05.155' N	014° 20.253' E	Hydrophon an Deck
10.9.	SO277_22-1	OBE M	07:12:57	168,20	36° 05.299' N	014° 20.410' E	OBMT 02 an Deck
10.9.	SO277_22-1	OBE M	07:39:50	127,00	36° 03.608' N	014° 20.832' E	Hydrophon zu Wasser
10.9.	SO277_22-1	OBE M	07:41:50	128,20	36° 03.614' N	014° 20.846' E	OBMT 03 ausgelöst
10.9.	SO277_22-1	OBE M	07:46:11	128,00	36° 03.611' N	014° 20.852' E	Hydrophon an Deck
10.9.	SO277_22-1	OBE M	07:56:43	154,00	36° 03.822' N	014° 21.026' E	OBMT 03 an Deck
10.9.	SO277_22-1	OBE M	08:17:46	149,20	36° 03.572' N	014° 23.578' E	Hydrophon zu Wasser
10.9.	SO277_22-1	OBE M	08:19:01	151,20	36° 03.571' N	014° 23.576' E	OBMT 04 ausgelöst
10.9.	SO277_22-1	OBE M	08:23:55	150,70	36° 03.570' N	014° 23.571' E	Hydrophon an Deck
10.9.	SO277_22-1	OBE M	08:35:00	153,20	36° 03.788' N	014° 23.636' E	OBMT 04 an Deck
10.9.	SO277_23-1	CTD	10:05:56	175,20	36° 06.035' N	014° 14.726' E	clean ship liegt an
10.9.	SO277_23-1	CTD	10:20:14	173,00	36° 06.035' N	014° 14.723' E	wg tech Probleme
10.9.	SO277_23-1	CTD	10:43:38	172,00	36° 06.036' N	014° 14.724' E	BOSI, SL: 177m

Date	Station	Gear	Time	Depth	Latitude	Longitude	Remarks
2020	SONNE		UTC	[m]	[°N]	[°E]	
10.9.	SO277 24-1	CTD	11:40:12	133,50	36° 03.427' N	014° 21.543' E	Clean Ship
10.9.	SO277 24-1	CTD	11:50:12	132,70	36° 03.427' N	014° 21.550' E	Transponder bei SL: 10m angebracht und zu Wasser
10.9.	SO277 24-1	CTD	11:58:44	133,00	36° 03.430' N	014° 21.550' E	BOSI, SL: 136m
10.9.	SO277 24-1	CTD	13:18:47	135,58	36° 03.464' N	014° 21.598' E	Beginn Hieven
10.9.	SO277 24-1	CTD	13:26:15	135,77	36° 03.465' N	014° 21.594' E	Transponder an Deck
10.9.	SO277 25-1	CSE M	14:25:23	63,00	36° 02.372' N	014° 21.375' E	1. Messkette zu Wasser
10.9.	SO277 25-1	CSE M	14:29:14	63,50	36° 02.382' N	014° 21.356' E	BOKO 1.Messkette
10.9.	SO277 25-1	CSE M	14:34:34	64,50	36° 02.406' N	014° 21.311' E	2.Messkette zu Wasser
10.9.	SO277 25-1	CSE M	14:35:59	64,70	36° 02.411' N	014° 21.299' E	3.Messkette zu Wasser
10.9.	SO277 25-1	CSE M	14:41:55	65,50	36° 02.435' N	014° 21.254' E	4.Messkette zu Wasser
10.9.	SO277 25-1	CSE M	15:05:51	65,00	36° 02.502' N	014° 21.123' E	Schweinchen zu Wasser
10.9.	SO277 25-1	CSE M	15:13:34	65,00	36° 02.502' N	014° 21.120' E	Schweinchen an Deck
10.9.	SO277 25-1	CSE M	15:17:25	65,20	36° 02.501' N	014° 21.123' E	Schweinchen zu Wasser
10.9.	SO277 25-1	CSE M	15:29:49	65,20	36° 02.501' N	014° 21.123' E	rwK = 302°, d=2nm
10.9.	SO277 25-1	CSE M	22:06:51	60,50	36° 03.263' N	014° 19.615' E	rwK: 311°, d: 1nm
11.9.	SO277 25-1	CSE M	03:51:19	62,50	36° 03.972' N	014° 18.612' E	Beginn hieven
11.9.	SO277 25-1	CSE M	04:00:56	62,70	36° 03.972' N	014° 18.612' E	Schweinchen an Deck
11.9.	SO277 25-1	CSE M	04:29:44	61,00	36° 03.948' N	014° 18.666' E	1.Messkette an Deck
11.9.	SO277 25-1	CSE M	04:36:20	61,50	36° 03.948' N	014° 18.674' E	2.Messkette an Deck
11.9.	SO277 25-1	CSE M	04:38:26	61,50	36° 03.948' N	014° 18.672' E	3.Messkette an Deck
11.9.	SO277 25-1	CSE M	04:41:42	61,00	36° 03.948' N	014° 18.670' E	frei vom Grund
11.9.	SO277 25-1	CSE M	04:44:46	61,20	36° 03.949' N	014° 18.665' E	Streamer an Deck
11.9.	SO277 26-1	OBE M	07:35:05	56,50	36° 00.326' N	014° 26.857' E	OBMT 13 zu Wasser
11.9.	SO277 26-1	OBE M	07:49:46	51,70	36° 00.070' N	014° 26.934' E	OBMT 14 zu Wasser
11.9.	SO277 26-1	OBE M	08:05:37	49,00	35° 59.857' N	014° 26.995' E	OBMT 15 zu Wasser
11.9.	SO277 26-1	OBE M	08:22:30	50,50	35° 59.637' N	014° 27.064' E	OBMT 16 zu Wasser
11.9.	SO277 27-1	GC	09:09:55	65,70	36° 01.654' N	014° 22.995' E	GC 3m
11.9.	SO277 27-1	GC	09:12:47	65,50	36° 01.657' N	014° 22.988' E	FW2/SPW2
11.9.	SO277 27-1	GC	09:15:03	66,00	36° 01.656' N	014° 22.986' E	Boko, SLmax: 78m
11.9.	SO277 27-1	GC	09:15:28	66,50	36° 01.656' N	014° 22.985' E	SZmax: 16,6kN
11.9.	SO277 28-1	GC	11:05:58	56,50	36° 01.593' N	014° 23.229' E	GC 3m
11.9.	SO277 28-1	GC	11:11:26	56,70	36° 01.592' N	014° 23.228' E	BOKO, SLmax: 67m
11.9.	SO277 28-1	GC	11:12:11	57,50	36° 01.592' N	014° 23.228' E	Beginn Hieven, SZmax: 14kN
11.9.	SO277 29-1	GC	11:40:06	54,00	36° 01.459' N	014° 23.597' E	GC 3m
11.9.	SO277 29-1	GC	11:43:35	53,20	36° 01.461' N	014° 23.600' E	SLmax: 60m
11.9.	SO277 29-1	GC	11:43:56	53,20	36° 01.461' N	014° 23.600' E	Beginn Hieven, SZmax: 14kN
11.9.	SO277 29-1	GC	12:01:57	53,70	36° 01.458' N	014° 23.613' E	2. Versuch
11.9.	SO277 29-1	GC	12:03:45	53,70	36° 01.459' N	014° 23.613' E	BOKO, SLmax: 61m
11.9.	SO277 29-1	GC	12:04:03	53,20	36° 01.459' N	014° 23.613' E	Beginn Hieven, SZmax: 14kN

Date	Station	Gear	Time	Depth	Latitude	Longitude	Remarks
2020	SONNE		UTC	[m]	[°N]	[°E]	
11.9.	SO277_30-1	CSE M	14:18:07	185,00	36° 06.092' N	014° 17.692' E	Streamer zu Wassr
11.9.	SO277_30-1	CSE M	14:18:56	185,50	36° 06.091' N	014° 17.687' E	1.Messkette zu Wasser
11.9.	SO277_30-1	CSE M	14:25:37	185,20	36° 06.085' N	014° 17.647' E	2.Messkette zu Wasser
11.9.	SO277_30-1	CSE M	14:27:16	186,00	36° 06.084' N	014° 17.637' E	3.Messkette zu Wasser
11.9.	SO277_30-1	CSE M	14:33:48	186,20	36° 06.081' N	014° 17.614' E	4.Messkette zu Wasser
11.9.	SO277_30-1	CSE M	14:53:11	187,00	36° 06.070' N	014° 17.547' E	Schweinchen zu Wasser
11.9.	SO277_30-1	CSE M	15:37:48	164,20	36° 06.017' N	014° 17.174' E	komplett ausgesteckt SL = 320m
12.9.	SO277_30-1	CSE M	02:50:55	145,20	36° 05.407' N	014° 13.259' E	80m Kabel zusätzlich ausgesteckt
12.9.	SO277_30-1	CSE M	03:43:02	145,00	36° 05.409' N	014° 13.263' E	Beginn hieven
12.9.	SO277_30-1	CSE M	04:00:29	145,50	36° 05.410' N	014° 13.260' E	Schweinchen an Deck
12.9.	SO277_30-1	CSE M	04:23:33	145,70	36° 05.414' N	014° 13.287' E	1.Messkette an Deck
12.9.	SO277_30-1	CSE M	04:35:36	145,70	36° 05.411' N	014° 13.278' E	2.Messkette an Deck
12.9.	SO277_30-1	CSE M	04:38:21	145,50	36° 05.412' N	014° 13.277' E	3.Messkette an Deck
12.9.	SO277_30-1	CSE M	04:43:45	145,00	36° 05.412' N	014° 13.277' E	Streamer an Deck
12.9.	SO277_31-1	AUV_ L	06:30:55	32,50	36° 00.886' N	014° 22.117' E	AUV auf Mission
12.9.	SO277_31-1	AUV_ L	12:25:47	34,70	36° 00.900' N	014° 22.112' E	AUV aufgetaucht
12.9.	SO277_32-1	GC	07:40:54	44,00	36° 05.016' N	014° 16.104' E	GC - 3nm
12.9.	SO277_32-1	GC	07:43:49	44,00	36° 05.018' N	014° 16.100' E	FW2/SPW2
12.9.	SO277_32-1	GC	07:45:28	43,70	36° 05.017' N	014° 16.101' E	Boko, SLmax: 54m
12.9.	SO277_32-1	GC	07:45:58	43,70	36° 05.016' N	014° 16.101' E	Beginn hieven, SZmax: 14,2kN
12.9.	SO277_33-1	GC	08:15:38	91,00	36° 05.293' N	014° 16.473' E	GC - 3m
12.9.	SO277_33-1	GC	08:17:47	91,70	36° 05.298' N	014° 16.476' E	FW2/SPW2
12.9.	SO277_33-1	GC	08:20:30	92,00	36° 05.299' N	014° 16.477' E	Boko, SLmax: 105m
12.9.	SO277_33-1	GC	08:21:01	91,00	36° 05.299' N	014° 16.478' E	Beginn hieven, SZmax: 24,6kN
12.9.	SO277_33-2	GC	08:50:26	91,00	36° 05.297' N	014° 16.476' E	GC - 3m
12.9.	SO277_33-2	GC	08:52:04	93,70	36° 05.297' N	014° 16.475' E	FW2/SPW2
12.9.	SO277_33-2	GC	08:54:45	93,00	36° 05.296' N	014° 16.475' E	Boko, SLmax: 104m
12.9.	SO277_33-2	GC	08:55:55	91,00	36° 05.295' N	014° 16.474' E	Beginn hieven, SZmax: 22,9kN
12.9.	SO277_34-1	GC	11:07:10	70,20	36° 04.497' N	014° 17.621' E	GC 3m
12.9.	SO277_34-1	GC	11:11:25	70,20	36° 04.496' N	014° 17.622' E	BOKO, SLmax: 85m
12.9.	SO277_34-1	GC	11:11:48	70,50	36° 04.496' N	014° 17.622' E	Beginn Hieven, SZmax: 18kN
12.9.	SO277_35-1	PS	17:25:18	72,29	36° 01.722' N	014° 24.319' E	rwK = 120°, d = 2nm
12.9.	SO277_35-1	PS	17:40:12	57,32	36° 00.584' N	014° 26.514' E	rwK = 165°, d = 2nm
12.9.	SO277_35-1	PS	17:50:20	59,25	36° 00.530' N	014° 26.876' E	rwK = 300°, d = 4nm
12.9.	SO277_35-1	PS	18:19:34	90,56	36° 02.777' N	014° 22.286' E	rwK = 036°, d = 2nm
12.9.	SO277_35-1	PS	18:34:34	158,68	36° 04.440' N	014° 23.440' E	rwK: 128°, d: 3,2nm
12.9.	SO277_35-1	PS	18:56:25	150,35	36° 02.760' N	014° 26.515' E	rwK: 126°, d: 9,1nm
12.9.	SO277_35-1	PS	19:57:34	125,20	35° 57.418' N	014° 35.581' E	rwK: 183°, d: 1,3nm
12.9.	SO277_35-1	PS	20:06:37	122,59	35° 56.195' N	014° 35.677' E	rwK: 267°, d: 3nm
12.9.	SO277_35-1	PS	20:27:20	102,08	35° 55.807' N	014° 32.126' E	rwK: 308°, d: 3,3nm

Date	Station	Gear	Time	Depth	Latitude	Longitude	Remarks
2020	SONNE		UTC	[m]	[°N]	[°E]	
12.9.	SO277 35-1	PS	20:50:20	62,88	35° 57.793' N	014° 28.814' E	rwK: 226°, d: 2,3nm
12.9.	SO277 35-1	PS	21:05:45	57,33	35° 59.875' N	014° 27.655' E	rwK: 156°, d: 2,3nm
12.9.	SO277 35-1	PS	21:33:52	55,28	35° 57.809' N	014° 28.675' E	Ende Parasound Profil
12.9.	SO277 35-1	PS	21:36:11	47,49	35° 57.586' N	014° 28.950' E	Multibeam Profil Beginn, rwK: 129°, d: 0,9nm
12.9.	SO277 35-1	PS	21:51:05	54,45	35° 57.202' N	014° 29.891' E	rwK: 308°, d: 3,9nm
12.9.	SO277 35-1	PS	22:19:26	44,32	35° 59.778' N	014° 26.301' E	rwK: 128°, d: 4nm
12.9.	SO277 35-1	PS	22:52:09	65,25	35° 57.478' N	014° 30.171' E	rwK: 308°, d: 4nm
12.9.	SO277 35-1	PS	23:25:27	45,68	35° 59.892' N	014° 26.283' E	rwK: 128°, d: 4nm
12.9.	SO277 35-1	PS	23:57:09	62,63	35° 57.528' N	014° 30.217' E	rwK: 308°, d: 4nm
13.9.	SO277 35-1	PS	00:27:52	45,60	35° 59.897' N	014° 26.280' E	rwK: 128°, d: 4nm
13.9.	SO277 35-1	PS	00:58:51	65,04	35° 57.600' N	014° 30.284' E	rwK: 308°, d: 4nm
13.9.	SO277 35-1	PS	01:28:50	46,68	35° 59.957' N	014° 26.338' E	rwK: 128°, d: 4nm
13.9.	SO277 35-1	PS	02:00:00	65,48	35° 57.636' N	014° 30.292' E	rwK: 308°, d: 4nm
13.9.	SO277 35-1	PS	02:35:23	53,73	36° 00.239' N	014° 26.666' E	rwK: 128°, d: 4nm
13.9.	SO277 35-1	PS	03:08:30	57,16	35° 57.593' N	014° 30.031' E	rwK = 308°, d= 4nm
13.9.	SO277 35-1	PS	03:35:46	50,12	36° 00.132' N	014° 26.508' E	rwK = 128°, d= 4nm
13.9.	SO277 35-1	PS	04:06:36	86,80	35° 57.792' N	014° 30.468' E	rwK =308°, d=4nm
13.9.	SO277 35-1	PS	04:37:46	52,88	36° 00.197' N	014° 26.661' E	rwK = 128°, d=4nm
13.9.	SO277 35-1	PS	05:10:41	90,24	35° 57.731' N	014° 30.953' E	rwK= 308°, d= 4nm
13.9.	SO277 35-1	PS	05:42:14	53,04	36° 00.494' N	014° 26.748' E	Ende MBES Survey 06, Beginn MBES Survey 07, rwK = 299°, d= 2nm
13.9.	SO277 35-1	PS	06:08:34	129,90	36° 02.659' N	014° 22.880' E	rwK: 130°, d: 6,3nm
13.9.	SO277 35-1	PS	07:01:32	66,52	35° 59.273' N	014° 29.300' E	rwK: 037°, d: 1nm
13.9.	SO277 35-1	PS	07:09:00	115,04	35° 59.797' N	014° 30.130' E	rwK: 308°, d: 3,5nm
13.9.	SO277 36-1	CTD	08:12:24	34,00	36° 00.925' N	014° 22.212' E	FW2/ SPW2
13.9.	SO277 36-1	CTD	08:14:51	33,70	36° 00.928' N	014° 22.212' E	Bei SL 10m Transponder am Draht
13.9.	SO277 36-1	CTD	08:18:24	34,50	36° 00.928' N	014° 22.212' E	Bodensicht, SL: 28m
13.9.	SO277 36-1	CTD	09:41:26	33,04	36° 00.845' N	014° 22.281' E	Transponder an Deck
13.9.	SO277 37-1	AUV_L	12:35:56	64,70	36° 01.350' N	014° 25.317' E	AUV taucht ab
13.9.	SO277 38-1	CSE_M	14:56:43	66,70	36° 01.804' N	014° 24.242' E	1.Messkette zu Wasser
13.9.	SO277 38-1	CSE_M	14:57:46	66,70	36° 01.805' N	014° 24.244' E	2.Messkette zu Wasser
13.9.	SO277 38-1	CSE_M	15:03:55	67,70	36° 01.790' N	014° 24.261' E	3.Messkette zu Wasser
13.9.	SO277 38-1	CSE_M	15:05:16	66,50	36° 01.788' N	014° 24.267' E	4.Messkette zu Wasser
13.9.	SO277 38-1	CSE_M	15:11:30	69,00	36° 01.772' N	014° 24.309' E	5.Messkette zu Wasser
13.9.	SO277 38-1	CSE_M	15:50:50	66,20	36° 01.679' N	014° 24.524' E	Schweinchen zu Wasser
13.9.	SO277 38-1	CSE_M	16:00:20	66,70	36° 01.681' N	014° 24.522' E	rwK = 120°. d= 2nm
13.9.	SO277 38-1	CSE_M	16:02:53	65,70	36° 01.674' N	014° 24.537' E	Bodenkontakt
13.9.	SO277 38-1	CSE_M	16:17:50	67,50	36° 01.611' N	014° 24.663' E	Streamer komplett ausgesteckt, SL = 200m
13.9.	SO277 38-1	CSE_M	22:17:12	55,00	36° 00.675' N	014° 26.689' E	Hydrophon zu Wasser
13.9.	SO277 38-1	CSE_M	22:32:03	54,00	36° 00.675' N	014° 26.688' E	Hydrophon an Deck
13.9.	SO277 38-1	CSE_M	23:01:19	54,20	36° 00.613' N	014° 26.828' E	rwK: 165°, d: 2nm

Date	Station	Gear	Time	Depth	Latitude	Longitude	Remarks
2020	SONNE		UTC	[m]	[°N]	[°E]	
13.9.	SO277_38-1	CSE M	23:22:25	55,20	36° 00.453' N	014° 26.877' E	Hydrophon zu Wasser
13.9.	SO277_38-1	CSE M	23:27:20	57,00	36° 00.456' N	014° 26.875' E	Hydrophon an Deck
14.9.	SO277_38-1	CSE M	01:33:01	54,50	35° 59.798' N	014° 27.095' E	Hydrophon zu Wasser
14.9.	SO277_38-1	CSE M	01:42:15	55,20	35° 59.801' N	014° 27.096' E	Hydrophon an Deck
14.9.	SO277_38-1	CSE M	04:12:29	46,20	35° 59.278' N	014° 27.198' E	Schweinchen an Deck
14.9.	SO277_38-1	CSE M	04:53:54	45,50	35° 59.377' N	014° 27.163' E	1.Messkette an Deck
14.9.	SO277_38-1	CSE M	05:05:21	45,20	35° 59.433' N	014° 27.157' E	2.Messkette an Deck
14.9.	SO277_38-1	CSE M	05:06:33	45,70	35° 59.432' N	014° 27.154' E	3.Messkette an Deck
14.9.	SO277_38-1	CSE M	05:13:02	45,00	35° 59.441' N	014° 27.165' E	4.Messkette an Deck
14.9.	SO277_38-1	CSE M	05:13:46	45,20	35° 59.442' N	014° 27.166' E	Streamer an Deck
14.9.	SO277_38-1	CSE M	05:43:38	52,20	36° 00.066' N	014° 26.918' E	Hydrophon zu Wasser
14.9.	SO277_38-1	CSE M	06:06:00	52,50	36° 00.071' N	014° 26.937' E	Hydrophon an Deck
14.9.	SO277_39-1	MB	06:21:40	46,87	35° 58.910' N	014° 27.093' E	rwK: 125°, d: 1nm, v: 10kn ü.G.
14.9.	SO277_39-1	MB	06:27:43	50,37	35° 58.363' N	014° 28.058' E	rwK: 128°, d: 1,7nm
14.9.	SO277_39-1	MB	06:37:30	51,59	35° 57.356' N	014° 29.658' E	rwK: 123°, d: 1,9nm
14.9.	SO277_39-1	MB	06:48:38	99,43	35° 56.336' N	014° 31.593' E	rwK: 161°, d: 0,8nm
14.9.	SO277_39-1	MB	06:53:21	95,78	35° 55.664' N	014° 32.014' E	rwK: 128°, d: 3,1nm
14.9.	SO277_39-1	MB	07:13:32	95,55	35° 53.714' N	014° 35.215' E	rwK: 153°, d: 3,1nm
14.9.	SO277_39-1	MB	07:32:01	58,20	35° 51.058' N	014° 36.955' E	rwK: 333°, d: 3,2nm
14.9.	SO277_39-1	MB	07:56:24	107,75	35° 54.113' N	014° 35.615' E	rwK: 153°, d: 3,1nm
14.9.	SO277_39-1	MB	08:23:00	62,13	35° 51.098' N	014° 37.066' E	rwK: 333°, d: 3,2nm
14.9.	SO277_39-1	MB	08:47:56	106,29	35° 54.125' N	014° 35.780' E	rwK: 153°, d: 3,1nm
14.9.	SO277_39-1	MB	09:14:48	61,83	35° 50.975' N	014° 37.285' E	Ende Profil
14.9.	SO277_39-1	MB	09:42:13	99,32	35° 53.416' N	014° 35.884' E	Parasound Profil, rwK: 157°, d: 2,6nm, v: 7kn ü.G.
14.9.	SO277_39-1	MB	10:05:19	67,62	35° 50.962' N	014° 37.150' E	Ende Parasound Profil
14.9.	SO277_40-1	CTD	10:43:05	116,55	35° 54.794' N	014° 37.847' E	Clean Ship
14.9.	SO277_40-1	CTD	10:56:28	116,59	35° 54.794' N	014° 37.868' E	BOSI, SL: 119m
14.9.	SO277_40-1	CTD	11:16:12	115,74	35° 54.754' N	014° 37.878' E	Abbruch wg tech. Probleme
14.9.	SO277_40-1	CTD	11:16:20	116,00	35° 54.755' N	014° 37.878' E	Beginn Hieven
14.9.	SO277_40-1	CTD	11:48:24	115,41	35° 54.760' N	014° 37.880' E	BOSI, SL: 119m
14.9.	SO277_40-1	CTD	11:50:17	115,95	35° 54.757' N	014° 37.887' E	Fortsetzung Profil
14.9.	SO277_40-1	CTD	12:14:06	115,63	35° 54.770' N	014° 37.864' E	Beginn Hieven
14.9.	SO277_40-1	CTD	12:55:35	118,38	35° 55.076' N	014° 37.529' E	BOSI, SL: 122m
14.9.	SO277_40-1	CTD	12:56:08	118,52	35° 55.076' N	014° 37.530' E	rwK: 258°, d: 0,2nm
14.9.	SO277_41-1	CTD	14:37:40	62,50	35° 53.001' N	014° 34.851' E	BOKO, SLmax = 65m
14.9.	SO277_41-1	CTD	14:39:32	62,35	35° 53.002' N	014° 34.851' E	rwK = 210°
14.9.	SO277_42-1	CTD	15:43:25	96,58	35° 55.918' N	014° 31.721' E	Posidonia SL = 10m
14.9.	SO277_42-1	CTD	16:00:25	96,66	35° 55.919' N	014° 31.714' E	SL = 100m
14.9.	SO277_42-1	CTD	16:00:45	97,07	35° 55.918' N	014° 31.714' E	rwK = 120°
14.9.	SO277_42-1	CTD	17:23:34	99,36	35° 55.895' N	014° 31.980' E	Posidonia an Deck

Date	Station	Gear	Time	Depth	Latitude	Longitude	Remarks
2020	SONNE		UTC	[m]	[°N]	[°E]	
14.9.	SO277_43-1	PS	19:05:01	97,94	36° 01.681' N	014° 25.089' E	Beginn Profil, rwK: 046°, d: 8,6nm, v: 7kn ü.G.
14.9.	SO277_43-1	PS	20:18:31	142,18	36° 07.551' N	014° 32.539' E	Ende Parasound Profil
14.9.	SO277_43-1	PS	20:26:08	140,09	36° 06.914' N	014° 33.257' E	Beginn Multibeam Profil, rwK: 226°, d: 7nm, v: 10kn ü.G.
14.9.	SO277_43-1	PS	21:09:49	137,12	36° 01.845' N	014° 26.972' E	rwK: 046°, d: 7,1nm
14.9.	SO277_43-1	PS	21:53:19	140,20	36° 06.460' N	014° 33.448' E	rwK: 226°, d: 7,1nm
14.9.	SO277_43-1	PS	22:41:10	141,63	36° 02.029' N	014° 26.723' E	rwK: 046°, d: 7nm
14.9.	SO277_43-1	PS	23:29:52	139,04	36° 06.771' N	014° 33.364' E	rwK: 226°, d: 7nm
15.9.	SO277_43-1	PS	00:17:10	145,58	36° 02.281' N	014° 26.495' E	rwK: 046°, d: 7nm
15.9.	SO277_43-1	PS	01:08:54	142,49	36° 07.623' N	014° 32.299' E	rwK: 226°, d: 7nm
15.9.	SO277_43-1	PS	01:53:21	145,59	36° 02.643' N	014° 26.594' E	rwK: 046°, d: 7nm
15.9.	SO277_43-1	PS	02:44:09	144,12	36° 07.876' N	014° 32.061' E	rwK: 226°, d: 7nm
15.9.	SO277_43-1	PS	03:27:47	149,02	36° 03.580' N	014° 25.717' E	rwK = 046°, d= 7nm
15.9.	SO277_43-1	PS	04:15:45	144,48	36° 08.138' N	014° 31.791' E	rwK = 226°c = 7nm
15.9.	SO277_43-1	PS	05:00:17	147,97	36° 03.577' N	014° 25.758' E	rwK = 046°, d= 2nm
15.9.	SO277_44-1	AUV_L	05:55:52	38,20	36° 01.843' N	014° 21.102' E	Modem wird im Schacht hinab gelassen
15.9.	SO277_44-1	AUV_L	06:26:10	38,50	36° 01.846' N	014° 21.113' E	AUV Luise zu Wasser
15.9.	SO277_44-1	AUV_L	06:29:54	39,00	36° 01.847' N	014° 21.114' E	Mission wurde gestartet
15.9.	SO277_44-1	AUV_L	06:38:07	38,50	36° 01.843' N	014° 21.116' E	Modem wieder an Deck
15.9.	SO277_44-1	AUV_L	12:21:24	33,50	36° 01.730' N	014° 20.961' E	AUV gesichtet
15.9.	SO277_45-1	GC	07:17:31	124,70	36° 04.430' N	014° 19.257' E	GC - 3m
15.9.	SO277_45-1	GC	07:20:06	126,20	36° 04.428' N	014° 19.258' E	FW2/SPW2
15.9.	SO277_45-1	GC	07:23:19	126,00	36° 04.427' N	014° 19.258' E	SLmax: 138m
15.9.	SO277_45-1	GC	07:24:01	124,00	36° 04.425' N	014° 19.259' E	Beginn hieven, SZmax: 16,0kN
15.9.	SO277_45-2	GC	07:42:47	123,70	36° 04.427' N	014° 19.268' E	GC - 3m
15.9.	SO277_45-2	GC	07:45:38	125,20	36° 04.428' N	014° 19.265' E	FW2/SPW2
15.9.	SO277_45-2	GC	07:49:16	126,00	36° 04.426' N	014° 19.272' E	Boko, SLmax: 137m
15.9.	SO277_45-2	GC	07:50:05	123,70	36° 04.424' N	014° 19.270' E	Beginn hieven, SZmax: 23,5kN
15.9.	SO277_46-1	GC	08:20:48	147,00	36° 04.367' N	014° 19.740' E	GC - 3m
15.9.	SO277_46-1	GC	08:25:28	145,70	36° 04.364' N	014° 19.748' E	FW2/SPW2
15.9.	SO277_46-1	GC	08:30:40	147,70	36° 04.369' N	014° 19.748' E	Boko, SLmax: 161m
15.9.	SO277_46-1	GC	08:31:45	148,00	36° 04.369' N	014° 19.744' E	SZmax: 20,7kN
15.9.	SO277_47-1	GC	11:00:27	130,50	36° 03.958' N	014° 19.917' E	GC 3m
15.9.	SO277_47-1	GC	11:07:50	130,70	36° 03.958' N	014° 19.913' E	BOKO, SLmax: 142m
15.9.	SO277_47-1	GC	11:08:15	127,70	36° 03.957' N	014° 19.915' E	Beginn Hieven, Szmax: 19kN
15.9.	SO277_47-2	GC	11:28:42	127,50	36° 03.965' N	014° 19.918' E	GC 3m
15.9.	SO277_47-2	GC	11:32:43	129,20	36° 03.969' N	014° 19.919' E	BOKO, SLmax: 145m
15.9.	SO277_47-2	GC	11:33:11	129,50	36° 03.969' N	014° 19.919' E	SZmax: 19kN
15.9.	SO277_48-1	CSE M	14:31:39	47,20	35° 59.492' N	014° 27.089' E	Streamer zu Wasser / 1. Messkette
15.9.	SO277_48-1	CSE M	14:40:07	45,50	35° 59.493' N	014° 27.093' E	2.Messkette zu Wasser
15.9.	SO277_48-1	CSE M	14:51:51	46,50	35° 59.493' N	014° 27.091' E	Streamer komplett ausgesteckt, SL = 200m
15.9.	SO277_48-1	CSE M	16:03:50	44,20	35° 59.515' N	014° 27.111' E	rwK = 341°

Date	Station	Gear	Time	Depth	Latitude	Longitude	Remarks
2020	SONNE		UTC	[m]	[°N]	[°E]	
16.9.	SO277_48-1	CSE M	04:24:22	54,20	36° 00.483' N	014° 26.821' E	1.Messkette an Deck
16.9.	SO277_48-1	CSE M	04:33:06	53,50	36° 00.479' N	014° 26.819' E	Streamer an Deck
16.9.	SO277_49-1	AUV_ L	06:00:30	146,50	36° 03.542' N	014° 26.271' E	Mission gestartet
16.9.	SO277_49-1	AUV_ L	06:19:48	147,20	36° 03.540' N	014° 26.267' E	Modem an Deck
16.9.	SO277_49-1	AUV_ L	12:22:51	146,70	36° 03.623' N	014° 26.287' E	AUV gesichtet
16.9.	SO277_50-1	GC	07:03:12	50,36	35° 59.489' N	014° 27.599' E	GC - 3m
16.9.	SO277_50-1	GC	07:07:32	52,00	35° 59.489' N	014° 27.601' E	FW2/SPW2
16.9.	SO277_50-1	GC	07:09:04	50,70	35° 59.488' N	014° 27.600' E	Boko, SLmax: 60m
16.9.	SO277_50-1	GC	07:10:39	51,20	35° 59.488' N	014° 27.603' E	SZmax: 14,0kN
16.9.	SO277_50-2	GC	07:20:59	49,70	35° 59.494' N	014° 27.604' E	GC - 3m
16.9.	SO277_50-2	GC	07:23:32	49,20	35° 59.495' N	014° 27.601' E	FW2/SPW2
16.9.	SO277_50-2	GC	07:24:59	50,70	35° 59.496' N	014° 27.602' E	Boko, SLmax: 65m
16.9.	SO277_50-2	GC	07:26:00	49,00	35° 59.496' N	014° 27.603' E	Beginn hieven, SZmax: 14,3kN
16.9.	SO277_51-1	GC	08:16:04	68,70	36° 00.243' N	014° 27.424' E	GC - 3m
16.9.	SO277_51-1	GC	08:18:28	67,20	36° 00.241' N	014° 27.427' E	FW2/SPW2
16.9.	SO277_51-1	GC	08:20:36	68,20	36° 00.243' N	014° 27.425' E	Boko, SLmax: 83m
16.9.	SO277_51-1	GC	08:21:51	69,00	36° 00.244' N	014° 27.425' E	SZmax: 17,3kN
16.9.	SO277_52-1	GC	09:23:22	33,20	36° 00.935' N	014° 22.220' E	GC - 3m
16.9.	SO277_52-1	GC	09:25:47	33,50	36° 00.933' N	014° 22.218' E	FW2/SPW2
16.9.	SO277_52-1	GC	09:26:55	34,00	36° 00.933' N	014° 22.219' E	SLmax: 43m
16.9.	SO277_52-1	GC	09:27:55	34,20	36° 00.934' N	014° 22.220' E	SZmax: 14,4kN
16.9.	SO277_52-2	GC	11:00:40	34,50	36° 00.942' N	014° 22.220' E	GC 3m
16.9.	SO277_52-2	GC	11:01:55	34,00	36° 00.942' N	014° 22.220' E	BOKO, SLmax: 44m
16.9.	SO277_52-2	GC	11:02:11	33,50	36° 00.942' N	014° 22.220' E	SZmax: 14kN
16.9.	SO277_53-1	GC	11:19:01	34,00	36° 00.899' N	014° 22.241' E	BOKO, SLmax: 43m
16.9.	SO277_53-1	GC	11:19:17	33,70	36° 00.899' N	014° 22.242' E	SZmax: 14kN
16.9.	SO277_53-2	GC	11:32:10	34,20	36° 00.890' N	014° 22.246' E	BOKO, SLmax: 45m
16.9.	SO277_53-2	GC	11:32:21	33,20	36° 00.889' N	014° 22.246' E	SZmax: 14kN
16.9.	SO277_54-1	CTD	13:39:11	39,00	36° 01.936' N	014° 21.069' E	clean ship
16.9.	SO277_54-1	CTD	13:46:21	37,78	36° 01.934' N	014° 21.070' E	Transponder bei SL: 10m angebracht und zu Wasser
16.9.	SO277_54-1	CTD	14:12:07	38,04	36° 01.939' N	014° 21.076' E	Posidonia an Deck
16.9.	SO277_54-1	CTD	14:14:26	38,40	36° 01.940' N	014° 21.076' E	CTD an Deck
16.9.	SO277_54-1	CTD	14:31:31	37,81	36° 01.939' N	014° 21.075' E	Video-CTD zu Wasser
16.9.	SO277_54-1	CTD	14:34:50	38,83	36° 01.939' N	014° 21.076' E	Posidonia SL= 10m
16.9.	SO277_54-1	CTD	14:38:04	38,96	36° 01.939' N	014° 21.075' E	Bodensicht SL= 34m
16.9.	SO277_54-1	CTD	15:50:18	40,90	36° 01.771' N	014° 21.213' E	SLmax = 42m
16.9.	SO277_54-1	CTD	16:04:46	41,49	36° 01.772' N	014° 21.213' E	Posidonia an Deck
16.9.	SO277_54-1	CTD	16:07:09	41,66	36° 01.772' N	014° 21.212' E	CTD an Deck
16.9.	SO277_55-1	MB	16:31:30	30,16	36° 00.191' N	014° 22.688' E	rwK = 125°, d= 4nm
16.9.	SO277_55-1	MB	16:55:41	42,89	35° 58.089' N	014° 26.629' E	rwK = 111°, d= 3nm
16.9.	SO277_55-1	MB	17:12:12	48,06	35° 57.094' N	014° 29.672' E	rwK = 129°, d= 2nm
16.9.	SO277_55-1	MB	17:27:37	95,53	35° 55.588' N	014° 32.091' E	rwK = 127°, d= 3nm

Date	Station	Gear	Time	Depth	Latitude	Longitude	Remarks
2020	SONNE		UTC	[m]	[°N]	[°E]	
16.9.	SO277 55-1	MB	17:46:16	93,44	35° 53.818' N	014° 35.036' E	rwK = 125°, d = 2nm
16.9.	SO277 55-1	MB	17:57:17	95,18	35° 52.772' N	014° 36.702' E	rwK = 149°, dd= 1nm
16.9.	SO277 55-1	MB	18:05:03	66,26	35° 51.644' N	014° 37.228' E	viele kurze Kurse in unterschiedliche Richtungen
16.9.	SO277 55-1	MB	19:23:34	92,66	35° 54.561' N	014° 40.437' E	Begibnn Profil Nr. 2. rwK: 308°, d: 12,5nm
16.9.	SO277 55-1	MB	20:48:08	140,16	36° 02.272' N	014° 28.298' E	rwK: 048°, d: 0,7nm
16.9.	SO277 55-1	MB	20:53:53	141,99	36° 02.772' N	014° 28.644' E	rwK: 128°, d: 14nm
16.9.	SO277 55-1	MB	22:41:11	73,20	35° 54.215' N	014° 42.429' E	rwK: 308°, d: 14nm
17.9.	SO277 55-1	MB	00:20:06	143,22	36° 02.661' N	014° 28.650' E	rwK: 129°, d: 14nm
17.9.	SO277 55-1	MB	02:00:00	75,71	35° 54.465' N	014° 42.803' E	rwK: 308°, d: 14nm
17.9.	SO277 55-1	MB	03:40:05	142,23	36° 02.841' N	014° 28.863' E	rwK: 129°, d: 14nm
17.9.	SO277 56-1	CTD	06:02:46	121,70	35° 56.701' N	014° 35.667' E	clean ship liegt an
17.9.	SO277 56-1	CTD	06:04:20	121,70	35° 56.699' N	014° 35.669' E	FW1/SPW1
17.9.	SO277 56-1	CTD	06:07:26	121,20	35° 56.702' N	014° 35.669' E	Bei SL: 10m Transponder am Draht
17.9.	SO277 56-1	CTD	06:14:36	122,00	35° 56.700' N	014° 35.671' E	Fieren gestopt, warten auf Kamerabild, SL: 100m
17.9.	SO277 56-1	CTD	06:32:51	120,20	35° 56.703' N	014° 35.671' E	Bodensicht, SL: 125m
17.9.	SO277 56-1	CTD	06:34:35	120,50	35° 56.704' N	014° 35.671' E	rwK: 215°, d: 411m, v: 0,3kn
17.9.	SO277 56-1	CTD	07:21:53	120,08	35° 56.519' N	014° 35.513' E	rwK: 090°, d: 446m
17.9.	SO277 56-1	CTD	08:11:12	121,64	35° 56.520' N	014° 35.807' E	rwK: 297°, d: 737m, v: 0,5kn
17.9.	SO277 56-1	CTD	08:56:24	119,68	35° 56.686' N	014° 35.405' E	Beginn hieven, SL: 123m, SZmax: 3,3 kN
17.9.	SO277 56-1	CTD	09:01:49	121,35	35° 56.687' N	014° 35.406' E	Transponder an Deck
17.9.	SO277 57-1	CTD	10:19:21	54,50	36° 01.058' N	014° 25.243' E	clean ship liegt an
17.9.	SO277 57-1	CTD	10:29:00	55,20	36° 01.064' N	014° 25.242' E	Transponder bei SL: 10m angebracht und zu Wasser
17.9.	SO277 57-1	CTD	10:34:18	54,50	36° 01.065' N	014° 25.244' E	BOSI; SL: 57m
17.9.	SO277 57-1	CTD	10:34:50	55,20	36° 01.065' N	014° 25.245' E	rwK: 027°, d: 0,5nm
17.9.	SO277 57-1	CTD	11:46:09	64,20	36° 01.350' N	014° 25.415' E	Transponder an Deck
17.9.	SO277 58-1	GC	12:49:44	80,58	36° 03.298' N	014° 19.833' E	BOKO, SLmax: 92m
17.9.	SO277 58-1	GC	12:49:55	81,14	36° 03.298' N	014° 19.834' E	Beginn Hieven, SZmax: 19kN
17.9.	SO277 59-1	CSE M	14:10:04	143,99	36° 02.481' N	014° 27.435' E	rwK= 308°
17.9.	SO277 59-1	CSE M	14:11:17	143,50	36° 02.481' N	014° 27.435' E	1.Messkette zu Wasser
17.9.	SO277 59-1	CSE M	14:13:10	142,96	36° 02.479' N	014° 27.440' E	2. Messkette zu Wasser
17.9.	SO277 59-1	CSE M	14:22:15	143,59	36° 02.500' N	014° 27.411' E	3.Messkette zu Wasser
17.9.	SO277 59-1	CSE M	14:27:55	142,82	36° 02.517' N	014° 27.385' E	4.Messkette zu Wasser
17.9.	SO277 59-1	CSE M	14:33:27	143,38	36° 02.533' N	014° 27.357' E	4.Messkette zu Wasser
17.9.	SO277 59-1	CSE M	14:50:09	143,85	36° 02.558' N	014° 27.321' E	Schweinchen zu Wasser
17.9.	SO277 59-1	CSE M	15:03:00	144,62	36° 02.578' N	014° 27.288' E	Schweinchen auf Grund
17.9.	SO277 59-1	CSE M	15:45:34	145,00	36° 02.854' N	014° 26.846' E	Streamer vollständig ausgesteckt, SL = 320m
18.9.	SO277 59-1	CSE M	06:07:27	157,20	36° 05.289' N	014° 23.007' E	Schweinchen an Deck
18.9.	SO277 59-1	CSE M	06:32:01	159,20	36° 05.234' N	014° 23.086' E	1. Messkette an Deck
18.9.	SO277 59-1	CSE M	06:38:48	158,50	36° 05.211' N	014° 23.121' E	2. Messkette an Deck
18.9.	SO277 59-1	CSE M	06:44:51	156,20	36° 05.193' N	014° 23.147' E	3. Messkette an Deck

Date	Station	Gear	Time	Depth	Latitude	Longitude	Remarks
2020	SONNE		UTC	[m]	[°N]	[°E]	
18.9.	SO277_59-1	CSE M	06:53:01	155,70	36° 05.177' N	014° 23.173' E	4. Messkette an Deck
18.9.	SO277_60-1	OBE M	07:50:54	46,50	35° 59.505' N	014° 27.336' E	Hydrophon zu Wasser
18.9.	SO277_60-1	OBE M	07:51:11	45,70	35° 59.504' N	014° 27.336' E	OBMT # 01 ausgelöst
18.9.	SO277_60-1	OBE M	07:52:34	46,20	35° 59.502' N	014° 27.335' E	OBMT an der Oberfläche
18.9.	SO277_60-1	OBE M	07:53:26	46,50	35° 59.501' N	014° 27.334' E	Hydrophon an Deck
18.9.	SO277_60-1	OBE M	08:12:21	51,00	35° 59.651' N	014° 27.095' E	OBMT # 1 an Deck
18.9.	SO277_60-1	OBE M	08:16:18	52,50	35° 59.652' N	014° 27.094' E	Hydrophon zu Wasser
18.9.	SO277_60-1	OBE M	08:16:48	52,20	35° 59.651' N	014° 27.094' E	OBMT # 02 ausgelöst
18.9.	SO277_60-1	OBE M	08:17:37	51,50	35° 59.651' N	014° 27.093' E	OBMT # 02 an der Oberfläche
18.9.	SO277_60-1	OBE M	08:18:11	52,00	35° 59.651' N	014° 27.093' E	Hydrophon an Deck
18.9.	SO277_60-1	OBE M	08:34:28	50,00	35° 59.821' N	014° 27.068' E	OBMT # 02 an Deck
18.9.	SO277_60-1	OBE M	08:35:30	50,20	35° 59.822' N	014° 27.072' E	Hydrophon zu Wasser
18.9.	SO277_60-1	OBE M	08:37:56	49,70	35° 59.821' N	014° 27.068' E	OBMT #03 ausgelöst
18.9.	SO277_60-1	OBE M	08:39:13	49,70	35° 59.820' N	014° 27.066' E	OBMT # 03 aufgetaucht
18.9.	SO277_60-1	OBE M	08:40:30	50,00	35° 59.819' N	014° 27.067' E	Hydrophon an Deck
18.9.	SO277_60-1	OBE M	08:55:26	51,20	36° 00.053' N	014° 26.996' E	OBMT # 03 an Deck
18.9.	SO277_60-1	OBE M	08:56:00	51,70	36° 00.052' N	014° 26.994' E	Hydrophon zu Wasser
18.9.	SO277_60-1	OBE M	08:57:03	52,20	36° 00.051' N	014° 26.992' E	OBMT #04 ausgelöst
18.9.	SO277_60-1	OBE M	08:58:13	51,70	36° 00.051' N	014° 26.992' E	OBMT #04 an der Oberfläche
18.9.	SO277_60-1	OBE M	08:59:37	52,20	36° 00.052' N	014° 26.994' E	Hydrophon an Deck
18.9.	SO277_60-1	OBE M	09:16:49	56,20	36° 00.245' N	014° 26.904' E	OBMT #04 an Deck
18.9.	SO277_60-1	OBE M	10:01:15	54,20	36° 00.533' N	014° 27.023' E	OBMT 05 ausgelöst
18.9.	SO277_60-1	OBE M	10:15:10	56,00	36° 00.633' N	014° 27.078' E	OBMT 05
18.9.	SO277_60-1	OBE M	10:40:48	57,00	36° 01.147' N	014° 25.282' E	OBMT 06 ausgelöst
18.9.	SO277_60-1	OBE M	10:51:58	58,00	36° 01.246' N	014° 25.154' E	OBMT 06
18.9.	SO277_60-1	OBE M	11:09:47	64,50	36° 01.740' N	014° 24.035' E	OBMT 07 ausgelöst
18.9.	SO277_60-1	OBE M	11:20:04	66,50	36° 01.849' N	014° 23.949' E	OBMT 07
18.9.	SO277_60-1	OBE M	11:39:25	58,50	36° 01.794' N	014° 22.603' E	OBMT 08 ausgelöst
18.9.	SO277_60-1	OBE M	11:50:26	62,20	36° 01.907' N	014° 22.491' E	OBMT 08
18.9.	SO277_60-1	OBE M	12:09:38	66,20	36° 02.428' N	014° 21.289' E	OBMT 09 ausgelöst
18.9.	SO277_60-1	OBE M	12:22:17	67,50	36° 02.565' N	014° 21.109' E	OBMT 09
18.9.	SO277_60-1	OBE M	12:43:03	81,50	36° 03.565' N	014° 19.744' E	OBMT 10 ausgelöst
18.9.	SO277_60-1	OBE M	12:52:27	85,00	36° 03.655' N	014° 19.631' E	OBMT 10
18.9.	SO277_60-1	OBE M	13:10:25	65,50	36° 03.971' N	014° 18.660' E	OBMT 11 ausgelöst
18.9.	SO277_60-1	OBE M	13:21:07	68,50	36° 04.078' N	014° 18.515' E	OBMT 11
18.9.	SO277_60-1	OBE M	13:51:35	143,70	36° 05.706' N	014° 15.178' E	OBMT 12 ausgelöst

Date	Station	Gear	Time	Depth	Latitude	Longitude	Remarks
2020	SONNE		UTC	[m]	[°N]	[°E]	
18.9.	SO277 60-1	OBE M	14:03:47	156,23	36° 05.852' N	014° 15.088' E	OBMT 12
18.9.	SO277 60-1	OBE M	14:05:17	160,55	36° 05.909' N	014° 15.070' E	
18.9.	SO277 61-1	CTD	15:06:26	33,84	36° 00.882' N	014° 22.285' E	
18.9.	SO277 61-1	CTD	15:07:17	34,46	36° 00.881' N	014° 22.285' E	
18.9.	SO277 61-1	CTD	15:11:48	34,03	36° 00.882' N	014° 22.280' E	Posidonia SL= 10m
18.9.	SO277 61-1	CTD	15:15:36	34,25	36° 00.882' N	014° 22.275' E	Bodensicht SL= 33m
18.9.	SO277 61-1	CTD	15:16:06	33,84	36° 00.883' N	014° 22.274' E	
18.9.	SO277 61-1	CTD	16:13:02	34,80	36° 00.880' N	014° 22.219' E	
18.9.	SO277 61-1	CTD	16:13:17	34,13	36° 00.880' N	014° 22.219' E	
18.9.	SO277 61-1	CTD	16:18:04	34,40	36° 00.880' N	014° 22.219' E	Posidonia an Deck
18.9.	SO277 61-1	CTD	16:20:39	34,66	36° 00.879' N	014° 22.217' E	CTD an Deck
18.9.	SO277 61-1	CTD	16:25:29	34,36	36° 00.879' N	014° 22.216' E	
18.9.	SO277 62-1 wurde wegen falscher Einträge gelöscht und unter SO277 63-1 neu angelegt. Gesamtsumme der Stationen 69						
18.9.	SO277 63-1	EM71 0	21:37:06	108,93	36° 36.534' N	015° 19.069' E	Beginn Profil, rwK: 035°, d: 19,9nm
18.9.	SO277 63-1	EM71 0	23:31:00	2747,57	36° 52.190' N	015° 32.485' E	rwK: 356°, d: 25nm
19.9.	SO277 63-1	EM71 0	02:00:00	2253,68	37° 17.282' N	015° 30.519' E	rwK: 341°, d: 8nm
19.9.	SO277 63-1	EM71 0	02:50:40	2154,94	37° 24.885' N	015° 27.326' E	rwK = 313°, d = 4nm
19.9.	SO277 63-1	EM71 0	03:28:31	2044,01	37° 27.546' N	015° 23.715' E	rwk= 316°, d= 2nm
19.9.	SO277 63-1	EM71 0	03:46:38	1971,02	37° 28.893' N	015° 22.099' E	rwK = 310°, d = 2nm
19.9.	SO277 63-1	EM71 0	04:08:25	1807,06	37° 30.348' N	015° 19.894' E	rwK = 298°, d= 1nm
19.9.	SO277 63-1	EM71 0	04:20:02	1810,15	37° 30.943' N	015° 18.525' E	rwK = 300°, d= 3nm
19.9.	SO277 63-1	AGSS	05:10:25	0,00	37° 32.372' N	015° 15.514' E	Einmessen
19.9.	SO277 64-1	AGSS	05:13:43	0,00	37° 32.374' N	015° 15.513' E	Modem zu Wasser
19.9.	SO277 64-1	AGSS	05:21:04	0,00	37° 32.374' N	015° 15.517' E	Modem auf SLmax = 30m
19.9.	SO277 64-1	CTD	07:02:02	1192,54	37° 32.133' N	015° 15.892' E	clean ship liegt an
19.9.	SO277 65-1	CTD	07:05:10	1196,16	37° 32.127' N	015° 15.891' E	FW1/SPW1
19.9.	SO277 65-1	CTD	07:07:15	1194,31	37° 32.126' N	015° 15.895' E	Bei SL: 10m Transponder am Draht
19.9.	SO277 65-1	CTD	07:49:15	1192,32	37° 32.161' N	015° 15.878' E	Bodensicht, SL: 1196m
19.9.	SO277 65-1	CTD	07:54:12	1201,29	37° 32.181' N	015° 15.878' E	rwK: 117°, d: 0,1nm, v: 0,5kn
19.9.	SO277 65-1	CTD	08:27:58	1208,17	37° 32.111' N	015° 15.953' E	rwK: 268°, d: 0,3nm
19.9.	SO277 65-1	CTD	08:46:49	1197,46	37° 32.111' N	015° 15.835' E	Abbruch Profil
19.9.	SO277 65-1	CTD	08:48:02	1199,65	37° 32.110' N	015° 15.835' E	Beginn hieven, SZmax: 11,4kN
19.9.	SO277 65-1	CTD	09:29:56	1198,79	37° 32.113' N	015° 15.838' E	Transponder an Deck
19.9.	SO277 65-1	SEIS OBR	10:06:08	814,35	37° 33.173' N	015° 14.554' E	OBS # 01 zu Wasser
19.9.	SO277 66-1	SEIS OBR	10:26:03	1166,93	37° 32.928' N	015° 15.825' E	OBS 02
19.9.	SO277 66-1	SEIS OBR	10:36:09	1275,52	37° 32.590' N	015° 16.334' E	OBS 03

Date	Station	Gear	Time	Depth	Latitude	Longitude	Remarks
2020	SONNE		UTC	[m]	[°N]	[°E]	
19.9.	SO277_66-1	SEIS OBR	10:49:03	1378,31	37° 31.939' N	015° 16.497' E	OBS 04
19.9.	SO277_66-1	SEIS OBR	11:06:31	1145,15	37° 32.140' N	015° 15.339' E	OBS 05
19.9.	SO277_66-1	SEIS OBR	11:20:21	913,98	37° 32.426' N	015° 14.438' E	OBS 06
19.9.	SO277_67-1	CTD	14:23:59	1967,68	37° 25.778' N	015° 26.670' E	Posidonia SL = 10m
19.9.	SO277_67-1	CTD	15:20:09	1964,50	37° 25.786' N	015° 26.670' E	Bodensicht, SL = 1972m
19.9.	SO277_67-1	CTD	15:21:27	1959,97	37° 25.786' N	015° 26.670' E	rwK = 272°, d= 0,7nm
19.9.	SO277_67-1	CTD	17:14:45	2109,89	37° 25.819' N	015° 25.703' E	SLmax = 2123m
19.9.	SO277_67-1	CTD	18:33:53	2110,31	37° 25.818' N	015° 25.704' E	Transponder an Deck
19.9.	SO277_67-1	CTD	18:37:40	2111,00	37° 25.820' N	015° 25.702' E	CTD an Deck
19.9.	SO277_67-1	MB	19:20:45	2144,66	37° 24.098' N	015° 25.426' E	Beginn Profil, rwK: 044°, d: 13nm, v: 6kn
19.9.	SO277_68-1	MB	21:29:13	2008,59	37° 33.479' N	015° 36.856' E	rwK: 134°, d: 1nm
19.9.	SO277_68-1	MB	21:39:52	2129,25	37° 33.024' N	015° 37.821' E	rwK: 224°, d: 13,2nm
19.9.	SO277_68-1	MB	23:49:51	2160,63	37° 23.462' N	015° 26.560' E	rwK: 134°, d: 1nm
20.9.	SO277_68-1	MB	00:01:47	2166,36	37° 22.702' N	015° 27.308' E	rwK: 041°, d: 2nm
20.9.	SO277_68-1	MB	00:21:32	2182,59	37° 23.893' N	015° 28.813' E	rwK: 312°, d: 8nm
20.9.	SO277_68-1	MB	01:39:09	1941,01	37° 29.084' N	015° 21.790' E	rwK: 307°, d: 3nm
20.9.	SO277_68-1	MB	02:09:03	1823,00	37° 30.868' N	015° 18.772' E	rwK = 263°, d=2nm
20.9.	SO277_68-1	MB	02:27:55	1427,45	37° 30.657' N	015° 16.265' E	rwK = 013°, d=1nm
20.9.	SO277_68-1	MB	02:39:26	1490,63	37° 31.615' N	015° 16.346' E	rwK = 256°, d= 1nm
20.9.	SO277_68-1	MB	02:47:52	1387,71	37° 31.592' N	015° 15.388' E	rwK = 114°, d= 1nm
20.9.	SO277_68-1	MB	02:57:06	1492,46	37° 31.134' N	015° 16.031' E	rwK = 076°, d= 1nm
20.9.	SO277_68-1	MB	03:07:05	1652,71	37° 31.365' N	015° 17.330' E	rwK= 095°, d= 2nm
20.9.	SO277_68-1	MB	03:27:18	1824,32	37° 31.205' N	015° 20.049' E	rwK =281°, d = 3nm
20.9.	SO277_68-1	MB	03:57:34	1444,97	37° 31.999' N	015° 16.932' E	rwK = 294°, d= 2nm
20.9.	SO277_68-1	MB	04:13:09	891,81	37° 32.683' N	015° 14.976' E	rwK = 285°, d 2nm
20.9.	SO277_68-1	MB	04:29:58	430,17	37° 33.281' N	015° 12.749' E	rwK =302°, d= 1nm
20.9.	SO277_68-1	MB	04:53:40	433,71	37° 32.910' N	015° 12.601' E	rwK = 104°, d = 3nm
20.9.	SO277_68-1	MB	05:10:05	915,06	37° 32.531' N	015° 14.746' E	rwK = 114°, d = 2nm
20.9.	SO277_68-1	MB	05:34:13	1445,78	37° 31.551' N	015° 15.961' E	rwK = 002°, d = 2nm
20.9.	SO277_68-1	CTD	12:05:03	1577,05	38° 41.529' N	015° 16.335' E	clean ship
20.9.	SO277_69-1	CTD	13:10:35	1577,07	38° 41.529' N	015° 16.333' E	BOSI, SL: 1575m
20.9.	SO277_69-1	CTD	13:12:24	1578,36	38° 41.529' N	015° 16.333' E	SLmax: 1577m
20.9.	SO277_69-1	CTD	13:13:42	1576,87	38° 41.530' N	015° 16.334' E	Beginn Hieven
20.9.	SO277_69-1	MB	15:26:08	363,51	38° 47.673' N	015° 10.698' E	rwK = 048°, d = 2nm
20.9.	SO277_70-1	MB	15:42:53	340,57	38° 49.096' N	015° 12.764' E	rwK = 070°, d = 2nm
20.9.	SO277_70-1	MB	15:50:28	174,17	38° 49.434' N	015° 13.947' E	rwK = 248°, d = 2nm
20.9.	SO277_70-1	MB	16:00:02	123,79	38° 49.450' N	015° 14.320' E	rwK = 219°, d = 1nm
20.9.	SO277_70-1	MB	16:18:42	358,91	38° 48.232' N	015° 11.612' E	rwK = 237°, d = 1nm
20.9.	SO277_70-1	MB	16:25:18	359,28	38° 47.714' N	015° 10.722' E	rwK = 053°, d = 2nm
20.9.	SO277_70-1	MB	16:43:53	460,69	38° 49.191' N	015° 12.595' E	rwK = 070°, d = 1nm
20.9.	SO277_70-1	MB	16:56:29	351,75	38° 50.004' N	015° 14.328' E	rwK = 236°, d = 4nm
20.9.	SO277_70-1	MB	17:29:27	904,85	38° 47.905' N	015° 09.874' E	Unterbrechung Profil
20.9.	SO277_70-1	MB	18:55:05	2916,99	38° 52.480' N	014° 50.688' E	Fortsetzung Profil, rwK: 100°, d: 6,6nm, v: 6kn ü. G.

Date	Station	Gear	Time	Depth	Latitude	Longitude	Remarks
2020	SONNE		UTC	[m]	[°N]	[°E]	
20.9.	SO277 70-1	MB	20:01:24	2267,15	38° 51.370' N	014° 59.008' E	rwK: 054°, d: 16nm
20.9.	SO277 70-1	MB	22:42:43	2488,38	39° 00.714' N	015° 15.687' E	rwK: 234°, d: 16nm
21.9.	SO277 70-1	MB	01:34:15	2226,12	38° 50.462' N	015° 00.161' E	rwK: 054°, d: 17nm
21.9.	SO277 70-1	MB	04:26:42	2334,57	38° 59.369' N	015° 18.232' E	rwk= 234°, d =14nm
21.9.	SO277 70-1	MB	06:45:33	2207,83	38° 50.615' N	015° 05.000' E	rwK: 146°, d: 1nm
21.9.	SO277 70-1	MB	06:53:24	2134,49	38° 49.902' N	015° 05.388' E	rwK: 054°, d: 8,7nm, v: 8kn ü. G.
21.9.	SO277 70-1	MB	07:57:59	2415,97	38° 54.753' N	015° 14.362' E	rwK: 174°, d: 1nm
21.9.	SO277 70-1	MB	08:06:25	2345,21	38° 54.085' N	015° 14.737' E	rwK: 234°, d: 7,1nm
21.9.	SO277 70-1	MB	09:00:29	1827,54	38° 49.781' N	015° 07.548' E	rwK: 132°, d: 0,5nm
21.9.	SO277 70-1	MB	09:05:50	1778,89	38° 49.371' N	015° 07.687' E	rwK: 056°, d: 5,4nm
21.9.	SO277 70-1	MB	09:46:26	1940,12	38° 52.223' N	015° 13.417' E	rwK: 162°, d: 0,6nm
21.9.	SO277 70-1	MB	09:52:11	1701,69	38° 51.934' N	015° 13.872' E	rwK: 236°, d: 5,1nm
21.9.	SO277 70-1	MB	10:32:50	1530,23	38° 48.946' N	015° 08.565' E	rwK: 055°, d: 5nm
21.9.	SO277 70-1	MB	11:14:50	1302,99	38° 51.209' N	015° 14.057' E	rwK: 236°, d: 4nm
21.9.	SO277 70-1	MB	11:56:00	1054,93	38° 48.138' N	015° 09.575' E	Profilwechsel, rwK: 176°, d: 8nm
21.9.	SO277 70-1	MB	12:39:04	902,51	38° 41.487' N	015° 10.252' E	Beginn Panarea Profil, rwK: 253°, d: 7nm
21.9.	SO277 70-1	MB	13:30:47	677,34	38° 39.539' N	015° 01.811' E	rwK: 073°, d: 7nm
21.9.	SO277 70-1	MB	14:38:58	1196,22	38° 42.447' N	015° 10.213' E	Profilende Panarea
21.9.	SO277 70-1	MB	15:13:43	1253,06	38° 48.189' N	015° 09.107' E	rwK = 56°, d= 5nm

7 Data and Sample Storage and Availability

The data were collected within the SMART project. These data gathered during SO277 are stored in facilities of GEOMAR Helmholtz-Zentrum für Ozeanforschung Kiel and visible within the Ocean Science Information System (OSIS-Kiel). All metadata are immediately available publicly via the following link pointing to OSIS-Kiel in the GEOMAR data management portal (<https://portal.geomar.de/metadata/leg/show/356226>). In addition, the portal provides a single downloadable KML formatted file (<https://portal.geomar.de/metadata/leg/kmlexport/356226>), which retrieves and combines up-to-date cruise (SO277) related information, links to restricted data and to published data for visualization e.g. in GoogleEarth.

After a three-year moratorium the GEOMAR data management will assist to publish these data by dissemination to national and international data archives, i.e. the data will be submitted to PANGAEA no later than October 2023.

Sediment and rock samples will be stored at the Core and Rock Repository at GEOMAR in Kiel (responsible: Dr. Mark Schmidt).

Table 2: Overview of data availability

Type	Database	Available	Free Access	Contact
Hydrographic data	PANGAEA	01/2021	09/2023	gdv@geomar.de
CTD, ADCP	PANGAEA	01/2021	09/2023	gdv@geomar.de
OBS data	OSIS	01/2021	09/2023	gdv@geomar.de

Reflection seismic data	OSIS	01/2021	09/2023	gdy@geomar.de
CTD video data	OSIS	01/2021	09/2023	gdy@geomar.de
Gravity core samples	OSIS	01/2021	09/2023	gdy@geomar.de
AUV photography	OSIS	01/2021	09/2023	gdy@geomar.de
EM data	OSIS	01/2021	09/2023	gdy@geomar.de

8 Acknowledgements

We thank captain Oliver Meyer of R/V Sonne and his crew for relentless support throughout the entire cruise and the many extra efforts that this cruise involved in times of coronavirus. Particular thanks go to our partners at the University of Malta who could not join the cruise because of coronavirus. We like to thank the Maltese Department of Continental Shelf and the superintendent for Cultural Heritage for granting work permits and the German embassy in Malta for their support on the ground. The cruise would not have been possible without financial support by the Helmholtz Association for the SMART project through the Helmholtz European Partnering program.

9 References

- Adkins, J. F., McIntyre, K. Schrag, D. P. (2002). The salinity, temperature, and $\delta^{18}\text{O}$ of the glacial deep ocean. *Science* 298, 1769-1773.
- Bakalowicz, M.(2018). Coastal Karst Groundwater in the Mediterranean: A Resource to Be Preferably Exploited Onshore, Not from Karst Submarine Springs. *Geosciences* 8, 258.
- Bakken, T. H., Ruden, F., Magset, L. E. (2012). Submarine Groundwater: A New Concept
- Bates, B.C., Z.W. Kundzewicz, S. Wu and J.P. Palutikof, Eds. (2008). *Climate Change and Water. Technical Paper of the Intergovernmental Panel on Climate Change, IPCC Secretariat, Geneva, 210 pp.*
- Bayon, G., Dupré, S., Ponzevera, E., Etoubleau, J., Chéron, S., Pierre, C., ... & De Lange, G. J. (2013). Formation of carbonate chimneys in the Mediterranean Sea linked to deep-water oxygen depletion. *Nature Geoscience*, 6(9), 755-760.
- Bonforte, A., Guglielmino, F., Coltelli, M., Ferretti, A., & Puglisi, G. (2011). Structural assessment of Mount Etna volcano from Permanent Scatterers analysis. *Geochemistry, Geophysics, Geosystems*, 12(2).
- Bonforte, A., Guglielmino, F., Coltelli, M., Ferretti, A., & Puglisi, G. (2011). Structural assessment of Mount Etna volcano from Permanent Scatterers analysis. *Geochemistry, Geophysics, Geosystems*, 12(2).
- Borgia, A., Ferrari, L., & Pasquare, G. (1992). Importance of gravitational spreading in the tectonic and volcanic evolution of Mount Etna. *Nature*, 357(6375), 231.
- Bratton, J. F. (2010). The Three Scales of Submarine Groundwater Flow and Discharge across Passive Continental Margins. *The Journal of Geology* 118, 565-575.

- Burnett, W., Aggarwal, P., Aureli, A., Bokuniewicz, H. (2006): Quantifying submarine groundwater discharge in the coastal zone via multiple methods. *Science of the total Environment* 367, 498-543.
- Chiocci, F. L., Coltelli, M., Bosman, A., & Cavallaro, D. (2011). Continental margin large-scale instability controlling the flank sliding of Etna volcano. *Earth and Planetary Science Letters*, 305(1), 57-64.
- Cohen, D., Person, M., Wang, P., Gable, C.W., Hutchinson, D., Marksamer, A., Dugan, B., Kooi, H., Groen, K., Lizarralde, D., Evans, R.L., Day-Lewis, F.D. and Lane, J.W., Jr. (2010). Origin and Extent of Fresh Paleowaters on the Atlantic Continental Shelf, USA. *Groundwater*, 48: 143-158. <https://doi.org/10.1111/j.1745-6584.2009.00627.x>
- D'Alessandro, W., De Gregorio, S., Dongarrà, G., Gurrieri, S., Parello, F., & Parisi, B. (1997). Chemical and isotopic characterization of the gases of Mount Etna (Italy). *Journal of Volcanology and Geothermal Research*, 78(1-2), 65-76.
- Evans, R. L. (2007). Using CSEM techniques to map the shallow section of seafloor: From the coastline to the edges of the continental slope. *Geophysics* 72, WA105-WA116.
- Gatt, P.A. Carbonate Facies, depositional sequences and tectonostratigraphy of the Paleogene Malta Platform (2012) PhD thesis, Durham University.
- Grasshoff K., Ehrhardt M., Kremling K. (1999) *Methods of Seawater Analysis*. Wiley-VCH, Weinheim, 600 pages. ISBN: 978-3527295890
- Greenlee, L. F., Lawer, D. F., Freeman, B. D., Marrot, B., Moulin, P. (2009). Reverse osmosis desalination: Water sources, technology, and today's challenges. *Water research* 43, 2317-2348.
- Gross, F., Krastel, S., Geersen, J., Behrmann, J.-H., Ridente D., Chiocci, F.L., Bialas, J., Papenberg, C., Cukur, D., Urlaub, M., Micallef, A. (2016). The limits of seaward spreading and slope instability at the continental margin offshore Mt Etna, imaged by high-resolution 2D seismic data, *Tectonophysics*, 667, 63-76.
- Gutscher, M. A., Dominguez, S., Lepinay, B. M., Pinheiro, L., Gallais, F., Babonneau, N., ... & Rovere, M. (2016). Tectonic expression of an active slab tear from high-resolution seismic and bathymetric data offshore Sicily (Ionian Sea). *Tectonics*, 35(1), 39-54.
- Gutscher, M. A., Kopp, H., Krastel, S., Bohrmann, G., Garlan, T., Zaragosi, S., ... & San Pedro, L. (2017). Active tectonics of the Calabrian subduction revealed by new multi-beam bathymetric data and high-resolution seismic profiles in the Ionian Sea (Central Mediterranean). *Earth and Planetary Science Letters*, 461, 61-72.
- Johnson, K.S., Coletti, L.J. (2002) In situ ultraviolet spectrophotometry for high resolution and long-term monitoring of nitrate, bromide and bisulfide in the ocean. *Deep-Sea Research I*, 49, 1291–1305.
- Johnston, R. H. (1983). The saltwater-freshwater interface in the Tertiary limestone aquifer, southeast Atlantic outer-continental shelf of the U.S.A.. *Journal of Hydrology* 61, 239-249.
- Kooi, H., Groen, J. (2001). Offshore continuation of coastal groundwater systems: predictions using sharp-interface approximations and variable density flow modeling. *Journal of Hydrology* 246, 19-35.
- Kopp, H., Lange, D., Steffen, K. P. und Petersen, F. Antragsteller/Inhaber: GEOMAR Helmholtz-Zentrum für Ozeanforschung Kiel (2017) Vorrichtung zur lösbaren Verbindung eines Drahtes und Verfahren zum Ausbringen des Gerätes in ein Gewässer mit der Vorrichtung. Patent: DE 102016107558 A1 2017.10.26.

- Linke P., Schmidt M., Rohleder M., Al-Barakati A., Al-Farawati R. (2015) Novel online digital video and high-speed data broadcasting via standard coaxial cable onboard marine operating vessels. *Marine Technology Society Journal* 49(1), 7-18.
- Micallef, A., Berndt, C., Debono, G. (2011). Fluid flow systems of the Malta Plateau, Central Mediterranean Sea. *Marine Geology* 284, 74-85 (2011).
- Micallef, A., Foglini, F., Le Bas, T., Angeletti, L., Maselli, V., Pasuto, A., & Taviani, M. (2013). The submerged paleolandscape of the Maltese Islands: Morphology, evolution and relation to Quaternary environmental change. *Marine Geology*, 335, 129-147. <https://doi.org/10.1016/j.margeo.2012.10.017>
- Nicolosi, I., Caracciolo, F. A., Branca, S., Ventura, G., & Chiappini, M. (2014). Volcanic conduit migration over a basement landslide at Mount Etna (Italy). *Scientific reports*, 4.
- P. Leahy and Meisler, H. (1982). An analysis of fresh and saline groundwater in the New Jersey Coastall Plain and Continental Shelf (abs.) EOS (American Geophysical Union Transactions) 63, 322.
- Palano, M. (2016). Episodic slow slip events and seaward flank motion at Mt. Etna volcano (Italy). *Journal of Volcanology and Geothermal Research*, 324, 8-14.
- Person, M., Dugan, B., Swenson, J. B., Urbano, L., Stott, C., Taylor, J., Willett, M. (2003). Pleistocene hydrogeology of the Atlantic continental shelf, New England. *Geological Society of America Bulletin* 115, 1324-1343.
- Petersen, F., Kopp, H., Lange, D., Hannemann, K., Urlaub, M. (2019). Measuring tectonic seafloor deformation and strain-build up with acoustic direct-path ranging, *Journal of Geodynamics*, 124, 14-24.
- Poland, M. P., Peltier, A., Bonforte, A., & Puglisi, G. (2017). The spectrum of persistent volcanic flank instability: A review and proposed framework based on Kīlauea, Piton de la Fournaise, and Etna. *Journal of Volcanology and Geothermal Research*.
- Polonia, A., Torelli, L., Gasperini, L., Cocchi, L., Muccini, F., Bonatti, E., ... & Carlini, M. (2017). Lower plate serpentinite diapirism in the Calabrian Arc subduction complex. *Nature communications*, 8(1), 1-13.
- Polonia, A., Torelli, L., Gasperini, L., Cocchi, L., Muccini, F., Bonatti, E., Hensen, C., Schmidt, M., Romano, S., Artoni, A. and Carlini, M. (2017) Lower plate serpentinite diapirism in the Calabrian Arc subduction complex. *Nature Communications*, 8 (2172). DOI 10.1038/s41467-017-02273-x.
- Post, V. (2005). Fresh and saline groundwater interaction in coastal aquifers: Is our technology ready for the problems ahead? *Hydrogeology Journal* 13, 120-123.
- Post, V. E., Groen, J., Kooi, H., Person, M. (2013). Offshore fresh groundwater as a global phenomenon. *Nature* 504, 71 (2013).
- Puglisi, G., Bonforte, A., & Maugeri, S. R. (2001). Ground deformation patterns on Mount Etna, 1992 to 1994, inferred from GPS data. *Bulletin of volcanology*, 62(6-7), 371-384.
- Schmidt M., Linke P., Esser D. (2013) Recent development in IR-sensor technology for monitoring subsea methane discharge. *Marine Technology Society Journal* 47(3), 27-35.
- Schmidt, M., Linke, P., Sommer, S., Esser, D., Cherednichenko, S. (2015) Natural CO₂ seeps offshore Panarea – A test site for subsea CO₂ leak detection technology. *Marine Technology Society Journal* 49 (1), 19-30.

- Schrenk, M. O., Brazelton, W. J., & Lang, S. Q. (2013). Serpentinization, carbon, and deep life. *Reviews in Mineralogy and Geochemistry*, 75(1), 575-606.
- Sciberras, M., Rizzo, M., Mifsud, J. R., Camilleri, K., Borg, J. A., Lanfranco, E., & Schembri, P. J. (2009). Habitat structure and biological characteristics of a maerl bed off the northeastern coast of the Maltese Islands (central Mediterranean). *Marine biodiversity*, 39(4), 251-264.
- Sea-Bird Electronics, Inc., 2017: Seasoftware V2: Seasave V7 CTD Real-Time Data Acquisition Software for Windows. Retrieved from <https://www.seabird.com/profiling/sbe-911plus-ctd/family-downloads?productCategoryId=54627473769>
- Seeberg-Elverfeldt, J., Schlüter, M., Feseker, T., Kölling, M. (2005). Rhizon sampling of porewaters near the sediment-water interface of aquatic systems. *Limnology and Oceanography: Methods*, 3(8), 361–371.
- Small, C., Nicholls, R. J. (2003). A global analysis of human settlement in coastal zones. *Journal of coastal research*, 584-599.
- Sommer, S., Linke, P., Pfannkuche, O., Schleicher, T., Schneider von Deimling, J., Reitz, A., et al. (2009). Seabed methane emissions and the habitat of frenulate tubeworms on the Captain Arutyunov mud volcano (Gulf of Cadiz). *Marine Ecology Progress Series*, 382, 69–86. <https://doi.org/10.3354/meps07956>
- Stuart, M., Maurice, L., Heaton, T. H. E., Sapiano, M. (2010). Groundwater residence time and movement in the Maltese islands – A geochemical approach. *Applied Geochemistry* 25, 609-620 (2010).
- Tibaldi, A., Corazzato, C., Marani, M., Gamberi, F. (2009). Subaerial-submarine evidence of structures feeding magma to Stromboli Volcano, Italy, and relations with edifice flank failure and creep. *Tectonophysics*, 469(1), 112–136.
- Urlaub, M., Petersen, F., Gross, F., Bonforte, A., Puglisi, G., Guglielmino, F., Krastel, S., Lange, D., and Kopp, H. (2018). Gravitational collapse of Mount Etna's southeastern flank, *Science Advances*, 4 (10), eaat9700.
- Vargas-Yáñez, M., García-Martínez, M.C., Moya, F., Balbín, R., López-Jurado, J.L., Serra, M., Zunino, P., Pascual, J., Salat, J. (2017) Updating temperature and salinity mean values and trends in the Western Mediterranean: The RADMED project. *Progress in Oceanography* 157, 27-46. <https://doi.org/10.1016/j.pocean.2017.09.004>.
- Walter, T. R., Haghighi, M. H., Schneider, F. M., Coppola, D., Motagh, M., Saul, J., ... & Heimann, S. (2019). Complex hazard cascade culminating in the Anak Krakatau sector collapse. *Nature Communications*, 10(1), 1-11.
- Wilson, W. D. (1960). Speed of sound in sea water as a function of temperature, pressure, and salinity. *The Journal of the Acoustical Society of America*, 32(6), 641-644.

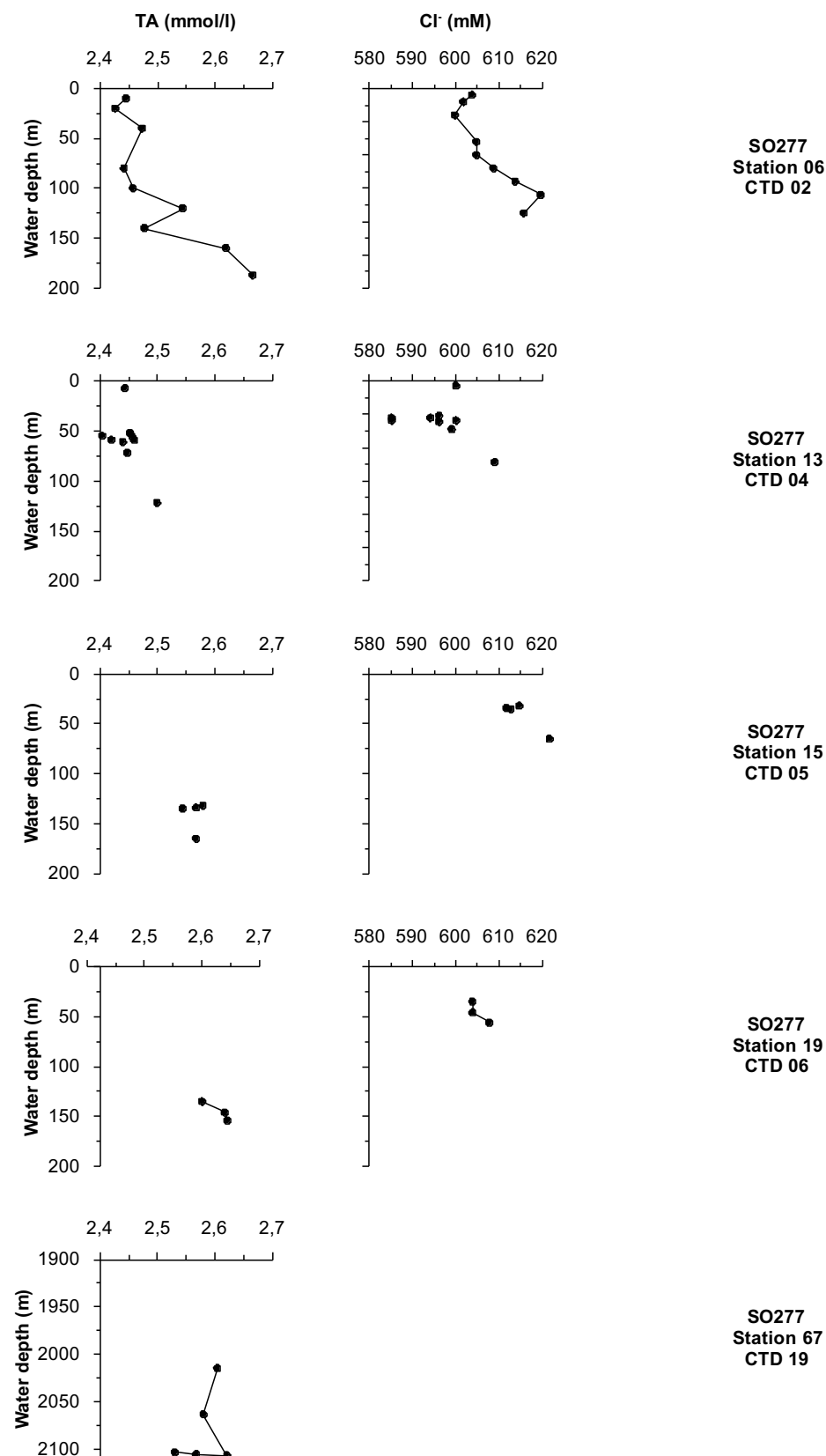
10 Abbreviations

ADC	Analog digital converter
AUV	Autonomous underwater vehicle
CSEM	Controlled source electromagnetic
CTD	Conductivity Temperature Depth sensor (also used to refer to the instrument)
DIC	Dissolved inorganic carbon


DVL	Doppler velocity log
EM	Electromagnetics
GC	Gravity corer
GPS	Global Positioning System
HD	high-density (video)
ICP-OES	Inductively-coupled plasma optical emission spectroscopy
InSAR	Interferometric synthetic aperture radar
mbsf	meters below seafloor
MCS	Multi-channel seismic
MMR	Magnetometric resistivity
MT	magnetotellurics
OA	Offshore aquifer
OBEM	Ocean bottom electromagnetic receiver
OBS	Ocean bottom seismometer
OMAX	Offshore Malta Aquifer Exploration (cruise name)
RU	Bird remote unit
USBL	Ultra-short baseline interferometry
UTC	Coordinated Universal Time
VCTD	Video CTD

11 Appendices


Appendix 1: Total alkalinity and chloride concentrations plotted against water depths of all VCTD stations where water samples were taken.




Appendix 2: GC 01, 0 – 96cm

SO277 - 27	GC 01		Date: 11.09.2020		
Core length: 1,96 m	Water depth: 66 m		Lat: 36° 01,654 Lon: 14° 22,995		
	0	Depth, cm	Colour	Lithology	Remarks
	10	0-96	Pale Olive 10Y 6/2	Well-mixed, not sorted silty sand	"hairs", most likely rotted seagrass throughout the core, Fragments of shells/snails, wood, corals
	20				
	30				
	40				
	50				
	60				
	70				
	80				
	90				
	96				


Appendix 3: GC 01, 96 - 196cm

		GC 01			
	96	Depth, cm	Colour	Lithology	Remarks
	106	96-145	Pale Olive 10Y 6/2	Mixed silty-sand with low clay content	Fragments of shells, corals
	116				
	126				
	136				
	146	145	Pale Olive 10Y 6/2	Mixed silty-sand with low clay content	Tooth fragment, approximately 1.5 cm long
	156	146-168	Pale Olive 10Y 6/2	Mixed silty-sand with low clay content	Fragments of shells, corals
	166				
	176	168-172	Pale Olive 10Y 6/2	Mixed silty-sand with low clay content	Mussel fragments (cm- size), age determination?
		172-177	Pale Olive 10Y 6/2	Mixed silty-sand with low clay content	Fragments of shells, corals
	186	177	black	Well rounded	Sand lense
		178-196	Pale Olive 10Y 6/2	Mixed silty-sand with low clay content	Fragments of shells, corals
	196				


Appendix 4: GC 05, 0 - 72cm

SO277 - 33		GC 05		Date: 12.09.2020	
Core length: 2,72 m		Water depth: 92 m		Lat: 36° 05,293 Lon: 14° 16,473	
					
0		Depth, cm	Colour	Lithology	Remarks
0		0	Light Olive, grey 5Y 5/2	Silty sand	Seafloor
10		0-24	Dusky yellow 5GY 5/2	Silty sand	Large fragments of shells, corals (up to 3 cm long), hairy seagrass
20					
30					
40		24-72		Silt	
50					
60					
70					
72					


Appendix 1: GC 05, 72 - 172cm

		GC 05				
	72	Depth, cm	Colour	Lithology	Remarks	
	82	72-94	Light Olive grey 5Y 5/2	Silt	Fragments of shells, hairy seagrass	
	92					
	102	94-115	Greyish olive green 5GY 3/2	Mixed clay and silt		
	112					
	122	115-117	Light Olive, grey 5Y 5/2	Silt		
	132	117-138	Greyish olive green 5GY 3/2	Mixed clay and silt	Lenses with shell fragments	
	142	138-168	Light Olive grey 5Y 5/2	Sandy silt	Hairy seagrass, large fragments of shells and corals (up to 3 cm)	
	152					
	162					
	172					


Appendix 2: GC 05, 172 - 272cm

		GC 05			
	172	Depth, cm	Colour	Lithology	Remarks
	182	168-224	Moderate olive brown	Mixed coarse-grained and fine-grained sand	Up to 3 cm large fragments (dominant facies), hairy seagrass, sediment gap 198-211 cm (crumbled out during core splitting)
	192				
	202				
	212				
	222				
	232	224-272	reddish	Coarse sand to gravel	Mainly composed of snails (0.5 cm long)
	242				
	252				
	262				
	272				


Appendix 3: GC 06, 0 - 78cm

SO277 - 34	GC 06		Date: 12.09.2020		
Core length: 2,78 m	Water depth: 71 m		Lat: 36° 04,497 Lon: 14° 17,621		
	0	Depth, cm	Colour	Lithology	Remarks
	10	0-78	Grayish olive 10Y 4/2	Silty sand	hairy, rotted seagrass (40-65 cm), seagrass and silty sand (65-78 cm)
	20				
	30				
	40				
	50				
	60				
	70				
	78				


Appendix 4: GC 06, 78 - 178cm

		GC 06			
	78	Depth, cm	Colour	Lithology	Remarks
	88	78-116	Grayish olive 10Y 4/2	Silty sand	
	98				
	108				
	118				
	128				
	138				
	148				
	158				
	168				
	178				
		177	Grayish olive 10Y 4/2	Sandy silt	Rests of algae and seagrass (116-130 cm), no algae visible (130-145 cm), thick algae and seagrass (145- 178 cm)


Appendix 5: GC 06, 178 - 278cm

		GC 06			
	178	Depth, cm	Colour	Lithology	Remarks
	188	178-236	Grayish olive 10Y 4/2	Sandy silt	Traces of algae and seagrass sequence, a single shell, less water content than above
	198				
	208				
	218				
	228				
	238	178-236	Grayish olive 10Y 4/2	Sandy silt	Traces of algae and seagrass sequence, a single shell, less water content than above
	248				
	258				
	268				
	278				


Appendix 6: GC 07, 0 - 67cm

SO277 - 45_1	GC 07		Date: 15.09.2020		
Core length: 0,67 m	Water depth: 125 m		Lat: 36° 04,430 Lon: 14° 19,257		
	0	Depth, cm	Colour	Lithology	Remarks
	10	0-28	Moderate greenish yellow 10Y 7/4	Sand to fine sand	Little hairy seagrass, shell fragments (< 0,5cm long)
	20				
	30				
	40	28-40	Dusty yellow green 5GY 5/2	Sandy silt	Well sorted with minor fragments of shells
	50	40-49	Dusty yellow green 5GY 5/2	Clayey silt	Mixed with big fragments of corals, lense of coarse black sand at 42 cm
	60	49-67	Dusty yellow green 5GY 5/2	Coarse sand	Most sediment is missing, heavily disturbed, gravel-sized fragments of corals and shells, Matrix mainly consisting of well-rounded black sand
	67				


Appendix 7: GC 07A, 0 - 85cm

SO277 - 45_2	GC 07A		Date: 15.09.2020		
Core length: 0,85 m	Water depth: 124 m		Lat: 36° 04.427 Lon: 14° 19,268		
	0	Depth, cm	Colour	Lithology	Remarks
	10	0-31	Moderate greenish yellow 10Y 7/4	Sandy silt, fining downwards	6-8cm: path of seagrass 18cm: seagrass Small shell fragments (<0,5cm)
	20				
	30				
	40	31-59	Dusty yellow green 5GY 5/2	Silty clay	Organic-rich black patches 37cm: 1cm long sand lense (black sand)
	50				
	60				
	70	59-85	Pale Olive 10Y 6/2	Silt/Sandy silt	Several large fragments (coral?) of 1-2cm length (but not dominant)
	80				
	85				


Appendix 8: GC 08, 0 - 55cm

SO277 - 46	GC 08		Date: 15.09.2020		
Core length: 1,55 m	Water depth: 146 m		Lat: 36° 04,367 Lon: 14° 19,740		
	0	Depth, cm	Colour	Lithology	Remarks
		0-5	Light brown 5YR 6/4	Gravel/Coarse sand	Slightly rounded grains of sand (mostly black) with sand-sized fragments of shells/coral some larger shell/coral fragments (<1cm)
	10	5-55	Dark greenish grey 5GY 4/1	Poorly sorted clayey silt with sand intraclasts	Organic-rich black patches, 2- 3cm thick sand clasts consisting of dark grains and shell fragments, clasts increase in size and frequency towards the bottom
	20				
	30				
	40				
	50				
55					


Appendix 9: GC 08, 55 - 155cm

		GC 08			
	55	Depth, cm	Colour	Lithology	Remarks
	65	55-141	Dark greenish grey 5GY 4/1	Silty sand	Black sand lenses throughout this segment 85cm: bioturbation From 110cm downwards: slightly coarser and larger fragments of shells (0,5-1 cm)
	75				
	85				
	95				
	105				
	115				
	125				
	135				
	145	141-155	Dark greenish grey 5GY 4/1	Sand	8*6cm large conglomerate surrounded by black sandy matrix
	155				

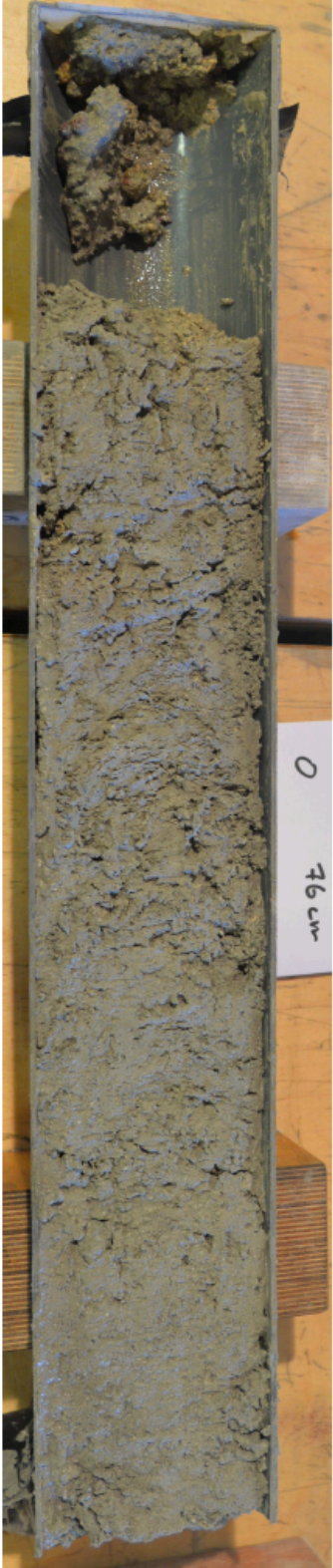
Appendix 10: GC 09, 0 - 40cm

SO277 - 47_1	GC 09		Date: 15.09.2020		
Core length: 1,4 m	Water depth: 130 m		Lat: 36° 03,958 Lon: 14° 19,917		
	0	Depth, cm	Colour	Lithology	Remarks
	10	0-32	Greenish grey 5GY 6/1	Clayey silt	1cm: 1cm clast. Hard, black/reddish (vesicular clast) Black organic- rich patches between 11-40cm
	20				
	30				
	40	32-40	Greenish grey 5GY 6/1	Silty clay	Hairy seagrass in small patches (18cm, 26cm, 33cm)


Appendix 11: GC 09, 40 - 140cm

		GC 09				
	40	Depth, cm	Colour	Lithology	Remarks	
	50	40-120	Greenish grey 5GY 6/1	clay	58cm: approximately 2cm long snail	
	60					
	70					
	80					
	90					
	100					
	110					
	120					
	130	120-140	Greenish grey 5GY 6/1	Clayey silt coarsening downwards to mixed coarse grained sand/gravel	Seagrass, fragments of corals and shell (larger towards bottom)	
	140					


Appendix 12: GC 11, 0 - 76cm

SO277 - 51	GC 11		Date: 16.09.2020		
Core length: 0,67 m	Water depth: 68 m		Lat: 36° 00,243 Lon: 14° 27,424		
	0	Depth, cm	Colour	Lithology	Remarks
	10	0-76	Dusky yellow green 5GY 5/2	Silty sand	Sand-sized coral and shell fragments with larger (up to 2cm) coral pieces
	20				
	30				
	40				
	50				
	60				
	70				
	76				


Appendix 13: GC 14, 0 - 88cm

SO277 - 58	GC 14		Date: 17.09.2020		
Core length: 2,88 m	Water depth: 68 m		Lat: 36° 03,298 Lon: 14° 19,833		
	0	Depth, cm	Colour	Lithology	Remarks
	10	0-37	Dusky yellow green 5GY 5/2	Silty sand, poorly sorted	Fragments of shells, hairy seagrass H ₂ S smell in pore waters throughout the whole gravity core
	20				
	30				
	40	37-48	Dusky yellow green 5GY 5/2	Silty sand	Bunch of seagrass
	50	48-67	Dusky yellow green 5GY 5/2	Silty sand	Seagrass almost absent, slightly larger shell fragments 56cm: organic-rich black lens
	60				
	70	67-88	Dusky yellow green 5GY 5/2	Silty sand (higher silt content)	Seagrass, larger (2cm) fragments of crab "needles" (largely intact)
	80				
	88				

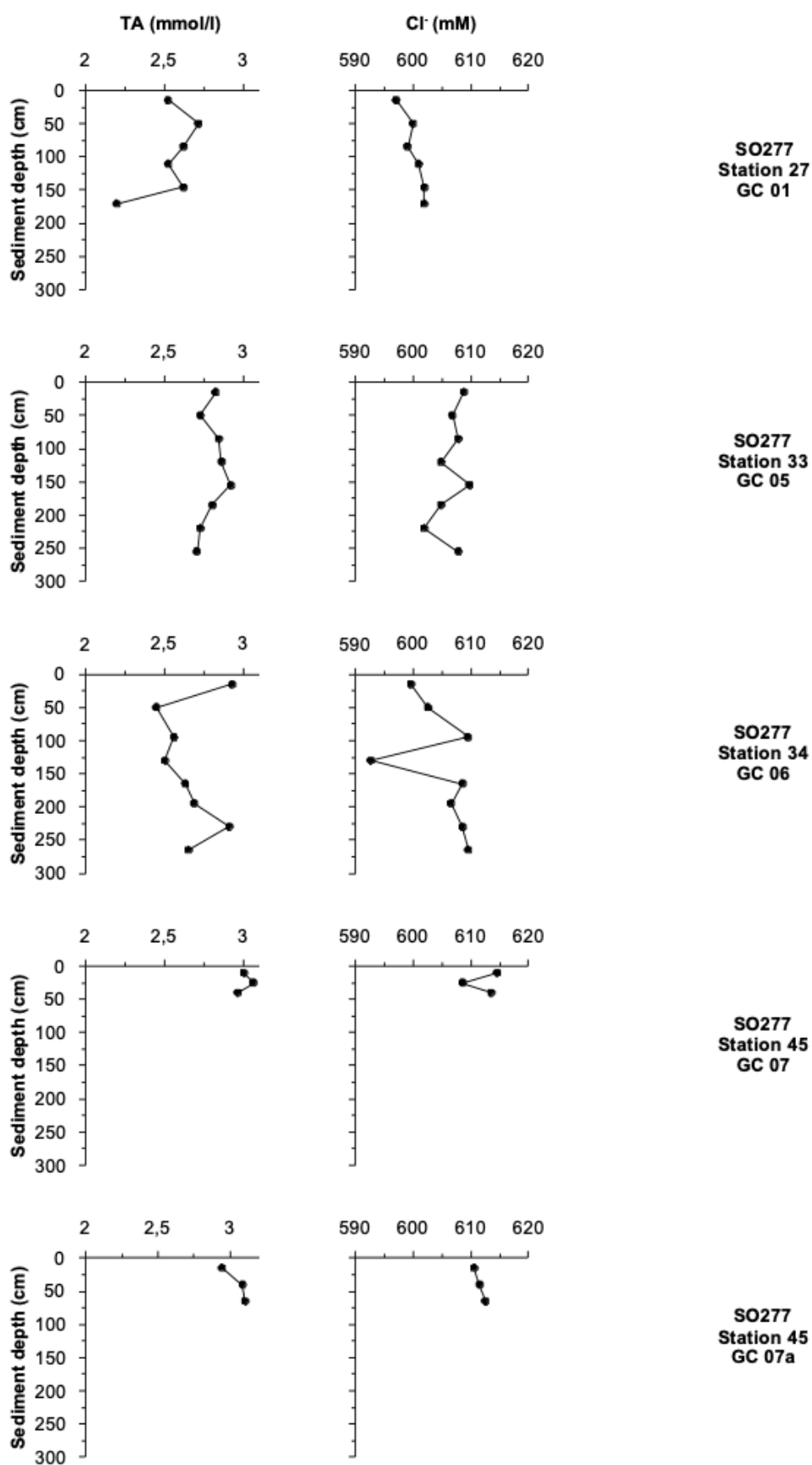
Appendix 14: GC 14, 88 - 188cm

		GC 14			
	88	Depth, cm	Colour	Lithology	Remarks
	98	88-176	Dusky yellow green 5GY 5/2	Silty sand/Sandy silt	Fragments of shells, some entire snails (<0,5cm) 122-148: slightly drier and finer grained 150-152: bunch of seagrass 168-169: seagrass 169-175: some larger fragments (1cm)
	108				
	118				
	128				
	138				
	148				
	158				
	168				
	178				
	188	176-188	Light olive 10Y 5/4	Clayey silt	Very little seagrass, small sand-sized shell fragments

Appendix 15: GC 14, 188 - 288cm

		GC 14			
	188	Depth, cm	Colour	Lithology	Remarks
	198	188-224	Light olive 10Y 5/4	Clayey silt	195-197: about 1cm wide black patch (organic/pyrite?), some fragments of coral and shells
	208				
	218				
	228				
	238	224-278	Light olive 10Y 5/4	Clayey silt	Fragments of shells (<0,5cm) 252cm: black lense (pyrite?)
	248				
	258				
	268				
	278				
	288	278-288	Light olive 10Y 5/4	Silty clay	Hairy seagrass Smell of H ₂ S when opened

Appendix 16: Total alkalinity and chloride concentrations plotted against sediment depth of the gravity cores.



Appendix 17: SO277 participants



GEOMAR Reports

No.

- 1 FS POSEIDON Fahrtbericht / Cruise Report POS421, 08. – 18.11.2011, Kiel - Las Palmas, Ed.: T.J. Müller, 26 pp, DOI: 10.3289/GEOMAR_REP_NS_1_2012
- 2 Nitrous Oxide Time Series Measurements off Peru – A Collaboration between SFB 754 and IMARPE –, Annual Report 2011, Eds.: Baustian, T., M. Graco, H.W. Bange, G. Flores, J. Ledesma, M. Sarmiento, V. Leon, C. Robles, O. Moron, 20 pp, DOI: 10.3289/GEOMAR_REP_NS_2_2012
- 3 FS POSEIDON Fahrtbericht / Cruise Report POS427 – Fluid emissions from mud volcanoes, cold seeps and fluid circulation at the Don_Kuban deep sea fan (Kerch peninsula, Crimea, Black Sea) – 23.02. – 19.03.2012, Burgas, Bulgaria - Heraklion, Greece, Ed.: J. Bialas, 32 pp, DOI: 10.3289/GEOMAR_REP_NS_3_2012
- 4 RV CELTIC EXPLORER EUROFLEETS Cruise Report, CE12010 – ECO2@NorthSea, 20.07. – 06.08.2012, Bremerhaven – Hamburg, Eds.: P. Linke et al., 65 pp, DOI: 10.3289/GEOMAR_REP_NS_4_2012
- 5 RV PELAGIA Fahrtbericht / Cruise Report 64PE350/64PE351 – JEDDAH-TRANSECT –, 08.03. – 05.04.2012, Jeddah – Jeddah, 06.04 - 22.04.2012, Jeddah – Duba, Eds.: M. Schmidt, R. Al-Farawati, A. Al-Aidaroos, B. Kürten and the shipboard scientific party, 154 pp, DOI: 10.3289/GEOMAR_REP_NS_5_2013
- 6 RV SONNE Fahrtbericht / Cruise Report SO225 - MANIHIKI II Leg 2 The Manihiki Plateau - Origin, Structure and Effects of Oceanic Plateaus and Pleistocene Dynamic of the West Pacific Warm Water Pool, 19.11.2012 - 06.01.2013 Suva / Fiji – Auckland / New Zealand, Eds.: R. Werner, D. Nürnberg, and F. Hauff and the shipboard scientific party, 176 pp, DOI: 10.3289/GEOMAR_REP_NS_6_2013
- 7 RV SONNE Fahrtbericht / Cruise Report SO226 – CHRIMP CHatham RIse Methane Pockmarks, 07.01. – 06.02.2013 / Auckland – Lyttleton & 07.02. – 01.03.2013 / Lyttleton – Wellington, Eds.: Jörg Bialas / Ingo Klaucke / Jasmin Mögeltönder, 126 pp, DOI: 10.3289/GEOMAR_REP_NS_7_2013
- 8 The SUGAR Toolbox - A library of numerical algorithms and data for modelling of gas hydrate systems and marine environments, Eds.: Elke Kossel, Nikolaus Bigalke, Elena Piñero, Matthias Haeckel, 168 pp, DOI: 10.3289/GEOMAR_REP_NS_8_2013
- 9 RV ALKOR Fahrtbericht / Cruise Report AL412, 22.03.-08.04.2013, Kiel – Kiel. Eds: Peter Linke and the shipboard scientific party, 38 pp, DOI: 10.3289/GEOMAR_REP_NS_9_2013
- 10 Literaturrecherche, Aus- und Bewertung der Datenbasis zur Meerforelle (*Salmo trutta trutta* L.) Grundlage für ein Projekt zur Optimierung des Meerforellenmanagements in Schleswig-Holstein. Eds.: Christoph Petereit, Thorsten Reusch, Jan Dierking, Albrecht Hahn, 158 pp, DOI: 10.3289/GEOMAR_REP_NS_10_2013
- 11 RV SONNE Fahrtbericht / Cruise Report SO227 TAIFLUX, 02.04. – 02.05.2013, Kaohsiung – Kaohsiung (Taiwan), Christian Berndt, 105 pp, DOI: 10.3289/GEOMAR_REP_NS_11_2013
- 12 RV SONNE Fahrtbericht / Cruise Report SO218 SHIVA (Stratospheric Ozone: Halogens in a Varying Atmosphere), 15.-29.11.2011, Singapore - Manila, Philippines, Part 1: SO218- SHIVA Summary Report (in German), Part 2: SO218- SHIVA English reports of participating groups, Eds.: Birgit Quack & Kirstin Krüger, 119 pp, DOI: 10.3289/GEOMAR_REP_NS_12_2013
- 13 KIEL276 Time Series Data from Moored Current Meters. Madeira Abyssal Plain, 33°N, 22°W, 5285 m water depth, March 1980 – April 2011. Background Information and Data Compilation. Eds.: Thomas J. Müller and Joanna J. Waniek, 239 pp, DOI: 10.3289/GEOMAR_REP_NS_13_2013

GEOMAR Reports

No.

- 14 RV POSEIDON Fahrtbericht / Cruise Report POS457: ICELAND HAZARDS Volcanic Risks from Iceland and Climate Change: The Late Quaternary to Anthropogenic Development Reykjavík / Iceland – Galway / Ireland, 7.-22. August 2013. Eds.: Reinhard Werner, Dirk Nürnberg and the shipboard scientific party, 88 pp, DOI: 10.3289/GEOMAR_REP_NS_14_2014
- 15 RV MARIA S. MERIAN Fahrtbericht / Cruise Report MSM-34 / 1 & 2, SUGAR Site, Varna – Varna, 06.12.13 – 16.01.14. Eds: Jörg Bialas, Ingo Klauke, Matthias Haeckel, 111 pp, DOI: 10.3289/GEOMAR_REP_NS_15_2014
- 16 RV POSEIDON Fahrtbericht / Cruise Report POS 442, "AUVinTYS" High-resolution geological investigations of hydrothermal sites in the Tyrrhenian Sea using the AUV "Abyss", 31.10. – 09.11.12, Messina – Messina, Ed.: Sven Petersen, 32 pp, DOI: 10.3289/GEOMAR_REP_NS_16_2014
- 17 RV SONNE, Fahrtbericht / Cruise Report, SO 234/1, "SPACES": Science or the Assessment of Complex Earth System Processes, 22.06. – 06.07.2014, Walvis Bay / Namibia - Durban / South Africa, Eds.: Reinhard Werner and Hans-Joachim Wagner and the shipboard scientific party, 44 pp, DOI: 10.3289/GEOMAR_REP_NS_17_2014
- 18 RV POSEIDON Fahrtbericht / Cruise Report POS 453 & 458, "COMM3D", Crustal Structure and Ocean Mixing observed with 3D Seismic Measurements, 20.05. – 12.06.2013 (POS453), Galway, Ireland – Vigo, Portugal, 24.09. – 17.10.2013 (POS458), Vigo, Portugal – Vigo, Portugal, Eds.: Cord Papenberg and Dirk Klaeschen, 66 pp, DOI: 10.3289/GEOMAR_REP_NS_18_2014
- 19 RV POSEIDON, Fahrtbericht / Cruise Report, POS469, "PANAREA", 02. – 22.05.2014, (Bari, Italy – Malaga, Spain) & Panarea shallow-water diving campaign, 10. – 19.05.2014, Ed.: Peter Linke, 55 pp, DOI: 10.3289/GEOMAR_REP_NS_19_2014
- 20 RV SONNE Fahrtbericht / Cruise Report SO234-2, 08.-20.07.2014, Durban, -South Africa - Port Louis, Mauritius, Eds.: Kirstin Krüger, Birgit Quack and Christa Marandino, 95 pp, DOI: 10.3289/GEOMAR_REP_NS_20_2014
- 21 RV SONNE Fahrtbericht / Cruise Report SO235, 23.07.-07.08.2014, Port Louis, Mauritius to Malé, Maldives, Eds.: Kirstin Krüger, Birgit Quack and Christa Marandino, 76 pp, DOI: 10.3289/GEOMAR_REP_NS_21_2014
- 22 RV SONNE Fahrtbericht / Cruise Report SO233 WALVIS II, 14.05-21.06.2014, Cape Town, South Africa - Walvis Bay, Namibia, Eds.: Kaj Hoernle, Reinhard Werner, and Carsten Lüter, 153 pp, DOI: 10.3289/GEOMAR_REP_NS_22_2014
- 23 RV SONNE Fahrtbericht / Cruise Report SO237 Vema-TRANSIT Bathymetry of the Vema-Fracture Zone and Puerto Rico Trench and Abyssal Atlantic Biodiversity Study, Las Palmas (Spain) - Santo Domingo (Dom. Rep.) 14.12.14 - 26.01.15, Ed.: Colin W. Devey, 130 pp, DOI: 10.3289/GEOMAR_REP_NS_23_2015
- 24 RV POSEIDON Fahrtbericht / Cruise Report POS430, POS440, POS460 & POS467 Seismic Hazards to the Southwest of Portugal; POS430 - La-Seyne-sur-Mer - Portimao (7.4. - 14.4.2012), POS440 - Lisbon - Faro (12.10. - 19.10.2012), POS460 - Funchal - Portimao (5.10. - 14.10.2013), POS467 - Funchal - Portimao (21.3. - 27.3.2014), Ed.: Ingo Grevemeyer, 43 pp, DOI: 10.3289/GEOMAR_REP_NS_24_2015
- 25 RV SONNE Fahrtbericht / Cruise Report SO239, EcoResponse Assessing the Ecology, Connectivity and Resilience of Polymetallic Nodule Field Systems, Balboa (Panama) – Manzanillo (Mexico), 11.03. -30.04.2015, Eds.: Pedro Martínez Arbizu and Matthias Haeckel, 204 pp, DOI: 10.3289/GEOMAR_REP_NS_25_2015

GEOMAR Reports

No.

- 26 RV SONNE Fahrtbericht / Cruise Report SO242-1, JPI OCEANS Ecological Aspects of Deep-Sea Mining, DISCOL Revisited, Guayaquil - Guayaquil (Ecuador), 29.07.-25.08.2015, Ed.: Jens Greinert, 290 pp, DOI: 10.3289/GEOMAR_REP_NS_26_2015
- 27 RV SONNE Fahrtbericht / Cruise Report SO242-2, JPI OCEANS Ecological Aspects of Deep-Sea Mining DISCOL Revisited, Guayaquil - Guayaquil (Ecuador), 28.08.-01.10.2015, Ed.: Antje Boetius, 552 pp, DOI: 10.3289/GEOMAR_REP_NS_27_2015
- 28 RV POSEIDON Fahrtbericht / Cruise Report POS493, AUV DEDAVE Test Cruise, Las Palmas - Las Palmas (Spain), 26.01.-01.02.2016, Ed.: Klas Lackschewitz, 17 pp, DOI: 10.3289/GEOMAR_REP_NS_28_2016
- 29 Integrated German Indian Ocean Study (IGIOS) - From the seafloor to the atmosphere - A possible German contribution to the International Indian Ocean Expedition 2 (IIOE-2) programme - A Science Prospectus, Eds.: Bange, H.W. , E.P. Achterberg, W. Bach, C. Beier, C. Berndt, A. Biastoch, G. Bohrmann, R. Czeschel, M. Dengler, B. Gaye, K. Haase, H. Herrmann, J. Lelieveld, M. Mohtadi, T. Rixen, R. Schneider, U. Schwarz-Schampera, J. Segsneider, M. Visbeck, M. Voß, and J. Williams, 77pp, DOI: 10.3289/GEOMAR_REP_NS_29_2016
- 30 RV SONNE Fahrtbericht / Cruise Report SO249, BERING – Origin and Evolution of the Bering Sea: An Integrated Geochronological, Volcanological, Petrological and Geochemical Approach, Leg 1: Dutch Harbor (U.S.A.) - Petropavlovsk-Kamchatsky (Russia), 05.06.2016-15.07.2016, Leg 2: Petropavlovsk-Kamchatsky (Russia) - Tomakomai (Japan), 16.07.2016-14.08.2016, Eds.: Reinhard Werner, et al., DOI: 10.3289/GEOMAR_REP_NS_30_2016
- 31 RV POSEIDON Fahrtbericht/ Cruise Report POS494/2, HIERROSEIS Leg 2: Assessment of the Ongoing Magmatic-Hydrothermal Discharge of the El Hierro Submarine Volcano, Canary Islands by the Submersible JAGO, Valverde – Las Palmas (Spain), 07.02.-15.02.2016, Eds.: Hannington, M.D. and Shipboard Scientific Party, DOI: 10.3289/GEOMAR_REP_NS_31_2016
- 32 RV METEOR Fahrtbericht/ Cruise Report M127, Extended Version, Metal fluxes and Resource Potential at the Slow-spreading TAG Mid-ocean Ridge Segment (26°N, MAR) – Blue Mining@Sea, Bridgetown (Barbados) – Ponta Delgada (Portugal) 25.05.-28.06.2016, Eds.: Petersen, S. and Shipboard Scientific Party, DOI: 10.3289/GEOMAR_REP_NS_32_2016
- 33 RV SONNE Fahrtbericht/Cruise Report SO244/1, GeoSEA: Geodetic Earthquake Observatory on the Seafloor, Antofagasta (Chile) – Antofagasta (Chile), 31.10.-24.11.2015, Eds.: Jan Behrmann, Ingo Klaucke, Michal Stipp, Jacob Geersen and Scientific Crew SO244/1, DOI: 10.3289/GEOMAR_REP_NS_33_2016
- 34 RV SONNE Fahrtbericht/Cruise Report SO244/2, GeoSEA: Geodetic Earthquake Observatory on the Seafloor, Antofagasta (Chile) – Antofagasta (Chile), 27.11.-13.12.2015, Eds.: Heidrun Kopp, Dietrich Lange, Katrin Hannemann, Anne Krabbenhoeft, Florian Petersen, Anina Timmermann and Scientific Crew SO244/2, DOI: 10.3289/GEOMAR_REP_NS_34_2016
- 35 RV SONNE Fahrtbericht/Cruise Report SO255, VITIAZ – The Life Cycle of the Vitiaz-Kermadec Arc / Backarc System: from Arc Initiation to Splitting and Backarc Basin Formation, Auckland (New Zealand) - Auckland (New Zealand), 02.03.-14.04.2017, Eds.: Kaj Hoernle, Folkmar Hauff, and Reinhard Werner with contributions from cruise participants, DOI: 10.3289/GEOMAR_REP_NS_35_2017

GEOMAR Reports

No.

- 36 RV POSEIDON Fahrtbericht/Cruise Report POS515, CALVADOS - CALabrian arc mud VolcAnoes: Deep Origin and internal Structure, Dubrovnik (Croatia) – Catania (Italy), 18.06.-13.07.2017, Eds.: M. Riedel, J. Bialas, A. Krabbenhoef, V. Bähre, F. Beeck, O. Candoni, M. Kühn, S. Muff, J. Rindfleisch, N. Stange, DOI: 10.3289/GEOMAR_REP_NS_36_2017
- 37 RV MARIA S. MERIAN Fahrtbericht/Cruise Report MSM63, PERMO, Southampton – Southampton (U.K.), 29.04.-25.05.2017, Eds.: Christian Berndt and Judith Elger with contributions from cruise participants C. Böttner, R. Gehrmann, J. Karstens, S. Muff, B. Pitcairn, B. Schramm, A. Lichtschlag, A.-M. Völsch, DOI: 10.3289/GEOMAR_REP_NS_37_2017
- 38 RV SONNE Fahrtbericht/Cruise Report SO258/1, INCON: The Indian - Antarctic Break-up Enigma, Fremantle (Australia) - Colombo (Sri Lanka), 07.06.-09.07.2017, 29.04.-25.05.2017, Eds.: Reinhard Werner, Hans-Joachim Wagner, and Folkmar Hauff with contributions from cruise participants, DOI: 10.3289/GEOMAR_REP_NS_38_2017
- 39 RV POSEIDON Fahrtbericht/Cruise Report POS509, ElectroPal 2: Geophysical investigations of sediment hosted massive sulfide deposits on the Palinuro Volcanic Complex in the Tyrrhenian Sea, Malaga (Spain) – Catania (Italy), 15.02.-03.03.2017, Ed.: Sebastian Hölz, DOI: 10.3289/GEOMAR_REP_NS_39_2017
- 40 RV POSEIDON Fahrtbericht/Cruise Report POS518, Baseline Study for the Environmental Monitoring of Subseafloor CO₂ Storage Operations, Leg 1: Bremerhaven – Bremerhaven (Germany), 25.09.-11.10.2017, Leg 2: Bremerhaven – Kiel (Germany), 12.10.-28.10.2017, Eds.: Peter Linke and Matthias Haeckel, DOI: 10.3289/GEOMAR_REP_NS_40_2018
- 41 RV MARIA S. MERIAN Fahrtbericht/Cruise Report MSM71, LOBSTER: Ligurian Ocean Bottom Seismology and Tectonics Research, Las Palmas (Spain) – Heraklion (Greece), 07.02.-27.02.2018, Eds.: H. Kopp, D. Lange, M. Thorwart, A. Paul, A. Dannowski, F. Petersen, C. Aubert, F. Beek, A. Beniest, S. Besançon, A. Brotzer, G. Caielli, W. Crawford, M. Deen, C. Lehmann, K. Marquardt, M. Neckel, L. Papanagnou, B. Schramm, P. Schröder, K.-P. Steffen, F. Wolf, Y. Xia, DOI: 10.3289/GEOMAR_REP_NS_41_2018
- 42 RV METEOR Fahrtbericht/Cruise Report M143, SLOGARO: Slope failures and active gas expulsion along the Romanian margin – investigating relations to gas hydrate distribution, Varna (Romania) – Heraklion (Greece), 12.12.-22.12.2017, Eds.: M. Riedel, F. Gausepohl, I. Gazis, L. Hähnel, M. Kampmeier, P. Urban, J. Bialas, DOI: 10.3289/GEOMAR_REP_NS_42_2018
- 43 RV POSEIDON Fahrtbericht/Cruise Report POS510, ANYDROS: Rifting and Hydrothermal Activity in the Cyclades Back-arc Basin, Catania (Italy) – Heraklion (Greece), 06.03.-29.03.2017, Ed.: M.D. Hannington, DOI: 10.3289/GEOMAR_REP_NS_43_2018
- 44 RV POSEIDON Fahrtbericht/Cruise Report POS524, GrimseyEM: Geophysical and geological investigations in the vicinity of the Grimsey Hydrothermal Field offshore Northern Iceland for the assessment of the geothermal potential and the exploration for potential mineralizations within the seafloor, Reykjavik (Iceland) – Bergen (Norway), 7.6 - 26.6.2018, Eds.: Sebastian Hölz and Sofia Martins, DOI: 10.3289/GEOMAR_REP_NS_44_2018
- 45 RV POSEIDON Fahrtbericht/Cruise Report POS527, Baseline Study for the Environmental Monitoring of Subseafloor CO₂ Storage Operations, Kiel – Kiel (Germany), 15.8. - 3.9.2018, Eds.: Eric Achterberg and Mario Esposito, DOI: 10.3289/GEOMAR_REP_NS_45_2018

GEOMAR Reports

No.

- 46 RV SONNE Fahrtbericht/Cruise Report SO264, SONNE-EMPEROR: The Plio/Pleistocene to Holocene development of the pelagic North Pacific from surface to depth – assessing its role for the global carbon budget and Earth's climate, Suva (Fiji) – Yokohama (Japan), 30.6. – 24.8.2018
Ed.: Dirk Nürnberg, DOI: 10.3289/GEOMAR_REP_NS_46_2018
- 47 RV SONNE Fahrtbericht/Cruise Report SO265, SHATSKY EVOLUTION: Evolution of the Shatsky Rise Hotspot System, Yokohama (Japan) – Kaohsiung (Taiwan), 26.08. – 11.10.2018, Eds.: Jörg Geldmacher, Reinhard Werner, and Folkmar Hauff with contributions from cruise participants, DOI: 10.3289/GEOMAR_REP_NS_47_2018
- 48 RV MARIA S. MERIAN Fahrtbericht/Cruise Report MSM78, PERMO 2, Edinburgh – Edinburgh (U.K.), 16.10. – 25.10.2018, Eds.: Jens Karstens, Christoph Böttner, Mike Edwards, Ismael Falcon-Suarez, Anita Flohr, Rachael James, Anna Lichtschlag, Doris Maicher, Iain Pheasant, Ben Roche, Bettina Schramm, Michael Wilson, DOI: 10.3289/GEOMAR_REP_NS_48_2019
- 49 RV SONNE Fahrtbericht/Cruise Report SO267, ARCHIMEDES I: Arc Rifting, Metallogeny and Microplate Evolution – an Integrated Geodynamic, Magmatic and Hydrothermal Study of the Fonualei Rift System, NE Lau Basin, Suva (Fiji) – Suva (Fiji), 11.12.2018 – 26.01.2019, Eds.: Mark Hannington, Heidrun Kopp, Michael Schnabel, DOI: 10.3289/GEOMAR_REP_NS_49_2019
- 50 RV Pelagia Fahrtbericht/Cruise Report 64PE-445, SALTAX: Geomorphology and geophysics of submarine salt flows in the Red Sea Rift, Limassol (Cyprus) – Safaga (Egypt), 27.08. – 21.09.2018, Eds.: Nico Augustin, Neil C. Mitchell, Froukje M. van der Zwan & Scientific Shipboard Party, DOI: 10.3289/GEOMAR_REP_NS_50_2019
- 51 RV POSEIDON Fahrtbericht/Cruise Report POS526, SeASOM: Semi-Autonomous Subsurface Optical Monitoring for methane seepage and cold-water coral studies in the North Sea, Bergen (Norway) – Doggerbank (Netherlands) – Hirtshals (Denmark) – Tisler (Norway) – Kiel (Germany), 23.07. – 11.08.2018, Eds.: Jens Greinert, Tim Schoening, DOI: 10.3289/GEOMAR_REP_NS_51_2019
- 52 RV POSEIDON Fahrtbericht/Cruise Report POS534, STEMM-CCS: Strategies for Environmental Monitoring of Marine Carbon Capture and Storage, Leg 1: Kiel (Germany) – Aberdeen (United Kingdom), 01.05. – 22.05.2019, Leg 2: Aberdeen (United Kingdom) – Bremerhaven (Germany), 23.05. – 29.05.2019, Ed.: Mark Schmidt, DOI: 10.3289/GEOMAR_REP_NS_52_2019
- 53 RV POSEIDON Fahrtbericht/Cruise Report POS535, Loki2GrimseyEM: Geophysical and geological investigations of massive sulfides at and in the vicinity of Loki's Castle (Norway) and similar experiments around the Grimsey Hydrothermal Field (Iceland) for the assessment of the geothermal potential and the exploration for potential mineralizations within the seafloor, Akureyri (Iceland) – Bremerhaven (Germany), 09.06 – 03.07.2019, Eds.: Sebastian Hölz, Amir Haroon and Sofia Martins, DOI: 10.3289/GEOMAR_REP_NS_53_2019
- 54 Practical Guide for Environmental Monitoring of Conventional Munitions in the Seas, Results from the BMBF funded project UDEMM "Umweltmonitoring für die Delaboration von Munition im Meer" Ed.: Jens Greinert, DOI: 10.3289/GEOMAR_REP_NS_54_2019
- 55 RV ALKOR Fahrtbericht/Cruise Report AL533, Mutual Field Trials of the Manned Submersible JAGO and the Hover-AUVs ANTON and LUISE off the Aeolian Islands, Mediterranean Sea, Catania (Italy) – La Seyne-sur-mer (France), 05.02. – 18.02.2020, Authors: Karen Hissmann, Marcel Rothenbeck, Emanuell Wenzlaff, Tim Weiß, Patrick Leibold, DOI: 10.3289/GEOMAR_REP_NS_55_2020

GEOMAR Reports

No.	Title
56	RV POSEIDON Fahrtbericht/Cruise Report POS536/Leg 1, DIPLANOAGAP: Distribution of Plastics in the North Atlantic Garbage Patch, Ponta Delgada (Portugal) – Malaga (Spain), 17.08. – 12.09.2019, Author: Mark Lenz, DOI: 10.3289/GEOMAR_REP_NS_56_2020
57	RV SONNE Fahrtbericht/Cruise Report SO277, OMAX: Offshore Malta Aquifer Exploration, Emden (Germany) – Emden (Germany), 14.08. – 03.10.2020, Autor / Author: Christian Berndt with contributions by Morelia Urlaub, Marion Jegen, Zarah Faghih, Konstantin Reeck, Gesa Franz, Kim Carolin Barnscheidt, Martin Wollatz-Vogt, Jonas Liebsch, Bettina Schramm, Judith Elger, Michel Kühn, Thomas Müller, Mark Schmidt, Timo Spiegel, Henrike Timm, Anina-Kaja Hinz, Thore Sager, Helene Hilbert, Lea Rohde, Torge Korbjuhn, Silvia Reissmann, Nicolaj Diller, DOI 10.3289/GEOMAR_REP_NS_57_2021

For GEOMAR Reports, please visit:
https://oceanrep.geomar.de/view/series/GEOMAR_Report.html

Reports of the former IFM-GEOMAR series can be found under:
https://oceanrep.geomar.de/view/series/IFM-GEOMAR_Report.html



Das GEOMAR Helmholtz-Zentrum für Ozeanforschung Kiel
ist Mitglied der Helmholtz-Gemeinschaft
Deutscher Forschungszentren e.V.

The GEOMAR Helmholtz Centre for Ocean Research Kiel
is a member of the Helmholtz Association of
German Research Centres

Helmholtz-Zentrum für Ozeanforschung Kiel / Helmholtz Centre for Ocean Research Kiel

GEOMAR
Dienstgebäude Westufer / West Shore Building
Düsternbrooker Weg 20
D-24105 Kiel
Germany

Helmholtz-Zentrum für Ozeanforschung Kiel / Helmholtz Centre for Ocean Research Kiel

GEOMAR
Dienstgebäude Ostufer / East Shore Building
Wischhofstr. 1-3
D-24148 Kiel
Germany

Tel.: +49 431 600-0
Fax: +49 431 600-2805
www.geomar.de